COMPARISON OF CFD SIMULATION AND EXPERIMENTAL DATA FOR HEATING AND COOLING IN LOW N PACKED BEDS OF SPHERICAL PARTICLES

By

Ashley Morgan

A Thesis
Submitted to the Faculty of
Worcester Polytechnic Institute
In partial fulfillment of the requirements for the
Degree of Master of Science
In Chemical Engineering

May 2014

Approved:

Prof. Dr. Anthony G. Dixon, Advisor

Prof. Dr. David DiBiasio, Department Head

ABSTRACT

Packed beds reactors are used in industry for many reactions that require a solid particle, often a catalyst, reacting with fluid. These reactions can be endothermic, with heat supplied in the column jacket, or exothermic, with a cooling fluid in the column jacket. In order for these columns to operate safely it is necessary to understand the heat transfer parameters within the bed and between the bed and column wall. At the column wall, wall effects can have a large impact on the heat transfer especially for columns that have a low column to particle diameter ratio (N). At values of N below 8, the wall effects account for a large percentage of the bed. These effects are difficult to model, so typically experiments are used to find the heat transfer parameters for a given set of conditions, with several scale up stages required.

Disadvantages of experimental results are that detailed flow patterns within the bed cannot be captured, and it can be difficult to obtain temperature readings at every point in the bed. This presents an opportunity to use Computational Fluid Dynamics (CFD) to supplement experimental data with theoretical results. CFD uses the conservation of mass, momentum and energy to solve for heat, mass and flow across the physics of interest. In order for CFD to be used confidently, these models must be validated against expected literature correlations as well as experimental data.

This research is built upon previous findings for comparisons of heating and cooling experiments (N=8) conducted at Worcester Polytechnic Institute (DiNino et. al, 2013). This study was one of the first that compared heating and cooling data collected under the same conditions. The goal of the study was to see if the heat transfer parameters between heating and cooling were the same. It was found that heating and cooling were comparable for the effective thermal conductivity, which is a measure of how much heat is transferred throughout the bed. However, for the wall Nusselt number, a measure of the heat transfer at the column wall, heating was found to be higher.

In this research, experimental data for heating and cooling (N=5.33) was collected and compared to theoretical CFD results. For the experiments, it was found that the effective thermal conductivity was comparable for heating and cooling, and the wall Nusselt number for heating was higher. These results were used to validate the CFD model, after appropriate corrections to the model set up were made. For the CFD results, it was found that both the wall Nusselt number and effective thermal conductivity were comparable for heating and cooling. The wall Nusselt number was slightly higher for cooling, however this difference decreased as the Reynolds number increased.

ACKNOWLEDGEMENTS

First I would like to sincerely thank my advisor Prof. Anthony Dixon for his support and guidance in both my undergraduate and graduate career. Without his help I would not have been able to complete my Masters under the 5 year program. I appreciate the time he put into helping me interpret my data as well as providing someone to bounce ideas off of and brainstorm possible solutions.

I would also like to thank the Chemical Engineering department as a whole for the caring and welcoming atmosphere provided by every member. I would like to especially thank Prof. David DiBiasio for providing my funding and being a wonderful Department Head. Also, Felicia and Tiffany for being extremely helpful administrative assistants, and also for providing moral support. Finally I would like to thank Prof. Steve Kmiotek for providing advice both professionally and personally, as well as always having an open door when I needed someone to talk to.

Within my research group I would like to acknowledge Nick Medeiros for moral support during late nights in the lab, as well as always being there to troubleshoot CFD problems and talk me through difficult concepts. Also, Behnam Partopour for being a helpful and kind lab mate.

Outside of the academic setting, my friends and family provided the support and encouragement I needed to finish my graduate degree. A large thanks to Lindsay, Paige, Kaitlyn, Ryan, Ron, and Eric for providing a source of humor when I needed a laugh, and also to Cody and Sterling for being welcome homework partners. Additionally I would like to thank Dave for always reminding me to be confident and that hard work pays off.

Last and not least I need to thank my family for always believing in and supporting me. I would like to thank my sister and Aunt Sharon for their random messages of encouragement. Finally I would like to especially thank my wonderful parents for their endless love and support. Without their help I never would have made it this far.

CONTENTS

LIST OF FIGURES

LIST OF TABLES

LIST OF EQUATIONS

CHAPTER 1 INTRODUCTION

Packed bed reactors are commonly used in industry for reactions between a fluid and solid particle such as oxidation, methane steam reforming, and other reactions that require a catalyst. These reactions can be endothermic and require heat supplied via a heating fluid in the column jacket, or exothermic in which heat is removed using a cooling fluid in the column jacket. For safety and economical purposes, it is important the correct amount of heat transfer occurs within the column. For an endothermic reaction, supplying too much heat results in wasted utility costs, and not enough heat will result in lower product yields. In an exothermic reaction, safety is a major concern since inadequate cooling can result in a dangerous runaway reaction. Therefore modeling of the heat transfer parameters is critical. This is usually done on smaller experimental scales, using several scale up columns before the full scale.

The disadvantages of this approach include increased cost, as well as incomplete information in the bed. Experimentally it is difficult to measure full flow patterns and the complete temperature profile within the bed. Flow and temperature values are especially valuable as the bed position approaches the tube wall. Near the tube wall, channeling effects can affect the flow and therefore the heat transfer parameters. When the diameter of the column is much larger than the particle diameter, these effects do not have a large impact on the heat transfer. However, for packed beds with a low column to particle diameter ratio, N, these wall effects account for a much larger portion of the bed and become important to model. It is generally thought that under a value of N=8 the wall effects become significant.

When modeling these wall effects two approaches can be used: allowing the effective thermal conductivity of the bed to vary with radial position, or introducing a heat transfer parameter at the tube wall (Winterberg, Tsotsas, Krische, & Vortmeyer, 2000) (Dixon, 2012b). By introducing this apparent wall heat transfer coefficient, h_w, the large increase in resistance due to wall channeling can be accounted for. This results in two main heat transfer parameters that can be used to analyze heat transfer in the packed bed: the effective thermal conductivity, and the wall Nusselt number. The effective thermal conductivity is a measure of how effective the bed transfer heat, while the wall Nusselt number measures heat transfer at the tube wall.

Experimentally, these parameters are found by taking radial temperature measurements in the packed bed at various packing heights, and then fitting them to an appropriate model. There is no known physical reasoning why these parameters should have different values, and most literature does not suggest a difference. The main author who reported a difference between the overall Nusselt numbers

in the bed was Leva (1947 & 1948). Leva reported different correlations for heating and cooling for packed beds with a value of D_P/D_T less than 0.35. These correlations suggested cooling had more overall heat transfer throughout the bed than heating at the same Reynolds number.

For the research performed by Leva, these results were presented in different papers and were not directly compared. There is a limited amount of research which directly compares heating and cooling for the same experimental set up, by the same researchers. This motivated the research that this current paper builds upon. DiNino, Judge, Hartzel, & Morgan (2013) studied both heating and cooling experimental data for N=8 using the same particles and set up. It was found for the effective thermal conductivity heating and cooling produced comparable values, and for the wall Nusselt number heating was higher. This research also determined to collect reliable experimental data, a constant bed height, with varying air flow, should be studied on a given day. Additionally, modifications to the model that fitted the data to heat transfer parameters were made to give interpolated temperatures that matched the found values. This motivated the current research, which aims to use computational fluid dynamics (CFD) combined with experimental data to draw comparisons between heating and cooling. For this study heating and cooling experiments were conducted at a value of N=5.33 and compared to a CFD model which simulated the experimental set up as accurately as possible.

Computational fluid dynamics is increasingly being used as a tool to model packed bed reactors in order to obtain detailed flow and temperature fields in packed beds. The theory beyond CFD uses momentum, mass, and energy balances over small cells within the domain of interest. The early uses of CFD were limited to 2D studies of two or three spheres (Dalman et al., 1986). With increasing computing power the complexity of the models has increased, allowing for realistic 3D models with hundreds of particles to be built that have been validated against experimental data (Magnico, 200) (Augier et al., 2010). The advantages of CFD include detailed fluid flow and temperature information within the packing, speed of results compared to design an experimental set up, as well as the ability to model both ideal and realistic situations (Patankar, 1980). An example of the available flow and temperature information is shown below. The figures show the center plane of the column for a cooling run at a Reynolds number of 876, for both the temperature contours as well as velocity vectors. For the velocity vectors, the picture is zoomed in on the column to show more details.

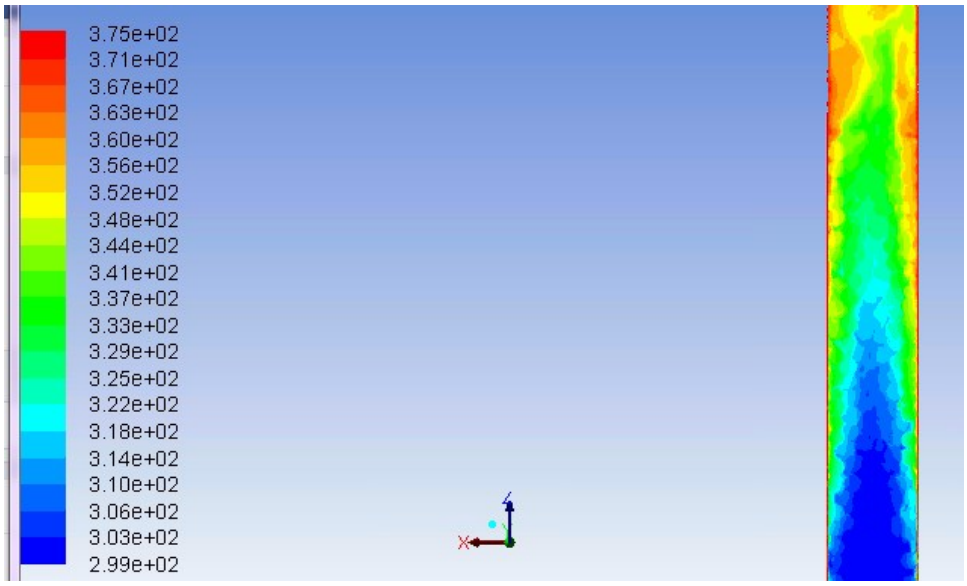

Figure 1-1. Example of Temperature contours [K] for a Cooling Simulation Re=876

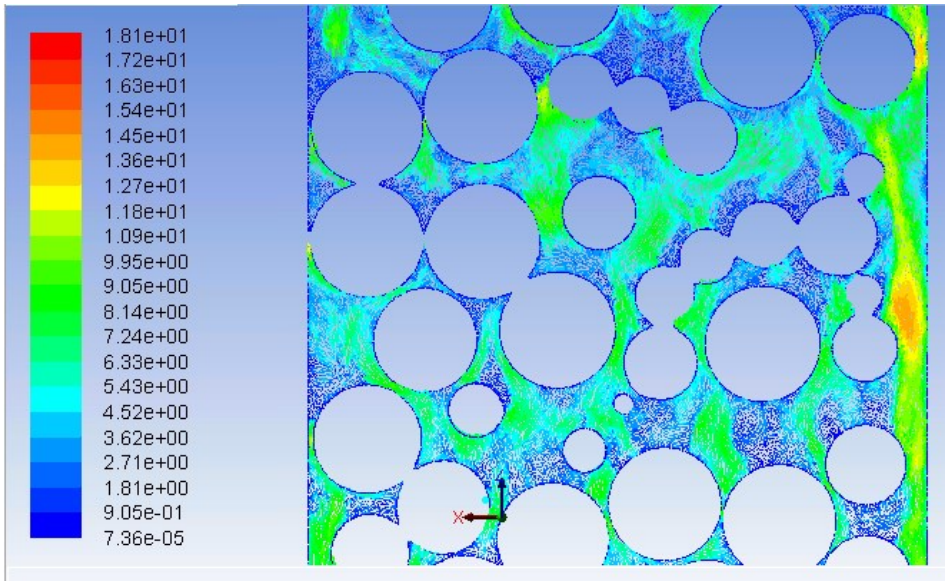

Figure 1-2. Example of Velocity Vectors for a Cooling Simulation Re=876

For this research, experimental runs were conducted, and the CFD was run to match the temperatures as well as mass flow rate for each run. Temperatures in the simulation bed were taken at the same point as the experimental data and fitted to the Generalized Inlet Plug Flow model (GIPPF). From the GIPPF model, the heat transfer parameters were found by solving a shell balance within the bed assuming: two dimensional, steady state, no reaction, constant physical properties, no pressure drop, pseudo-homogenous, plug flow, no axial dispersion of heat, no free convention of heat, and no radiation. The resulting heat transfer parameters were compared between: heating and cooling experiment, heating

experimental to CFD, cooling experimental to CFD, and heating and cooling CFD. The experimental results were used to identify any shortcomings in the CFD, and then once these were addressed the CFD was validated against the experimental data. This step is important to ensure the CFD makes physical sense and therefore confidence can be put into the simulation results. After the CFD models were validated, heating and cooling were compared in the theoretical case to see if there was any physical basis for a discrepancy between heating and cooling.

CHAPTER 2 Background

Packed bed reactors are commonly used in industry for reactions such as oxidation, methane steam reforming, and various other catalytic reactions. The main mechanisms for heat transfer in these packed beds are convection and conduction as air flows past the particle, and also via conduction between particles (Adeyanju & Manohar, 2009). For packed beds at lower temperatures, the third from of heat transfer, radiation, is generally neglected and will be for this research. When the reactors are large, the heat effects at the column wall do not greatly affect the bed of particles. When the column to particle diameter ratio, N, is lower than 8 the wall heat transfer becomes a large portion of the bed resistance. Therefore, the wall effects drastically affect the entire bed. These wall effects are difficult to model, making Computational Fluid Dynamics (CFD) a useful tool to better understand the heat transfer in packed beds. This is valuable information for modeling extremely exothermic and endothermic reactions to ensure the correct amount of heat is removed, or added, to the bed for safety purposes.

HEAT TRANSFER PARAMETERS

To analyze the heat transfer in a packed bed, two main dimensionless parameters are found: the effective thermal conductivity, and the wall Nusselt number. The Biot number and radial Peclet number are different ways of expressing the effective radial thermal conductivity ratio, k_r/k_f, and the wall Nusselt number, Nu_w, and are found in literature but will not be the focus of this research. However, for completeness the definitions of the radial Peclet and Biot numbers will be given.

The radial Peclet number is a ratio of the advection to the rate of diffusion. Advection is the movement of a fluid due to its bulk motion. The Peclet number gives an understanding of how much heat is being transferred in the axial direction to the radial position.

Equation 2-1. *Radial Peclet Number*

$$Pe_r = \frac{\rho v c_p d_p}{k_r}$$

Where ρ is the fluid density, v is the fluid velocity, C_p is fluid heat capacity, d_p is the diameter of the particles, and k_r is the effective radial thermal conductivity (Pantankar, 1980). The effective radial thermal conductivity is a measure of the thermal conductivity of both the bed particles, and the fluid between the particles. For a pseudo-homogenous model, it assumes a constant value for a given fluid velocity.

The Biot number gives a ratio of the resistance to heat transfer at the wall to the resistance of the particles within the packed bed. Where h_w is the apparent wall heat transfer coefficient, R is the tower's radius, and k_r is the effective radial thermal conductivity. The apparent wall heat transfer coefficient accounts for the large jump in resistance to heat transfer that is seen at the tube wall, which causes the sudden change in temperature as the position in the bed approaches the tube wall. In packed bed heat transfer experiments, the Biot number is expected to decrease as the fluid flow rate increases (DeWitt, 2007).

Equation 2-2. Biot Number

$$Bi = \frac{h_w R}{k_r}$$

The effective thermal conductivity a measure of the radial heat transfer through the bed to that of the fluid. The radial heat transfer through the bed includes all possible heat transfer such as: conduction in the fluid, particle to particle conduction, conduction between stagnant fluid and the particles, radial dispersion, and particle to fluid conduction. As the flow in the bed increase, this value is expected to increase as well.

Equation 2-3. Effective Thermal Conductivity

$$\frac{k_r}{k_f} = \frac{RePr}{Pe_r}$$

The wall Nusselt number compares the rate of convection to the rate of conduction at the wall. Since the radius of the column, and generally the thermal conductivity, remain constant the wall Nusselt number provides insight into the apparent heat transfer coefficient at the wall.

Equation 2-4. Wall Nusselt Number

$$Nu_w = \frac{h_w R}{k_f}$$

The parameters are affected by the material used for the particles, the shape of the particle, and most importantly the ratio of the tube to particle diameters (N). As mentioned before, at a small value of N, the wall effects affect a large percentage of the bed, and it is critical that they are understood for safety and product quality purposes.

There is no physical reasoning to believe these parameters would have different relationships to Reynolds number between heating and cooling, and most of the literature gives the same relation between the two. However, Leva (1947 & 1948) found a difference between heating and cooling when fitting the plots of Nusselt number against Reynolds number. Leva (1947) first studied heating of air and carbon dioxide in both a 2 inch and ½ inch column using spherical particles. He measured the temperature of the bed for five different packing materials at various flow rates and found the data fit the following correlation for particle to column diameters ratios less than 0.35:

Equation 2-5. Leva Correlation for Heating

$$Nu_o = 0.813 * \exp\left(-6\frac{D_p}{D_T}\right) * \left(\frac{D_p G}{\mu}\right)^{0.9}$$

Where Nu_o is the overall Nusselt number in the bed. Leva next studied cooling of air and carbon dioxide in packed bed (1948) and found the following correlation, also for D_p/D_T less than 0.35, which is clearly different than the one found for heating:

Equation 2-6. Leva Correlation for Cooling

$$Nu_o = 3.50 * \exp\left(-4.6\frac{D_p}{D_T}\right) * \left(\frac{D_p G}{\mu}\right)^{0.7}$$

MODELING

In order to obtain these heat transfer parameters, models are used to relate the temperature in the bed to the above parameters. In order to develop these models, first simplifying assumptions must be determined.

The simplest models assume heat is only transferred in one direction, axially, requiring that an average temperature be taken across the radial positions of the bed (Dixon & van Dongeren, 1998). To find this average a mean-cup average is used, and this in conjunction with the wall temperature allows for an overall heat transfer coefficient, U, to be found. However, the average temperature found in this way can drastically vary from the true radial mean temperature. This caused high errors in the values of U and led to the development of a two dimensional model which allows for heat transfer in both the radial and axial directions.

There are two ways to model the particles and fluid in a packed bed, heterogeneously which accounts for the differences between the particles and air, or pseudo-homogeneous which considers the particles

and the air to be a homogenous medium. A pseudo-homogenous approach simplifies the model, and can be applied in situations where the bulk fluid and particles have similar temperatures (Wen & Din, 2006). It has been found that this is a valid assumption for steady state systems in which no reaction is occurring (Dixon, A.G., 2012b). In addition to the particles and fluids, the velocity itself must be modeled in the bed; either with a constant plug flow model or by a model that has a radial velocity dependence (Winterberg, Tsotsas, Krische, & Vortmeyer, 2000). If a plug flow model is chosen, axial convection of heat is accounted for, however a constant radial conductivity must be used (Dixon, A.G, 2012b). At the wall, there is a sharp decrease in the conductivity due to a thin film of air which increases the resistance to heat transfer. In order to help with this, when using a constant thermal conductivity a wall heat transfer coefficient, $h_{w,}$ is introduced.

The advantage to using a radial dependence of velocity is now thermal conductivity can also have a radial dependence, resulting from the channeling effects that occur between the packing (Borkink & Westerterp, 1992). Since the thermal conductivity is allowed to vary across the bed, there is no need for the wall heat transfer coefficient. However, to determine the velocity profile, which in turn allows you to find the thermal conductivity's dependence on position, the bed porosity must be known. This requires a knowledge on how the bed is packed, so for simplicity the plug flow model is used.

One possible issue that can arise during modeling is length effects, in which the parameters h_w and k_r vary with increasing bed height (Dixon, A.G, 2012b). The radial conductivity was found to decrease to an asymptotic value, as well as the wall heat transfer coefficient, but to a lesser degree. It was found that using the correct inlet temperature profile was essential in eliminating length effects: using a radially flat profile provided effects, while a parabolic profile eliminated them. Also, Dixon (1985) found that heat loss in the calming section also produced length effects. Therefore, to establish a parabolic profile and to eliminate any heat loss effects, the first bed height is used as the inlet profile.

For this research the following assumptions were made: two dimensional, steady state, no reaction, constant physical properties, no pressure drop, pseudo-homogenous, plug flow, no axial dispersion of heat, no free convention of heat, and no radiation. This model was developed by Dixon and is termed the Generalized Initial Profile Plug Flow, GIPPF model. To develop this model, first an energy balance on a disc shaped region is performed (Dixon, A.G., 2012 a):

Equation 2-7. Heat Transfer Equation

$$0 = -\frac{1}{r}\frac{\delta}{\delta r}(rq_r) - \frac{\delta q_z}{\delta z}$$

Since a plug flow velocity profile is assumed that accounts for the axial convection of heat, all other heat transfer can be lumped into effective terms that are constant and follow Fourier's law. The other heat transfer is convective.

Equation 2-8. Fourier's Law

$$q_r = -k_r\frac{\delta T}{\delta r}$$

Equation 2-9. Convective Heat Transfer

$$q_z = v\rho c_p(T - T_{ref})$$

Since convection is considered the only method for heat transfer to occur in the axially direction, equations 5 and 6 are plugged into equation 4 to yield:

Equation 2-10. Modified Heat Transfer Equation

$$v\rho c_p\frac{\delta T}{\delta z} = k_r\frac{1}{r}\frac{\delta}{\delta r}(r\frac{\delta T}{\delta r}) = k_r(\frac{\delta^2 T}{\delta r^2} + \frac{1}{r}\frac{\delta T}{\delta r})$$

Assuming an axisymmetric column allows for the temperature gradient at the center of the bed to be zero. For the wall boundary condition, the wall heat transfer coefficient is used in conjunction with the observed wall temperature to give:

Equation 2-11. Boundary Condition at the Column Wall

$$-k_r\frac{\delta T}{\delta r}_R = h_W(T_R - T_W)$$

To make the axial length, radial position, and temperature dimensionless, the following parameters were defined:

Equation 2-12. Dimensionless Radial Position

$$y = \frac{r}{R}$$

Equation 2-13. Dimensionless Axial Length

$$x = \frac{z}{R}$$

Equation 2-14. Dimensionless Temperature

$$\Theta = \frac{T - T_w}{T_o - T_W}$$

These dimensionless parameters are used to make equation 7 and the boundary conditions dimensionless:

Equation 2-15. Dimensionless Heat Transfer Equation

$$\frac{\delta\Theta}{\delta x} = \frac{k_r}{v\rho c_p R}\left(\frac{\delta^2\Theta}{\delta y^2} + \frac{1}{y}\frac{\delta\Theta}{\delta y}\right) = \frac{1}{Pe_R}\left(\frac{\delta^2\Theta}{\delta y^2} + \frac{1}{y}\frac{\delta\Theta}{\delta y}\right)$$

Equation 2-16. Boundary Conditions

$$\frac{\delta\Theta}{\delta y} = 0 \quad at\ y = 0$$

$$\frac{\delta\Theta}{\delta y} + Bi\,\Theta = 0 \quad at\ y = 1$$

To solve the above equation separation of variables was used. It was assumed theta could be written as:

Equation 2-17. Assumption for Separation of Variables

$$\Theta(y, x) = Y(y)X(x)$$

This was substituted into the original partial differential equation, and divided through by XY.

Equation 2-18. Partial Differential Equation

$$Pe\left(\frac{R}{d_p}\right)\frac{X'}{X} = \left(\frac{Y''}{Y} + \frac{1}{y}\frac{Y'}{Y}\right) = k$$

Setting k equal to a constant :

Equation 2-19. Partial Differential Equation Set Constant

$$Y'' + \frac{1}{y}Y' = kY$$

With the following boundary conditions:

Equation 2-20. Boundary Conditions

$$XY' = 0 \; at \; y = 0$$
$$Y'(0) = 0$$

$$XY'(1) + Bi \; XY(1) = 0$$
$$Y'(1) + Bi \; Y(1) = 0$$

This yields a Bessel's equation of zero order with to solutions $J_0(y)$ and $Y_0(y)$ which gives:

Equation 2-21. Bessel's Equation

$$\lambda J_1(\lambda) - BiJ_0(\lambda) = 0$$

Which to satisfy the boundary conditions the eigenvalues needs to satisfy the above characteristic equation, and the constant k is set equal to the negative of the squared eigenvalues.

Equation 2-22. Solution for X Variable

$$X_i = \exp\{-\frac{\lambda_i x}{Pe * \frac{R}{d_p}}\}$$

For each infinite number of eigenvalues there is an infinite number of eigenfunctions $J_0(\lambda_i)$ allowing the following:

Equation 2-23. Eigen function Solution

$$\Theta(y,x) = \sum_{i=1}^{\infty} A_i J_0(\lambda_i y)\exp\{-\lambda_i^2 x \; / \; Pe * \frac{R}{d_p}\}$$

To determine the A_i the initial conditions are used, along with the Lommels integrals to give the final answer of the Generalized Initial Profile Plug Flow (GIPPF) model:

Equation 2-24. GIPPF Model

$$\Theta(y,x) = 2\sum_{i=1}^{\infty} \frac{\lambda_i^2 J_o(\lambda_{ij})}{\{J_o(\lambda_{ij})\}^2} \exp\left(\frac{-\lambda_i^2 (x - x_o)}{Pe_r \frac{R}{d_p}}\right) x \int_0^1 \Theta_o(y) J_o\,(\lambda_{ij}) y dy$$

EXPERIMENTAL

It has been found that a proper experimental technique strongly impacts the quality and accuracy of results. Several Major Qualifying Projects (MQPs) at Worcester Polytechnic Institute have focused on improving the experimental procedure to obtain the most accurate results. Typically, a vertical column is packed with catalyst carriers, or other packing material, and temperature readings are taken so a model can be used to find the effective thermal conductivity as well as the wall heat transfer coefficient. The column has a heated or cooled section where the heat transfer occurs, downstream from a calming section which establishes the flow profile into the bed. It is recommended that materials with low thermal conductivity, such as nylon, be used for the calming section to limit pre-heating or heat loss (Dixon, A.G., 1985).

There are several methods which have been developed to collect the temperature data in the packed bed, and they fall into two main categories: embedded methods which are directly in the packing, or suspended methods which take temperature readings above the packing (Thomeo, Rouiller, & Freire, 2004). Embedded methods include ladder frames, axial thermowells, and radial thermowells. The ladder frame is essentially a ladder that supports the thermocouples at various radial and axial positions. An axial thermowell is a long tube in the center of the bed, and a radial thermowell is pushed through the tube wall and across the bed at various axial positions. The advantage to embedded devices is the complete set of axially and radially data points are collected at once, requiring only one experimental run. However, these embedded devices have been found to disturb the packing structure of the column, which can affect the velocity profile in the bed as well as the temperature profiles. If embedded devices are used, it is important that low thermal conductivity materials are used, to avoid artificially high temperature readings in the thermocouples.

For suspended methods, the two main methods are crosses and rings. A cross generally has several arms that can measure temperature at different angular positions in the bed, as well as radial positions. Dixon (1985) for example used an eight armed cross with four angular replicates of six radial positions. These replicates showed scatter, which could be used to provide statistical information as to how the

temperature varies at the same radial position in the bed. The rings method has thermocouples that are within concentric metal rings at different radial positions, which allowed for an average temperature to be obtained (Kwong & Smith, 1957). However, it was argued by Dixon (2012b) that the scatter in temperature across the bed is valuable information.

The main advantages to suspended methods are the packing in the bed is not disturbed, so the velocity profile, and possibly temperature profile are not disturbed. However, there are some disadvantages and some perceived shortcomings of the suspended method. The main criticism is that since the thermocouples are suspended above the packing, they may not be representative of the profile within the packing since flow patterns are expected to change after leaving the packing (Thomeo, Rouiller, & Freiere, 2004). Dixon (1998) found that by placing the thermocouples directly on the surface of the bed, he obtained scattered results, and recommended that the thermocouples be placed 3-5mm above the packing.

Another concern with using the suspended methods is the amount of time the cross is inserted into the column while taking measurements. While Dixon (1985) showed that using a material with a low thermal conductivity was important to minimize any conduction effects, conduction could still occur. To investigate this, DiNino, Hartzel, Judge, & Morgan (2013) allowed the column to come to steady state before inserting the cross and collecting temperature data. After the cross was inserted, the column was run for another two hours, all the while collecting temperature data. This was done for two different bed heights. It was found that once the thermocouple cross was inserted, the difference in temperature readings initially, after one hour, and after two hours were within 1K of each other, with a standard deviation around 0.3K. They concluded that for a nylon cross conduction of the cross did not vary with immersion time, and did not result in artificially high temperature readings.

While both methods have their advantages and disadvantages, it was determined that the thermocouple cross would be the most accurate way to obtain temperature profiles. This allowed for minimal disturbance to the packing structure of the column, and also was determined to not have conduction effects due to immersion times.

After the method of data collection is determined, there are several options for the experimental set up: such as how to vary the bed height and air flow, as well as how to analyze the collected data. This review will focus on work done at Worcester Polytechnic Institute to determine the best methods for the equipment available for this research. Three main groups have focused on equipment set up at

Worcester Polytechnic Institute: DiNino, Hartzel, Judge, and Morgan (2013), Alexander, Ledwith, and Linskey (2011), and Ashman, Rybak, and Skene (2009).

When Ashman et al. (2009) conducted experiments, they only studied cooling experiments, meaning pre-heated air was run through a column with a cooling water jacket on the walls. Experiments were run by packing the column to one bed height per day, and varying the air flow in the column throughout the day. This allowed for all of the Reynolds numbers to be collected for a specific bed height in a single day. The thought behind this was to decrease effects on varying air supply to the column, and also to have a consistent packing between Reynolds numbers. The group studied a variety of packing materials in both a two-inch and four-inch column, and used an Inlet Profile Plug Flow model which assumes a parabolic inlet temperature profile, and does not interpolate the values. The group found strong correlations between their raschig ring study and literature values, and found values that trended higher for both effective thermal conductivity and wall Nusselt number for their spheres study.

When Alexander et al. (2011) conducted experiments, they studied both heating and cooling using raschig rings in the two and four inch columns. The goal of this study was to further resolve discrepancies found between heating and cooling studies conducted at WPI. During the early phases of data collection, nonsensical trends were observed in the dimensionless temperature profiles; such as the higher bed heights having larger values then the lower bed heights. This showed that as the bed heights increased, the temperature in the bed went further away from the wall temperature which does not make physical sense. In an attempt to fix these strange trends, the group altered the method by collecting all bed heights for one air flow in a day. This required the group to pack the column to the first bed height, start a run with a certain air flow and then increase the bed height after steady state was achieved. Since the bed was packed to all heights in one day, the packing needed to be removed at the end of an experimental run: so all Reynolds numbers had a different packing structure. The thought was day to day air variations would not skew temperature profiles.

In addition to the change in column packing, the group also added a correction factor for air expansion through the heater. The Reynolds number was multiplied by a factor of 1.2. However, this was discredited between Alexander et Al. (2011) and DiNino et al. (2013) since the conversation of mass applies to the Reynolds number calculation, and density and velocity would both vary as temperature changed to give a constant mass flow rate. The group also changed from the Inlet Profile Plug flow model to the GIPPF model discussed earlier, which interpolates the inlet profile based off of the first bed height.

DiNino et al. (2013) conducted research on heating and cooling experiments using ceramic spheres in the two inch column. Initially the group followed the recommendation of Alexander et al. (2011) and packed the column to all four heights with a constant air flow per experimental run. While conducting experiments, the group investigated the inlet profile used in the GIPPF to ensure it matched experimentally obtained results. It was found that for some profiles, the profile exceeded 1 at the bed center. This shows the program is interpreting the center of the bed to exceed the inlet temperature which is not physically reasonable. The GIPPF model was found to not be including the temperature reading at the center thermocouple, since there was only one reading instead of four like the other positions. Instead, the model used a cubic spline interpolation to find values below y=0.35, the smallest radial position available. A spline interpolation uses piecewise polynomials to interpolate the values at unknown points. For a cubic spline, the following equation is used with the constraint that first and second derivatives must be continuous:

Equation 2-25. Cubic Spline Interpolation Formula

$$S_i(x) = a_i(x - x_i)^3 + b_i(x - x_i)^2 + c_i(x - x_i) + d_i$$

Also, boundary conditions are used, in this case the known value at x=1 was used, and the derivative and x=0 was set to be zero, to guarantee a parabolic profile within the bed. In order to fix this overshoot that was being observed for some profiles, the cubic spline was modified to set the boundary condition at the center of the bed to be the experimentally measured temperature value. This showed a dramatic improvement in the temperature profiles, with all of them matching the experimentally found profiles.

Even with this improvement in the GIPPF model, there was still a large amount of unexplained scatter in the data collected by DiNino et al. (2013). In order to explain this, the group ran experiments using the procedure used by Ashman et al. (2009), of having one bed height per day and changing the air flow. After examining the dimensionless temperature profiles to ensure they made physical since, it was found by using this procedure the obtained results matched past experimental data and literature values. Alexander et al. (2011) was the only group to obtain non-physical temperature profiles, so DiNino et al. (2013) recommended to return to the procedure of one bed height per day with varying air flow. This allows for a constant packing structure for all Reynolds numbers, eliminating the possibility of bed void fraction affecting heat transfer parameters. Also since each air flow rate is run on the same day, any effects from air quality will be the same for all Reynolds numbers.

COMPUTATIONAL FLUID DYNAMICS

Computational fluid dynamics (CFD) is increasingly being used to model complex flow systems with heat and mass transfer. As computer capability increases, so does the complexity of the systems that are being modeled. The advantages of CFD modeling include lower cost than full scale experiments, speed with which results can be obtained, complete information such as velocity details, and the ability to model both real and idealistic situations (Patankar, 1980). The basics of CFD rely on momentum, energy and mass balances across small regions within the larger system being examined.

For CFD the two main approaches commonly used are finite elements (FE) and finite volume (FV). Fluent uses the FV method so it will be the focus of this discussion. In the FV method the domain of interest is divided into small control volumes, allowing for discretization of the problem. Over these control volumes the governing equations are integrated and the resulting equations are solved in an iterative fashion, using method of weighted residual ideas modified so that the conservation principle is upheld (Dixon, 2014a).

Early work using CFD in packed beds was greatly limited by computational resources, limiting studies to 2D with a small number of spheres. Dalman et. al (1986) studied the flow and heat transfer for a row of spheres in a cylindrical tube, by modeling the flow past two spheres, in a 2D study. This study was the first to show high detail flow patterns in between spheres, and pointed to eddies forming which caused poor heat transfer. As computing power increased, 3D models were introduced. In one of the early 3D studies, a three sphere model was used by Derkx and Dixon (1996). A ten-sphere model added in wall to particle contact points and focused on finding typical heat transfer parameters and validated them against experimentally obtained data (Logtenberg & Dixon, 1998a,b). Nijemeisland and Dixon (2001) created a 44 sphere model, with structured packed beds, for both N=2 and N=4 situations and modeled heat and flow within the bed, and validated CFD against experimental data.

With increasing computing power, CFD models in packed beds were able to become larger, more complex, and thus more realistic. Since this research focus on heat transfer, without reaction, in a lab scale packed bed this review will focus on similar studies. One of the early CFD studies of heat transfer in a more realistic fashion used a 44 sphere model with a non-regular packing (Guardo, et al., 2004). The spheres were packed by building an 11-sphere section, which was combined using four layers. Each layer was rotated 60 degrees around the beds axis before it was added. In this study, both laminar and turbulent flow of air through a packed bed were studied. The air was modeled using the incompressible

ideal gas law for the density, and a power law viscosity function. The velocity and temperature profiles in the bed were examined to ensure they followed expected trends, and the pressure drop and wall Nusselt number were compared to literature correlations. The study found good agreement between the correlations, and showed that CFD could be used to study a bed packed in a nonregular fashion, for laminar and turbulent flow. In 2005, Guardo et. al built on these findings by using the 44 sphere model above to study turbulence models, and also looked into contact points between the particles by overlapping the particles. Then in 2006 Guardo et. al once again used the 44 sphere model to show CFD could model forced convection at low pressure, with air as the heat transfer fluid, as well as mixed convection at high pressure.

For a larger scale packed bed, Magnico (2009) modeled 236 spheres with an N value of 5.96 and also 620 spheres with an N value of 7.8 in an unsteady state study of laminar flow and heat transfer. In this simulation, a cool gas entered the column at 273K and was heated by a wall at 373K. This study found 3D CFD could model the macroscopic properties of heat transfer, and these results agreed well with experimental results. The CFD was found to overestimate the radial heat transfer that occurred in the bed, and could only be used on the microscopic level when there was a small temperature gradient. This study did demonstrate that larger scale packed beds could be modeled using CFD and provide results that were comparable to experimental data and expected correlations.

This result was also mirrored by Augier et al. (2010) with their model of 620 densely packed particles. In this model, the wall effects were considered. Augier also ran a model with 440 particles which were considered to be infinitely large to ignore wall effects. To address the contact points issue, the particles were contradicted by 2%, so they were 98% of the original size and thus removing any contact between particles. This study found that locally there was some disagreement between the literature correlations and the CFD results. However, it was found that the 3D CFD model found global heat transfer parameters that agreed with the expected literature values.

GOVERNING EQUATIONS

For this research, the focus was on heat transfer in a fluid flow, therefore reaction equations will not be examined.

FLOW

When flow is modeled in Fluent the Navier-Stokes equations are used for momentum and mass conservation. Additionally, turbulence equations are needed for turbulent flow but since this research focus on laminar flow these will not be discussed. The general continuity equation is defined as follows:

Equation 2-26. General Continuity Equation

$$\frac{\delta \rho}{\delta t} + \frac{\delta(\rho u_i)}{\delta x_i} = S_m$$

With u_i being the velocity in the i-direction, ρ being the density, and S_m being any source terms. For this research the source terms were set to zero. The equation for conservation of momentum in direction i in a non-accelerating reference frame is given by:

Equation 2-27. Modified Conversation of Mass

$$\frac{\delta(\rho u_i)}{\delta t} + \frac{\delta(\rho u_i u_j)}{\delta x_i} = -\frac{\delta P}{\delta x_i} + \frac{\delta \tau_{ij}}{\delta x_i} + \rho g_i + F_i$$

Where P is the static pressure, τ_{ij} is the stress tensor, ρg_i is the gravitational body force, and F_i is any external body forces. For single-phase flow in packed beds it is usually zero. For a Newtonian fluid, the stress tensor is defined by:

Equation 2-28. Stress Tensor for Newtonian Fluid

$$\tau_{ij} = \left[\mu\left(\frac{\delta u_i}{\delta x_j} + \frac{\delta u_j}{\delta x_i}\right)\right] - \frac{2}{3}\mu\frac{\delta u_1}{\delta x_1}\delta_{ij}$$

Where μ is the molecular viscosity and the second term on the right is the effect of volume dilation.

PRESSURE-VELOCITY COUPLING

From the flow equations above, it can be observed that pressure appears in all three momentum equations (Patankar, 1980). The treatment of pressure is difficult since there is no explicit pressure equation, therefore pressure-velocity coupling is used to find equations for pressure using the momentum equations as well as the continuity equation. The most commonly used approach is termed SIMPLE (Semi-Implicit Method for Pressure-Linked Equations) which finds a pressure correction after every iteration. The SIMPLE method uses the fact that pressure is given indirectly, and when the correct pressure field is used the momentum equations will yield the velocity field which satisfies the continuity equation (Dixon, 2014c). For the flow field a co-located grid is used, since the mesh is unstructured, and the momentum values are interpolated. The steps of the SIMPLE algorithm are as follows:

1. Guess a pressure field (P*)
2. Solve the momentum equations for the velocity field (u*,v*, and w*)
3. Solve the pressure correction equation (P')
4. Calculate the new pressure based on the correction to the initial guess
5. Calculate the new velocity field from the velocity corrections
6. Solve discretization equations for other variables that may influence flow field (Temperature for this research)
7. Set the new pressure as the guess for pressure field and return to step 2

To help aid in convergence and increase stability, the correction equations have a relaxation factor, which will be discussed later in the Numerical Methods section.

ENERGY

Heat is transferred in three main ways: conduction, convection, and radiation. For experimental packed beds, radiation is generally neglected due to the relatively low temperatures observed in experimental settings. In reactions such as steam reforming, and other high temperature applications, radiation needs to be accounted for. Therefore, for this research, heat transfer will occur as conduction and convection between the particles, fluid, and tube wall. Therefore, the generalized energy balance equation, in the *i*-direction is:

Equation 2-29. Generalized Energy Balance

$$\frac{\delta(\rho E)}{\delta t}+\frac{\delta}{\delta x_i}\left(u_i(\rho E+\rho)\right)=\frac{\delta}{\delta x_i}\left(k_{eff}\frac{\delta T}{\delta x_i}-\sum h_j\overrightarrow{J_J}+\left(\overline{\overline{\tau_{eff}}}u_i\right)\right)+S_h$$

Where k_{eff} is the effective conductivity, and $\overrightarrow{J_J}$ is the diffusive flux of species J. The terms within the partial derivative on the right hand side represent the conduction, species diffusion and viscous dissipation. Any source terms are represented in the S_h term.

Within equation 29, the energy equation is defined as:

Equation 2-30. Energy Equation

$$E=h-\frac{p}{\rho}+\frac{u_i^2}{2}$$

For the solid particles within the packing, the energy balance is given below:

Equation 2-31. Solid Phase Energy Balance

$$\frac{\delta(\rho h)}{\delta t} + \frac{\delta}{\delta x_i}(u_i \rho h) = \frac{\delta}{\delta x_i}\left(k \frac{\delta T}{\delta x_i}\right) + S_h$$

For our model of steady state with no source terms, the time derivative term and source term are neglected.

NUMERICAL SOLUTIONS

These governing equations for momentum and energy are solved over the control volumes by integrating to solve for unknowns and linearizing the discretized equations. Fluent allows for the choice of two methods, coupled or segregated (Taskin, 2007). The segregated method solves for a single variable by considering all of cells in the domain and then solves for the next variable, and is an implicit solver. A coupled solver can solve both implicitly or explicitly. In the implicit approach, all the variables are solved in all the cells at the same time. For the explicit method solves for all variables in one cell at a time. Since the governing equations are highly nonlinear, and the problem is of a complex nature, the segregated approach was chosen. In this method, the following steps are used:

1. Fluid properties are updated based on previous solution, or set to initialized values if problem has just started.
2. The momentum equations for each direction (x, y, and z) are solved to update the velocity field.
3. A pressure correction is derived from the continuity equation based on the solution in step 2, and then this correction equation is solved for the needed corrections to pressure and velocity fields
4. Equations for energy are solved using the updated variables
5. If interphase coupling is included the source terms in the phase equations are updated.
6. A check for convergence of the equation is made. If convergence is not within a given tolerance, the process is repeated from step 1.

When this approach is taken, a relaxation factor is generally used to aid in convergence (Pantankar, 1980). This relaxation factor weights how much the new predicted values influences the old solution.

Equation 2-32. Relaxation Formula

$$\varphi_p^{new,used} = \varphi_p^{old} + U(\varphi_p^{new,predicted} - \varphi_p^{old})$$

If the relaxation factor, U, is below one it is under relaxed. This slows convergence but helps with stability. If U is equal to one there is no relaxation, and the predicted value is used. If U is over one it is over relaxed and can be used to speed up convergence or quickly propagate changes, although it decreases the stability of the calculation. For the momentum field values of 0.6 -0.7 are typically used for the under relaxation factors, energy typically uses a factor of 0.95, pressure a value of 0.3 and density and body forces values of 0.7 -0.8 are commonly used (Dixon, 2013a).

DISCRETIZATION

When using the finite volume method, the equations discretized so the continuous exact solution of the governing equations is replaced with values at the grid points (Dixon, 2014a). These grid points are usually in the center of the control volumes, and the variables are discretized using piecewise linear functions. The discretization of the governing equations can be showed by considering the steady-state conservation equation for a general scalar, ϕ (Taskin, 2007). The following equation is the integration of the general conservation over a control volume V:

Equation 2-33. Integral Form of General Conservation Equation

$$\oint \rho\varphi\vec{v} \cdot d\vec{A} = \oint \Gamma_{\varphi}\nabla\varphi \cdot d\vec{A} + \int_{V} S_{\varphi} dV$$

Where ρ is the density, $\vec{v}$ is the velocity field, $\vec{A}$ is the surface area vector, Γ_{φ} is the diffusion coefficient and S_{φ} is the source term for the unit volume. The above equation is applied to every cell in the domain, and the discretization on one cell gives:

Equation 2-34. Discretization of General Conservation Equation over One Cell

$$\sum_{f}^{N_{faces}} \rho_f \vec{v}_f \varphi_f \cdot \vec{A}_f = \sum_{f}^{N_{faces}} \Gamma_{\varphi}(\nabla\varphi)_n \cdot \overrightarrow{A_f} + S_{\varphi}V$$

Where N_{faces} is the numbers of faces the control volume has. When these equations are solved, Fluent stores the values at the cell centers. For convection however, the values at the faces must be known (Dixon, 2014b). If the average between the central grid points is taken, problems can arise therefore several different schemes are commonly used: first-order upwind, power-law, second-order upwind, and QUICK scheme. When using the first-order upwind scheme the value of the scalar at the interface is taken to be equal to the grid point on the upwind side of the face. This is done since the values are not

strongly affected by the value of the points downstream. This method is very stable and is generally used to help establish the flow field, however it is not very accurate and can led to false diffusion.

For the power-law scheme the value is interpolated using an exponential profile based on the exact solution to the 1D equation. The points used in the interpolation are the grid points upwind and downstream to the interface. The disadvantage to this approach is that exponentials are computationally expensive. With the second-order upwind scheme, the value at the face is linearly interpolated from the two upwind values (Patankar, 1980). This method is commonly used since it is both stable and accurate, although regions with strong gradients can result in values outside the surrounding cell values. Therefore limitations must be applied. Finally, the QUICK scheme uses a quadratic curve fitted through the two upstream values, and one downstream value. A downside to this scheme is overshoots can occur in regions with strong gradients, although it is an extremely accurate scheme.

Mesh

In finite volume method, the collection of control volumes which make up the domain is referred to as the mesh. One of the advantages to the FV method is both a structured and unstructured mesh can be used. For a structured mesh, the control volumes are set up rigorously and can be well defined using an indexing system (Patankar, 1980). These meshes are restricted to simple geometries. For a more complex geometry, an unstructured mesh is used in which the control volumes are placed arbitrarily and cannot be indexed. While generating the mesh, it is important to use enough cells to capture the physics within the system. If too coarse of a grid, not enough cells, is used the results may not accurately represent the system. However, as more cells are introduced into the mesh, computation time increases and if too many cells are used, too fine a mesh, the simulation may never converge. In order to find the balance of mesh density and computational accuracy, mesh independence studies are used were the mesh is refined until the results no longer vary.

Contact Points

When a discrete particle CFD method is used, the contact points between the particles can become problematic (Dixon, Nijemesiland, & Stitt, 2012). The contact points become difficult to mesh, and result in Fluent attempting to model infinitesimally small regions. In order to properly model these contact points, four main approaches have been used to replace the contact points with easy to model geometry. The four main approaches to this contact points issue are gaps, caps, bridges, or overlap.

These four methods fall into two categories, global and local methods. Global methods change the particles sizes and ths the void fraction in the bed: gaps and overlap. A drastic change in bed void fraction can lead to changes in pressure drop and velocity profiles in the bed, so local methods were investigated. The local methods, bridges and caps, only change near the contact point. These have a small effect on the bed void fraction, and hence minimal impact on the pressure drop and fluid flow, ideally.

For the gaps method, all of the particles in the bed are shrunk so they no longer have any contact points; but instead have a film of fluid between the particles. This method is applied to the entire bed of particles so it is a global method. In work done by Dixon, Nijemesiland, and Stitt (2003) it was found that shrinking the spheres to 99.5% of their nominal diameter allowed for this method to be implemented at higher Reynolds numbers, without causing jetting. Jetting causes changes to the velocity field downstream of the particles, which can led to changes in the flow field. The other global method is overlapping. This method, developed by Guardo et al. (2004) expanded the size of the particles by 1% to allow overlap between a particles and its neighbors. This was done to model real contact points, and to help with convergence issues that were found if the particles were not altered. This method is also a global method since all particles were affected.

The local methods, the caps and bridges, did not change every particle in the bed, but only the contact points of particles and their immediate neighbors. For the caps method, any particles that were within a predefined distance of each other, were flattened so they became the desired distance apart from each other. Finally, the bridges method took particles within a predefined distance of each other and added a small cylinder between them, linking the two particles. In this method, it is important to properly model the thermal properties of these bridges so they match the particle-fluid-particle conduction observed with the actual contact point. Dixon et al. (2012) did this by considering conduction from a plane through the contact point which is perpendicular to the line contacting the two particles, and then modeling another parallel plane inside the particle. The planes are held at two constant temperatures, and then by equating fluxes through the planes an effective thermal conductivity of the bridge can be found.

Dixon et al. (2012) studied the effect each of these contacts points had on the drag coefficient, temperature, and heat flow at Reynolds numbers of 500, 2000, and 10,000. Since this study is focusing on Reynolds number below 1,000 these results will be applicable. It was found that the flow field is more affected by openings in the field, as with the gaps and caps method, than blockages. The openings

in the particle bed produce jetting effects which affect fluid flow downstream. When the heat transfer was looked at, it was found that the gaps method doesn't allow for enough conduction between the particles, while the overlap method produces too much conduction. Similarly to the gaps method, the caps method had an under prediction of temperature and heat flow, due to the lack of conduction between the two particles. This left the bridges method as being the most accurate for matching benchmark temperature profiles, given the effective thermal conductivity of the bridge was modeled, allowing for the appropriate amount of conduction between the particles and across the bed. It was found that having the ratio of bridge radius to particle diameter of 0.2 yielded nearly the same heat flow for all Reynolds numbers.

CHAPTER 3 METHODOLOGY

For this research two forms of data collection were performed: experimental data and modeling using Computational Fluid Dynamics (CFD). The CFD modeled the actual physical column used for experimental data as accurately as possible. In both scenarios a column of 2 inch diameter was packed to heights of 4, 6, 8, and 10 inches using 3/8 inch alpha-alumina porous ceramic spheres. Before air entered the column, it was first passed through a 6 inch calming section packed with ½ inch steel spheres. This calming section is made of nylon to reduce heat transfer before the column, and is used to establish the velocity profile of the air before it is exposed to heat transfer in the column. The experimental procedure was modified from previous work done at Worcester Polytechnic Institute (DiNino, Hartzell, Judge, & Morgan, 2013).

EXPERIMENTAL

The column used was a brass column consisting of two concentric tubes, which were welded together using a brass plate on the top and bottom. The inner diameter of 2 inches was open to the top and bottom, and had a height of 18 5/8 inches. The space between the outer tube and inner tube was sealed, allowing either cooling water or steam to pass along the walls of the inner column, in order to provide a constant temperature for heat transfer. This column was attached to the nylon calming section with four screws.

To collect temperature data throughout the column, three thermocouples were placed along the column wall, five in the calming section, and twenty-five on a cross which was inserted into the column. This cross was placed 5 millimeters above the column packing to obtain exit gas temperature profiles from the bed. The cross had one center thermocouple (A) and then four repetitive thermocouples in six different radial positions (B-G), as seen in Figure 1. The thermocouples in the same radial position were spaced 90 degrees apart. After data was collected from the first position, the cross would be rotated by 45 degrees in order to collect data from eight points in the bed for each radial position.

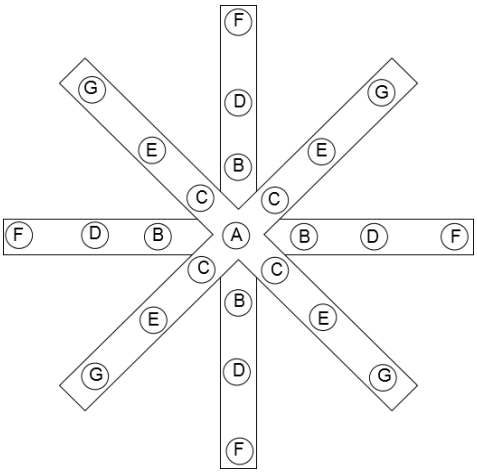

Thermocouple	Radial Position [mm]	Dimensional Position
B	12	0.47244
C	9	0.35433
D	18	0.70866
E	15	0.59055
F	23	0.90551
G	21	0.82677

Figure 3-1*. Diagram of Thermocouple Cross*

To begin a new experimental run at four inches, the packing from the previous experiment was carefully removed from the column by unscrewing the column from the calming section. The column was then slid over a box to catch the packing. The column was reattached to the calming section. If the column was covered in insulation, then the screws were obstructed. In this case, two people must carefully tip the column section over and pour the packing into a box. Care must be taken to avoid putting unnecessary tension on the thermocouple wires attached to the column.

When the packing was ready to be added to the column it was added incrementally, and after every addition it was compressed several times by being tapped with a metal rod to ensure a tight packing arrangement. The height of the packing was checked, and if appropriate, more packing was added. Once the desired height was reached, the thermocouple cross was adjusted so it would be five millimeters above the bed, by measuring the length from the top of the column to the packing and adjusting the cross using the apparatus shown in figure 2. The support bar was L shaped, with the longer portion wrapping around the column. Therefore it was important to measure from the tips of the thermocouples to the bar right next to the rod.

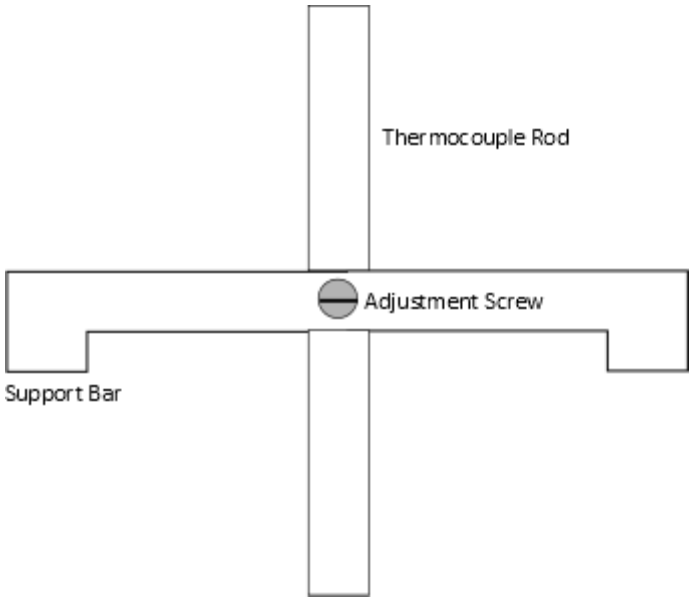

Figure 3-2. Thermocouple Adjustment Apparatus

For cooling experiments, air was passed through a dryer to remove any water vapor and then heated to approximately 95°C before entering the calming section. Once the air entered the column, cooling water was passed through the jacket countercurrent to the air. The process of starting a cooling experiment begins with turning the water in the cooling jacket on, using the water valve. Next the air is turned on by turning the first globe valve, shown as AV1 in Figure 3. Then the purge valve is opened to allow any condensate to flow out, and then closed again. Next AV2 is adjusted to yield the desired air flow rate in the rotameter. Finally, taking extreme caution to ensure a high enough air flow is being used, the heater is turned on; if there is not sufficient airflow through the heater, it will overheat and potentially become a safety hazard. The figure below also shows a cross section of the column; showing the packing in both the calming section and test section, as well as the thermocouple cross lowered into the column. The water enters the top of the column, fills the entire column jacket, shown in the figure as empty space between the insulation and packing, before flowing out the bottom of the column.

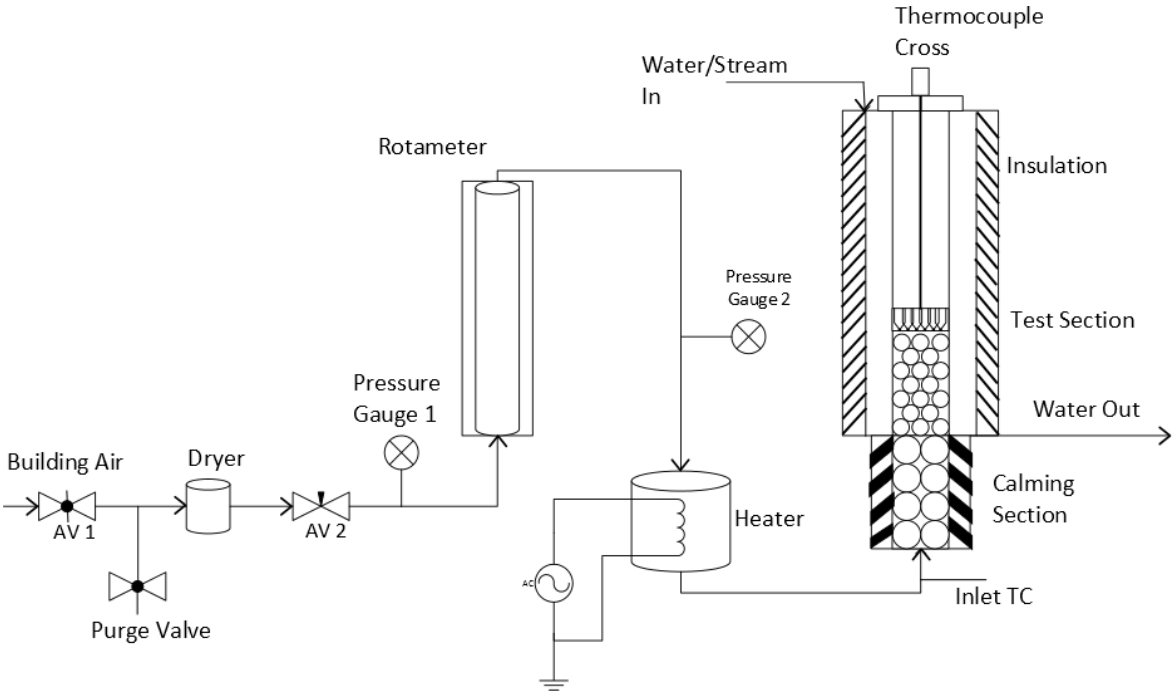

Figure 3-3. Column Flow Diagram

For heating experiments, the air flow is supplied to the column in the same fashion as cooling, although the heater is not turned on. Also steam now enters the column jacket, and exits as mostly condensed steam, however it is still near the boiling point so it enters a condenser to be safely disposed. Since the air step up is very similar to cooling, for simplicity only the process flow for turning the steam on shall be shown, with a simplified column diagram. For the heating experiments, the insulation in Figure 3 is applied to the column for safety reasons. Once the airflow has been turned on to the column, the water valve for the condenser is turned on. Before the steam is turned on, insulated gloves should be put on both hands for safety purposes. Now, the first globe valve, SV1 is turned, supplying steam to the line (Figure 4). The lines will become hot so caution must be taken to avoid contact with the pipes. To purge condensed steam that may be in the line, purge valve 1 should be slowly turned until steam is seen in the drain. Steam passes through the regulator to bring it down to a safe 5 psi. Once SV2 is turned, the second purge valve should be turned until steam is seen in the drain. Finally, steam is supplied to the column jacket and the third purge valve should be turned to clear any remaining condensed steam from the system. The steam from the column is passed through the condenser and then safely disposed of as water.

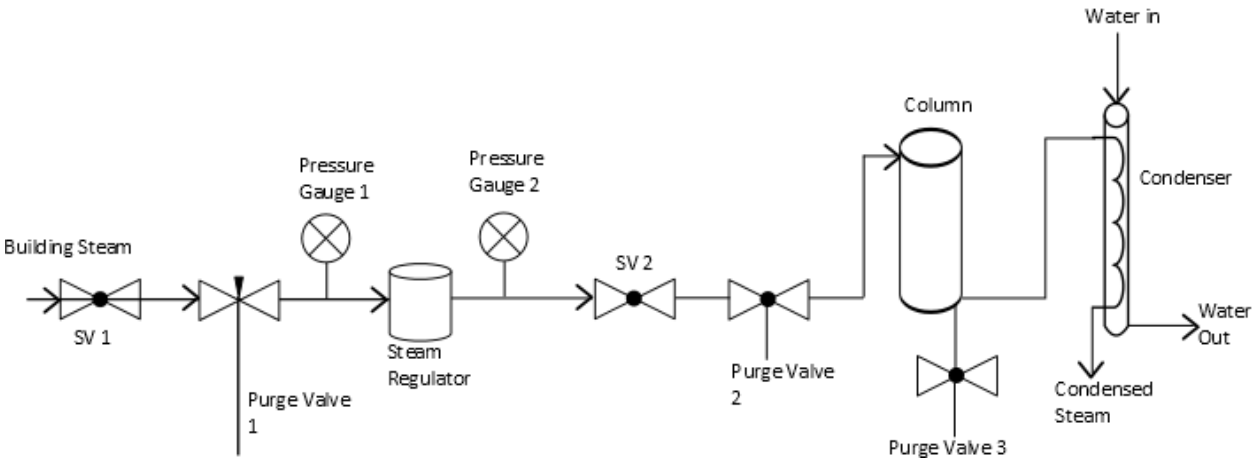

Figure 3-4. Flow Diagram for Steam

Once the initial startup was done, the column was run for two hours to ensure steady state was achieved before data collection occurred. This two hour period was decided on from past research (Ashman, et. al 2009, & DiNino et. al. 2013) as well as from observing when the temperature profiles collected no longer varied with increasing time. Then, the rotameter flow rate and pressure gauges were all recorded. A Keithley Series 2007 Datalogger was used with an ExceLINX add on to measure the radial temperature profile of the bed using the thermocouple cross (Ashman, Rybak, & Skene, 2009). Data collection was stopped and the cross was rotated 45 degrees and a new data collection sheet was made. After operating for ten minutes at this rotated position, the same measurements as before were taken. For heating runs the steam lines were purged using the second and third valves; and for both heating and cooling the air was temporarily turned off and the airline was purged of any water vapor. The airflow was increased to the next flow, and the same procedure was repeated for the remaining air flow rates. For the increased airflows, only one hour was needed to allow the system to achieve steady state. When data collection was completed for that bed height, the air, water/steam and, if applicable, heater were turned off. For cooling experiments air was run through the heater for ten minutes to ensure it did not overheat and melt the elements in the heater. For the next day of data collection, the bed height was increased and the procedure was repeated for the same air flow rates. Using this procedure, the bed height remained constant during a day of data collection, and the air flows were varied (DiNino et al., 2013). Therefore, a complete experiment took four days, one day per bed height.

DATA COLLECTION

The temperature data was acquired using thermocouples placed in the column and collected using a Keithley Series 20007 Datalogger. This system and instructions were set up from previous work in the research lab (Ashman et al., 2009). The Datalogger was capable of collecting data from 200 channels at a time, but this experiment only utilized 34 of them. The data was recorded using a Microsoft Excel add-in called ExceLINX. In order to do this, go to Excel, click on Tools → 'Add In' and select 'ExceLINX.xla'. ExceLINX was then available in the dropdown menu bar in Excel.

ExceLINX

Since ExceLINX uses macros, it was highly suggested to turn the security settings for macros off. This ensured that the program was able to run correctly every time. In order to start collecting data the ExceLINX first had to be configured. To do this, a blank Excel spreadsheet was opened and Select ExceLINX→ 'Create' → 'DMM Config' was clicked.

In order for the Keithley instrument to be configured correctly the following selections were made:

In the drop down menu, 'Device' Ke2700_COM1 was selected and MM7700 was selected for both 'Slot 1 Module' and 'Slot 2 Module'. The drop down for 'Front Panel Lockout' should be 'off'. The remaining dropdowns were left as their defaults.

Below the drop down menus, there is a section titled Channel Scan List. Under the first column 'Channel', the 'List' was set as '101-120, 201-214' to make sure all of the data from the channels in use was being collected. Under the column labeled 'Measurement' under the 'Function' drop down 'TEMP' was selected. Without selecting this option, the wrong data would be collected and that run would be useless. Under the 'Range' dropdown, 'K' was selected and under 'Options' the 'Opt 1' dropdown 'INT' was selected, as illustrated in Figure 5.

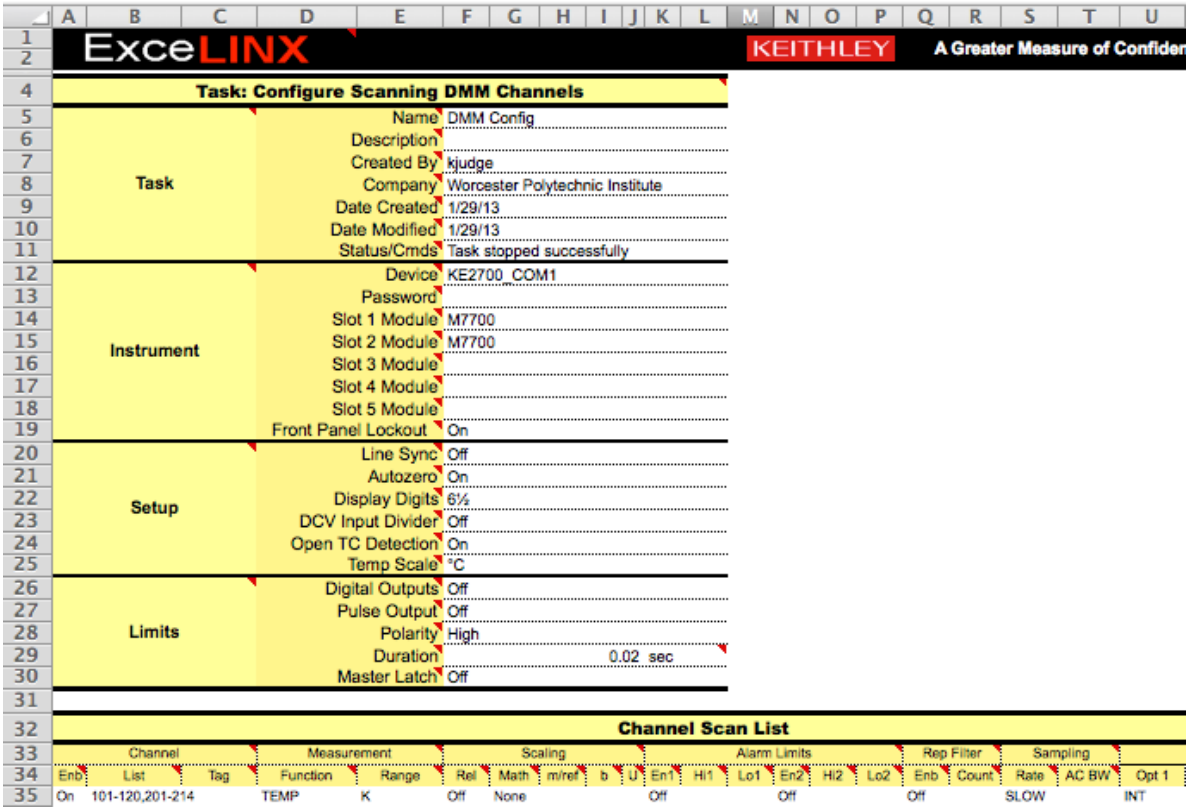

ExceLINX KEITHLEY A Greater Measure of Confider

Task: Configure Scanning DMM Channels

Task	Name	DMM Config
	Description	
	Created By	kjudge
	Company	Worcester Polytechnic Institute
	Date Created	1/29/13
	Date Modified	1/29/13
	Status/Cmds	Task stopped successfully
Instrument	Device	KE2700_COM1
	Password	
	Slot 1 Module	M7700
	Slot 2 Module	M7700
	Slot 3 Module	
	Slot 4 Module	
	Slot 5 Module	
	Front Panel Lockout	On
Setup	Line Sync	Off
	Autozero	On
	Display Digits	6½
	DCV Input Divider	Off
	Open TC Detection	On
	Temp Scale	°C
Limits	Digital Outputs	Off
	Pulse Output	Off
	Polarity	High
	Duration	0.02 sec
	Master Latch	Off

Channel Scan List

Channel			Measurement		Scaling					Alarm Limits						Rep Filter		Sampling		
Enb	List	Tag	Function	Range	Rel	Math	m/ref	b	U	En1	Hi1	Lo1	En2	Hi2	Lo2	Enb	Count	Rate	AC BW	Opt 1
On	101-120,201-214		TEMP	K	Off	None				Off			Off			Off		SLOW		INT

Figure 3-5: DMM Configuration Setup

After the correct selections had been made, the 'start' option was selected from the status/commands menu. The enter key must be hit to register the selection and to start the configuration of the Datalogger.

After the Datalogger was configured, a new tab was selected in the spreadsheet and ExceLINX→ 'Create'→ 'DMM Scan' was selected from the toolbar. Data for different runs was stored in the same spreadsheet by opening different scan tabs for each run. To ensure the data was collected properly, only one scan was run at a time.

To properly set up the data sheet the following options were chosen:

For the 'Reading Count' dropdown 'INF' was selected. This changed the number of data points to infinite to ensure the data was collected until steady state is achieved. Under the dropdowns for 'Add Channel Tags' and 'Add Channels', yes was selected. The update interval should be 100msec and all other options were left at their default, as illustrated in Figure 6.

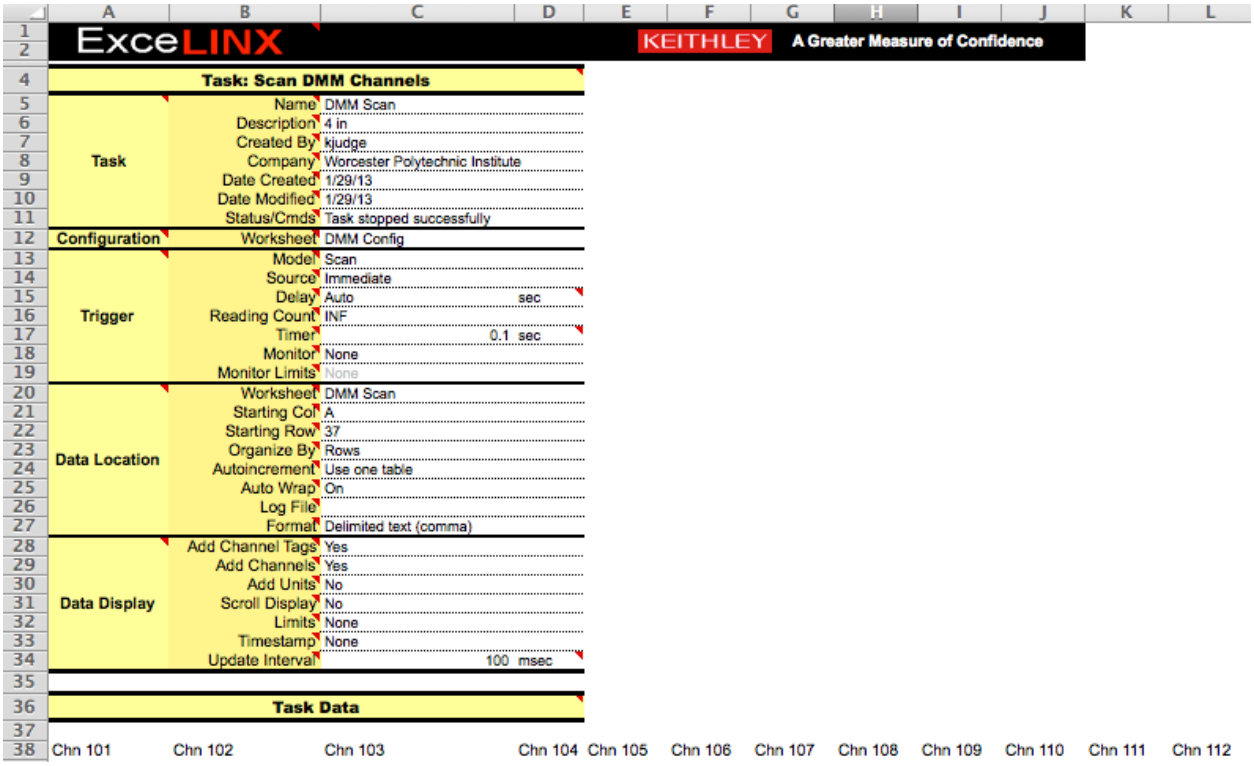

ExceLINX — KEITHLEY — A Greater Measure of Confidence

Task: Scan DMM Channels			
Task	Name	DMM Scan	
	Description	4 in	
	Created By	kjudge	
	Company	Worcester Polytechnic Institute	
	Date Created	1/29/13	
	Date Modified	1/29/13	
	Status/Cmds	Task stopped successfully	
Configuration	Worksheet	DMM Config	
Trigger	Model	Scan	
	Source	Immediate	
	Delay	Auto	sec
	Reading Count	INF	
	Timer	0.1	sec
	Monitor	None	
	Monitor Limits	None	
Data Location	Worksheet	DMM Scan	
	Starting Col	A	
	Starting Row	37	
	Organize By	Rows	
	Autoincrement	Use one table	
	Auto Wrap	On	
	Log File		
	Format	Delimited text (comma)	
Data Display	Add Channel Tags	Yes	
	Add Channels	Yes	
	Add Units	No	
	Scroll Display	No	
	Limits	None	
	Timestamp	None	
	Update Interval	100	msec

Task Data

Chn 101	Chn 102	Chn 103	Chn 104	Chn 105	Chn 106	Chn 107	Chn 108	Chn 109	Chn 110	Chn 111	Chn 112

Figure 3-6: DMM Scan Setup

After the column set up was complete and the thermocouple cross was put in the proper position, 'Start' was selected from the Status/Commands menu. In order to start the data collection, the enter key had to be hit. To stop data collection, the stop command was selected and the enter key was hit at the same time.

Lab Safety

While the column is in operation, proper lab attire should be worn: long pants with closed toe shoes, tying back long hair, and making sure long sleeves are rolled back to above the elbows. The main safety concern for both heating and cooling is the high temperatures. For cooling experiment the heater and column platform should not be touched to avoid burns, and during heating the steam lines should not be touched without insulated gloves.

To prevent damage to the heater during cooling experiments, the flow rate of the air should not drop below 25% of maximum flow using the ½-50-G-9 rotameter, to avoid overheating. For both cooling and heating experiments the air flow should not exceed 55% to avoid the column particles becoming fluidized, which could cause damage to the thermocouple cross.

COMPUTATIONAL FLUID DYNAMICS

In parallel to the experimental data collection, Fluent 14.0 was used to obtain theoretical CFD temperatures. The model was built using the SphGen in-house program (Dixon, 2013a) to match the experimental column as closely as possible. For the computer model, the calming section was six inches high, with an inner diameter of two inches to match the column. The metal screen that separated the calming packing from the column packing was excluded from the model. The model included ten inches of the 3/8 inch ceramic packing, with an additional three inches of empty space above the column to allow for the exiting air flow to become established. Without this empty air space, the chance of divergence increases due to reversed flow for both mass and heat transfer. The origin of the column was the center of the bed, at the beginning of the calming section. The z-direction was set to be the axial direction of the column. Similarly to the exit of the column, an inch of empty space was added before the entrance of the calming section.

The mesh was generated using the software Gambit (Dixon, 2013b), with a total of 43.66 million cells. Due to the large size, the mesh was created in three sections and then sewn together. The three sections were the calming section, the packed section, and the empty space after the packing. For the calming section and bed packing, the mesh size was 0.025" and 0.01875" respectively, determined by the diameter of the particle divided by twenty. In order to reduce the number of cells in the model, the section of empty space after the column had a size function applied, reducing the number of cells by 8 million cells. The size function started at the exit of the column, with a mesh size of 0.01875" to a maximum size of 0.0375" with a growth rate of 1.1. In order to refine the mesh on the walls, particle bridges, and particles, two boundary layers were applied with cell thicknesses of 0.000375 inches.

The CFD was run in multiple ways, in order to troubleshoot any issues that arose, as well as to find explanations to discrepancies observed. However, certain settings and approaches remained constant and will be discussed here. To match the experimental conditions in the column, the average conditions were inputted into Fluent. This included the mass flow into the column and the temperatures of the inlet air, and the column walls. The average temperatures of the inlet air and wall were taken by averaging the data for the four bed heights used to make the dimensionless temperature graphs. In order to find the mass flow, the average Reynolds number for a run was inputted into the following equation.

Equation 3-1. Mass Flow Calculation

$$\dot{m} = \frac{\mu * \pi * r_c^2 * Re}{d_p}$$

The viscosity was based off the average inlet air temperature for that Reynolds number. The mass flow rates used for all the runs can be found in table 1. The temperatures for each run can be found in the appendix.

Table 3-1. Summary of Reynolds Numbers and CFD Mass Flow Rates

Air Flow Rate	Experimental Cooling Re	Experimental Heating Re	CFD Mass Flow [kg/s]	CFD Cooling Re	CFD Heating Re
25%	503	630	0.00269671	503	689
32%	588	702	0.0031524	588	805
35%	658	789	0.003124	658	798
40%	775	901	0.00352773	775	901
45%	876	1018	0.004001	876	1022
50%	982	1139	0.00445958	982	1141
			0.0023487		600

To begin a CFD run, the boundary conditions were first inputted. For the inlet, a mass flow inlet was used with the mass flows above, as well as the inlet temperature of the air. An outflow condition was used for the exit, with a Backflow temperature of 350 Kelvin for heating experiments and 300 Kelvin for cooling experiments. For the calming section, a coupled wall condition was used, with zero heat flux and zero heat generation to reflect the low conductivity of the nylon wall, which ideally would result in perfect insulation. The column walls were set to a temperature boundary setting with the average wall temperature of the experiment. At the column wall, bridges were made between any particle close enough to be viewed as touching the wall. This criteria was set as the particle diameter divided by 50. This bridge was modeled as a separate particle with properties that combined the fluid and particle properties using Dixon et. al's (2012) approach of averaging. These bridges were given the same conditions as the wall which they were contacting, and the interface between the bridge and particle was set an interior boundary condition. An example of a contact between the tube wall and particle can be seen below.

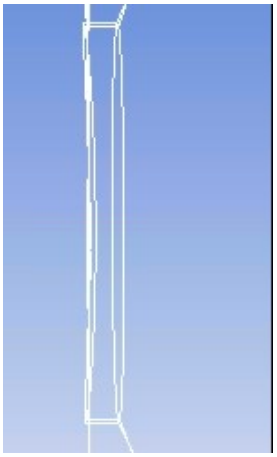

Figure 3-7. Particle and Wall Contact Point

For the particle-particle contact points within the bed, a slightly different approach was taken. A bridge was used to connect any particles within $d_p/50$, and then the bridge and adjacent particles were merged into one particle. To separate the particles, an interface was made in the midpoint of the bridge. In this approach half of the bridge was added onto each particle, with the same properties as that particle; therefore the bridges between particles no longer had an individual identity. The interfaces between these combined particle and bridges was set as interior. Since all of the particles are connected between these bridges, to save computational space these particles were lumped together. For this model the calming section was lumped together, and the packing section was also lumped together.

Below the bed is shown, as well as a zoomed in picture to better show the bridges between the particles. In the figure below, the split between the test section and calming section can also be seen, towards the bottom of the picture.

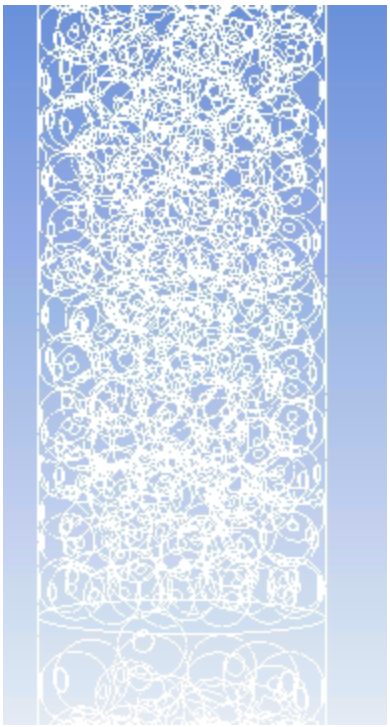

Figure 3-8. Packed Bed Mesh

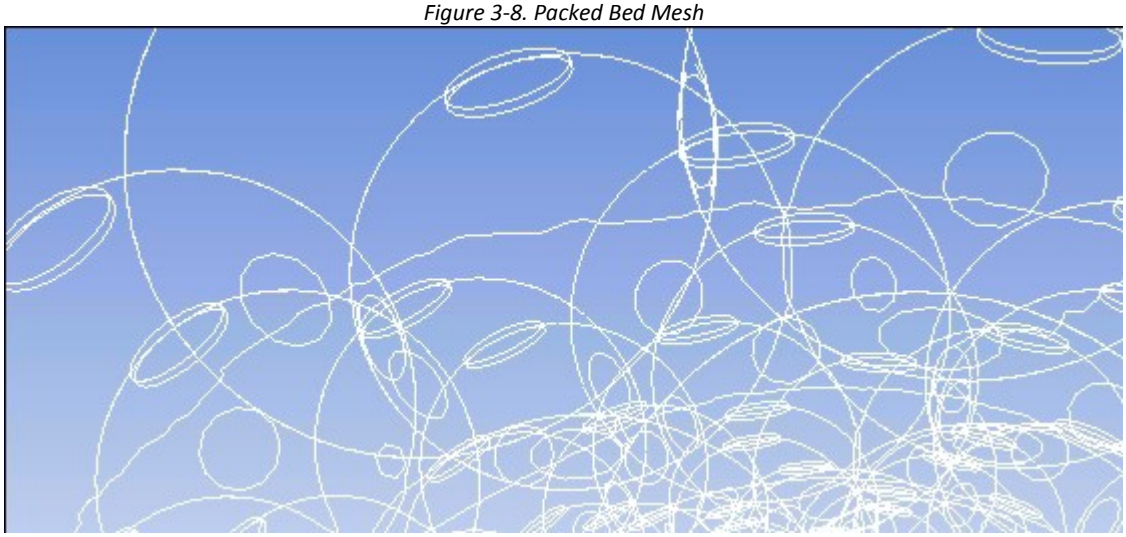

Figure 3-9. Zoomed In Particle Bridges

When the model was properly setup, the energy equation was turned off to establish the flow and aid initial convergence and it was initialized using a standard initialization with the velocity that corresponds to the Reynolds number. In order to turn off the energy equation, the density of air needed to be set to constant, instead of ideal gas. After initialization, the solution methods were set to the following: Scheme SIMPLE, Gradient Green-Gauss Cell Based, Pressure Standard, and Momentum First Order Upwind. The solution controls for the under-relaxation factors were set to Pressure 0.3, Body Forces 0.7 and Momentum 0.7. The calculation was run for 150 iterations to allow the flow to establish. Then, the

energy equation was turned on, and the air density was set to compressible ideal gas. The momentum solution method was changed to second order upwind, and density and energy were also set to second order upwind. The solution controls were set to Pressure 0.3, Density 0.8, Body Forces 0.8, Momentum 0.7, and Energy 0.95. Monitors were set up for the temperature on the bed of the column, as well as the slice of the column at a bed packing height of 4 inches. The calculation was run for 300 iterations, and then the Energy control was increased to 1 in order to quickly propagate the temperature into the bed, and the calculation was run for 5-20 iterations. The control was once again dropped to 0.95 and the calculation was run for an additional 200 iterations. Then the monitors and mass and heat flux difference were used to determine if more iterations were needed.

Once the monitors became constant, and the balances of net fluxes of heat and mass were below 0.75% the calculation was complete. Points were created in the column that corresponded to all of the experimental thermocouple positions in the bed, and the temperatures at these specified points in the column were recorded using an XY-Plot, writing to a text file. The exact positions of these points can be found in the appendix. The temperature and velocity contours down the center plane of the column were also recorded.

SIMULATION 1

For the first round of simulations, the properties of the solid materials were kept constant. For the α-alumina porous ceramic, the values of commonly accepted density and heat capacity were used (Ochiai, Ogura, Ozao, & Tsutsumi, 1997). For the thermal conductivity a large range was found in the literature for the α-alumina depending on the particles porosity and composition. For this reason the effective thermal conductivity was found using the y-intercept value for N=8 data (DiNino et. al, 2013) was multiplied by the thermal conductivity of air at an average of 60°C to yield an average thermal conductivity of the bed. For steel the accepted values for density, thermal conductivity, and heat capacity were used (AK Steel Corporation, 2007). For the air, an ideal gas model was used in Fluent for the density, while the heat capacity and thermal conductivity were taken at an average of 60°C, and viscosity were taken at the inlet air conditions (Microelectronic Heat Transfer Laboratory, 1997). For the bridges that modeled the connections between particles, results found from Dixon, Nijemeisland, & Stitt (2013b) were used to average the properties of the air and the material. A summary of the values used are listed in table 2.

Table 3-2. Summary of Properties Used for Simulation 1

	Ceramic	Air	Steel	Steel-Air	Ceramic-Air
Density [kg/m^3]	1,927	1.0468	8,030	4,015	960
Heat Capacity [J/kg*K]	850	1008.8	500	750	930
Thermal Conductivity [W/M*K]	0.4156	0.028592	18	0.1100	0.0728

For the first simulation, the inlet air temperature matched the value given by the inlet thermocouple.

SIMULATION 2

For the second round of simulations, it was observed that the CFD effective thermal conductivity was consistently lower than experimental. When reviewing how values were obtained, it was observed the method for simulation 1 was the effective thermal conductivity of the entire bed, not just the ceramic particles. Therefore, the value was changed to 1 following previous research done at WPI as well as general literature values for porous ceramic catalyst particles, the new thermal conductivities are summarized below.

Table 3-3. Updated Thermal Conductivities

	Ceramic	Air	Steel	Steel-Air	Ceramic-Air
Thermal Conductivity [W/M*K]	1	0.028592	18	0.1100	0.0858

This also affected the value of the ceramic-air bridge thermal conductivity. For the second simulation the viscosity was set as both constant at the inlet conditions, as well as using a piecewise linear function with the following three data points:

Table 3-4. Values used for Piecewise Linear Viscosity in CFD

Point	**Temperature [K]**	**Viscosity [kg /m*s]**
1	293.15	1.8205e-5
2	333.15	2.0061e-5
3	368.15	2.1595e-5

For the second simulation, possible heat loss and pre-heating was taken into account for the inlet air. Therefore the inlet temperature was corrected using experimentally measured values, which will be

discussed more in the results section. The constant viscosity value was taken at this corrected temperature.

Data Analysis

Once the data was collected it was analyzed in two ways. First, dimensionless graphs were made. This was done to ensure that the profiles made physical sense and followed the expected trends. The second way used a FORTRAN program in Microsoft Developer Studio that fit heat transfer parameters to the data.

Reynolds Number

The Reynolds Number had to be calculated from the data collected from the pressure gauges and rotameter. The maximum flow rate was calculated by using tabulated data for the ½-50-G-9 rotameter, based on the pressure gauge immediately before the heater. Using this maximum flow rate, the heater pressure, and the percent flow recorded by the rotameter, the flow in standard cubic feet per minute (SCFM) was found:

Equation 3-2. Air Flow Calculation

$$SCFM = (Air\ \%)(MAX)\frac{(14.7 + Heater\ Pressure)}{14.7}$$

This value was then converted to the superficial velocity using the cross sectional area of the column.

Equation 3-3. Superficial Velocity Calculation

$$v = \frac{SCFM}{\pi(r_C)^2} * \frac{1\ min}{60\ sec} * \frac{0.3048\ m}{1\ ft}$$

This velocity was multiplied by the particle diameter and air density, and then divided by the viscosity of the air to obtain the Reynolds number. For the calculation, the density of the air at room temperature should be used, since the SCFM was found using a pressure gauge before the heater. This is due to the fact that density multiplied by velocity is constant due to the conservation of mass. Viscosity however, should be used based off the temperature of the air at the inlet of the column.

Equation 3-4. Reynolds Number Calculation

$$Re = \frac{\rho * d_p * v}{\mu}$$

Dimensionless Temperature Plots

After the data was collected the dimensionless temperature was plotted against the dimensionless radial position. The dimensionless temperature was defined as:

Equation 3-5. Dimensionless Temperature

$$\theta = \frac{T - T_w}{T_o - T_w}$$

The dimensionless radial position was defined as:

Equation 3-6. Dimensionless Radial Position

$$y = r/R$$

To make the graphs for experimental data, lines approximately ten rows from the bottom of the ExceLINX data sheet were copied and pasted into a pre-made Excel spreadsheet. It was important that these lines were chosen from the data obtained during steady state, or else the resulting parameters would be incorrect. This spreadsheet was labeled to identify which column correlated to which thermocouple. All of the temperatures for one thermocouple position were then averaged together. This was done for the zero degree and the forty-five degree thermocouple cross rotation. This average was used as the temperature for that radial position. The wall temperature for the dimensionless equation was found by averaging the three wall thermocouples. The plots were created by taking this temperature profile for all four bed heights and plotting them on the same graph.

To make the graphs for the CFD data, points were made that corresponded to the thermocouple positions for each bed height, for both the original and rotated positions. Then a xy-plot was made that recorded the temperatures at each of these points, and these were written to a text file. The text files were made for each bed height and were copied and pasted into a pre-made excel sheet that automatically populated the correct cells. Then, in the same fashion as above, the dimensionless graphs were made.

Data Files for GIPPF Program

In order to analyze the data, it had to be entered in a certain format that the program could read. This was done by entering the information in the following format and saving the test file with a .cdat extension in Notepad:

Table 3-5: GIPPF Format

Number of Profiles	Number of Radial Positions	Number of Wall Readings	Number of Angles			
Column Diameter	Particle Diameter					
Radius 1	Radius 2	Radius 3	Radius 4	R5	R6	R7
Reynolds Number	Bed Depth	Angle of Rotation				
Inlet Temperature						
R1 TC1	-1	-1	-1			
R2 TC 1	R2 TC 2	R2 TC 3	R2 TC 4			
R3 TC 1	R3 TC 2	R3 TC 3	R3 TC 4			
R4 TC 1	R4 TC 2	R4 TC 3	R4 TC 4			
R5 TC 1	R5 TC 2	R5 TC 3	R5 TC 4			
R6 TC 1	R6 TC 2	R6 TC 3	R6 TC 4			
R7 TC 1	R7 TC 2	R7 TC 3	R7 TC 4			
Wall TC 1	Wall TC 2	Wall TC				
-1	-1	-1				

Since there was only one temperature reading for the center of the bed, -1 was inserted for the remaining thermocouple positions. The program recognized -1 as meaning no data when entered in a temperature position. Once all of the profiles were entered in this format, a new line of -1 -1 -1 had to be entered at the end in order for the computer program to recognize the end of the file. The temperatures are given in degrees Celsius to two decimal points and the lengths in millimeters. To run the program the following steps were taken:

1. Open Microsoft Developer Studio
2. Open the workplace “GIPPF_FIT.for” found under the Working folder
3. Click on Build → Click on Rebuild All
4. Click on Build → Execute GIPPF_FIT.exe
5. The following screen appears (See Figure 10)
6. Input the file name including the extension and hit enter
7. Enter the range of Reynolds number to be analyzed. One Reynolds number can be analyzed at a time and the model requires a symmetric input with the actual value between the two extremes (Example Min=410, Max=414, actual Re=412)
8. Enter the bed depths to be analyzed. To analyze all input 0.0 for minimum and 1000.0 for the maximum.

9. Enter a guess for Peclet number (Pe_r) and the Biot number (Bi). Starting guesses of 5.0 generally give results. Name output will an extension of .res
10. Run analysis
11. After the analysis is complete the file can be opened and fitted temperature profiles may be viewed.

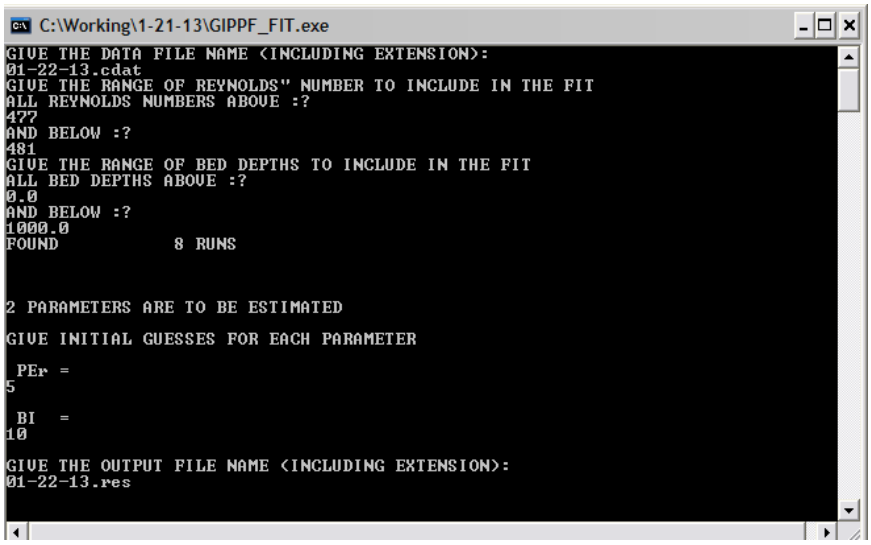

Figure 3-10: Screen Before Building the GIPPF Model

After the run was completed, the results were opened in Notepad. The program used the first bed depth as the inlet, so results for three heights are given. For these three heights, the dimensionless radial position and the correlating dimensionless temperature were given. For the heat transfer parameters the Peclet number and Biot number were estimated, and then the model derived the effective thermal conductivity and wall Nusselt number. With these four parameters, a 95% confidence interval was given along with an F-test critical value. The 95% confidence interval showed what values 95 of 100 experimental runs would give. The F-test is a measure of the explained variance to the unexplained variance. From this information, graphs were made comparing the heat transfer parameters with the Reynolds number to determine the patterns. For this research, the focus will be on the effective thermal conductivity and wall Nusselt number. These patterns were compared for between heating and cooling, and also comparing how the CFD compared to the experimental data.

CHAPTER 4 RESULTS AND DISCUSSION

Once all the data was collected, heating and cooling were compared between experimental and computer results. The first step for both the CFD and experimental results was to ensure the dimensional temperature profiles for every run made physical sense. In order to make physical sense, the profile should decrease as the bed height increases. A decrease in dimensional temperature ($\Theta = \frac{T-T_w}{T_{in}-T_w}$) shows the temperature in the bed is approaching the wall temperature. The dimensional temperature should also decrease as the position approaches the wall. An example profile is shown below for an experimental cooling (N=5.33) with a Reynolds number of 789.

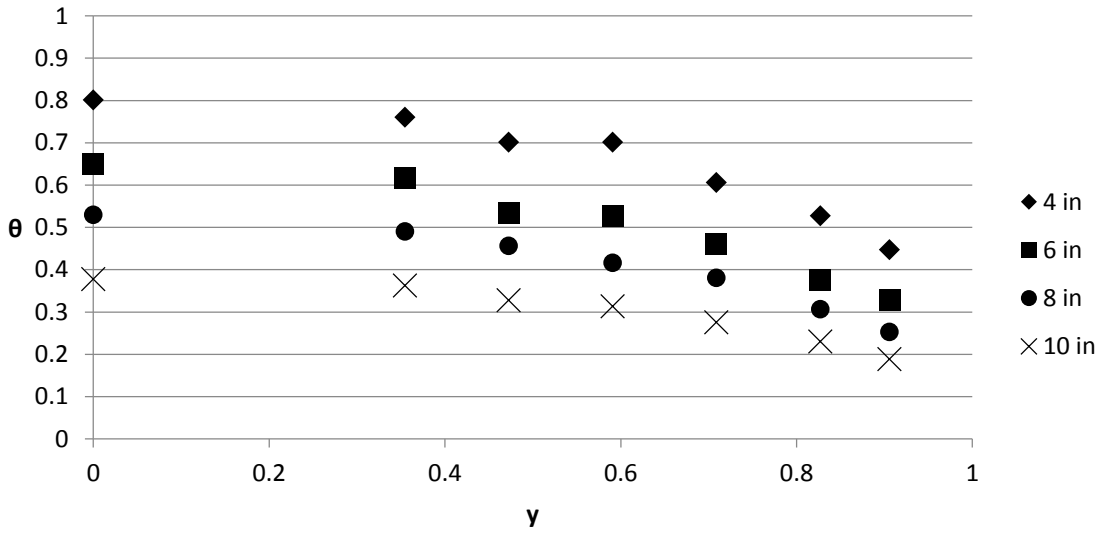

Figure 4-1. *Dimensionless Temperature Profile for Experimental Cooling at Re=789 (N=5.33)*

After it was confirmed that all the dimensionless profiles made physical sense, the heat transfer trends were analyzed to see if there were any discrepancies between experimental heating and cooling. Next, cooling and heating were compared between experimental and CFD results. By analyzing the differences between experimental and CFD, possible shortcomings in the CFD were theorized and then new simulations were run to test these theories. Once the CFD simulations were validated against experimental data, heating and cooling were compared between the CFD simulations.

EXPERIMENTAL HEATING VERSUS COOLING

The experimental results for the 2013 research (N=8) and the current research (N=5.33) were analyzed for trends and for any sources of experimental error that may have been overlooked.

Calculation of Reynolds Number Based on Inlet Air Viscosity

While reviewing results from previous research conducted in 2013, it was found the Reynolds number calculation did not include a temperature dependence for the viscosity.

Equation 4-1. Reynolds Number

$$Re = \frac{\rho v d_p}{\mu}$$

The density should not have a temperature dependence since density multiplied by velocity is constant, due to the conservation of mass. Velocity is found using a pressure gauge at room temperature, therefore density should also be at room temperature. For viscosity however, it would make physical sense to use the value based on the inlet temperature of the column. Therefore, the research from 2013 (N=8) was revisited to examine the effect on Reynolds number, and the heat transfer parameters, if the inlet temperature viscosity was used. Since the previous research used viscosity at room temperature, the heating data was relatively unaffected, and the small percent change of 1.9% was a result of changing from English to SI units. The Reynolds number comparison for heating can be found in the appendix. For cooling however, a difference of 14.1% was observed, as seen in the table below.

Table 4-1. Comparison of Cooling Experiment (N=8) Reynolds Number Using Temperature Dependence of Viscosity

2013 Reynolds Number	Reynolds Number Using Inlet Viscosity	Delta
376	323	-53
420	361	-59
474	407	-67
539	463	-76
602	517	-85
667	573	-94
758	651	-107
838	720	-118
867	745	-122
956	821	-135
1037	891	-146

In order to study the effect of changing the Reynolds number based on the viscosity of the inlet air, the data from the N=8 experimental runs was re-fitted to heat transfer parameters both for the original Reynolds number as well as the new Reynolds number. This change also had a small effect on the model

used to fit the experimental data to find the heat transfer parameters. The model directly fits the data to the Peclet number and Biot, and then derives the effective thermal conductivity and wall Nusselt number. The effective thermal conductivity is found using the following equation:

Equation 4-2. Effective Thermal Conductivity

$$\frac{k_r}{k_f} = \frac{RePr}{Pe_r}$$

Since the Reynolds number is now being found using the viscosity at the inlet conditions, the Prandtl number should also be taken at the inlet conditions. For cooling runs this was taken at 20^0C to be 0.71 and for heating it was taken at 95^0C to be 0.72. The wall Nusselt number depends on the effective thermal conductivity, so both of the derived values are influenced by the change.

When the experimental results were re-fitted for heating, there was no effect as expected. Since the Prandtl number in the original model was set at room temperature, the results should only vary by 1.4% due to changing from English to SI units. This is shown for the effective thermal conductivity in the figure below. In the figure below, inlet temperature denotes the data which is corrected for SI units.

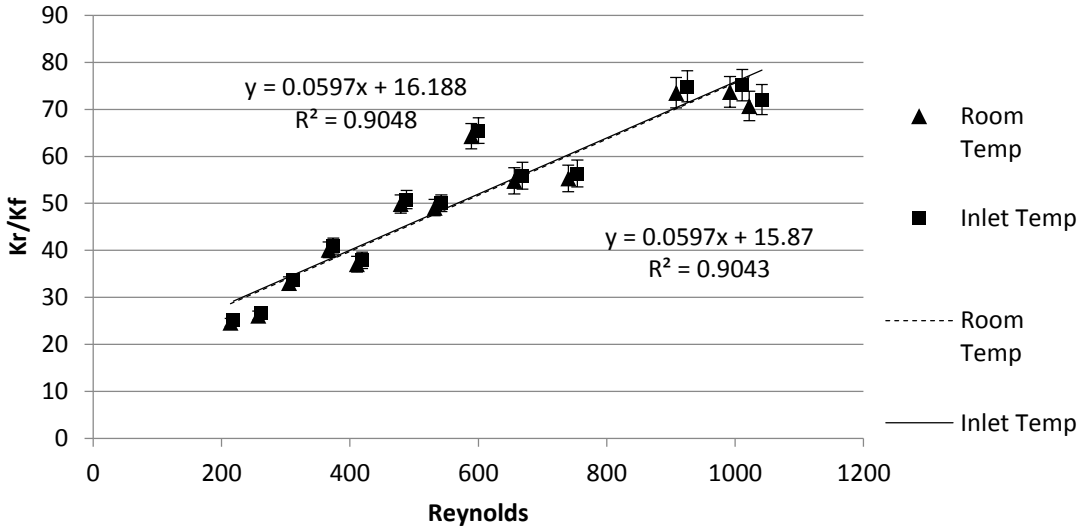

Figure 4-2. Effective Thermal Conductivity Compared to Reynolds Number Based on Viscosity at Room and Inlet Temperature for Heating Experiments (N=8)

As with the effective thermal conductivity, the wall Nusselt number remained relatively unchanged. The slight shift in Reynolds number is more apparent, as shown in the figure below, but the values for the wall Nusselt number do not change outside of this expected 1.4% shift.

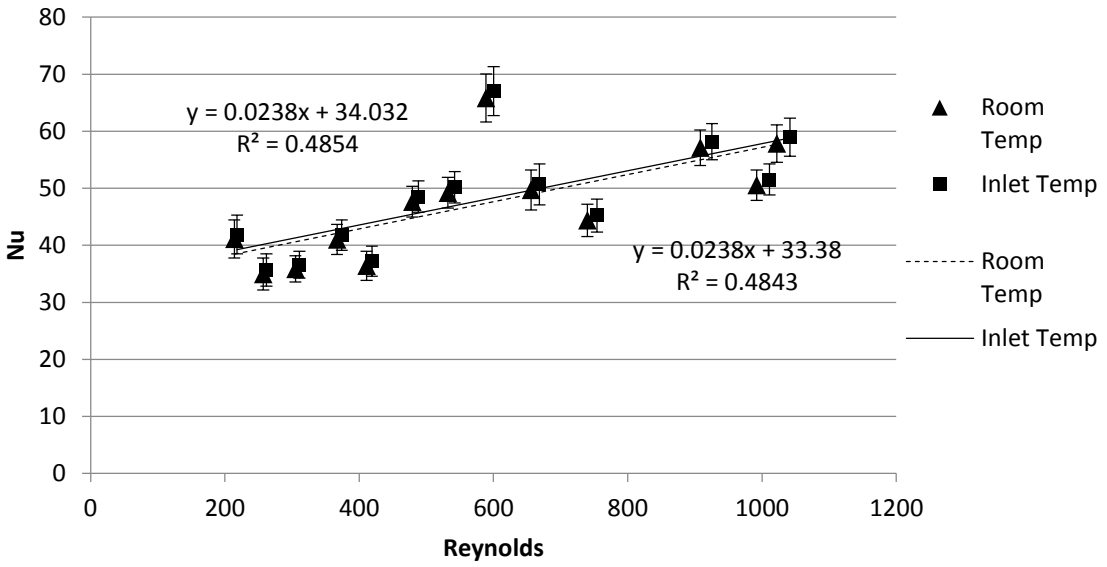

Figure 4-3. Wall Nusselt Number Compared to Reynolds Number Based on Viscosity at Room and Inlet Temperature for Heating Experiments (N=8)

Once the re-fitted heating parameters gave the expected results, the cooling results were examined. For the re-fitting of the Reynolds number based on the room temperature viscosity, the higher Prandtl number of 0.72 was used. For the effective thermal conductivity, changing the Reynolds number based on the inlet temperature caused a shift downwards, by 18%. This large of a shift is expected, since the Reynolds number changed by 14% and a different value was used for the Prandtl number.

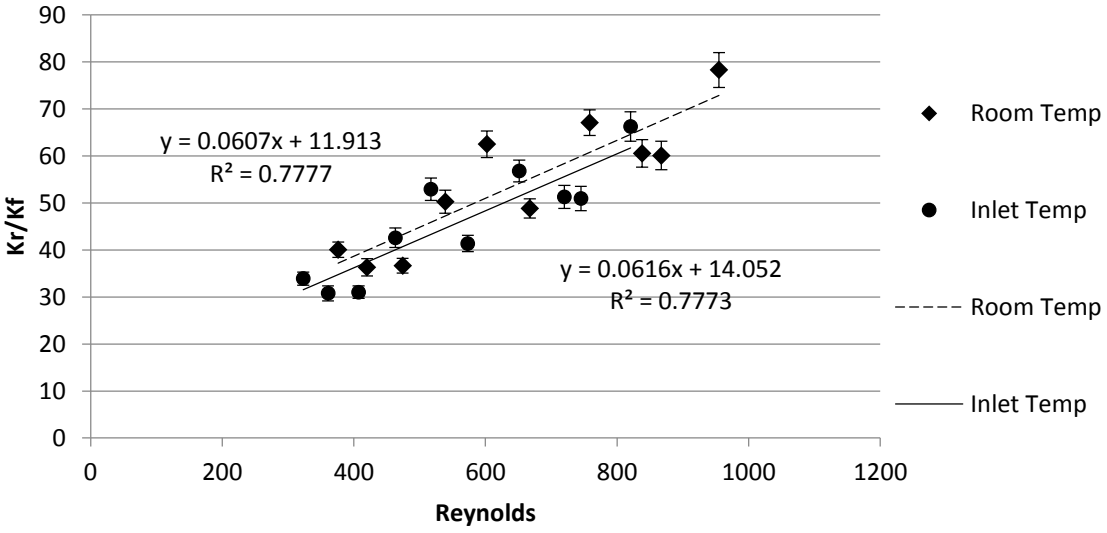

Figure 4-4. Effective Thermal Conductivity Compared to Reynolds Number Based on Viscosity at Room and Inlet Temperature for Cooling Experiments (N=8)

The wall Nusselt number also saw a downward shift of 18% when the Reynolds number was corrected for the inlet air properties.

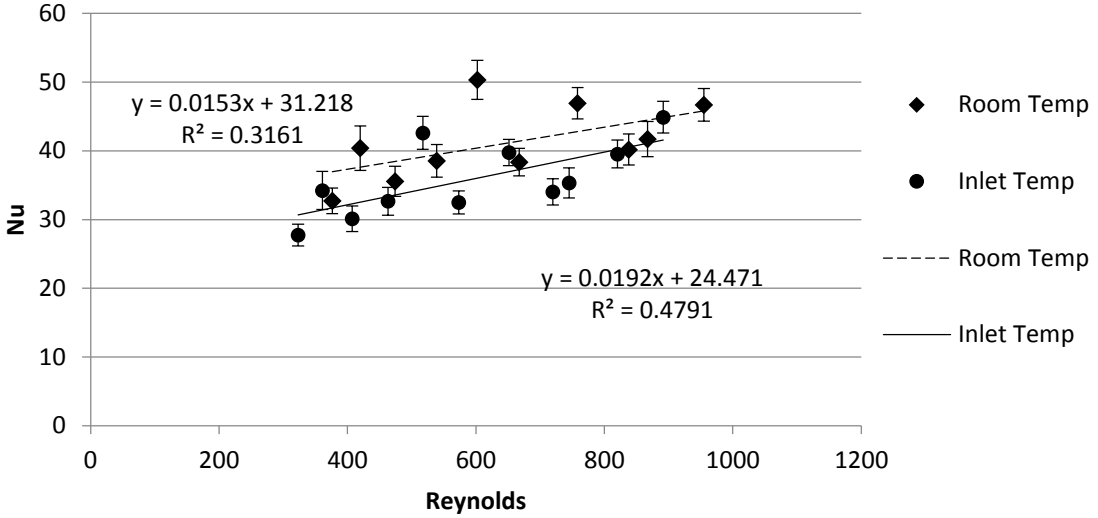

Figure 4-5. Wall Nusselt Compared to Reynolds Number Based on Viscosity at Room and Inlet Temperature for Cooling Experiments (N=8)

After seeing how calculating the Reynolds number based upon the inlet air to the column affects cooling, the data can be compared between heating and cooling. For comparative purposes the graphs using Reynolds number based on the room temperature air are given below. For the effective thermal conductivity, the difference between heating and cooling is within experimental error.

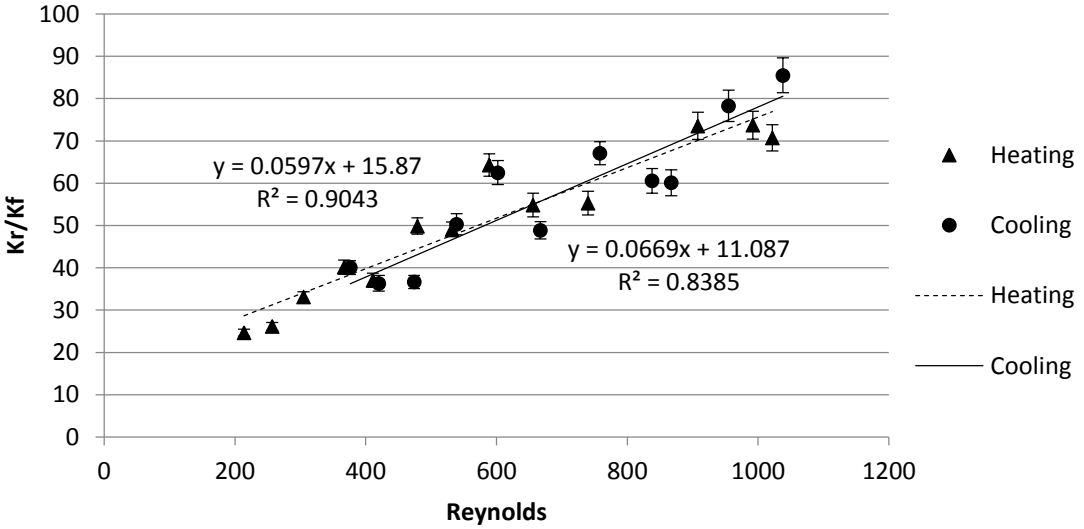

Figure 4-6. Effective Thermal Conductivity Compared to Reynolds Number Based on Viscosity at Room Temperature for Heating and Cooling Experiments (N=8)

For the wall Nusselt number, heating trends higher the cooling with most data points being well outside of the range of the 95% confidence range.

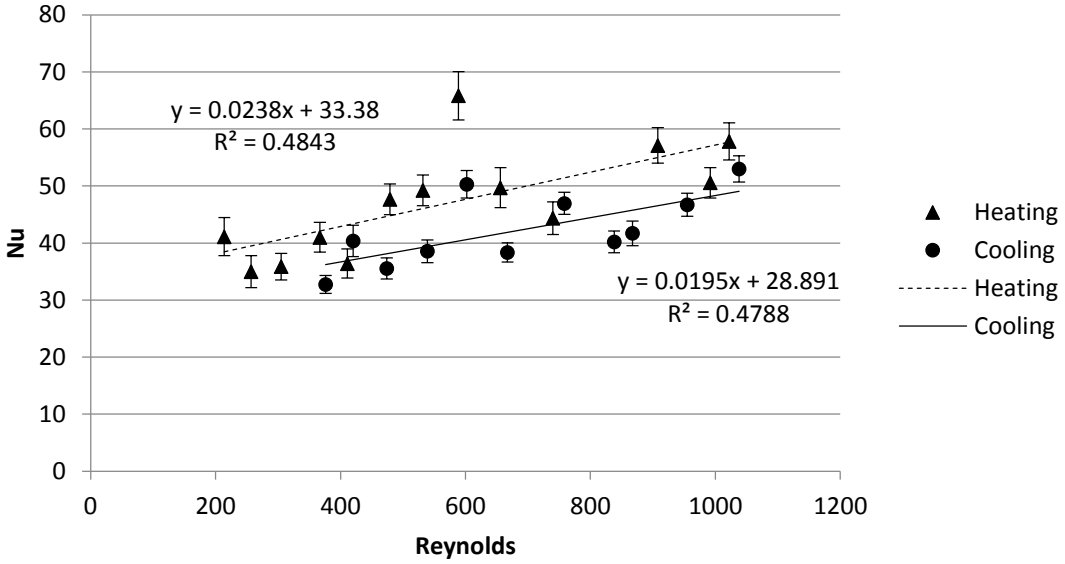

Figure 4-7. Wall Nusselt Number Compared to Reynolds Number Based on Viscosity at Room Temperature for Heating and Cooling Experiments (N=8)

After the Reynolds number was adjusted for the inlet viscosity, heating and cooling were still comparable within experimental error. This is due to the fact the cooling data shifted downwards following the same trend as the original data.

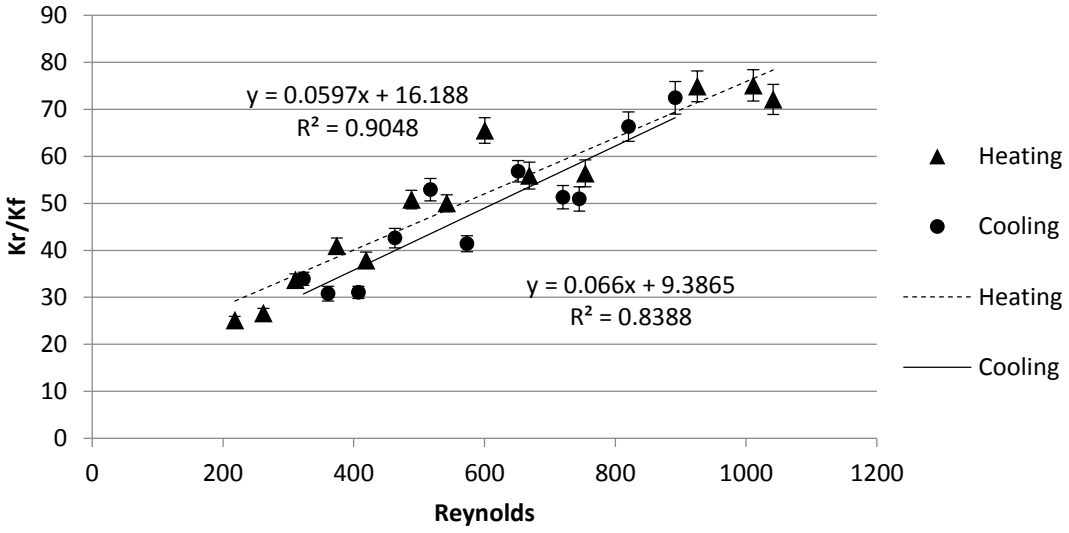

Figure 4-8. Effective Thermal Conductivity Compared to Reynolds Number Based on Viscosity at Inlet Temperature for Heating and Cooling Experiments (N=8)

For the wall Nusselt number, the difference between heating and cooling is still apparent, however cooling is now always lower than heating for a given Reynolds number.

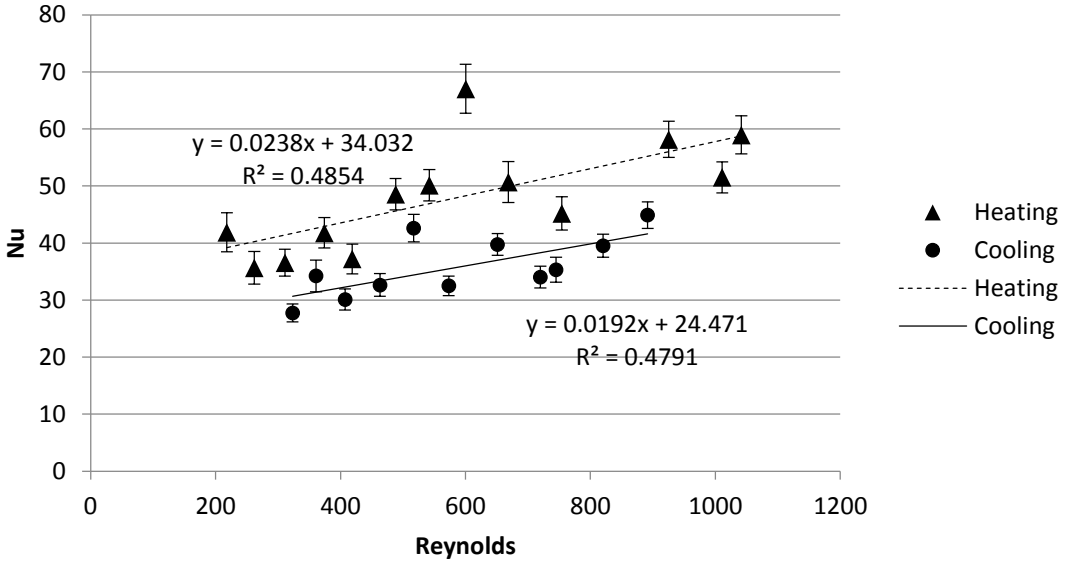

Figure 4-9. Wall Nusselt Number Compared to Reynolds Number Based on Viscosity at Inlet Temperature for Heating and Cooling Experiments (N=8)

Based on the physical reasoning, as well as the resulting graphs still following expected trends, it was decided calculating the Reynolds number based on the inlet air was a better representation of what was physically occurring. Therefore, for this research (N=5.33) the Reynolds number was calculated using the viscosity based on the inlet temperature.

Experimental Results (N=5.33)

When the heating and cooling results were compared for experimentally collected data (N=5.33), it was found there was essentially no difference in the effective thermal conductivity, as show in Figure 10 below. While the trend for the heating data is slightly higher, the heating and cooling points are within 95% confidence of each other. This is shown by the error bars, and represents where the data points would be 95 times if the data was collected 100 times. Since these confidence regions overlap, it is concluded heating and cooling are comparable within experimental error. Physically, this means heating and cooling are both capable of the same level of heat transfer across the bed.

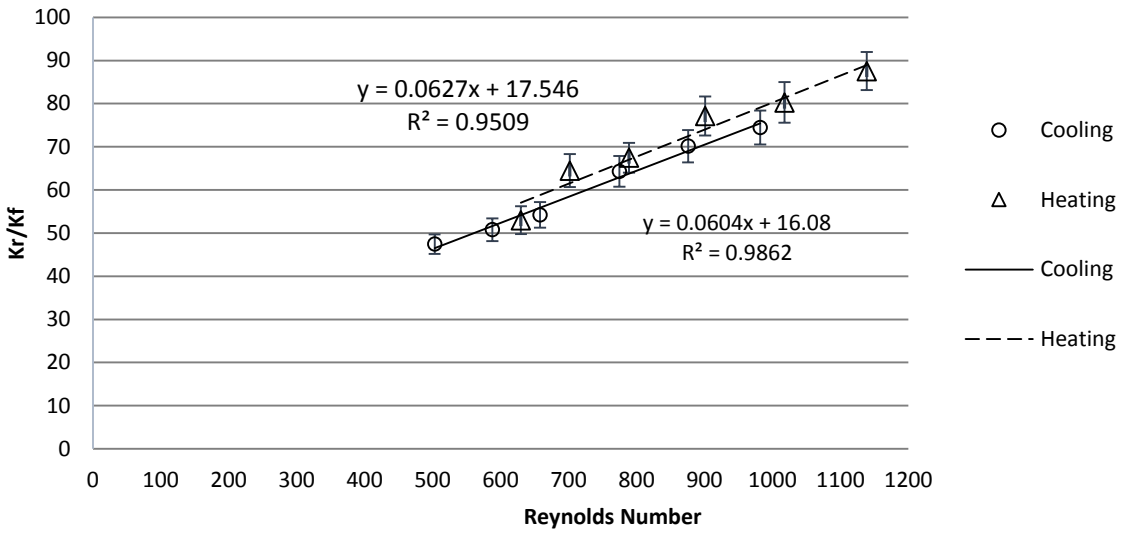

Figure 4-10. Effective Thermal Conductivity for Experimental Heating and Cooling Data (N=5.33)

However, when the wall Nusselt number showed a difference between heating and cooling as shown below in Figure 11. The values for heating are about 30% higher than those for cooling, which is well beyond the confidence range of the data points.

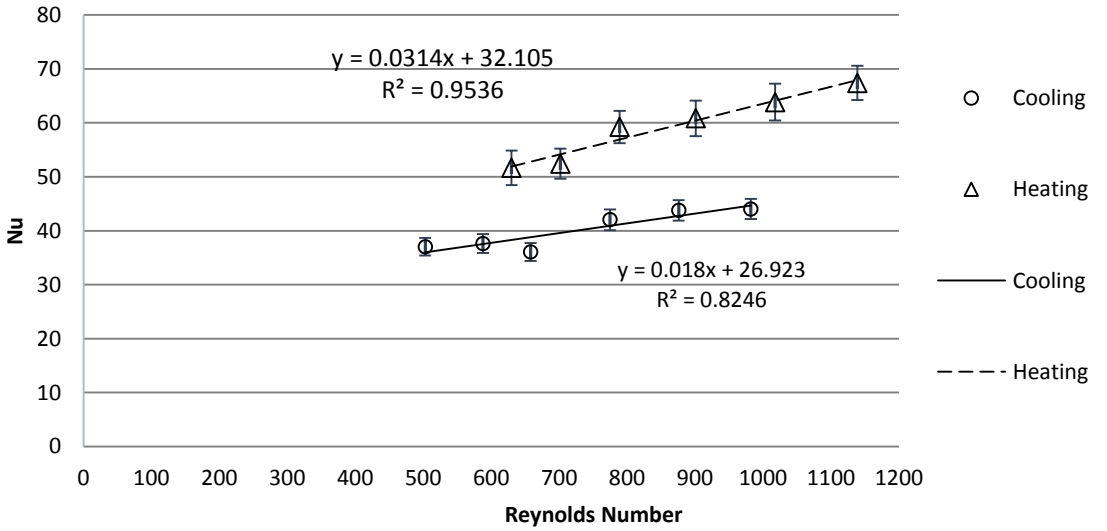

Figure 4-11. Wall Nusselt Number for Experimental Heating and Cooling Data (N=5.33)

In order to explain this discrepancy, the definition of the wall Nusselt number is looked at:

Equation 4-3. Wall Nusselt Number

$$Nu_w = \frac{h_w d_p}{k_f}$$

The only variable is the heat transfer parameter at the wall, h_w, since the particle diameter and thermal conductivity of the fluid is relatively constant. Therefore, a consistently higher Nusselt number shows there is a higher value of heat transfer between the bed and tube wall. A possible explanation for this could the consistency of the tube wall temperature. For the heating runs, the condensing steam provides a fairly uniform wall temperature. In past research, a difference as large as 4 degrees Celsius was observed from the top and bottom of the column during cooling runs (DiNino, et al., 2013). When the wall temperatures for this research were looked at, it was found the temperature on the column wall varied by up to 5.7 degrees Celsius, with an average of 3.2 degrees. All of the temperature differences can be viewed in the appendix. Although this is not a huge difference, it could lower the driving force for heat transfer, which would result in a lower Nusselt number.

To confirm that the effective thermal conductivity should be similar for both heating and cooling, the dimensionless temperature profiles were compared for heating and cooling experiments. Since the heat transfer parameters are derived from these profiles, similar profiles should result in similar parameters. For the initial bed heights, heating is slightly higher than cooling near the center of the bed. This shows that cooling is closer to the wall temperature, so more heat has been transferred in the cooling run. However, as the bed position approaches the wall, heating becomes lower than cooling. This could result in a perceived higher conduction throughout the bed for heating, resulting in the slightly higher values of effective thermal conductivity for heating. For the remaining bed heights heating and cooling are comparable.

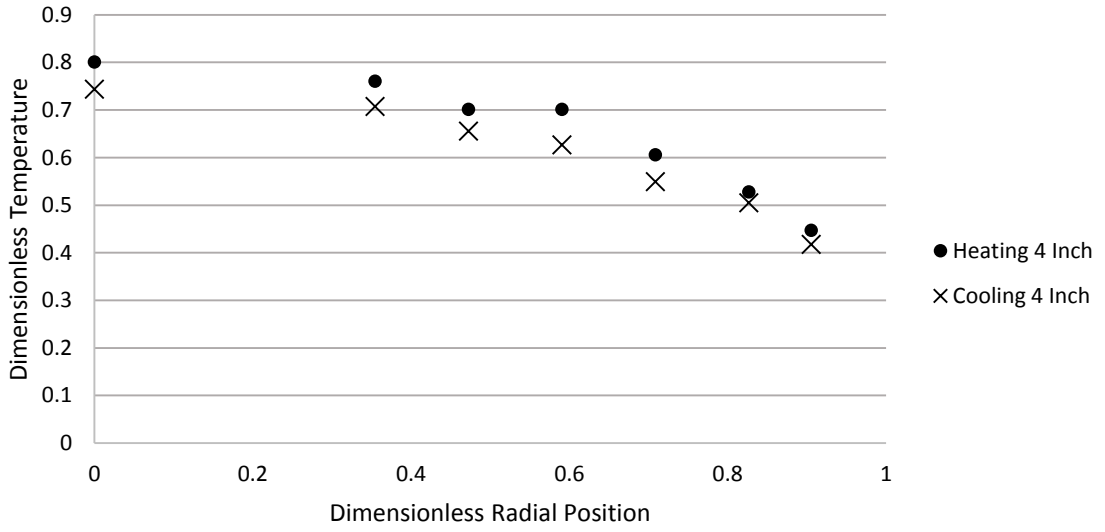

Figure 4-12. Dimensionless Temperature Profile for Experimental Heating (Re=789) and Cooling (Re=658) at an Air Flow of 35% and Bed Height of Four Inches (N=5.33)

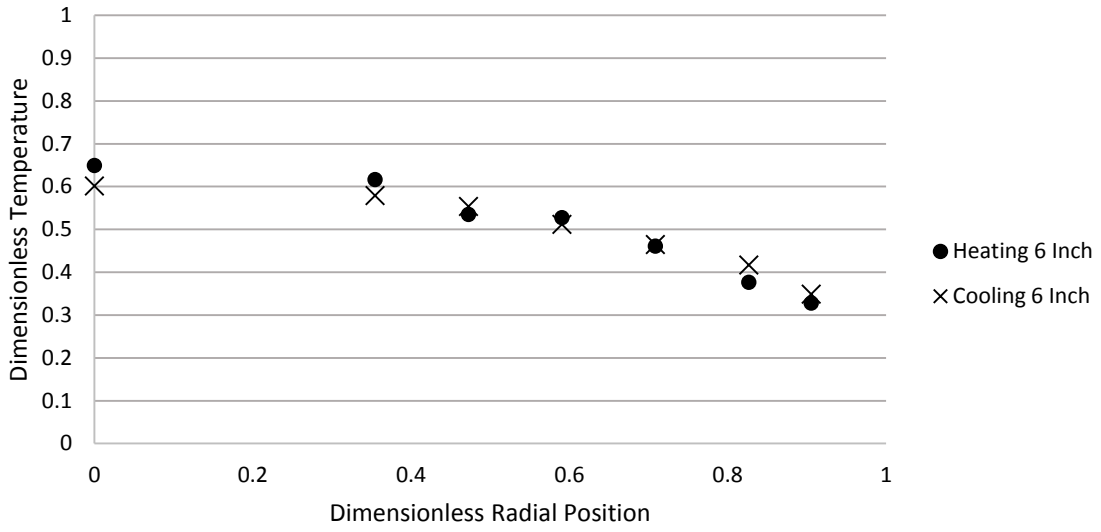

Figure 4-13. Dimensionless Temperature Profile for Experimental Heating (Re=789) and Cooling (Re=658) at an Air Flow of 35% and Bed Height of Six Inches (N=5.33)

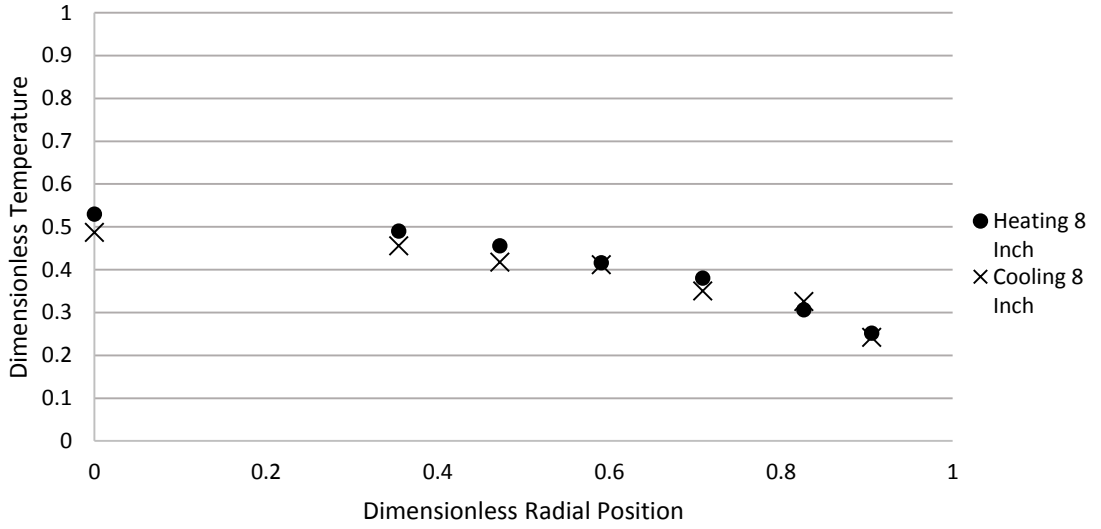

Figure 4-14. Dimensionless Temperature Profile for Experimental Heating (Re=789) and Cooling (Re=658) at an Air Flow of 35% and Bed Height of Eight Inches (N=5.33)

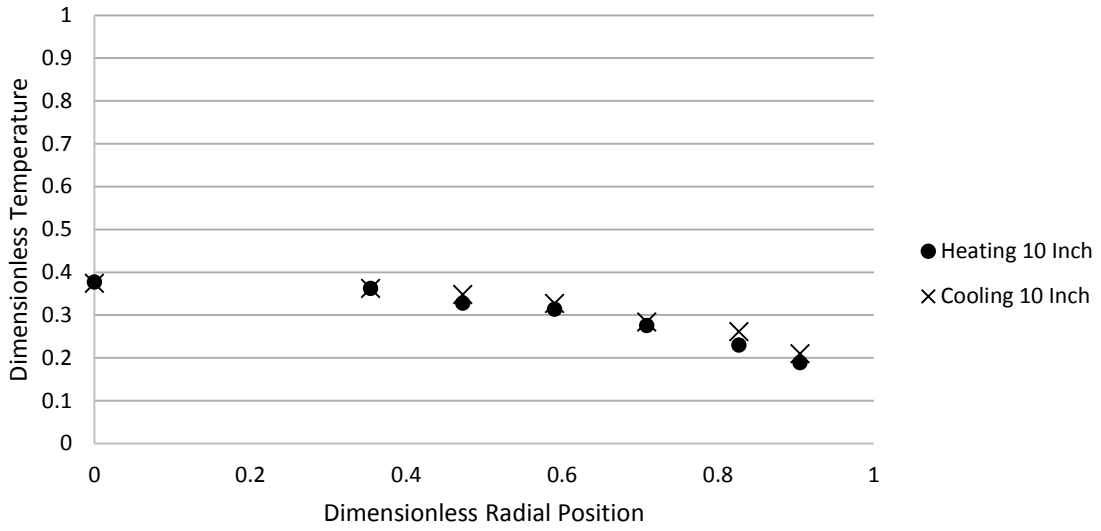

Figure 4-15. Dimensionless Temperature Profile for Experimental Heating (Re=789) and Cooling (Re=658) at an Air Flow of 35% and Bed Height of Ten Inches (N=5.33)

A similar trend is observed for the other air flows, and these graphs can be found in the appendix. For the wall Nusselt number, the graphs must be analyzed a bit more. The GIPPF model finds the value of the wall Nusselt number using the following formula:

Equation 4-4. Wall Nusselt Number Relation

$$Nu_w = \frac{h_w d_p}{k_f} = \frac{h_w R}{k_r}\frac{d_p}{R}\frac{k_r}{k_f} = Bi\frac{d_p}{R}\frac{k_r}{k_f}$$

The model uses the convection boundary condition at the wall to find the Biot number, and then uses the previously found value for the effective thermal conductivity as well as the given particle diameter and column radius to find the value of the wall Nusselt number.

Equation 4-5. Boundary Condition at Tube Wall

$$-k_r\frac{d\Theta}{dy} = h_w R(\Theta\,|_{r=R} - \Theta_w) \quad or \quad \frac{d\Theta}{dy} = Bi(\Theta\,|_{r=R} - \Theta_w)$$

In order to examine why the wall Nusselt number is always higher for heating, the dimensionless profiles provided by the model were studied. A third order polynomial fit was used to find the interpolated value of theta at the wall, and also to find the flux. To find the flux, the derivative of the polynomial fit was evaluated at the tube wall. Using equation 5, a value of the Biot Number (h_wR/k_r) was found for the all runs, at the bed heights of six, eight, and ten inches. It was found that for all of these conditions, the

value for heating was higher, as can been seen in the table below. The details of the interpolated dimensionless temperatures and fluxes can be found in the appendix.

Table 4-2. Comparison of Biot Number for Heating and Cooling Experimental (N=5.33)

Air Flow	Heating 6 Inches	Cooling 6 Inches	Heating 8 Inches	Cooling 8 Inches	Heating 10 Inches	Cooling 10 Inches
28%	5.079	2.104	2.744	2.322	2.716	2.153
32%	2.238	1.968	2.222	1.992	2.169	2.018
35%	2.404	1.726	2.470	1.856	2.372	1.800
40%	2.148	1.775	2.146	1.846	2.154	1.809
45%	2.166	1.700	2.194	1.734	2.164	1.736
50%	2.066	1.621	2.090	1.623	2.055	1.648

A possible reason for this trend could be the more uniform wall temperatures observed for the heating runs. This results in a higher driving force at the wall, which causes a higher flux and a lower dimensionless wall temperature. Therefore, the Biot number is larger for heating, which in turn yields in a higher wall Nusselt number. The best way to test this theory would using CFD in which both heating and cooling have a uniform wall temperature.

EXPERIMENTAL VERSUS CFD (N=5.33)

Once the experimental data was collected, the run conditions for the CFD were found. These conditions included the mass flow rate, inlet air temperature, and wall temperature. The mass flow rate was calculated using the cooling experimental runs, so the experimental and CFD Reynolds numbers are identical. However, for heating the same mass flow rate was used which sometimes caused a discrepancy between the experimental and CFD Reynolds numbers. For the cooling runs with air flows of 32% and 35%, the mass flow rates were very similar, but due to differences in inlet temperatures the Reynolds numbers are different. However, for heating this led to almost identical Reynolds numbers at 800. In order to have a stronger correlation between the heating CFD, an additional run was done using the temperatures from the 28% flow rate run at a mass flow that yielded a Reynolds number of 600. Before the heating and cooling results could be compared to anything, the temperature contours and velocity vectors at the column center plane were looked at to ensure they made physical sense. Examples of these expected profiles are shown below. For cooling this is hot air coming in with the temperatures first decreasing at the wall. The as the axial position increases the temperature at the center of the bed should slowly decrease, as in Figure 16.

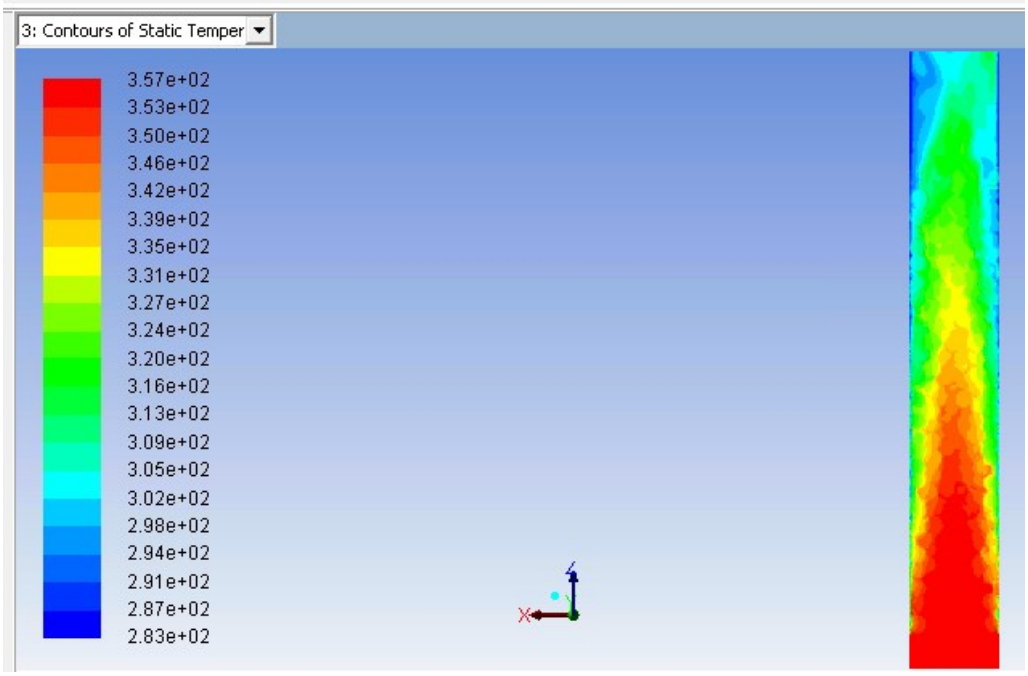

Figure 4-16. Temperature Contours at Center Plane of Bed for Cooling Simulation 2 Constant Viscosity (Re=775)

For heating simulations, the cooler air enters the column, and the temperature should increase first and the wall, and the center of the bed should become warmer as the axial position increases, as shown in the figure below.

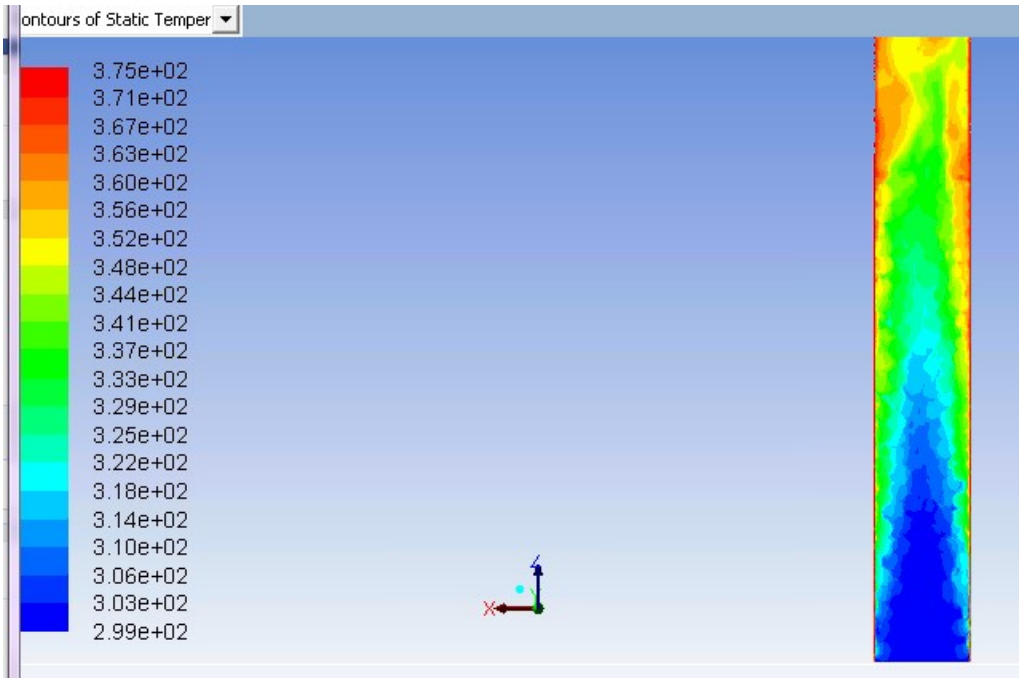

Figure 4-17. Temperature Contours at Center Plane of Bed for Heating Simulation 2 Constant Viscosity (Re=901)

Cooling Results Simulation 1

For the first simulation run, the inlet temperature and average wall temperature obtained from the experimental data were used in the CFD boundary conditions. The mass flow rates for the CFD runs were found using the Reynolds number from the experimental run. After the CFD runs were completed, the heat transfer trends were compared between CFD and experiments. For the effective thermal conductivity, the experimental values trended higher than the CFD by 14-25%. This suggests that the CFD is not modeling as much heat transfer across the bed as is actually occurring in the experiment.

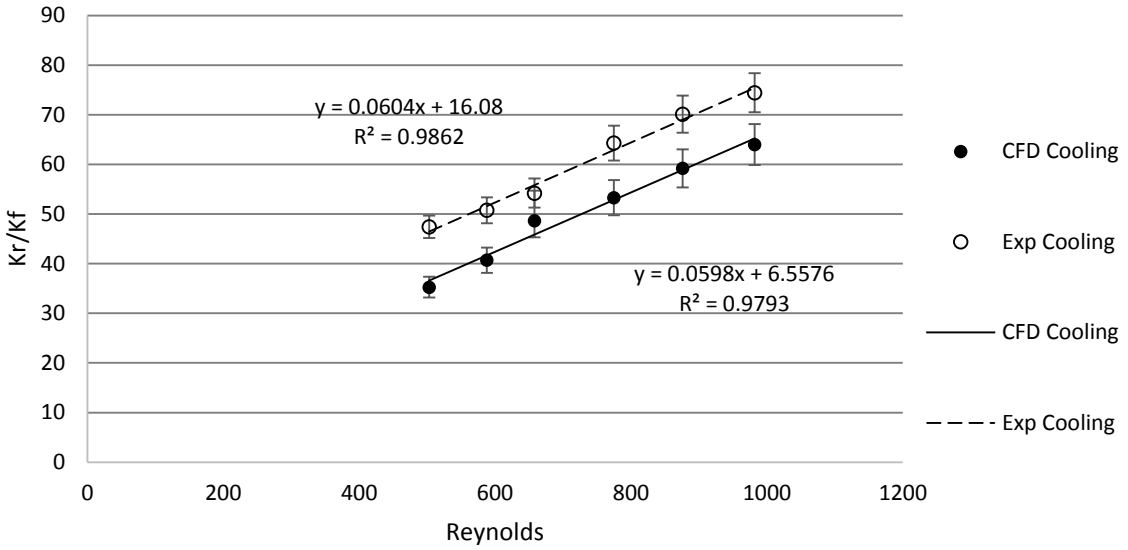

Figure 4-18. Effective Thermal Conductivity Comparison for CFD and Experimental Cooling (N=5.33)

A possible explanation for this difference could be the assumption of a perfectly insulated calming section used for the CFD. The inlet temperature is taken before the calming section, allowing for possible heat loss to occur before the air enters the test section. In the CFD this would result in a hotter bed, which may result in a lower thermal conductivity. The lower effective thermal conductivity would be a result of the higher inlet temperatures making it seem that less heat is being removed from the bed.

Before a conclusion can definitely be made about the root cause of the discrepancy, the wall Nusselt number also needs to be examined. When looking at the wall Nusselt number, the opposite trend was observed, with the CFD data being 20-25% higher than the experimental data. These findings support the idea brought up in the Experimental Heating vs. Cooling section that a more uniform wall temperature results in a higher wall Nusselt number.

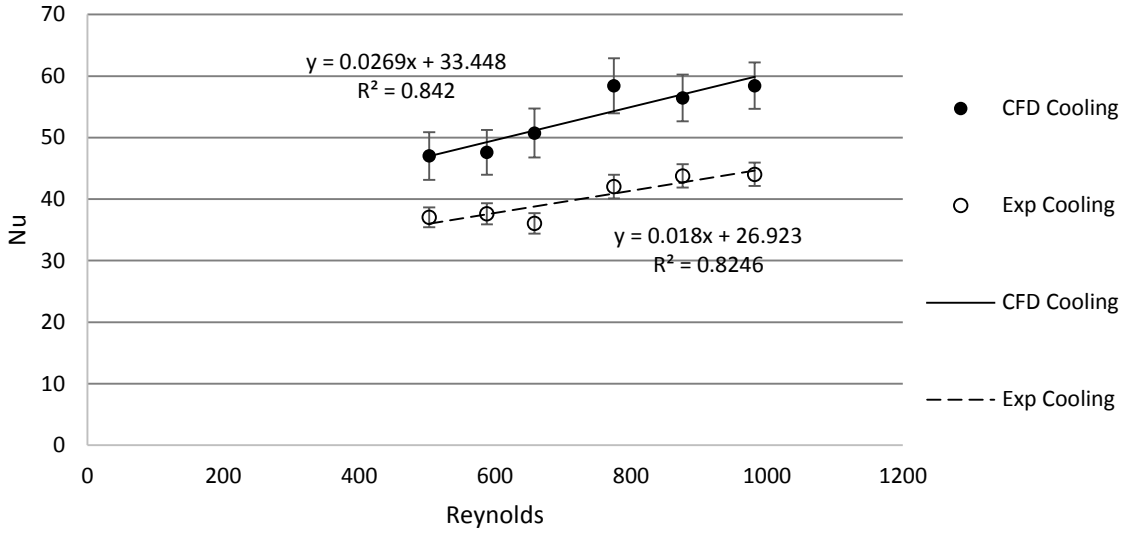

Figure 4-19. Wall Nusselt Number Comparison for CFD and Experimental Cooling (N=5.33)

In order to test these theories, the dimensionless temperature profiles of all the runs were examined. The results are most apparent at four inches, so that is all that will be shown here, but all of the graphs for all Reynolds numbers and bed heights can be found in the appendix. The example below shows that the CFD temperatures are consistently higher, with the difference being largest at the center of the bed. This would support the idea that heat is lost in the calming section in experiments, but not in the CFD simulations, leading to higher CFD dimensionless temperatures. For the wall Nusselt number, the flux at the wall is clearly higher, due to the steeper dimensionless profiles. Although the value at the wall is higher, the difference between the slopes is larger. Therefore the profiles support the higher wall Nusselt number for the CFD, possibly due to the more uniform wall temperatures in the CFD.

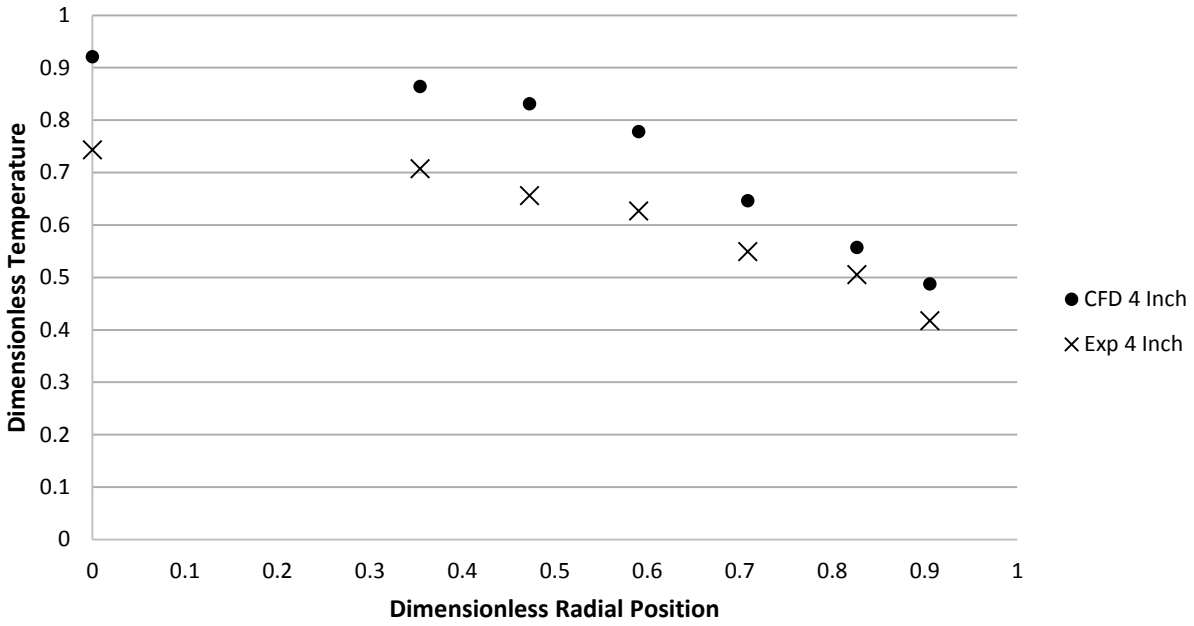

Figure 4-20. Dimensionless Profile Comparing CFD to Experimental Cooling at Re=658 (Air Flow of 35%) at a Bed Height of Four Inches (N=5.33)

In order to get a better idea of the difference in bed temperatures, the temperature profiles of CFD and experimental were compared.

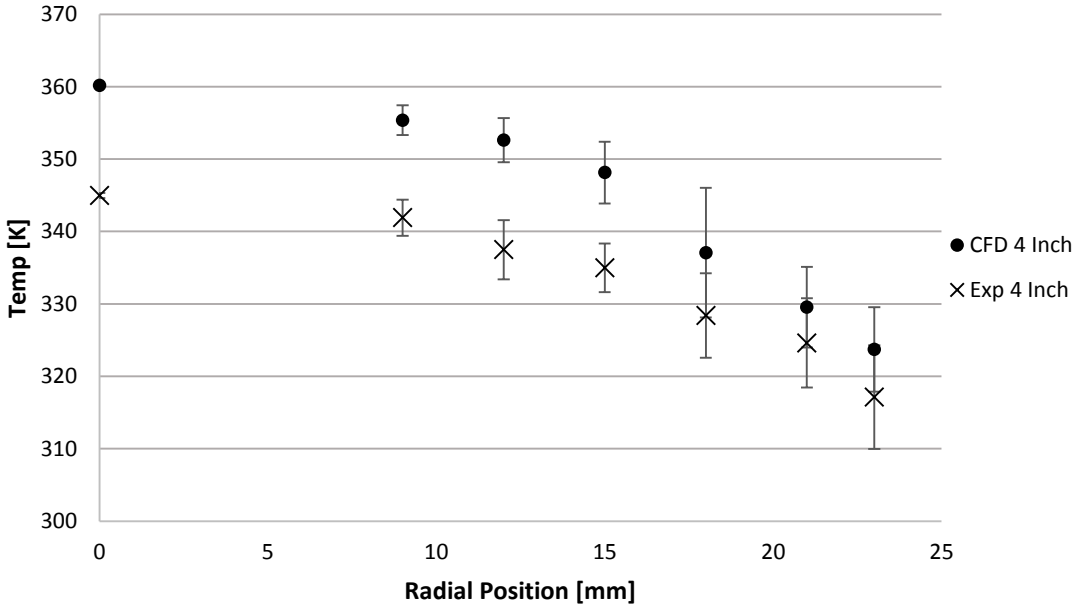

Figure 4-21. Temperature Profile Comparing CFD to Experimental Cooling at Re=658 (Air Flow of 35%) at a Bed Height of Four Inches (N=5.33)

The difference in the center of the bed is about 15K, and 5K as the bed position approaches the wall. After it was confirmed that the CFD modeled a hotter bed than was observed for experimental data, it was decided that the heat loss that occurs in the calming section should be found.

Heat Loss in the Calming Section

To find the heat loss in the calming section, all of the packing was removed from the column. The thermocouple cross was lowered so it rested five millimeters above the entrance of the test section. The airflow was run as if an experiment was being conducted, and the heater was turned on. The system was allowed to come to steady state, and the same six experimental air flows were used to collect temperature data. The difference between the inlet and each thermocouple position was recorded for each air flow, and the average difference was found. It was noted that for the radial positions closest to the wall, at 25 mm, the difference seemed to be much higher, probably due to wall effects. So a second average was taken, excluding these four replicated thermocouples.

Table 4-3. Heat Loss in the Calming Section for Each Air Flow

Air Flow	Average [K]	Excluding 25 mm Average [K]
28%	11.66	10.753
32%	11.18	10.337
35%	10.45	9.629
40%	9.72	8.906
45%	9.02	8.229
50%	8.20	7.390

From this data, it was found that the calming section loss averages about 10K. With this knowledge the next round of CFD simulations were run correcting the inlet temperature to better match what is observed experimentally.

Heating Results Simulation 1

As with the cooling runs, for the first simulation the inlet temperature and wall averages matched the experimentally collected data. The mass flow rate was made to identically match the cooling runs. The heating comparison follows the similar trend to cooling; the effective thermal conductivity for the CFD data is about 15-20% lower than the experimental data.

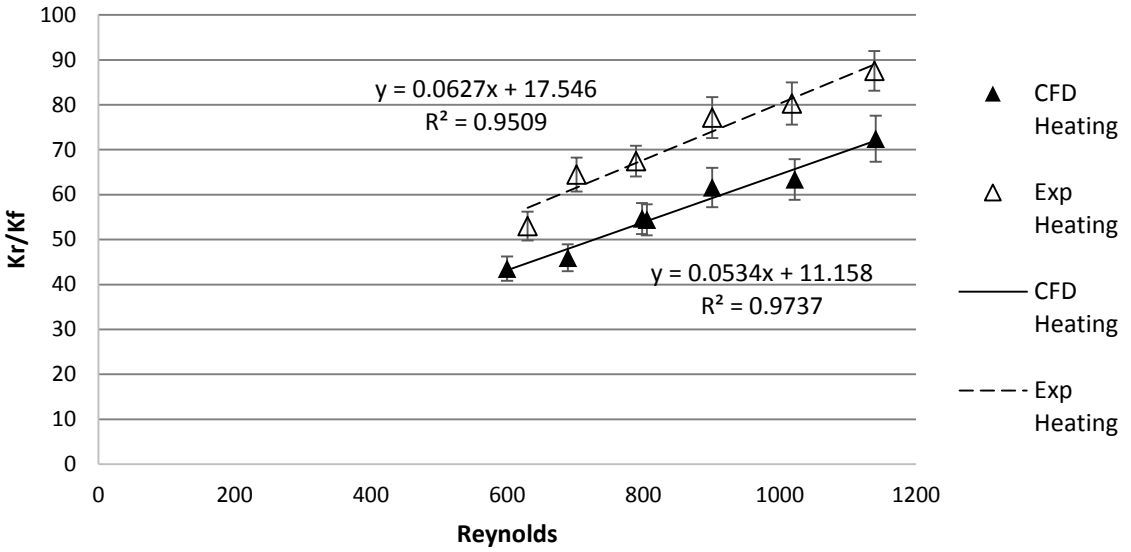

Figure 4-22. Effective Thermal Conductivity Comparison for CFD and Experimental Heating (N=5.33)

For the wall Nusselt number, the data points for experimental and CFD were within 95% confidence of each other, with the CFD trending slightly higher. This supports the theory that the difference between the wall Nusselt numbers for cooling are a result of the temperature gradient observed in the wall. For heating experiments, the phase change of the steam provides a much more consistent wall temperature, and the CFD modeled the column wall with a uniform temperature.

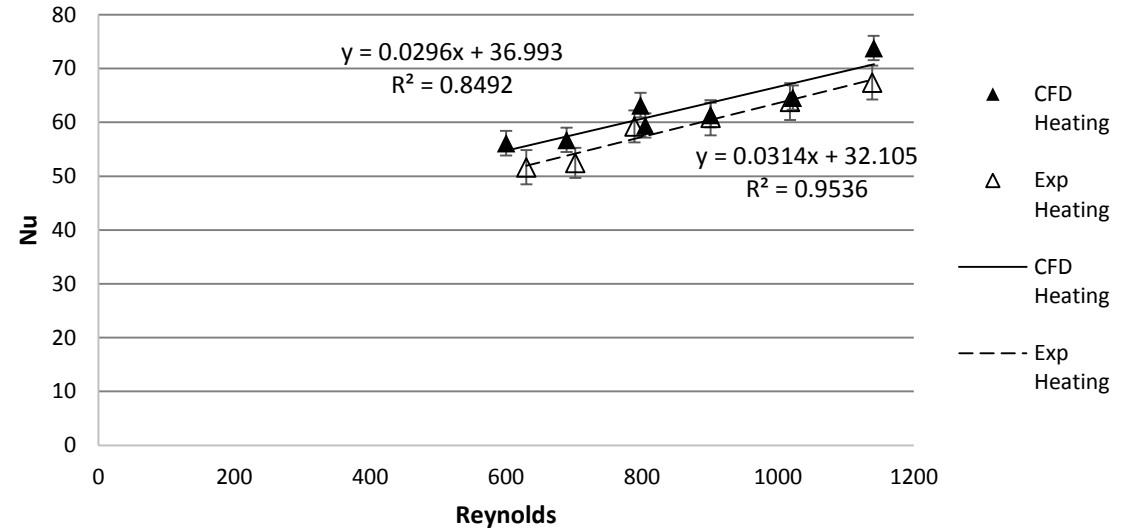

Figure 4-23. Wall Nusselt Number Comparison for CFD and Experimental Heating (N=5.33)

To look into what may be causing the lower effective thermal conductivity, it is useful to look at the dimensionless temperature profiles, as well as the actual temperature readings. As with cooling the air

flow of 35% at the four inch bed height will be discussed, and the remaining graphs can be found in the appendix.

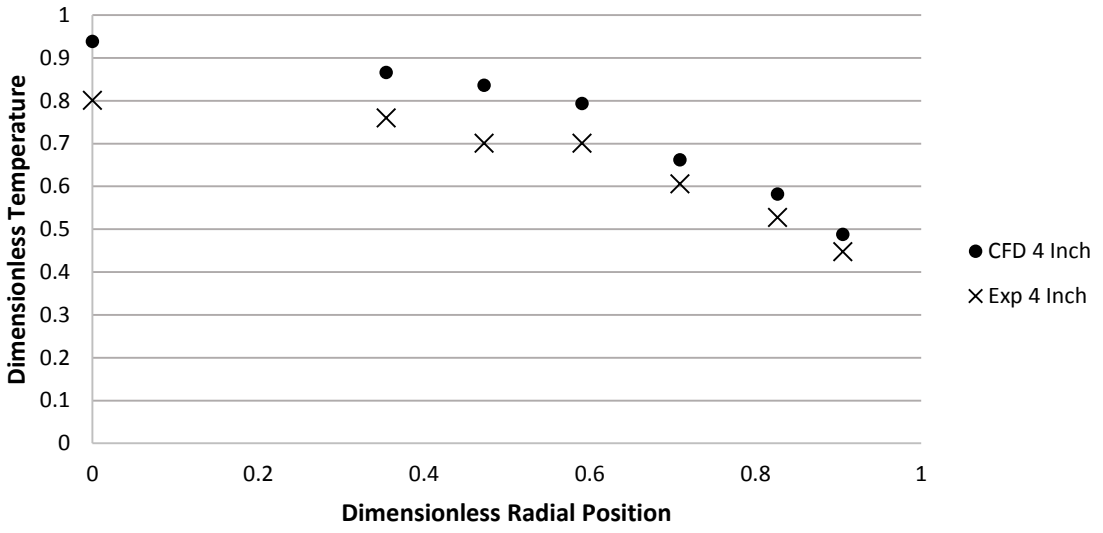

Figure 4-24. Dimensionless Profile Comparing CFD (Re= 798) to Experimental (Re=789) Heating at a Bed Height of Four Inches (N=5.33)

The values for the CFD data are observed to be higher than experimental at the center of the bed, and come to closer agreement as the bed position approaches the tube wall. This mirrors the trend observed for cooling, with the CFD dimensionless temperatures being higher, and therefore further away from the wall temperatures. This suggests that for heating there is some pre-heating of the air that occurs within the calming section. Pre-heating of the air would bring the experimental values closer to the wall temperatures. To understand the temperature difference better, the actual temperature profiles were looked at to see how large of a temperature difference there was between the CFD and experimental results.

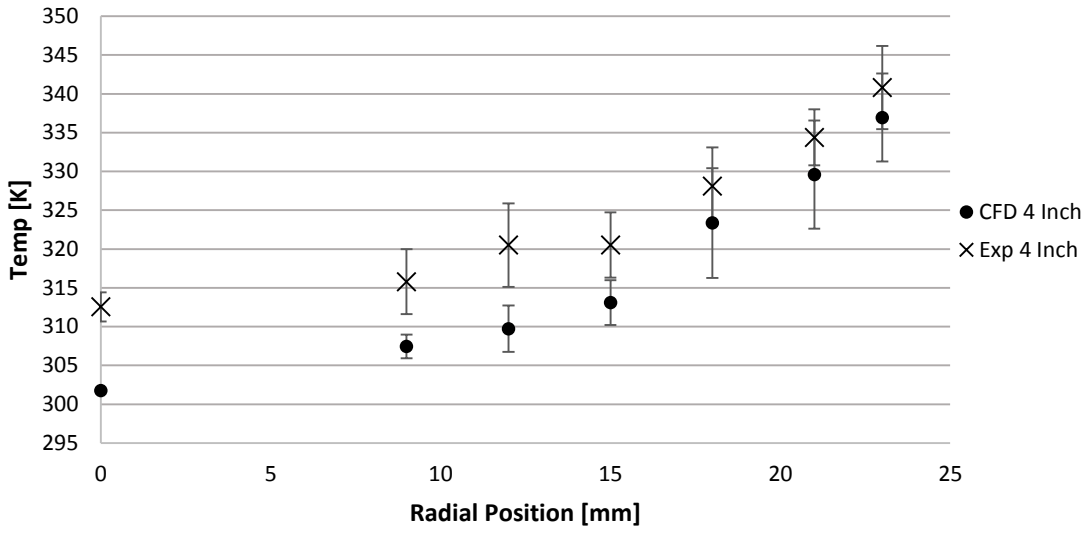

Figure 4-25. Temperature Profile Comparing CFD (Re= 798) to Experimental (Re=789) Heating at a Bed Height of Four Inches (N=5.33)

The difference at the bed center between the CFD and experimental is 10K, similar to what was found for cooling. This difference drops to 5K near the tube wall. This data suggests there is pre-heating in the calming section, so this was investigated.

Pre-Heating in the Calming Section

Once the packing was removed from the column, the thermocouple cross was lowered to 5 millimeters above the bed entrance. The steam was turned on and the air flows were set to match the experimental flows. For the first air flow, the system was allowed two hours to reach steady state, and the remaining flows only required one hour. The temperatures were recorded, and the difference in the inlet thermocouple was compared to each of the positions on the thermocouple cross. It was observed that the furthest positions, at 25mm, had much larger differences that were most likely due to wall effects. As a result, two averages were taken: one with all of the positions and one excluding the four thermocouples positioned at 25 mm. The average difference between the inlet thermocouple and the cross is about 2K for heating runs. This is quite a bit lower than the 10K difference observed for cooling, as expected. Since the calming section is nylon, and therefore an insulator, it makes sense that more heat would be lost from the hot air than heat gained through conduction of the column against the calming section which then would be transferred to the incoming air.

Table 4-4. Pre-Heating in the Calming Section for Each Air Flow

Air Flow	Average [K]	Excluding 25 mm Average [K]
28%	3.58	2.289
32%	3.42	2.191
35%	3.15	1.996
40%	2.87	1.847
45%	2.74	1.802
50%	2.63	1.783

COOLING RESULTS SIMULATION 2

From the findings in the first simulation, the cooling CFD runs were rerun using the corrected inlet temperatures which accounted for heat loss in the calming section. Since inlet conditions could not be set between the calming section and test section, this was done by setting the temperature into the calming section at the corrected value. After the first simulation was run for the 28% air flow condition, there was still a large discrepancy between the CFD results and the experimental data, as shown below in the dimensionless graph for four inches of packing.

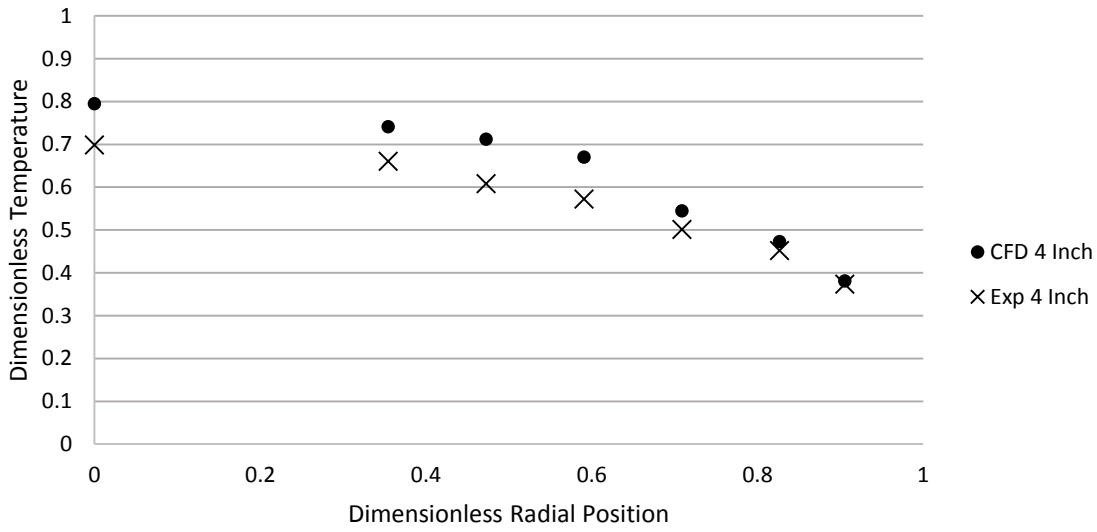

Figure 4-26. Dimensionless Profile Comparing CFD (Re= 503) to Experimental (Re=503) Cooling at a Bed Height of Four Inches (N=5.33) with Lower Particle Thermal Conductivity (k=0.4156)

While the difference was not as large as it was for the first simulation, the points were still not as comparable as expected. This prompted a closer look at the CFD set-up, particularly the thermal properties of the packing material and air. For the ceramic packing, it was decided the approach of using the y-intercept of the N=8 experimental data (DiNino et. al, 2013) could have resulted in a thermal

conductivity value that was representative of the particle and fluid, and not the independent α-alumina particles. Therefore literature values and values used for previous research at WPI were investigated and it was found a value of 1 may be more appropriate for the α-alumina. This was considerably higher than the 0.4156 that was used before, and should result in more reasonable CFD temperatures. After the thermal properties were modified, the resulting dimensionless graphs came into a much closer agreement, as shown below. Therefore for the remaining simulations, the higher thermal conductivity of the α-alumina particles was used.

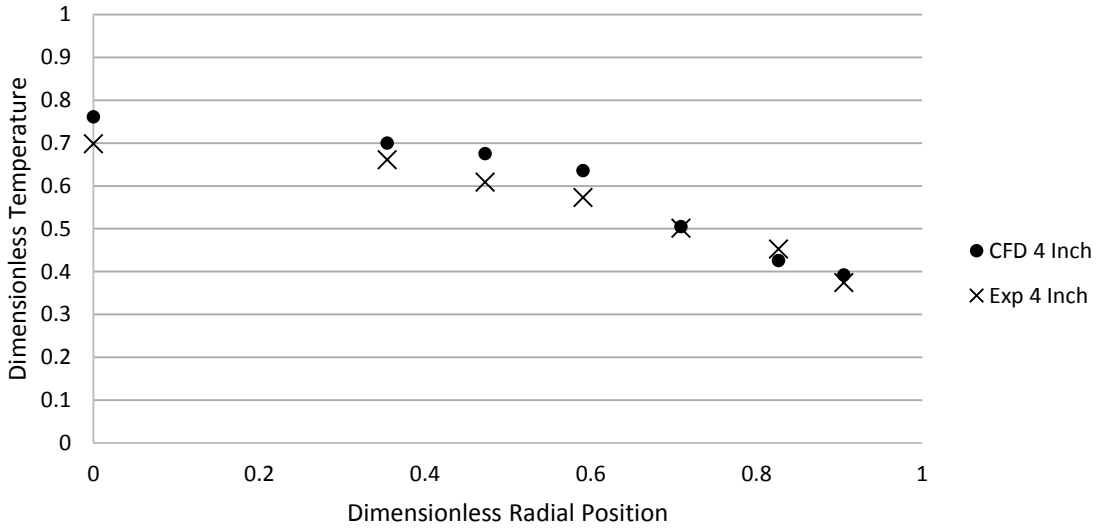

Figure 4-27. Dimensionless Profile Comparing CFD (Re= 503) Constant Viscosity to Experimental (Re=503) Cooling at a Bed Height of Four Inches (N=5.33) with Higher Particle Thermal Conductivity (k=1)

In addition to the α-alumina thermal conductivity, the physical properties of the air were also investigated. Since the viscosity of air changes with temperature, it was decided each simulation would be run with a constant viscosity based on the corrected inlet temperature, as well as with a viscosity having a piecewise linear dependence on temperature. This was done to see how the temperature dependence of viscosity affected the theoretical temperatures obtained, as well as the parameters found. All of the dimensionless graphs for all these differing conditions can be found in the appendix. The Reynolds number was still calculated to match the nominal inlet temperature taken before the calming section, in order to match the experimental conditions.

Constant Viscosity Results

For the simulations using the viscosity as constant based on the corrected inlet temperature, the effective thermal conductivity was found to shift up by 10-15%. This confirms that adjusting both the

inlet temperature for heat loss in the calming section, as well as the adjustment for the thermal conductivity of the α-alumina had the desired effect.

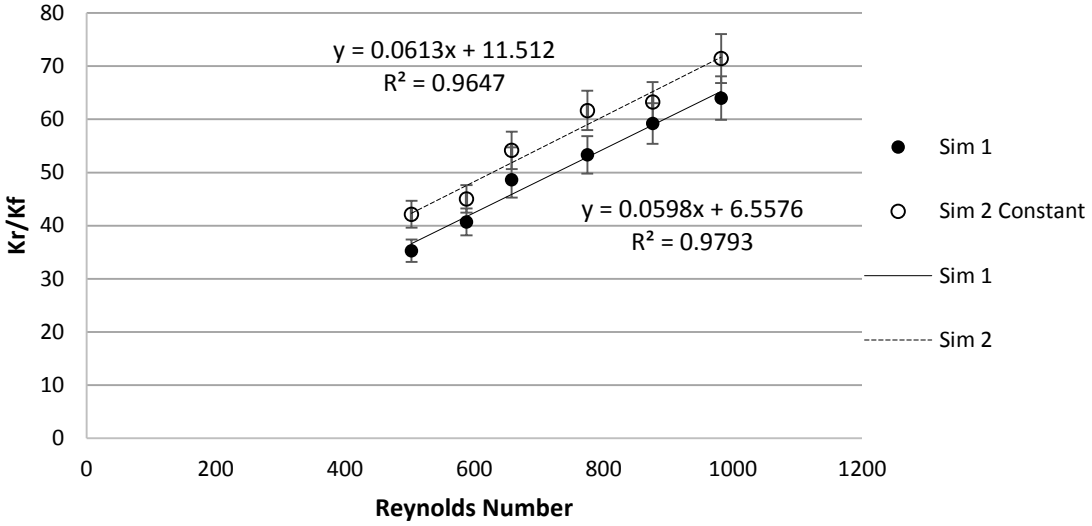

Figure 4-28. Effective Thermal Conductivity Comparison for CFD Simulation 1 and CFD Simulation 2 with Constant Air Viscosity Cooling (N=5.33)

Once it was found the changes had the expected effect on the effective thermal conductivity, the results were compared to the experimental data. As the graph below shows, the CFD results match the experimentally obtained data relatively well, with half of the points being within the 95% confidence range. The three points that are not within this range are just outside. Since the CFD data is still slightly lower, this suggests the value of 1 for the α-alumina may not identically match the particles used in the column. However the relative agreement between the CFD and experiment validates the CFD model.

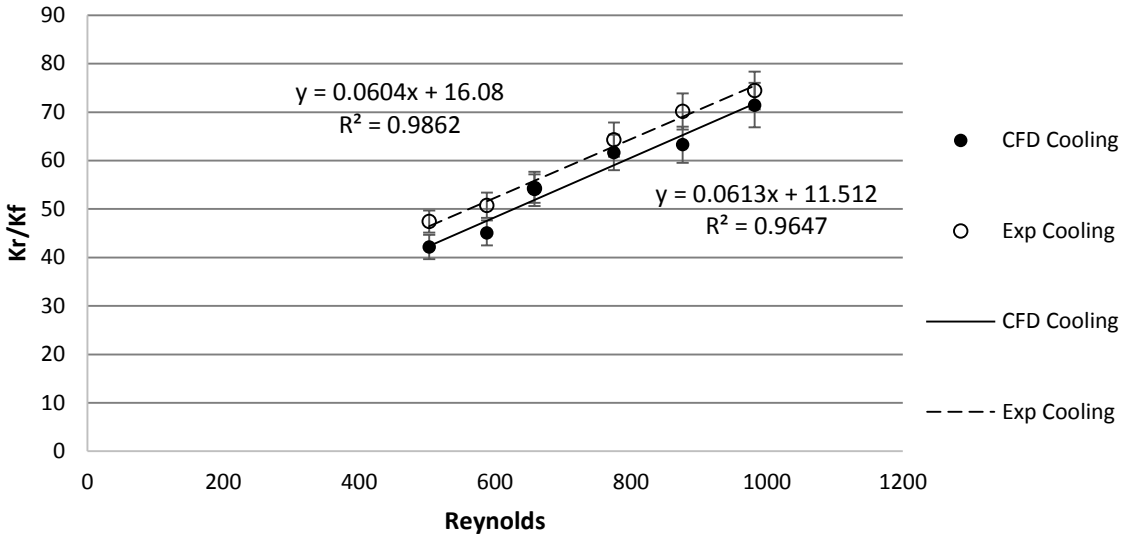

Figure 4-29. Effective Thermal Conductivity Comparison for CFD Simulation 2 with Constant Air Viscosity to Experimental Cooling (N=5.33)

For the wall Nusselt number, the adjustment was not expected to have a large effect since the changes affect the properties of the bed itself, not the interaction at the tube wall. This was confirmed by the graph below which shows essentially overlapping points for both simulations.

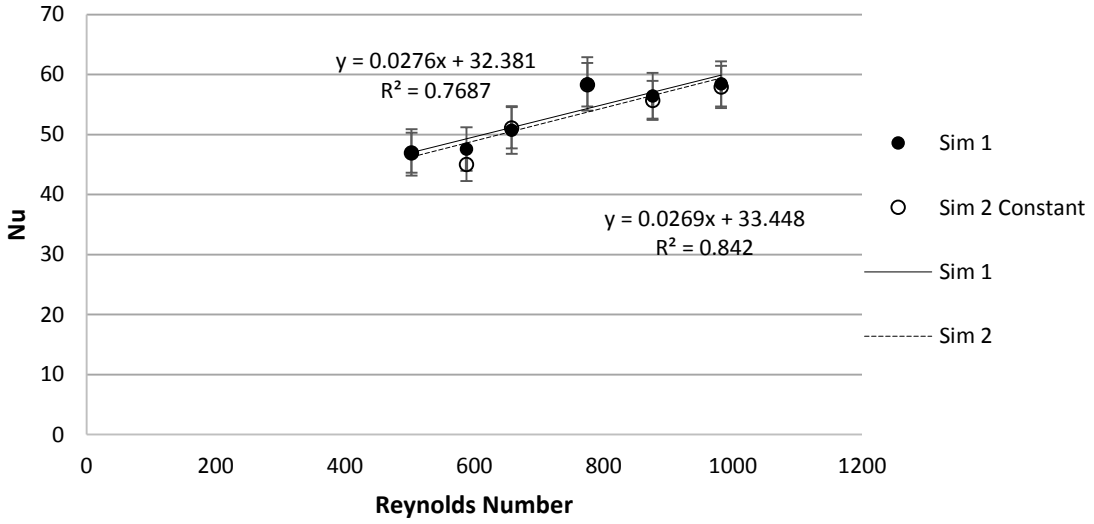

Figure 4-30. Wall Nusselt Number Comparison for CFD Simulation 1 and CFD Simulation 2 with Constant Air Viscosity Cooling (N=5.33)

Temperature Dependence of Viscosity Results

After each run had converged for a constant viscosity based on the corrected inlet temperature, a piecewise linear temperature dependence of viscosity was used for the air. To confirm the piecewise

linear function caused the viscosity to change with temperature, first the contours of viscosity were checked in the center plane of the bed, with an example shown below. The empty space in the contours represents the particles in the bed the fluid is flowing around. Since filled contours were not selected, areas with no changes are showed as empty space.

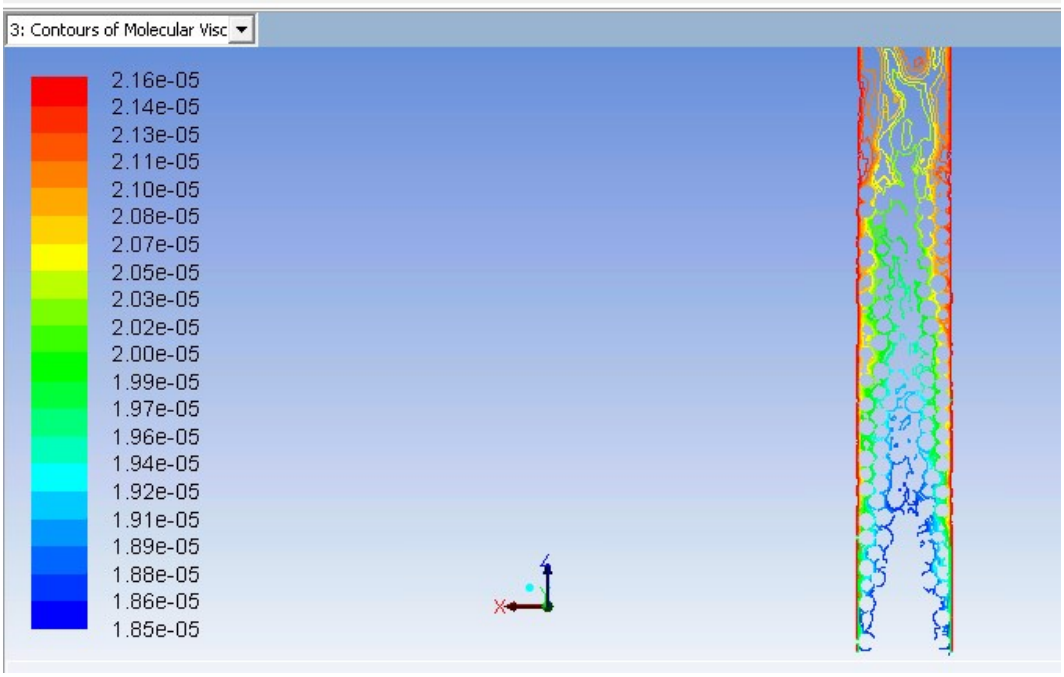

Figure 4-31. Viscosity Contours at Center Plane of Bed for Heating Simulation 2 (RE=901)

For the effective thermal conductivity, there was a small difference between the constant and varying viscosity. When there was an observable difference between the points, the runs with constant viscosity were slightly higher. For the varying viscosity results, the points are slightly less scattered, which pulls the y-intercept up slightly. However the general trend between the two conditions is the same.

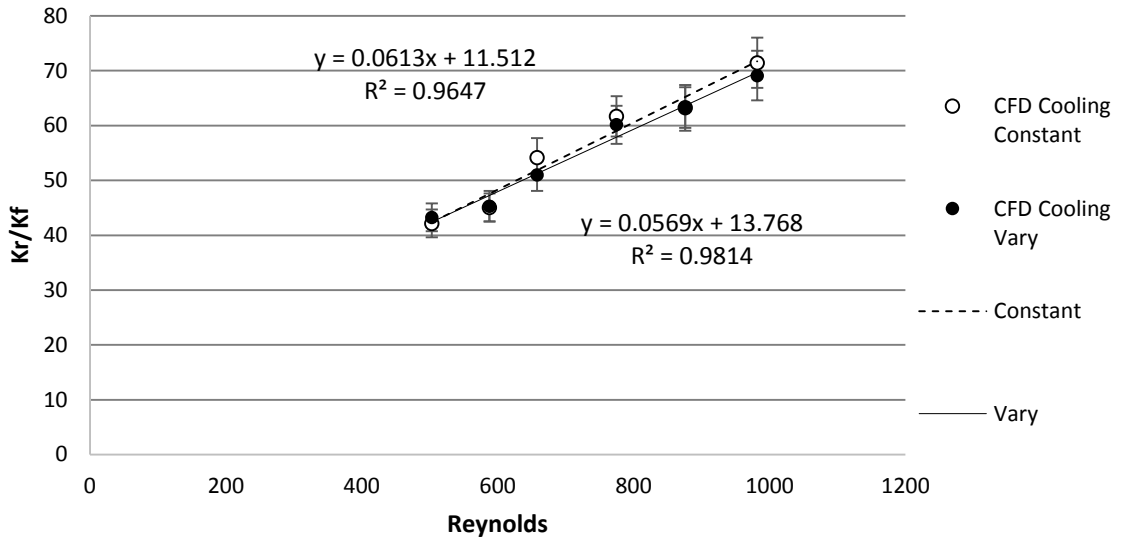

Figure 4-32. Effective Thermal Conductivity Comparison for CFD Simulation 2 for Constant Viscosity and a Piecewise Linear Temperature Dependence of Viscosity Cooling (N=5.33)

This slight shift downwards for the varying viscosity does not affect the comparison between the experimental data and the CFD results, as shown in the comparison below. The same comments made for the constant viscosity case can be made for the varying viscosity; half of the data points are within 95% confidence of each other, and the points that are not are just outside of this range.

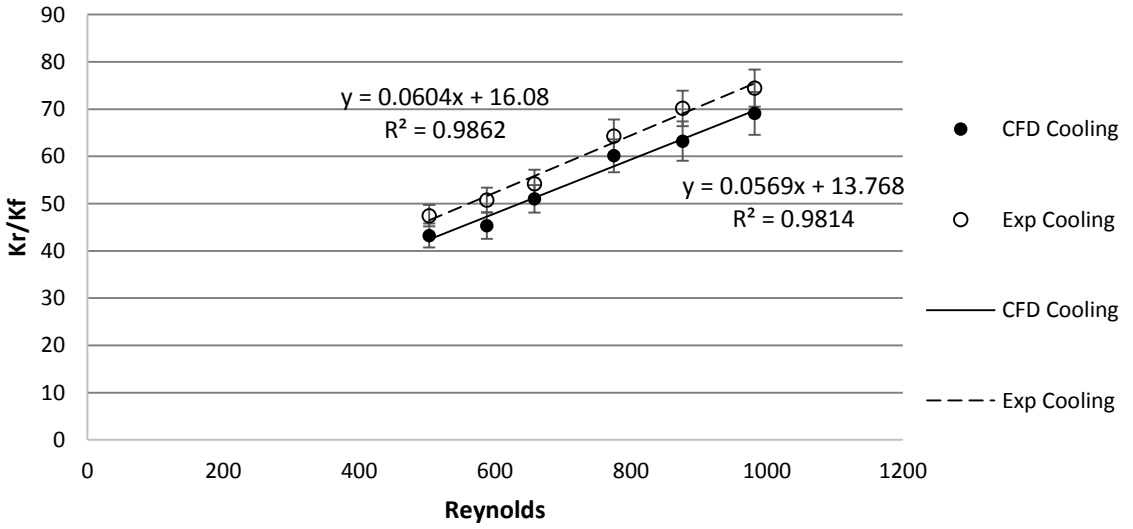

Figure 4-33. Effective Thermal Conductivity Comparison for CFD Simulation 2 with Piecewise Linear Temperature Dependence of Viscosity to Experimental Cooling (N=5.33)

For the wall Nusselt number, the difference between the constant and carrying viscosity is also very slight. As shown in the figure below, all of the points are within 95% confidence for the same Reynolds number, and the trend lines between the two are essentially identical.

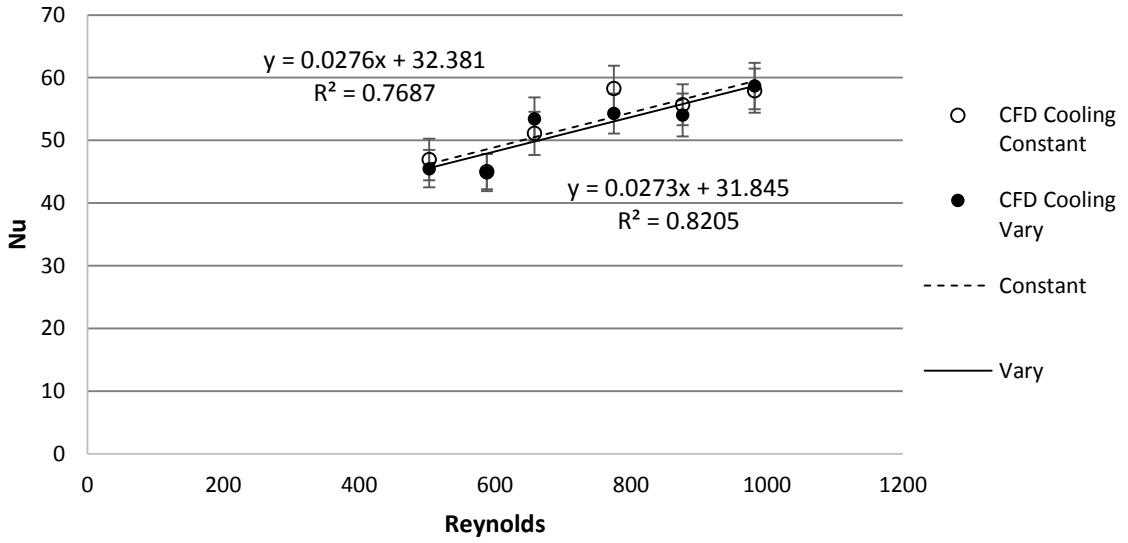

Figure 4-34. Wall Nusselt Number Comparison for CFD Simulation 2 with Piecewise Liner Temperature Dependence of Viscosity to Experimental Cooling (N=5.33)

These results demonstrate using the proper test section inlet temperature, as well as the correct thermal conductivity of the bed packing is critical for CFD results to match experimental data. Meanwhile, the temperature dependence of viscosity is not as critical to model. The results from this simulation compared to the experimental results validate the cooling CFD model and allow for confidence in the simulation results.

Heating Results Simulation 2

As with the cooling simulation, the heating simulations were run again using inlet temperatures corrected for any pre-heating, although this was to a smaller degree than the heat loss for cooling. The main difference between the first and second heating simulations was the thermal conductivity of the α-alumina particles. The heating runs were conducted first with a constant viscosity of air based on the corrected inlet temperature, and then using a piecewise linear temperature dependence of viscosity.

Constant Viscosity Results

For the second simulation for heating at a constant viscosity, the dimensionless profiles between CFD and experimental data matched relatively well, as shown below. There are a few points which are higher

for the CFD for the initial bed heights, but the profiles come into agreement for the remaining bed heights.

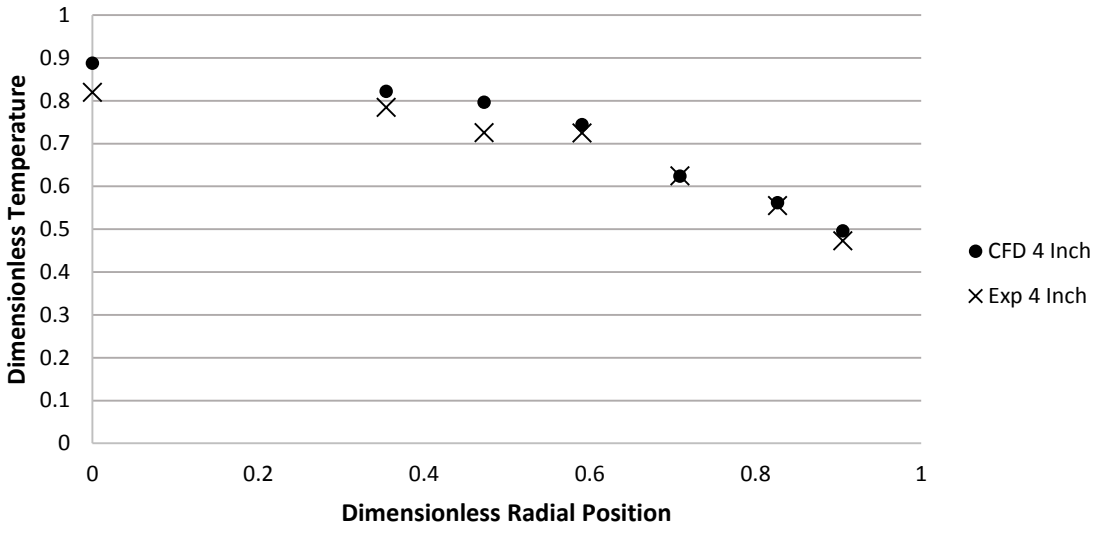

Figure 4-35. Dimensionless Profile Comparing CFD (Re= 901) Constant Viscosity to Experimental (Re=901) Heating at a Bed Height of Four Inches (N=5.33)

The trend in effective thermal conductivity was shifted upwards by 10-20%, similar to the results found for cooling. This showed the adjustments made to the inlet temperature and particle conductivity were valid for both heating and cooling, and both produced the same expected results.

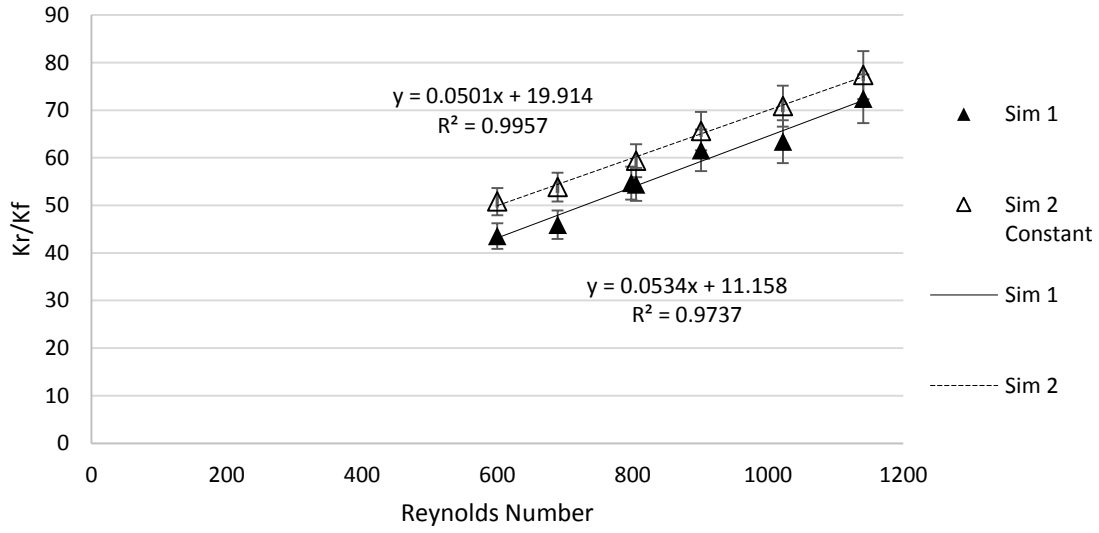

Figure 4-36. Effective Thermal Conductivity Comparison for CFD Simulation 1 and CFD Simulation 2 with Constant Air Viscosity Heating (N=5.33)

When the simulation data with constant viscosity was compared to the experimental heating data, it was found the experimental data trended slightly higher than the CFD results, in most cases just outside of the 95% confidence intervals at each Reynolds number. The CFD trending lower supports the higher values of dimensionless temperatures seen in the profiles.

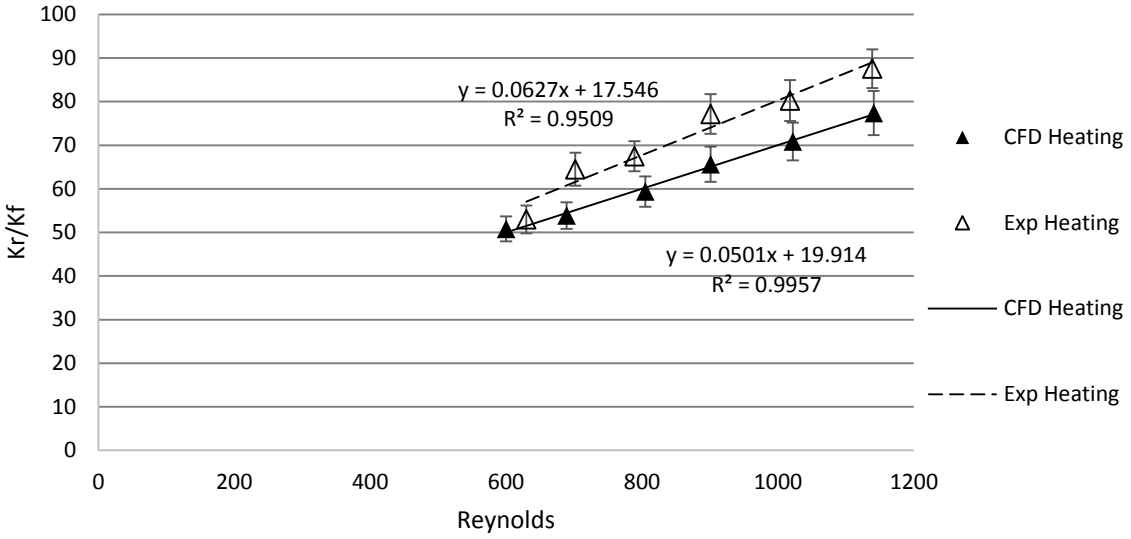

Figure 4-37. Effective Thermal Conductivity Comparison for CFD Simulation 2 with Constant Air Viscosity to Experimental Heating (N=5.33)

The difference between the heating CFD results and experimental data is slightly larger than that observed for cooling, however the discrepancy is still within reason. For the wall Nusselt number, there is almost no difference between the first and second simulation. The one exception are the points at Reynolds number of 1141, which appear to be due to a high value during simulation 1.

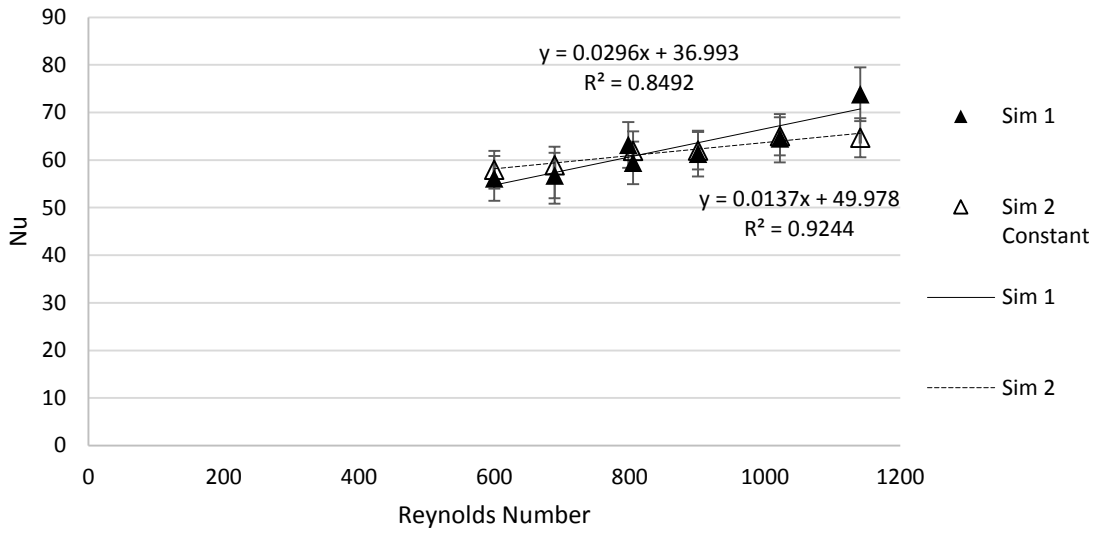

Figure 4-38. Wall Nusselt Number Comparison for CFD Simulation 1 and CFD Simulation 2 with Constant Air Viscosity Heating (N=5.33)

Temperature Dependence of Viscosity Results

When the temperature dependence of viscosity was added for the heating simulation, there was only a slight difference, as shown in the figure below. When a temperature dependence of viscosity was introduced, there is not clear pattern of the effective thermal conductivity increasing or decreasing. The changes between the two are within the 95% confidence intervals, although the constant viscosity results follow a linear trend more strongly than the varying viscosity results, due to an outlier for the varying viscosity at Re=805.

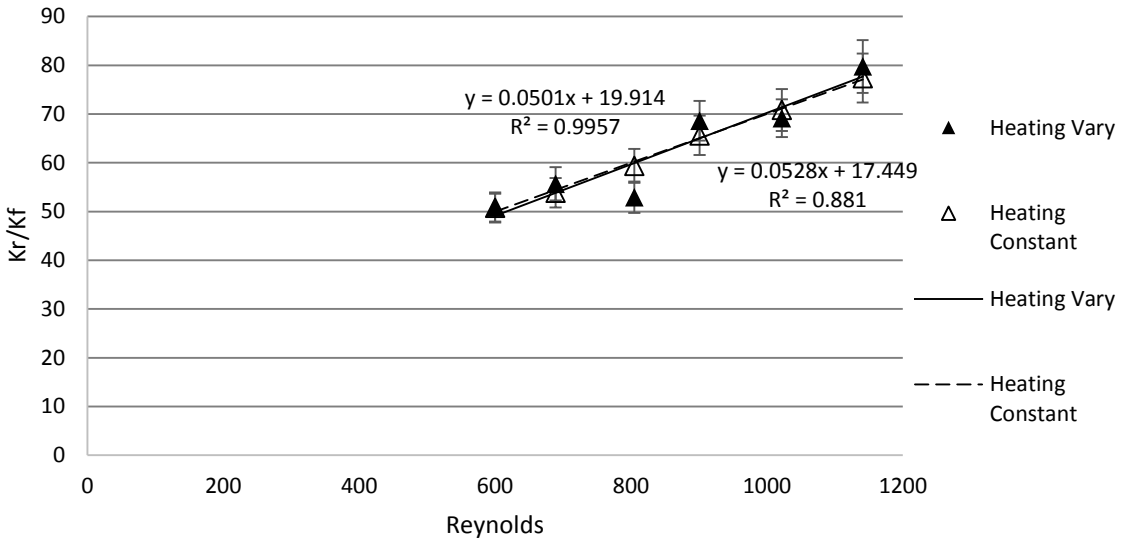

Figure 4-39. Effective Thermal Conductivity Comparison for CFD Simulation 2 for Constant Viscosity and a Piecewise Liner Temperature Dependence of Viscosity Heating (N=5.33)

For the wall Nusselt number, there is a very small difference between the constant and varying viscosity; however, the difference is small enough that the two are essentially the same, since all of the points are well within the 95% confidence ranges.

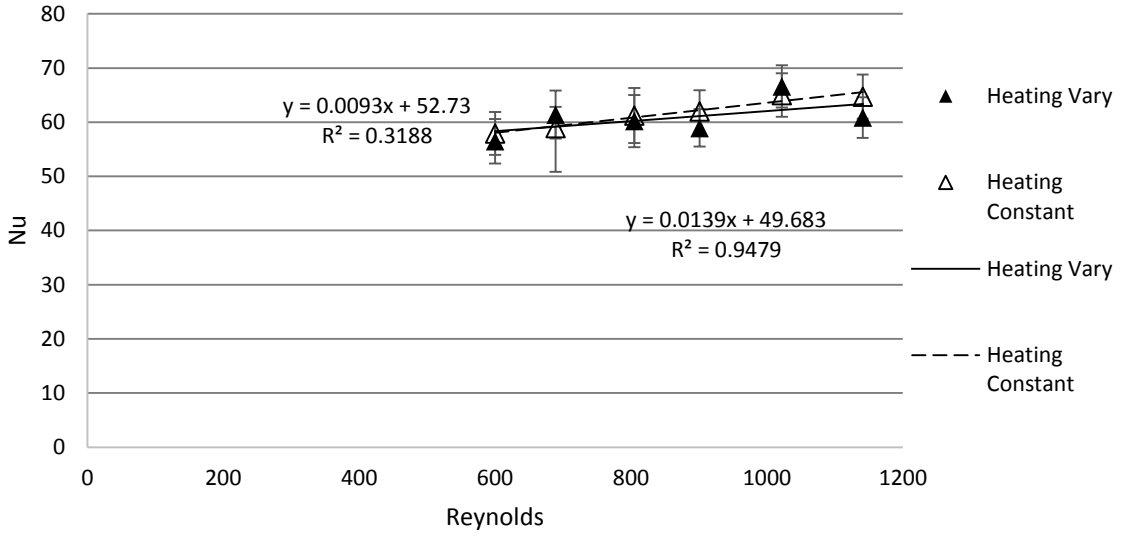

Figure 4-40. Wall Nusselt Number Comparison for CFD Simulation 2 for Constant Viscosity and a Piecewise Liner Temperature Dependence of Viscosity Heating (N=5.33)

As with the cooling results, these comparisons show increasing the thermal conductivity of the packing and accounting for pre-heating in the calming section results in CFD results which match experimental

data fairly well, and therefore the experimental results validate the CFD model for heating. The temperature dependence of the viscosity is not significant for heating when air is the heat transfer fluid.

CFD Heating versus Cooling

After the CFD data was validated against the experimental data, comparisons between heating and cooling CFD results could be made. This would allow for any difference between theoretical heating and cooling to be observed. While the second round of simulations was found to be the more reliable in comparison to experimental data, both simulations will be reported.

Simulation 1

Looking at the CFD comparison for heating and cooling for the first simulation, the effective thermal conductivity is essentially the same. Simulation one used the inlet temperatures measured before the calming section, and the lower value of thermal conductivity for the particles. All of the points for heating and cooling are within 95% confidence of each other, with no obvious outliers for either. The intersection of the heating line is higher than cooling, but due to the fact the slope and intercept can be heavily influenced by one point. This matches the trend observed for experimental data, although it is shifted downwards, due to using the lower value of the α-alumina particles thermal conductivity.

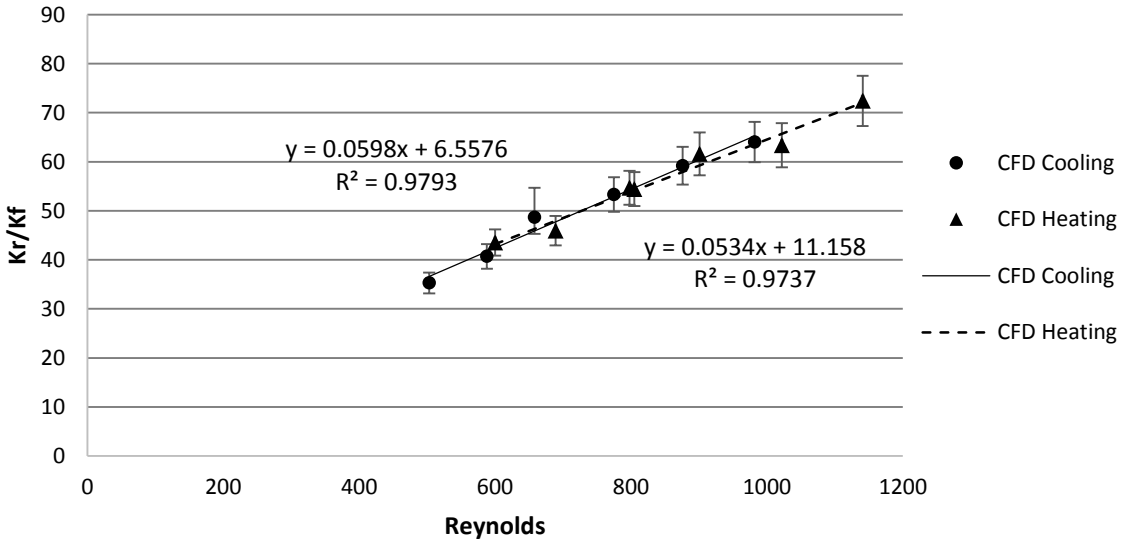

Figure 4-41. Effective Thermal Conductivity Comparison for CFD Heating and Cooling Data (N=5.33) Simulation 1

For the wall Nusselt number, the data points are not as closely matched as the effective thermal conductivity, but most points are within 95% confidence of each other. The heating points are always slightly higher than cooling, however not by a large enough amount to be considered significantly

different. Since the difference between the wall Nusselt number for heating and cooling is not as large as in the experimental data, it also supports the theory that the non-uniform wall temperature during experimental cooling runs results in a lower Nusselt number.

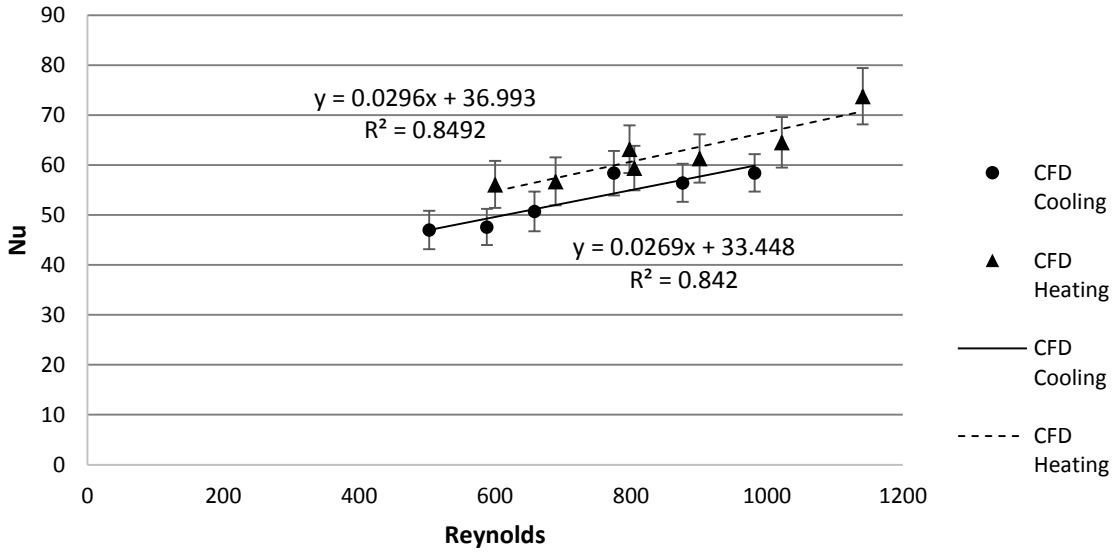

Figure 4-42. Wall Nusselt Number Comparison for CFD Heating and Cooling Data (N=5.33) Simulation 1

To confirm the observed similarities in the two heat transfer parameters, the dimensionless profiles for heating and cooling are compared. As with the other graphs, the graph at an air flow of 35% will be shown, only for the four inch bed height. The rest of the profiles can be found in the appendix. There is no difference between the heating and cooling results, except maybe slight variations which are negligible. This is the same for the other three bed heights, as well as all of the other air flows. The first simulation supports that there is not a difference between heating and cooling, as long as the temperature dependence of the air properties are properly modeled when calculating the Reynolds number.

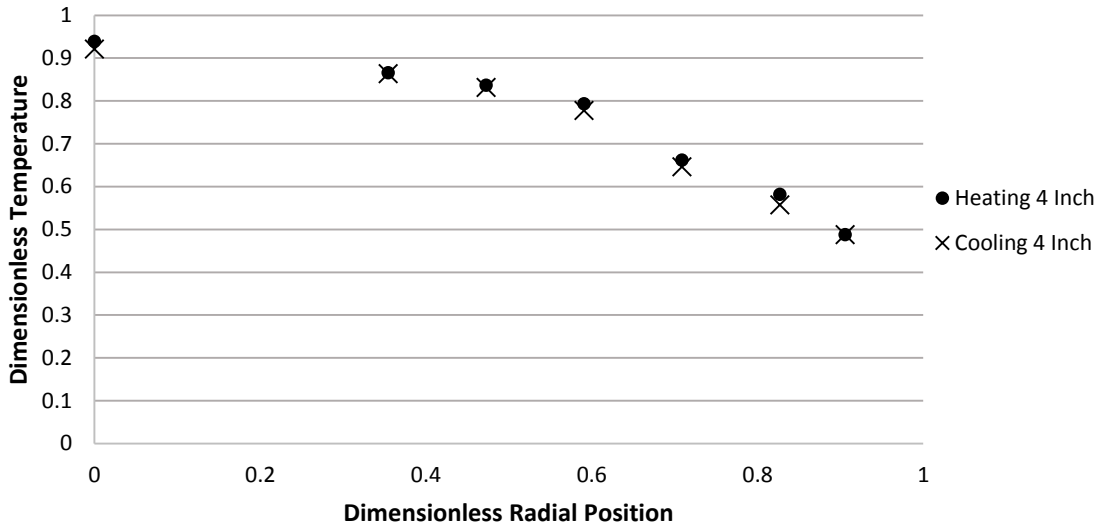

Figure 4-43. Dimensionless Temperature Profile for CFD Heating (Re=708) and Cooling (Re=658) Simulation1 at an Air Flow of 35% and Bed Height of Four Inches (N=5.33)

SIMULATION 2

After the second simulation was run with the appropriate corrections for the inlet temperature after the calming section and higher thermal conductivity for the particles (k=1), it was found to match the experimental data well. Therefore the models are validated as an appropriate computer model for the conditions being examined.

CONSTANT VISCOSITY RESULTS

When a constant viscosity, based on the corrected inlet temperature, was used for the second simulation there was once again a negligible difference between heating and cooling. To confirm this the dimensionless graphs were compared, however the inlet temperature was changed to match the inlet conditions to the CFD, not the experimental inlet.

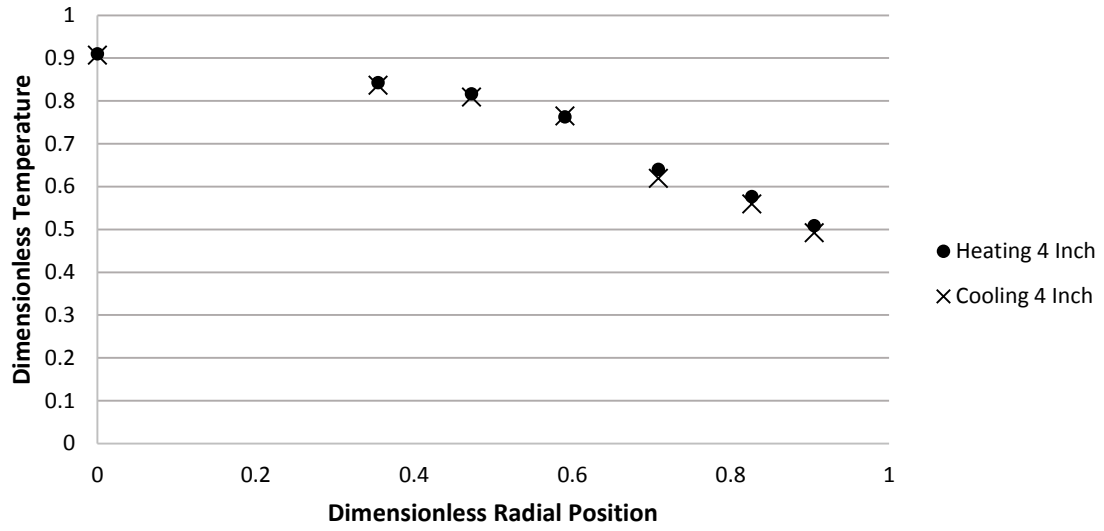

Figure 4-44. Dimensionless Temperature Profile for CFD Heating (Re=901) and Cooling (Re=775) Simulation 2 with Constant Viscosity at a Bed Height of Four Inches (N=5.33)

As the graph below shows, all of the points for effective thermal conductivity are well within the 95% confidence range. As with the first simulation, heating and cooling are comparable, and the trend in the CFD results match the experimental data.

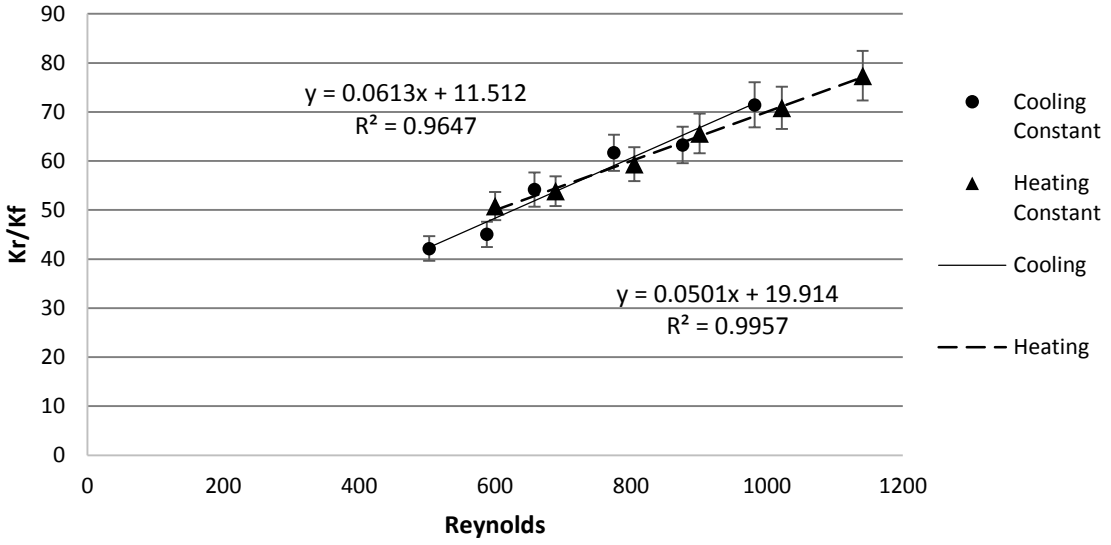

Figure 4-45. Effective Thermal Conductivity Comparison for CFD Heating and Cooling Data (N=5.33) Simulation 2 with Constant Air Viscosity

For the wall Nusselt number, heating trends higher than cooling data for every Reynolds number studied. The difference is more apparent at lower Reynolds number, and becomes within the 95% confidence levels of each other at a Reynolds of 600. The trend for heating is relatively flat, suggesting

an increase in air flow does not affect the wall heat transfer significantly. The trend for cooling increases with increasing Reynolds number in a more visible way, suggesting the wall heat transfer for cooling is more dependent on air flow.

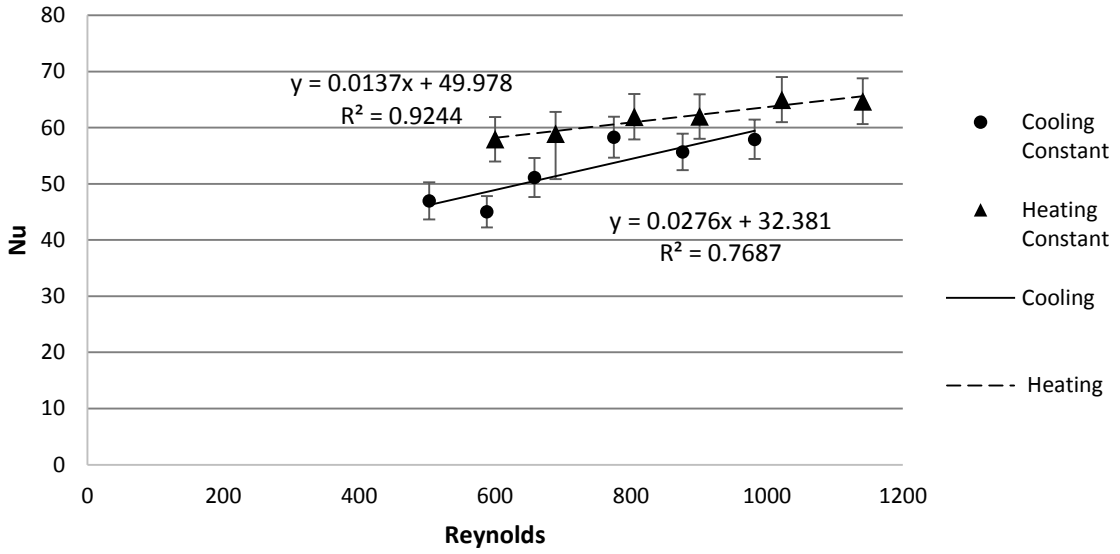

Figure 4-46. Wall Nusselt Number Comparison for CFD Heating and Cooling Data (N=5.33) Simulation 2 with Constant Air Viscosity

Temperature Dependence of Viscosity Results

When the viscosity of the air is allowed to depend upon temperature, the heating and cooling results again agree very well. There is one outlier for heating at a Reynolds of 805, but this may be due to the CFD run not obtaining proper convergence. When looking at the individual points, there is not a clear trend of heating or cooling being higher. All of the points are well within the 95% confidence range, which show any small effect viscosity plays on the results is of the same magnitude for heating and cooling simulations for the effective thermal conductivity.

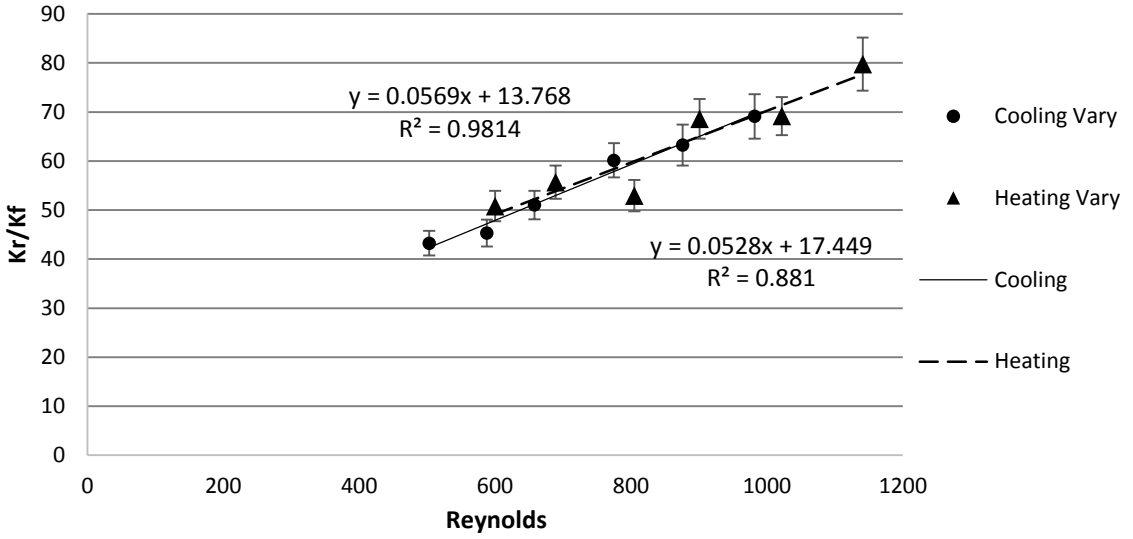

Figure 4-47. Effective Thermal Conductivity Comparison for CFD Heating and Cooling Data (N=5.33) Simulation 2 with Temperature Dependent Air Viscosity

When looking at the wall Nusselt number, heating still trends higher than cooling, and has a flatter slope. As the Reynolds number for cooling increases, the discrepancy between heating and cooling decreases, so the points are within the 95% confidence range. At Reynolds number lower than 600, the cooling points are outside the confidence region, and are about 10% lower than the heating values. Once again, the flat trend in heating suggests changing airflow does not affect the heating wall Nusselt number as strongly as the cooling results.

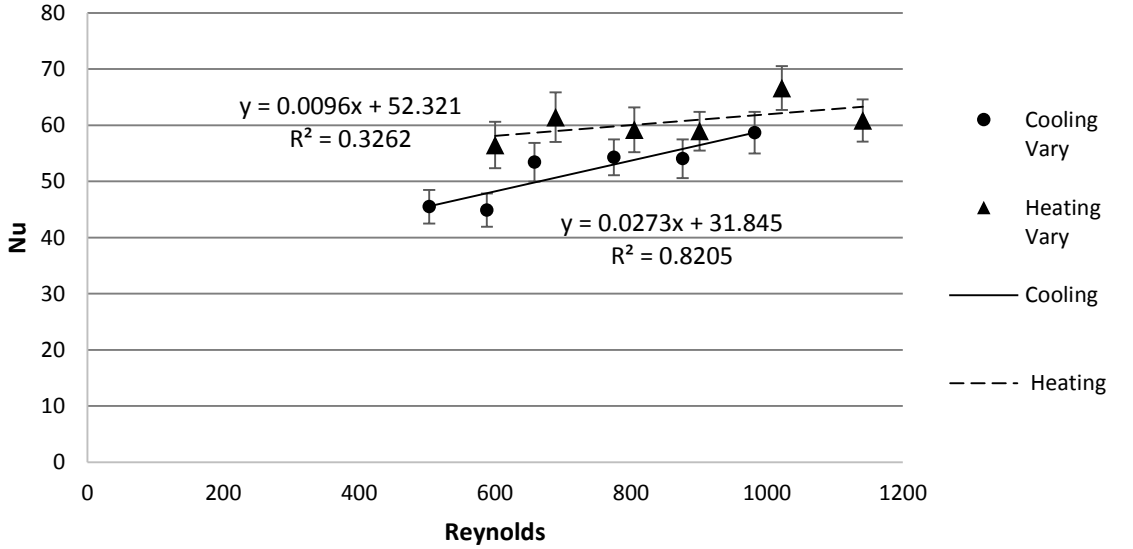

Figure 4-48. Wall Nusselt Number Comparison for CFD Heating and Cooling Data (N=5.33) Simulation 2 with Temperature Dependent Viscosity

The very slight difference in trends between the constant and varying viscosity suggests the physical properties of the heat transfer fluid have an effect on the observed parameters. However, for the conditions studied, the viscosity of air does not vary enough to greatly affect the parameters. To see to what degree, if any, the difference in viscosity can have on the parameters, the conditions at an air flow of 40%, corresponding to a mass flow of 0.003547 kg/s, were run using water as the heat transfer fluid. Water was chosen since the viscosity varies greatly with temperature. Between 20^0C and 95^0C the dynamic viscosity of water differs by 237% while air varies by 16% (Microelectronics Heat Transfer Laboratory, 1997). This vast difference will exaggerate any effects due to viscosity.

For the water run, a very preliminary study was done comparing heating and cooling at mass flow rate of 0.003547 kg/s. As shown below, the results vary by 23-27% based on changing from a constant viscosity based on the inlet air temperature to a temperature dependence. This shows that when the heat transfer fluid has a strong dependence on viscosity, this must be accounted for in the CFD.

Table 4-5. Water Run Results for a Mass Flow of 0.003547 kg/s

Condition	**Effective Thermal Conductivity**	**Percent Difference**	**Wall Nusselt Number**	**Percent Difference**
Cooling- Constant Viscosity	7.037 +/-.045	-22.6%	17.437 +/- 1.394	-26.9%
Cooling- Varying Viscosity	5.574 +/-0.44		13.745 +/- 1.173	
Heating- Constant Viscosity	6.595 +/- 0.050	27.9%	18.278 +/- 2.120	24.7%
Heating- Vary Viscosity	9.147 +/- 0.070		24.285 - 3.035	

CHAPTER 5 CONCLUSIONS AND RECOMMENDATIONS

For low N fixed beds, the wall effects have a large impact on the overall heat transfer within the bed. These effects are difficult to model, but they are critical to understand for safe and economical operation of industrial scale packed beds. To understand these effects experiments are conducted, and CFD is becoming increasingly prevalent. This research is aimed to help understand where heating and cooling are comparable for the heat transfer parameters, specifically the effective thermal conductivity and wall Nusselt number. In order to study the heat transfer in packed beds, both experimental and CFD results were obtained.

Experimental results were collected following the procedure suggested by DiNino et al. (2013) in which the column was packed to a constant bed height for a given day, and the air flow was varied so all six Reynolds numbers were collected in one day. This decreased variation between the Reynolds numbers due to re-packing of the column. The data was analyzed using the GIPPF model that was modified to use the actual temperature reading in the center of the bed as a boundary condition for the cubic spline that was fit to the dimensionless temperature profiles. This fit was used to find the heat transfer parameters, so a physically accurate profile was necessary.

When reviewing the results from DiNino et al. (2013) it was found the Reynolds number for heating and cooling was calculated using a value of viscosity at 20 degrees Celsius, since the velocity of the air was calculated at room temperature. Therefore, density should also be calculated at room temperature, due to conservation of mass. However, for the cooling runs the air is heated to approximately 95 degrees Celsius. It was suggested that the Reynolds number should be calculated based off of the inlet air temperature into the bed, which caused the cooling Reynolds numbers to be lowered by 14.1%. This also caused different values of the Prandtl number to be used in the GIPPF model when the data was being fitted. The data was re-fitted to the heat transfer parameters, and it was found heating and cooling were still comparable for effective thermal conductivity although the trend for cooling was shifted down. For the wall Nusselt number, heating trended higher than cooling, and the difference increased with increasing air flow.

For the experiments conducted for this research (N=5.33), calculating the Reynolds number based on the temperature of the air entering the calming section, it was found that heating and cooling were also comparable within experimental error for the effective thermal conductivity. However, for the wall Nusselt number a large discrepancy was observed between heating and cooling. The difference was larger than the one observed for N=8 data, which could be explained by the differing values of N for the

two studies. As with the N=8 studies, the difference between heating and cooling increased with increasing air flow.

After the experiments were completed, the run conditions for the CFD simulations were found so that the CFD matched the experiments as closely as possible. This was done by finding the mass flow rate that corresponded to the cooling run for each of the six air flows. This mass flow was used for both heating and cooling CFD simulations to provide a stronger comparison. For the inlet temperature, the average temperature of the air before the calming section for all the experiments was used for the first simulation. For the wall temperature, the average value of all the runs was used. When the first simulation CFD results were compared to heating and cooling, it was found the effective thermal conductivity was lower for the CFD simulations. When looking at the temperature profiles, it was found that the CFD temperatures were higher than the experimental ones for the cooling runs, and lower for the heating runs. This caused heat transfer in the calming section to be investigated. It was found for cooling runs the air lost about 10K in the calming section, and for heating runs the air was preheated by about 2K.

Therefore for the second simulation, the heat transfer in the calming section was taken into account. When this did not have the expected result for the Reynolds number of 503 cooling run, the setup of the CFD was studied. It was found that the thermal conductivity of the α-alumina particles was representative of the entire bed, and not the independent particles. Therefore the value was increased to match values used in other CFD research at WPI. The second simulation was also run using a constant viscosity based on the corrected inlet temperature, and a piecewise linear dependence on temperature. When the thermal conductivity of the particles was corrected, the CFD and experimental values for effective thermal conductivity become more comparable. Although they did not match, they were just outside of the confidence interval for both heating and cooling. This validated the CFD model.

For the wall Nusselt number the cooling CFD and experimental data did not compare; however, the heating CFD and experimental values did. This supported the idea that the discrepancy between the heating and cooling experimental data for the wall Nusselt number was due to the non-uniform wall temperature observed for cooling runs. For the comparison between a constant viscosity and temperature dependence, there was only a slight change in the parameters for both heating and cooling which did not affect any of the comparisons.

Finally, once the CFD simulations were validated, heating and cooling was compared for the CFD simulations. For the second simulation, it was found that heating and cooling are comparable for the effective thermal conductivity. For the wall Nusselt number, heating was found to be higher than cooling for all Reynolds numbers. For Reynolds numbers below 600, the difference was outside the confidence range; however above this the results were comparable within the 95% confidence range. From these results, it was found heating and cooling are comparable for the effective thermal conductivity. For the wall Nusselt number, the results appear to be dependent on the uniformity of the tube wall. Future work should attempt to include the observed temperature gradient at the tube wall for cooling CFD runs. If this results in better agreement between the CFD results and experimental data, it is confirmed the uniformity of the tube wall effects the wall Nusselt number.

When running experiments, it is recommended that a constant bed height be studied with the air flowing varying for given day. Also, when calculating the Reynolds number, it is suggested the viscosity at the inlet temperature of the calming section by used. When analyzing the results, the actual temperature at the center of the bed should be used to the GIPPF cubic spline interpolation.

For the CFD setup, the inlet temperature should account for heat loss in the calming section, and a proper particle thermal conductivity must be used. For the heat transfer fluid, a temperature dependence of viscosity should be used it, especially if the viscosity greatly depends on temperature. For the study here, it was not critical to have the viscosity vary with temperature, however for completeness it is recommended that it should be modeled as such. This will eliminate any small discrepancies that may arise, especially if the temperature range is larger than the one studied here. For future work, it is recommended the thermal conductivity of the packing used be experimentally determined to allow for a strong correlation between the CFD and experimental results.

This research showed heating and cooling have comparable values of effective thermal conductivity both experimentally and when CFD is used. For the wall Nusselt number, the CFD values matched relatively well between heating and cooling, while the experimental values did not. Disagreement between cooling CFD and experimental wall Nusselt numbers suggests this parameter is dependent on the uniformity of the tube wall.

NOMENCLATURE

$\theta = \frac{T-T_w}{T_o-T_w}$	Dimensionless Temperature
$y = r/R$	Dimensionless Radial Position
μ	Dynamic Viscosity of the Fluid
ρ	Density of Fluid
$Bi = \frac{h_w R}{k_r}$	Biot Number
d_p	Particle Diameter
d_T	Tower Diameter
h_w	Apparent wall heat transfer coefficient
k_r	Effective radial thermal conductivity
k_f	Thermal conductivity of the fluid
$\frac{k_r}{k_f} = \frac{RePr}{Pe_r}$	Effective Conductivity
$N = \frac{d_T}{d_P}$	Tube to Particle Diameter Ratio
$Nu_w = \frac{h_w d_p}{k_f}$	Wall Nusselt Number
$Pe_r = \frac{\rho v c_p d_p}{k_r}$	Radial Peclet Number
R	Tower Radius
$Re = \frac{\rho v d_p}{\mu}$	Reynolds Number
U	Overall Heat-Transfer Coefficient
v	Fluid Velocity

WORKS CITED

Adeyanju, A. A., & Manohar, K. (2009). Theoretical and Experimental Investigation of Heat Transfer in Packed Beds . *Research Journal of Applied Sciences, 4*(5), 166-177.

AK Steel Corporation. (2007). Product Data Sheet: Stainless Steel.

Alexander, T. E., Ledwith, B. C., & Linskey, M. M. (2011, April 27). Heat Transfer in Packed Bed Reactors -- Heating vs. Cooling.

Ashman, M., Ryback, D., & Skene, W. (2009). Heat Transfer Parameters of Cylindrical Catalyst Particles with Internal Voids in Fixed Bed Reactor Tubes. *Worcester Polytechnic Institute.*

Augier, F., Idoux, I., & Delenne, J.Y. (2010). Numerical Simulations of Transfer and Transport Propertires Inside Packed Beds of Spherical Particles. *Chemical Engineering Science, 65(3),* 1055-1064.

Borkink, J. G., & Westerterp, K. R. (1992 b, May). Influence of Tube and Particle Diameter on Heat Transfer in Packed Beds. *AIChE Journal, 38*(5), 703-715.

Dalman, M.T., Merkin, J.H, & McGreavy, C. (1986). Fluid Flow and Heat Transfer Past Two Spheres in a Cylindrical Tube. *Computers and Fluids, 14(3),* 267-281.

Derkx, O.R, & Dixon, A. G. (1996). Determination if the Fixed bed Wall Heat Transfer Coefficient Using Computational Fluid Dynamics. *Numerical Heat Transfer A, 29(8),* 777-794.

DiNino, A. R., Hartzell, E. J., Judge, K. E., & Morgan, A. T. (2013). Heating and Cooling in a Packed Bed. *Worcester Polytechnic Institute.*

Dixon, A. G. (1985, December). The Length Effect on Packed Bed Effective Heat Transfer Parameters. *Chemical Engineering Journal, 31*(3), 163–173.

Dixon, A. G. (2012 a, November 16). Heat Transfer Modelings. (A. DiNino, E. Hartzel, K. Judge, & A. Morgan, Interviewers)

Dixon, A. G. (2012 b, June). Fixed Bed Catalytic Reactor Modelling—the Radial Heat Transfer Problem. *The Canadian Journal of Chemical Engineering, 90*(3), 507-527.

Dixon, A.G., Personal Communication (2013a).

Dixon, A.G., (2014a). Finite Volume Method – Basics and steady 1-D conduction. Personal Collection of A. Dixon, Worcester Polytechnic Institute, Worcester, MA.

Dixon, A.G., (2014b). Finite Volume Method – convection and conduction. Personal Collection of A. Dixon, Worcester Polytechnic Institute, Worcester, MA.

Dixon, A.G., (2014c). Finite Volume Method Calculating the flow field. Personal Collection of A. Dixon, Worcester Polytechnic Institute, Worcester, MA.

Dixon, A.G., Nijemeisland, M., & Stitt, E. H. (2003). CFD Simulation of Reaction and Heat Transfer near the Wall of a Fixed Bed. *International Journal of Chemical Reactor Engineering, 1,* A22.

Dixon, A.G., Nijemeisland, M., & Stitt, E. H. (2013b). Systematic mesh development for 3D CFD Simulation of fixed beds: Contact points study. *Computers & Chemical Engineering, 48,* 135-153.

Dixon, A. G., & van Dongeren, J. H. (1998). The influence of the tube and particle diameters at constant ratio on heat transfer on packed beds . *Chemical Engineering and Processing, 37*, 23-32

Guardo, A., Coussirat, M., Larrayoz, M.A., Recasens, F., & Eguzquizza. E. (2004). CFD Flow and Heat Transfer in Nonregular Packings for Fixed Bed Equipment Design. *Industrial & Engineering Chemistry Research, 43(2),* 7049-7056.

Guardo, A., Coussirat, M., Larrayoz, M.A., Recasens, F., & Eguzquizza. E. (2005). Influence of the Turbulence Model in CFD Modeling of Wall-to Fluid Heat Transfer in Packed Beds. *Chemical Engineering Science, 60(6),* 1733-1742.

Guardo, A., Coussirat, M., Recasens, F ,Larrayoz, M.A., & Escaler, X. (2006). CFD Study on Particle-to Fluid Heat transfer in Fixed Bed Reactors: Convective Heat Transfer at Low and High Pressure. *Chemical Engineering Science, 61(13),* 4341-4353.

Kwong, S. S., & Smith, J. M. (1957, May). Radial Heat Transfer in Packed Beds. *Industrial & Engineering Chemistry, 49*(5), 894-903.

Leva, M. (1947). Heat Transfer to Gases through Packed Tubes. *Industrial and engineering Chemistry, 39(7),* 857-862.

Leva, M. (1948). Cooling of gases through Packed Tubes. *Industrial and engineering Chemistry, 40(4)*, 747-752.

Logtenberg, S.A. & Dixon, A.G. (1998a). Computational Fluid Dynamics Studies of Fixed Bed Heat Transfer. *Chemical Engineering and Processing, 37(1),* 7-21

Logtenberg, S.A. & Dixon, A.G. (1998b). Computational Fluid dynamics Simulations of Fluid Flow and Heat Transfer and the Wall-Particle Contact Points in a Fixed-Bed Reactor. *Chemical Engineering Science, 54(13),* 2433-2439.

Magnico, P. (2009). Pore-Scale Simulations of Unsteady Flow and Heat Transfer in Tubular Fixed Beds. *AIChE Journal, 55(4),* 849-867.

Microelectronics Heat Transfer Laboratory. (1997). Fluid Properties Calculator. Available online at: http://www.mhtl.uwaterloo.ca/old/onlinetools/airprop/airprop.html

Nijemeisland, M & Dixon, A.G &. (2001). CFD as a Design Tool for fixed-Bed Reactors. *Ind. Eng. Chem. Res.40,* 5246-5254.

Nijemeisland, M. & Dixon, A.G. (2004). CFD Study of Fluid Flow and Wall Heat Transfer in a Fixed Bed of Spheres. *AIChE Journal, 50(5),* 906-921.

Ochiai, M., Ogura, H., Ozao, R., & Tsutsumi, S. (1997). Thermal Analysis of Powered Alumina Materials. *Journal of Thermal Analysis, 49,* 961-970.

Patankar, S. V. (1980). *Numerical Heat Transfer and Fluid Flow.* New York: McGraw-Hill.

Taskin, M. (August 2007). CFD Simulation of Transport and Reaction in Cylindrical Catalyst Particles. *Worcester Polytechnic Institute.*

Thomeo, J. C., Rouiller, C. O., & Freire, J. T. (2004, June 11). Experimental Analysis of Heat Transfer in Packed Beds with Air Flow. *Industrial and Engineering Chemistry Research, 43*(15), 4140-4148.

Wen, D., & Ding, Y. (2006, Feburary 15). Heat transfer of gas flow through a packed bed. *Chemical Engineering Science, 61*, 3532-3542.

Winterberg, M., Tsotsas, E., Krischke, A., & Vortmeyer, D. (2000). A simple and coherent set of coefficients for modelling of heat and mass transport with and without chemical reaction in tubes filled with spheres. *Chemical Engineering Science, 55*(5), 967-979.

APPENDICES

APPENDIX A: TABLES

COMPARISON OF HEATING EXPERIMENT (N=8) REYNOLDS NUMBER USING TEMPERATURE DEPENDENCE OF VISCOSITY

2013 Reynolds Number	Reynolds Number Using Inlet Viscosity	Delta
214	218	4
257	262	5
305	311	6
367	374	7
411	419	8
479	488	9
532	542	10
589	600	11
656	669	13
740	754	14
908	925	17
992	1011	19
1022	1042	20

DIFFERENCE IN WALL TEMPERATURE FOR EXPERIMENTAL COOLING RUNS

Air Flow	Bed Height	Water TC 1	Water TC 2	Water TC 3	Delta
28%	4	7.23164892	7.56331778	8.91401005	1.68
Re 503		7.00755882	7.42866135	8.88940907	1.88
	6	9.10429096	9.3105545	10.8756609	1.77
		8.99199772	9.16261292	10.7382221	1.75
	8	8.25371456	8.20940876	10.5173883	2.26
		8.29293442	8.35025978	10.7010555	2.41
	10	10.0416927	10.5923061	12.9902468	2.95
		9.70487022	10.4186983	12.5874949	2.88
32%	4	6.86262941	7.69837141	8.43390369	1.57
Re 588		7.34457111	7.74335337	8.79862118	1.45
	6	7.29873228	7.92705822	9.53100681	2.23
		6.92632389	7.42612076	8.88526726	1.96
	8	8.98795986	9.06362534	12.0039396	3.02
		9.40667725	9.03420258	12.0210667	2.61
	10	9.46129608	10.4481258	12.1410666	2.68
		9.25645256	10.3027611	11.9675598	2.71

35%	4	7.97537994	7.90526915	9.40278721	1.43
Re 658		8.01250362	7.88724756	9.4452343	1.43
	6	7.78336048	8.09954548	10.3914509	2.61
		7.81593943	8.17358208	10.4509401	2.64
	8	9.23446465	8.99974346	12.3103542	3.08
		9.13093472	8.98124123	12.3545618	3.22
	10	9.11030865	10.0017681	13.2014313	4.09
		9.47328854	9.9013319	12.9716969	3.50
40%	4	8.31380749	8.53314114	10.3955679	2.08
Re 775		8.61396694	8.70796585	10.5356636	1.92
	6	9.45700741	9.59593773	12.2259779	2.77
		9.73873043	9.65862942	12.268343	2.53
	8	7.20157528	7.41838646	11.4516077	4.25
		7.17551613	7.56392813	11.6058168	4.43
	10	8.62681389	9.00171947	12.6892691	4.06
		8.32683277	8.93331051	12.6161518	4.29
45%	4	8.81252861	9.59401417	11.6434631	2.83
Re 876		9.52465248	10.1930542	12.3394833	2.81
	6	10.2876272	10.5233946	13.4112482	3.12
		10.0299091	10.5638819	13.6398544	3.61
	8	5.87362623	5.77210999	9.45651913	3.58
		6.34803724	6.4366951	11.0200577	4.67
	10	8.83185959	9.6821909	13.9732037	5.14
		9.15622139	9.70473385	14.0331087	4.88
50%	4	9.64727783	10.5943718	12.9373579	3.29
Re 982		9.78370285	10.5335245	12.8840199	3.10
	6	9.89869881	10.6935263	14.0319195	4.13
		9.84383583	10.5372648	14.0554094	4.21
	8	7.82478714	8.31815243	13.4405441	5.62
		8.29947376	8.20921612	13.3553591	5.06
	10	9.57540321	9.94231701	14.6331129	5.06
		9.24881744	10.0644674	14.952527	5.70

Summary of Interpolated Theta at Wall and Wall Fluxes for Experimental Runs

	Θ at R Heating	Θ at R Cooling	dΘ/dy at Wall Heating	dΘ/dy at Wall Cooling
28% 6 Inch	0.202	0.238	-1.027	-0.501
28% 8 Inch	0.179	0.182	-0.491	-0.422
28% 10 Inch	0.138	0.143	-0.375	-0.308
32% 6 Inch	0.270	0.265	-0.605	-0.522
32% 8 Inch	0.210	0.213	-0.466	-0.424
32% 10 Inch	0.163	0.169	-0.352	-0.340
35% 6 Inch	0.273	0.293	-0.656	-0.505
35% 8 Inch	0.213	0.239	-0.525	-0.444
35% 10 Inch	0.167	0.196	-0.397	-0.353
40% 6 Inch	0.300	0.312	-0.645	-0.554
40% 8 Inch	0.240	0.256	-0.514	-0.472
40% 10 Inch	0.189	0.210	-0.408	-0.380
45% 6 Inch	0.313	0.338	-0.678	-0.574
45% 8 Inch	0.252	0.281	-0.553	-0.488
45% 10 Inch	0.203	0.233	-0.440	-0.404
50% 6 Inch	0.327	0.361	-0.676	-0.586
50% 8 Inch	0.268	0.308	-0.560	-0.500
50% 10 Inch	0.219	0.259	-0.451	-0.427

Run Conditions for CFD Simulations 1 and 2

Cooling Sim 1	**Inlet Temp [K]**	**Wall Temp [K]**	**Viscosity [kg/m*s]**
503	368.0	282.6	2.5195E-05
588	367.2	282.3	2.1552E-05
658	366.8	282.7	2.2315E-05
775	365.8	282.7	2.1509E-05
876	364.8	283.2	2.1466E-05
982	363.6	284.1	2.1380E-05
Cooling Sim 2			
503	357.3	282.6	2.1121E-05
588	356.9	282.3	2.1121E-05
658	356.3	282.7	2.1077E-05
775	356.9	282.7	2.1077E-05
876	356.6	283.2	2.1077E-05
982	356.2	284.1	2.1077E-05
Heating Sim 1			
600	297.3	374.7	1.8396E-05
689	296.7	374.6	1.8996E-05

805	296.8	375	1.8396E-05
798	297.1	375	1.8396E-05
901	297.1	374.9	1.8396E-05
1022	297.3	374.8	1.8396E-05
1141	297.3	374.7	1.9397E-05
Heating Sim 2			
600	299.5	374.7	1.8497E-05
689	294.4	374.6	1.8497E-05
805	299	375	1.8497E-05
901	299	374.9	1.8491E-05
1022	299.1	374.8	1.8497E-05
1141	299	374.7	1.8497E-05

Coordinate Points for CFD Temperature readings to Match Experimental Thermocouple Readings

Position for z(4 inches) =0.0254m z(6 inches) = 0.3048m z(8 inches)= 0.03556m z(10 inches)=0.4064m

	0 Degree Rotation		45 Degree Rotation	
TC	x [m]	y [m]	x [m]	y [m]
A	0	0	0	0
B1	0	0.12	0.00849	0.00849
B2	0.12	0	-0.00849	0.00849
B3	0	-0.12	-0.00085	-0.00849
B4	-0.012	0	0.00849	-0.00849
C1	0.00636	0.00636	0	0.009
C2	-0.00636	0.00636	0.009	0
C3	-0.00636	-0.00636	0	-0.009
C4	0.00636	-0.00636	-0.009	0
D1	0	0.018	0.01273	0.01273
D2	0.018	0	-0.01273	0.01273
D3	0	-0.018	-0.01273	-0.01273
D4	-0.018	0	0.01273	-0.01273
E1	0.01061	0.01061	0	0.015
E2	-0.01061	0.01061	0.015	0
E3	-0.0161	-0.0161	0	-0.015
E4	0.01061	-0.01601	-0.015	0
F1	0	0.023	0.01626	0.01626
F2	0.023	0	-0.01626	0.01626
F3	0	-0.023	-0.01626	-0.01626
F4	-0.023	0	0.01626	-0.01626
G1	0.01485	0.01485	0	0.021
G2	-0.01485	0.01485	0.021	0
G3	-0.01485	-0.01485	0	-0.021
G4	0.01485	-0.01485	-0.021	0

Appendix B: Graphs

Wall Nusselt Number Comparison for CFD Simulation 2 with Constant Air Viscosity to Experimental Cooling (N=5.33)

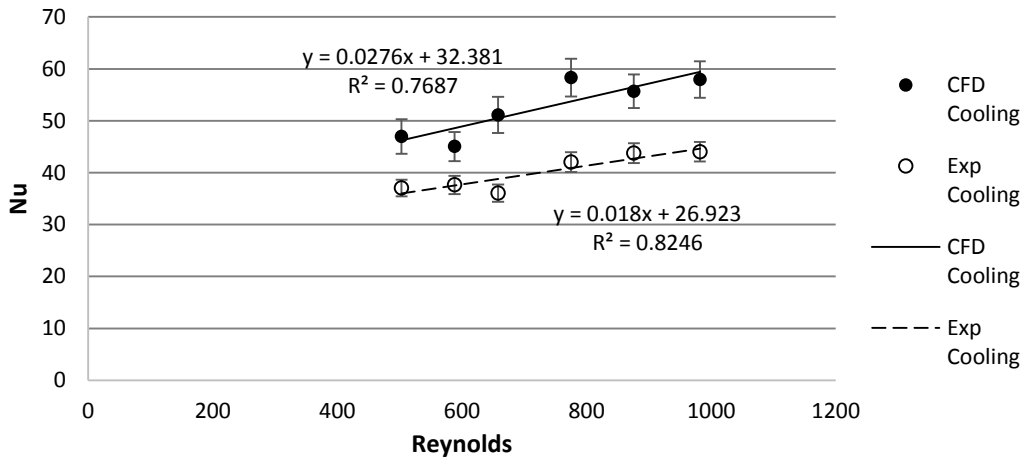

Wall Nusselt Number Comparison for CFD Simulation 2 with Varying Air Viscosity to Experimental Cooling (N=5.33)

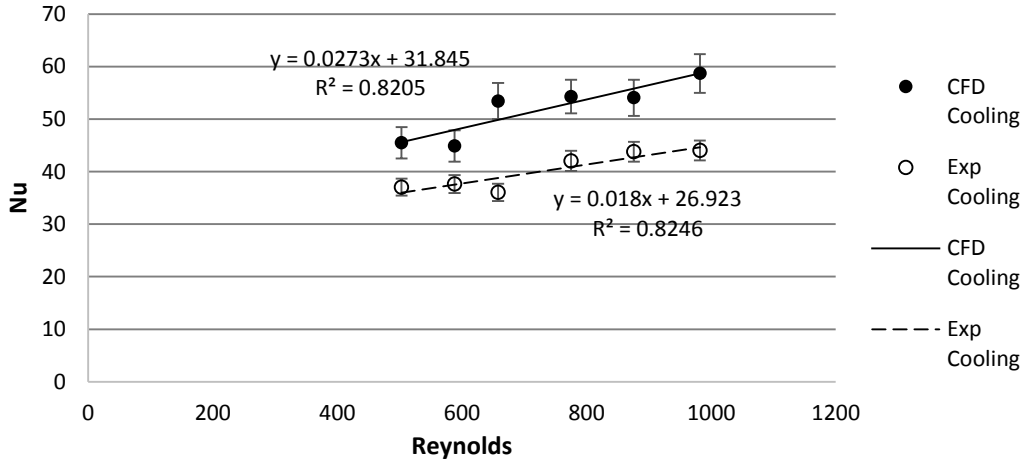

Wall Nusselt Number Comparison for CFD Simulation 2 with Constant Air Viscosity to Experimental Heating (N=5.33)

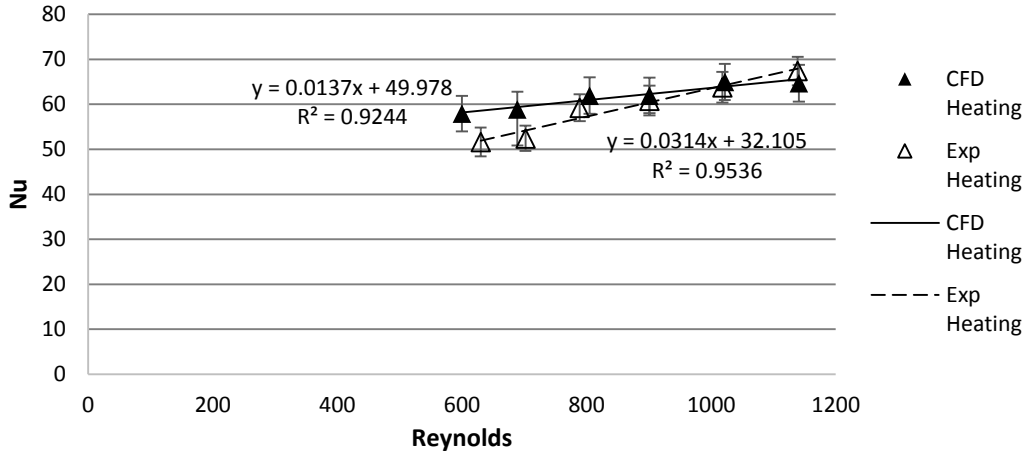

Wall Nusselt Number Comparison for CFD Simulation 2 with Varying Air Viscosity to Experimental Heating (N=5.33)

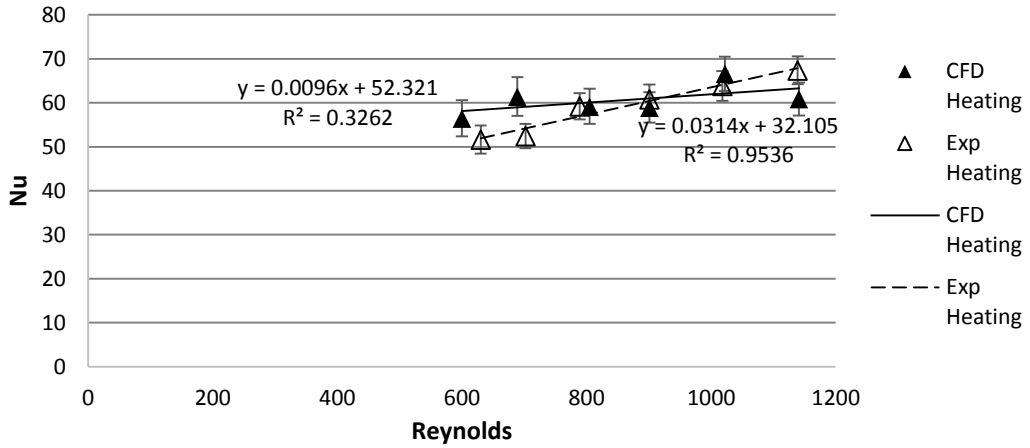

Appendix C: Dimensionless Temperature Profiles

Heating versus Cooling Experimental (N=5.33)

Air Flow 28% Cooling Re=503 and Heating Re=630 Bed Height 4 Inches

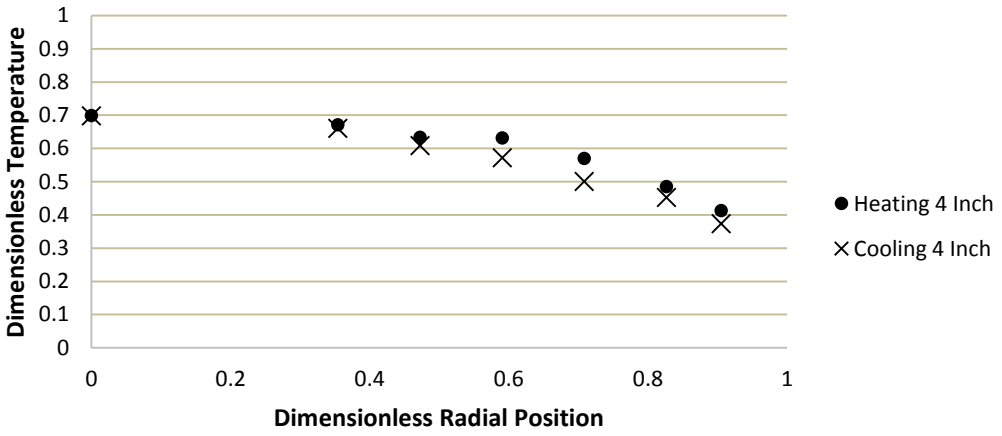

Air Flow 28% Cooling Re=503 and Heating Re=630 Bed Height 6 Inches

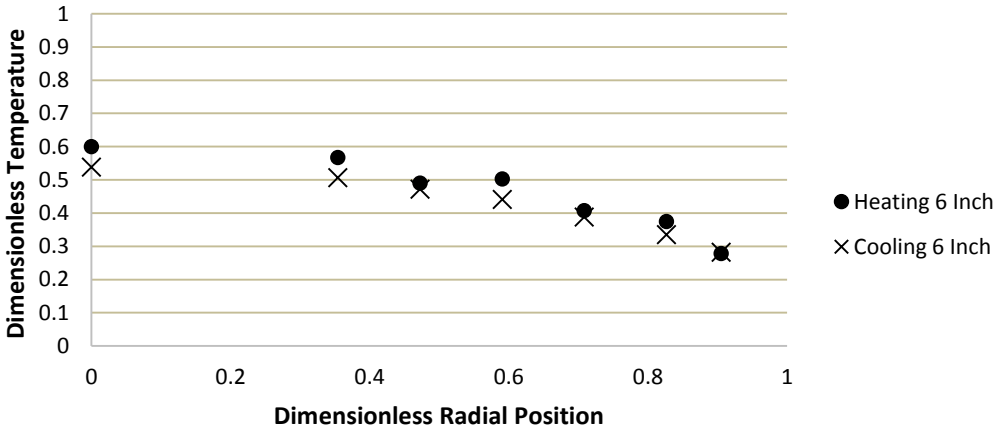

Air Flow 28% Cooling Re=503 and Heating Re=630 Bed Height 8 Inches

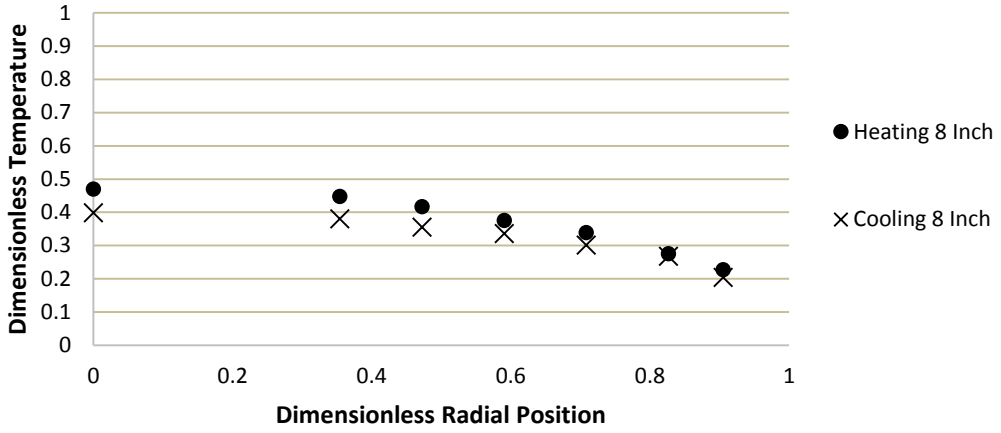

Air Flow 28% Cooling Re=503 and Heating Re=630 Bed Height 10 Inches

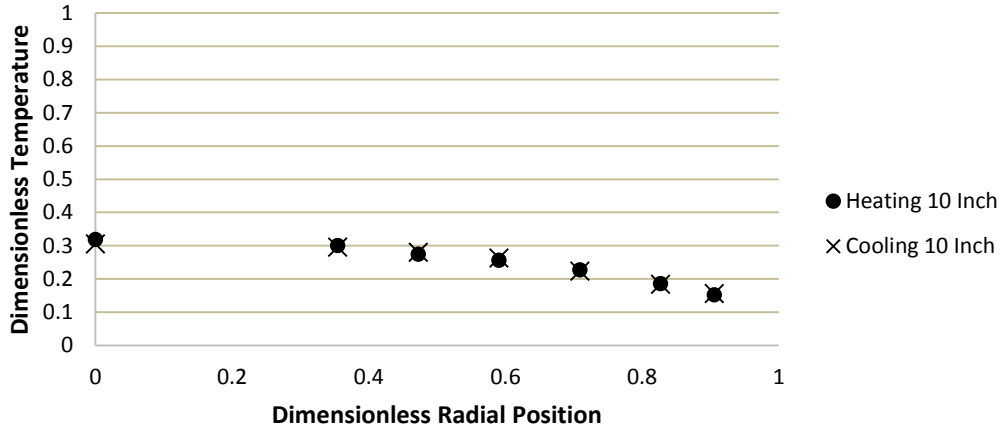

Air Flow 32% Cooling Re=588 and Heating Re=702 Bed Height 4 Inches

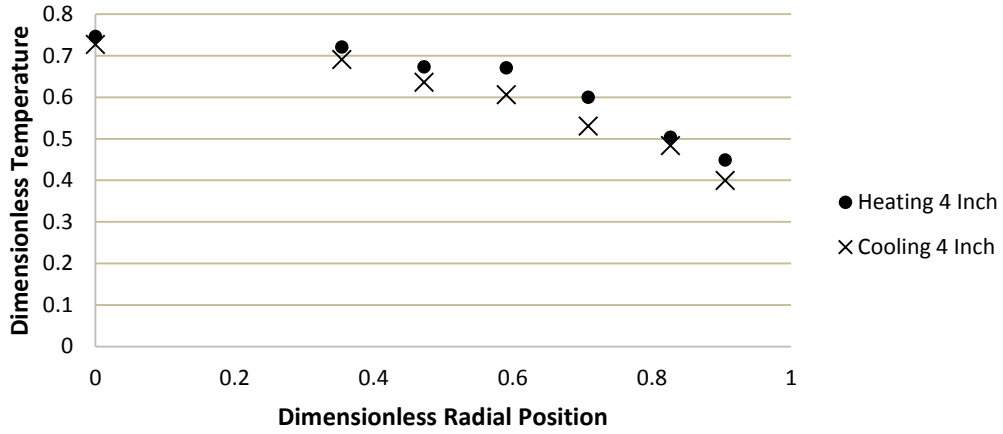

Air Flow 32% Cooling Re=588 and Heating Re=702 Bed Height 6 Inches

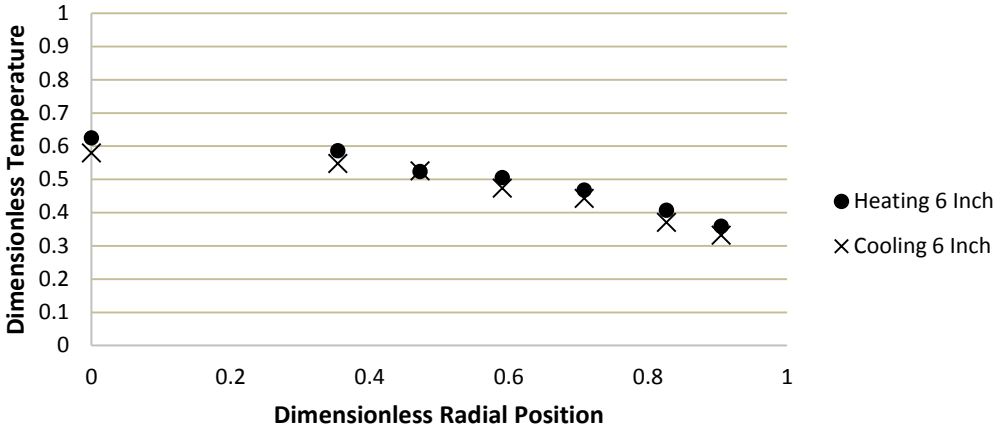

Air Flow 32% Cooling Re=588 and Heating Re=702 Bed Height 8 Inches

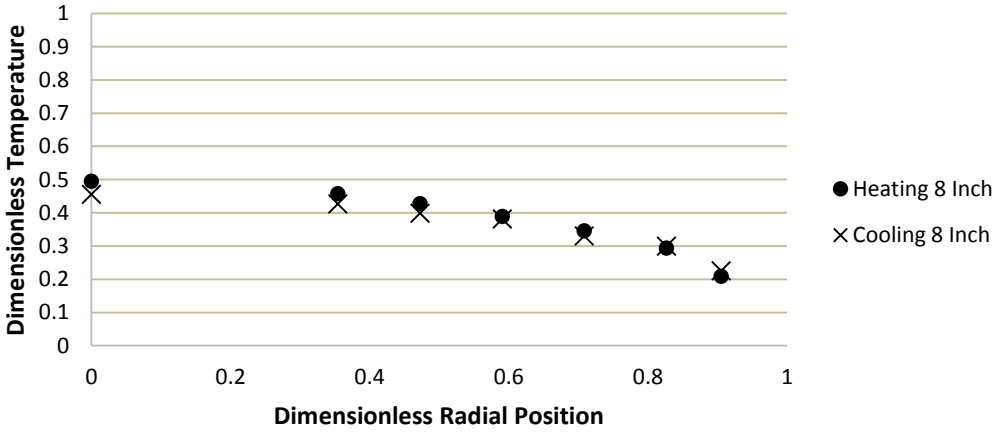

Air Flow 32% Cooling Re=588 and Heating Re=702 Bed Height 10 Inches

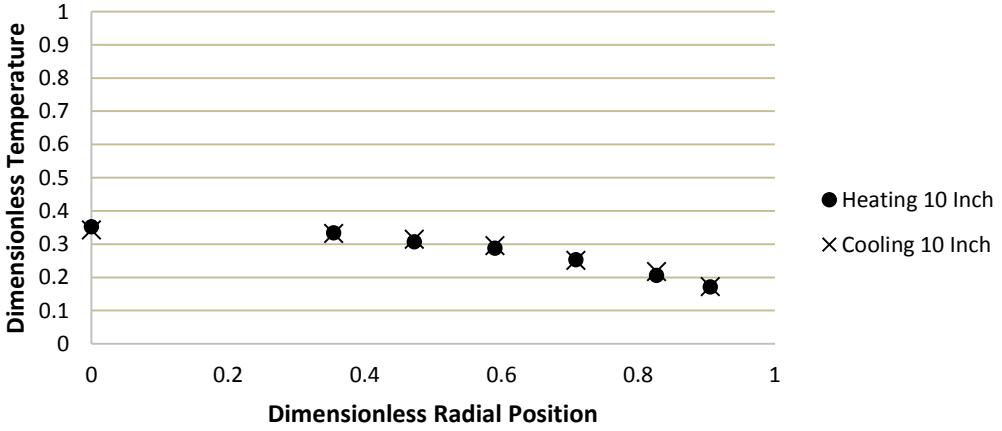

Air Flow 40% Cooling Re=775 and Heating Re=901 Bed Height 4 Inches

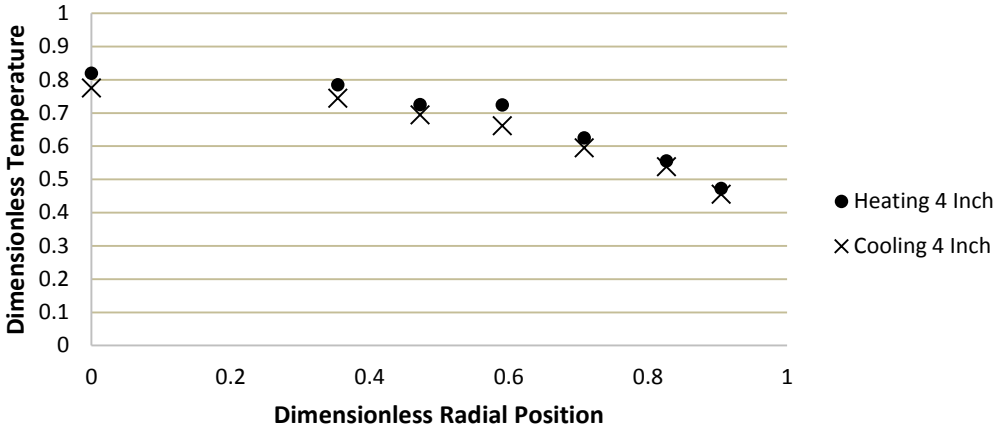

Air Flow 40% Cooling Re=775 and Heating Re=901 Bed Height 6 Inches

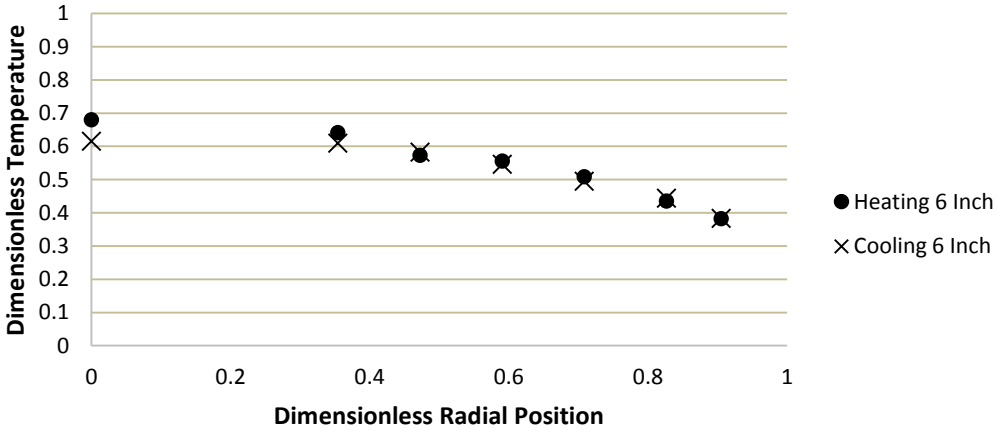

Air Flow 40% Cooling Re=775 and Heating Re=901 Bed Height 8 Inches

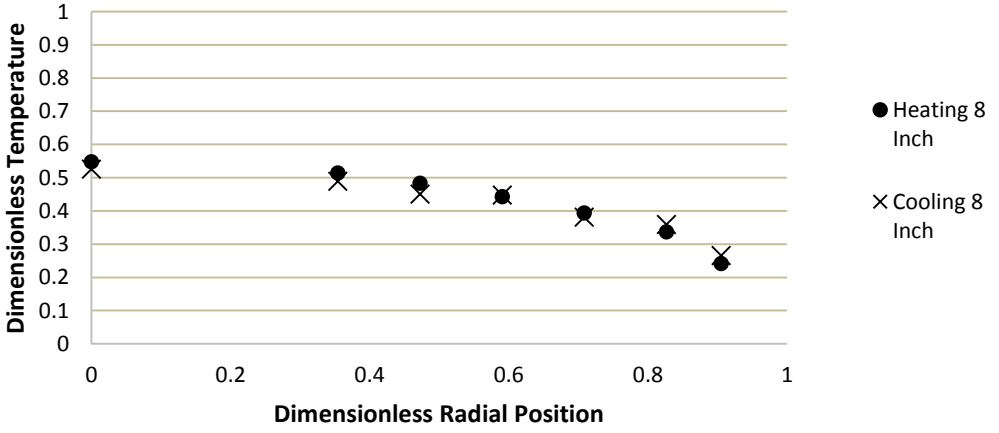

Air Flow 40% Cooling Re=775 and Heating Re=901 Bed Height 10 Inches

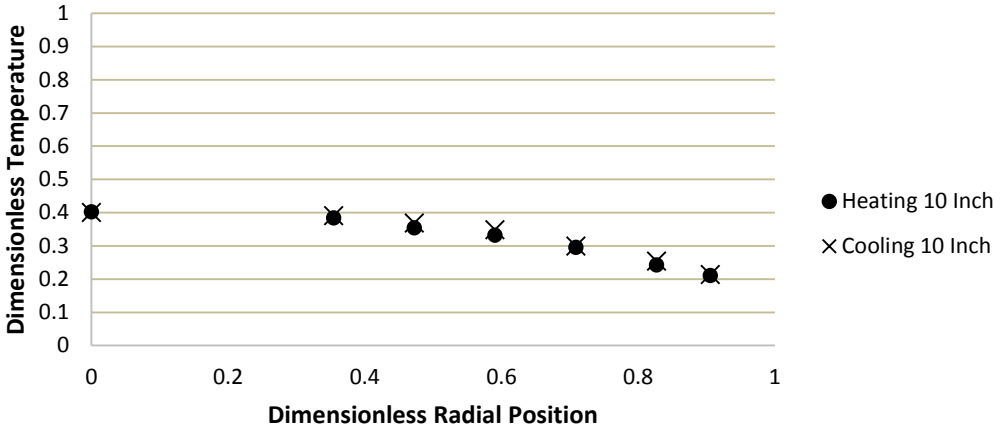

Air Flow 45% Cooling Re=876 and Heating Re=1018 Bed Height 4 Inches

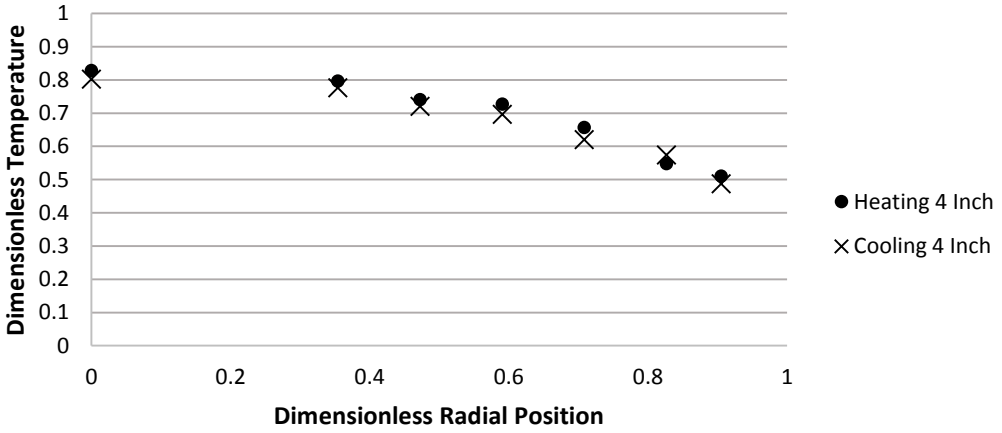

Air Flow 45% Cooling Re=876 and Heating Re=1018 Bed Height 6 Inches

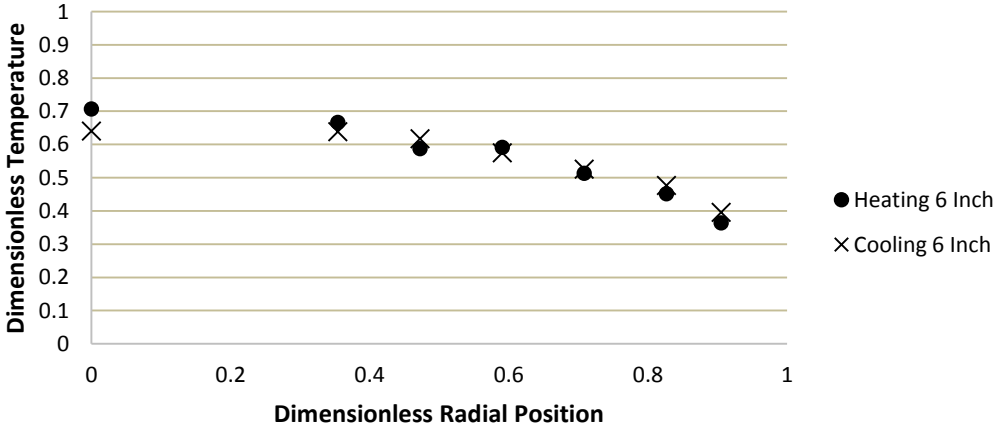

Air Flow 45% Cooling Re=876 and Heating Re=1018 Bed Height 8 Inches

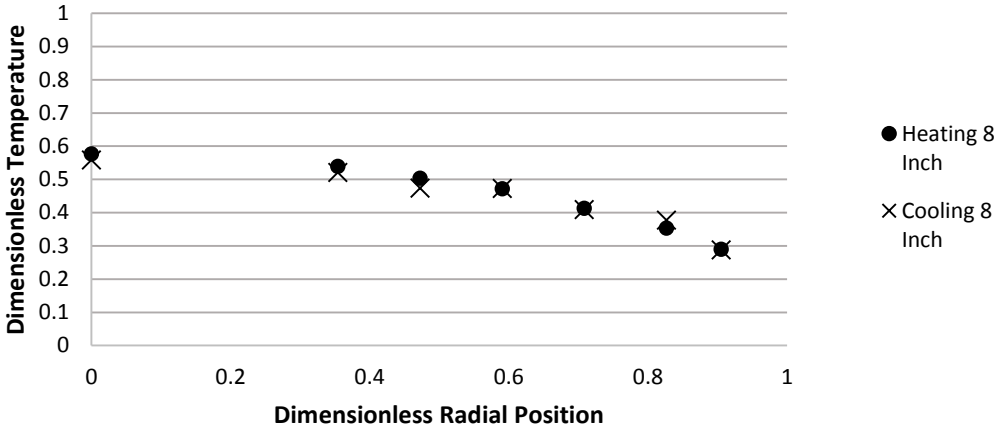

Air Flow 45% Cooling Re=876 and Heating Re=1018 Bed Height 10 Inches

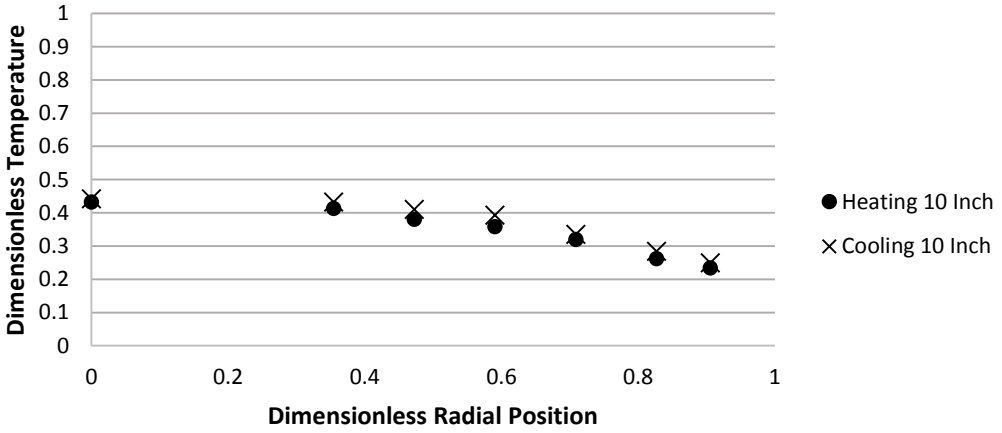

Air Flow 50% Cooling Re=982 and Heating Re=1139 Bed Height 4 Inches

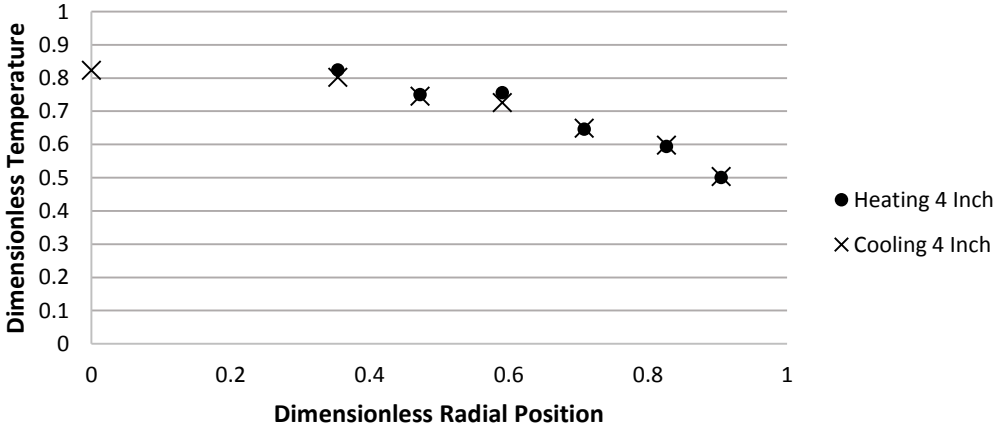

Air Flow 50% Cooling Re=982 and Heating Re=1139 Bed Height 6 Inches

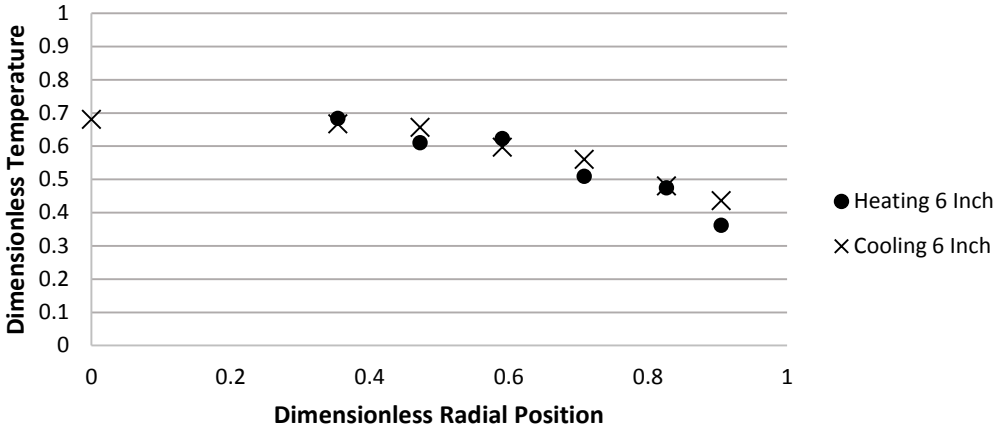

Air Flow 50% Cooling Re=982 and Heating Re=1139 Bed Height 8 Inches

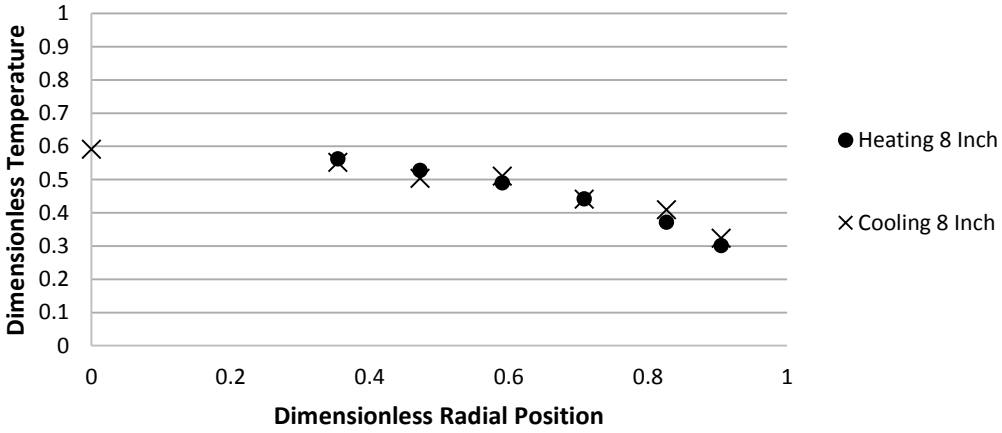

Air Flow 50% Cooling Re=982 and Heating Re=1139 Bed Height 10 Inches

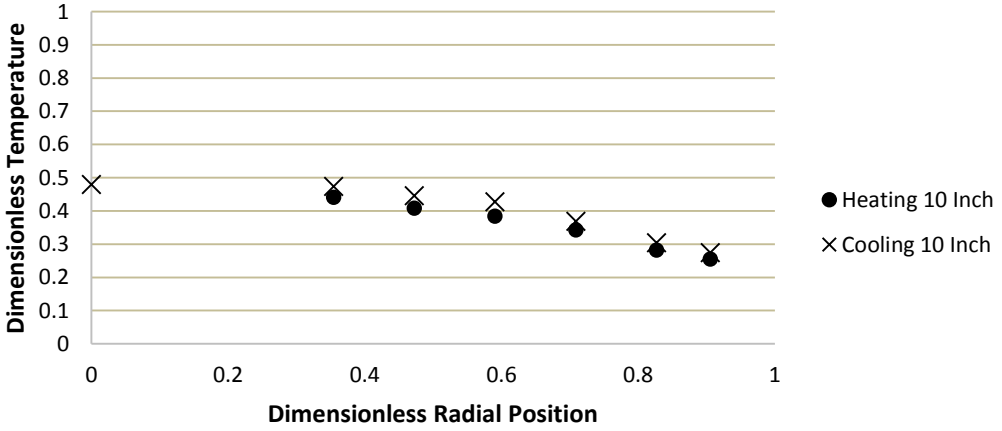

Simulation 1: Cooling Experimental versus CFD (N=5.33)

Air Flow 28% (Re=503) Bed Height 4 Inches

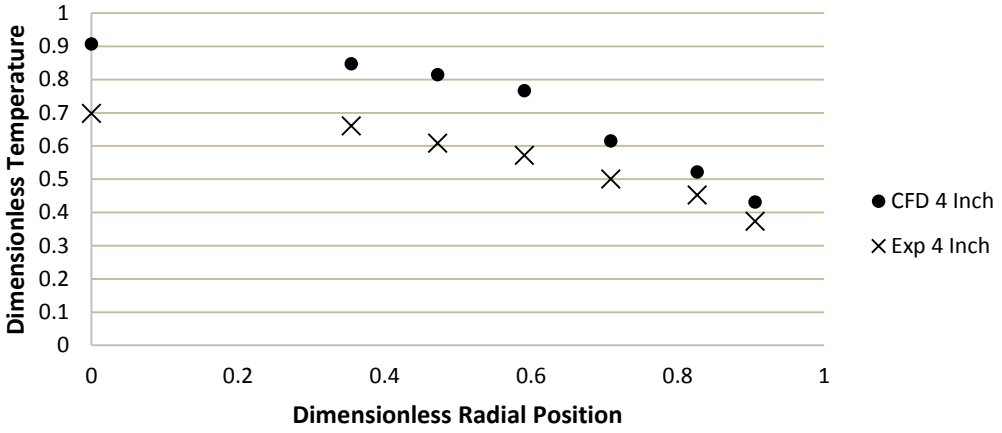

Air Flow 28% (Re=503) Bed Height 6 Inches

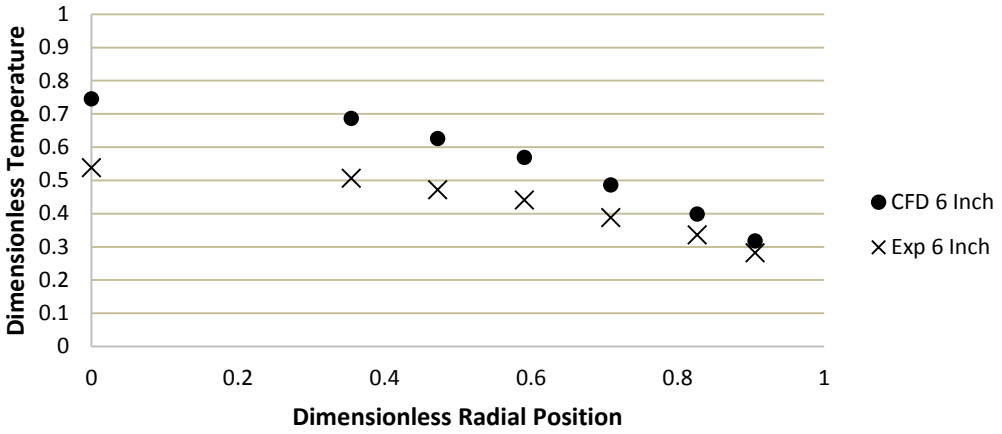

Air Flow 28% (Re=503) Bed Height 8 Inches

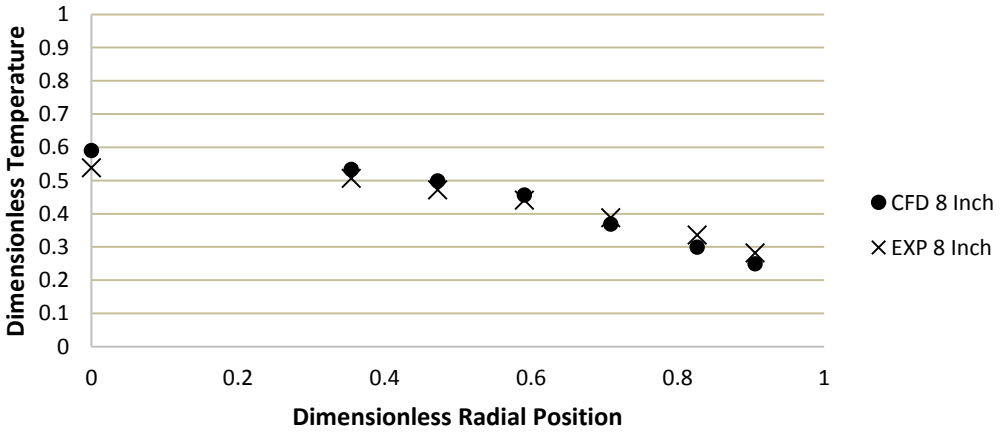

Air Flow 28% (Re=503) Bed Height 10 Inches

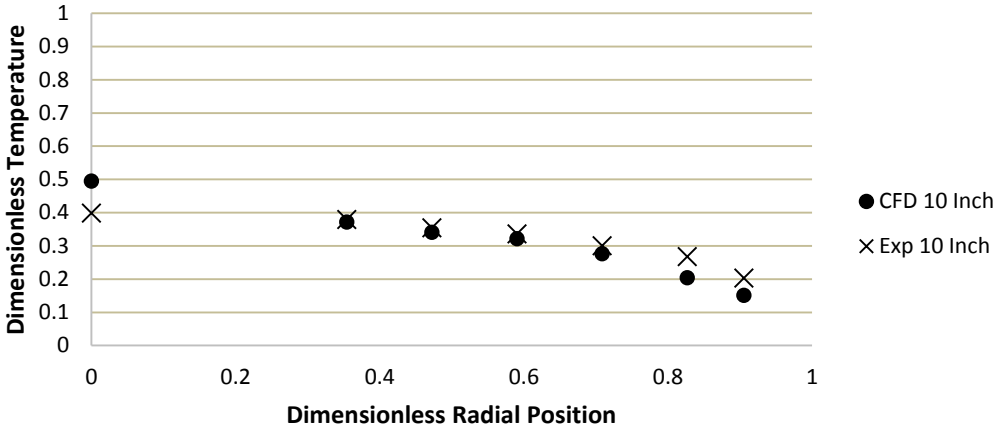

Air Flow 32% (Re=588) Bed Height 4 Inches

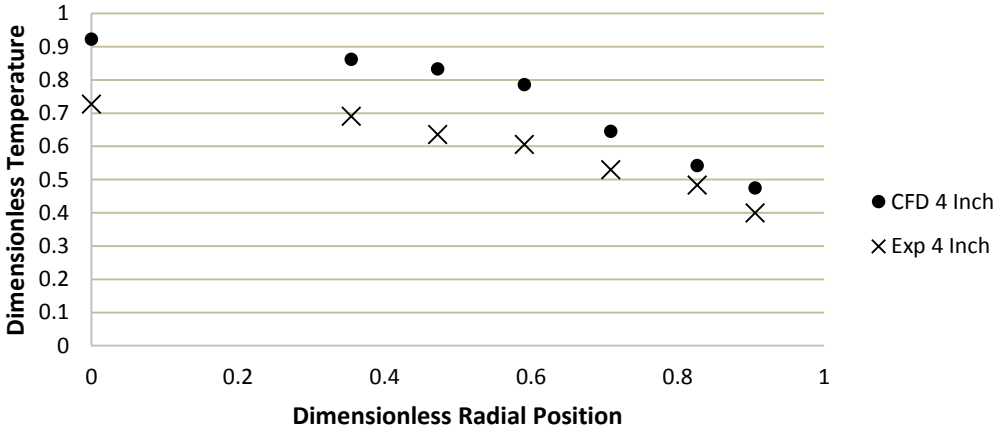

Air Flow 32% (Re=588) Bed Height 6 Inches

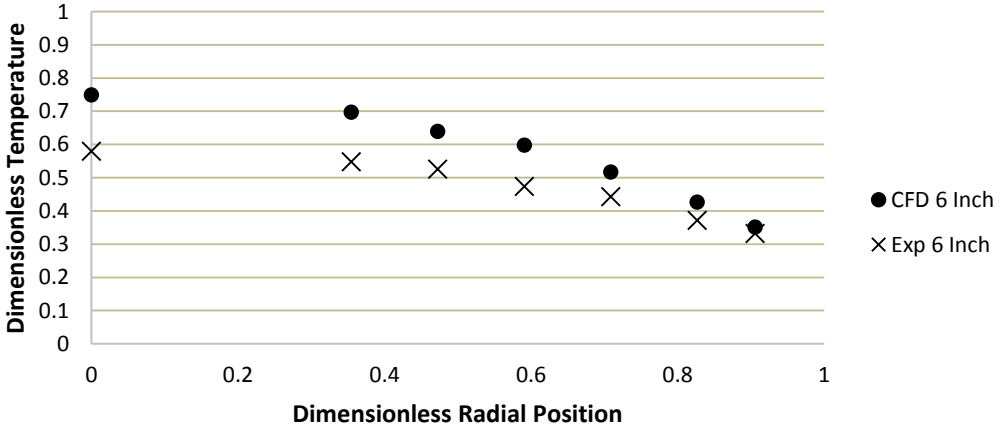

Air Flow 32% (Re=588) Bed Height 8 Inches

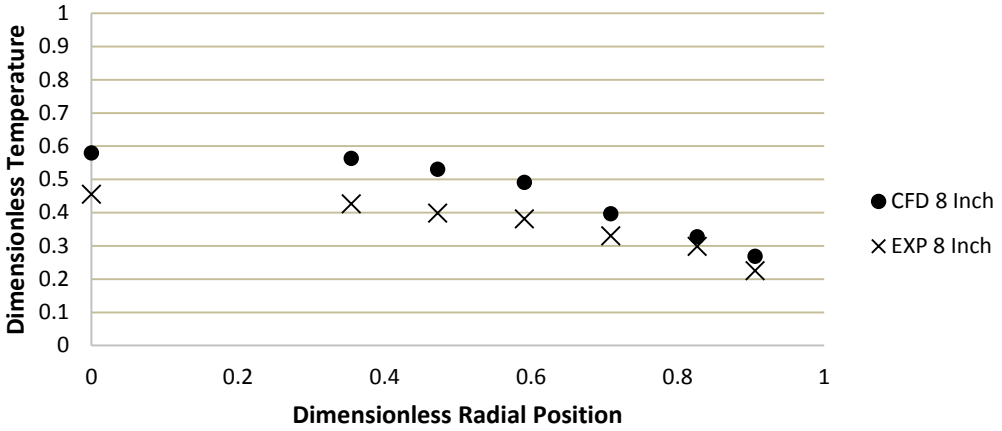

Air Flow 32% (Re=588) Bed Height 10 Inches

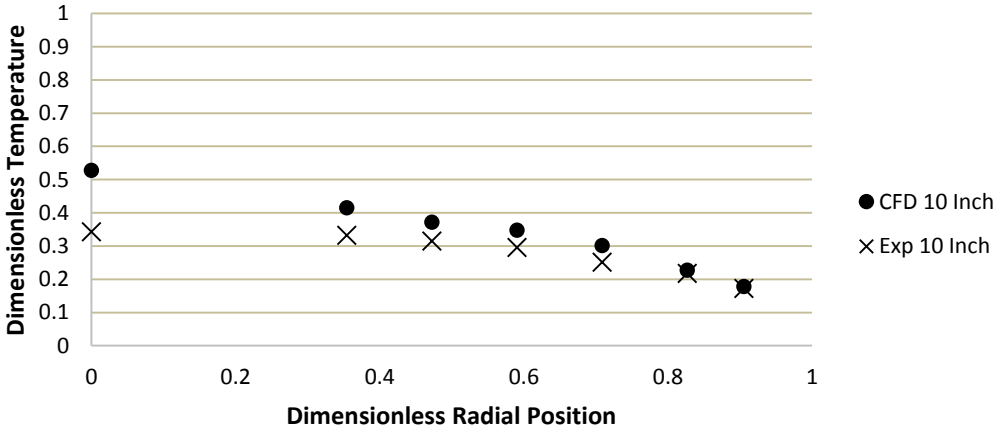

Air Flow 35% (Re=658) Bed Height 6 Inches

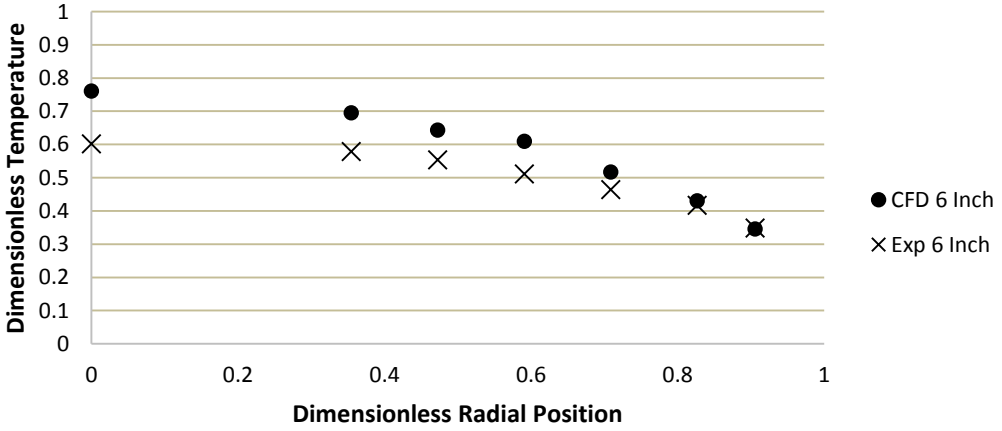

Air Flow 35% (Re=658) Bed Height 8 Inches

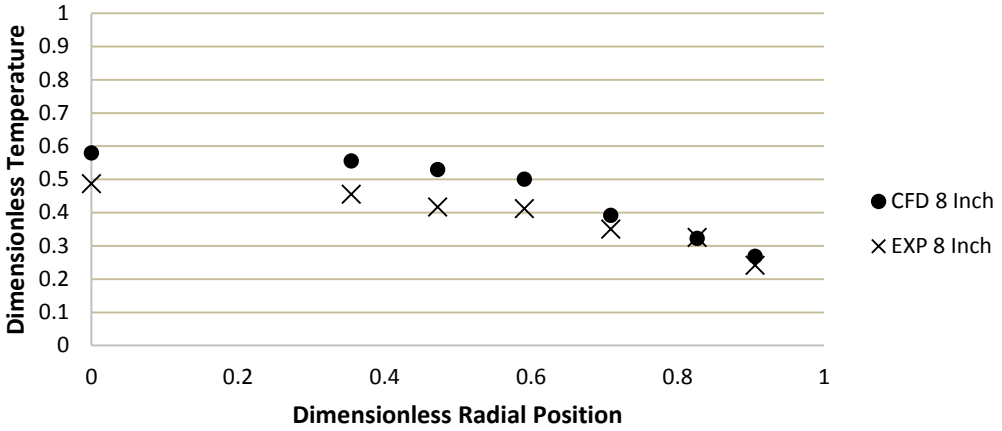

Air Flow 35% (Re=658) Bed Height 10 Inches

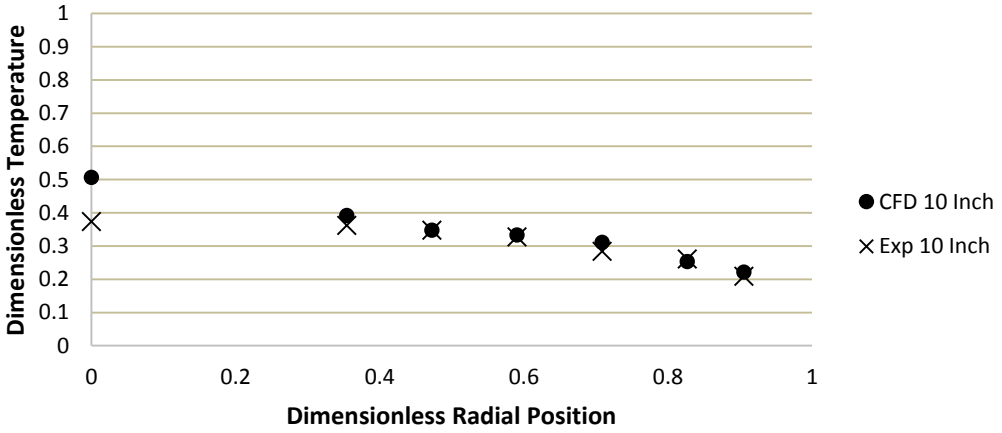

Air Flow 40% (Re=775) Bed Height 4 Inches

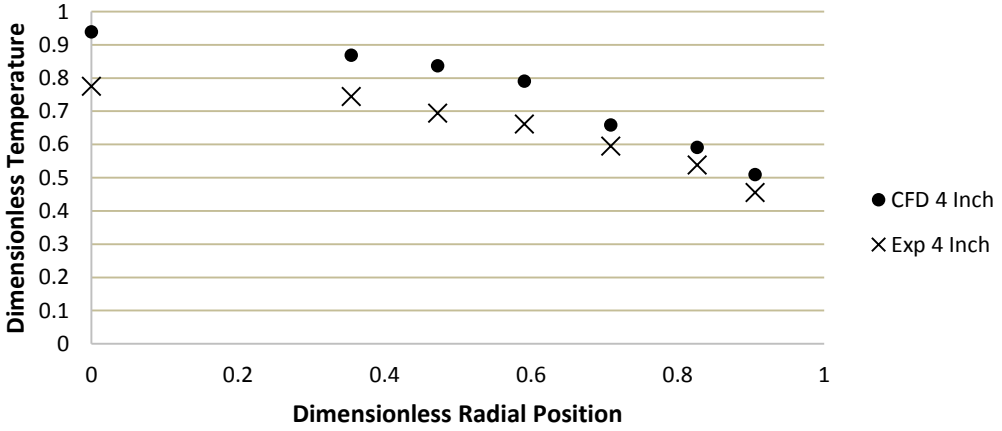

Air Flow 40% (Re=775) Bed Height 6 Inches

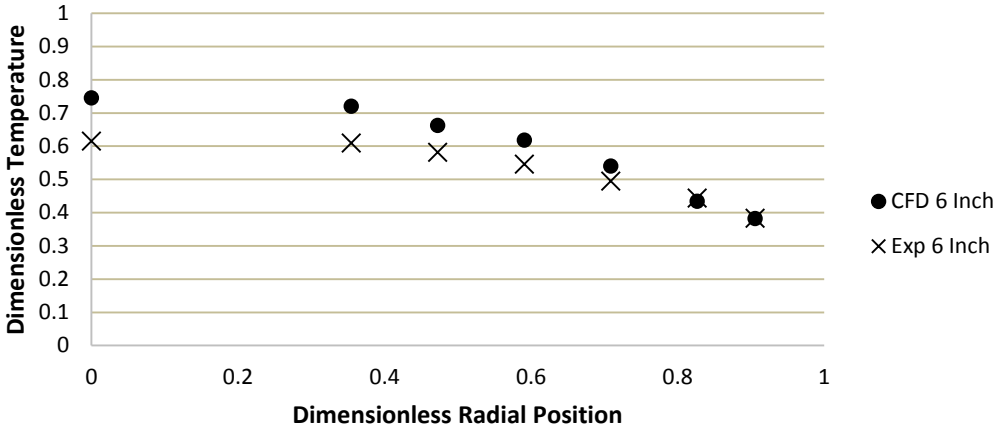

Air Flow 40% (Re=775) Bed Height 8 Inches

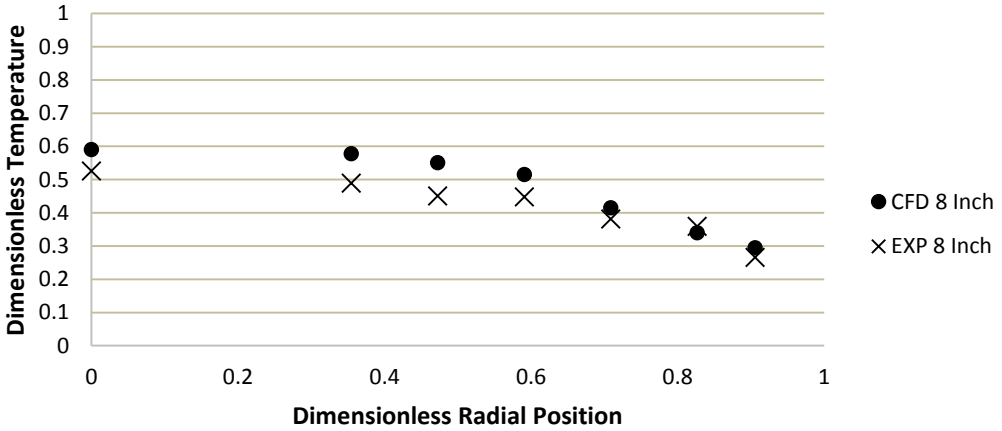

Air Flow 40% (Re=775) Bed Height 10 Inches

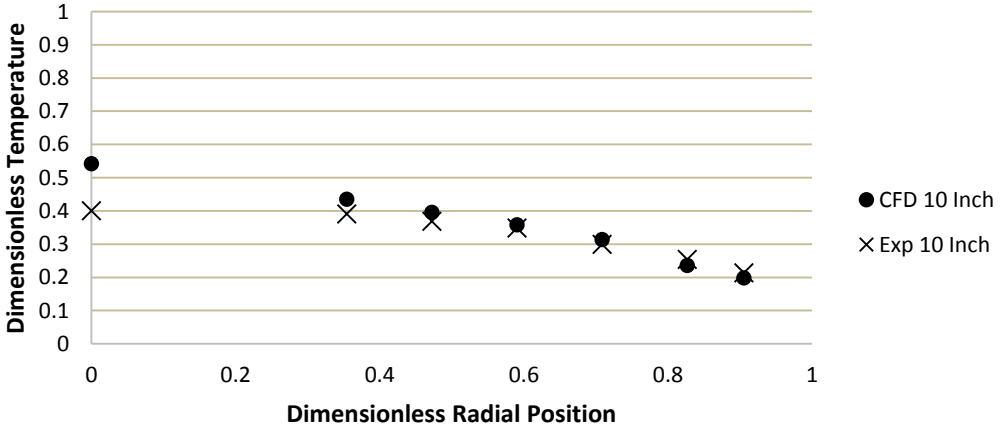

Air Flow 45% (Re=876) Bed Height 4 Inches

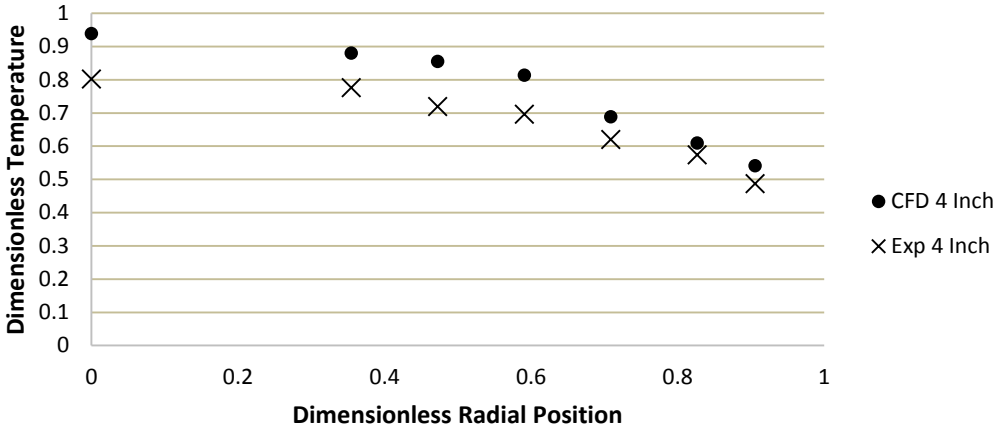

Air Flow 45% (Re=876) Bed Height 6 Inches

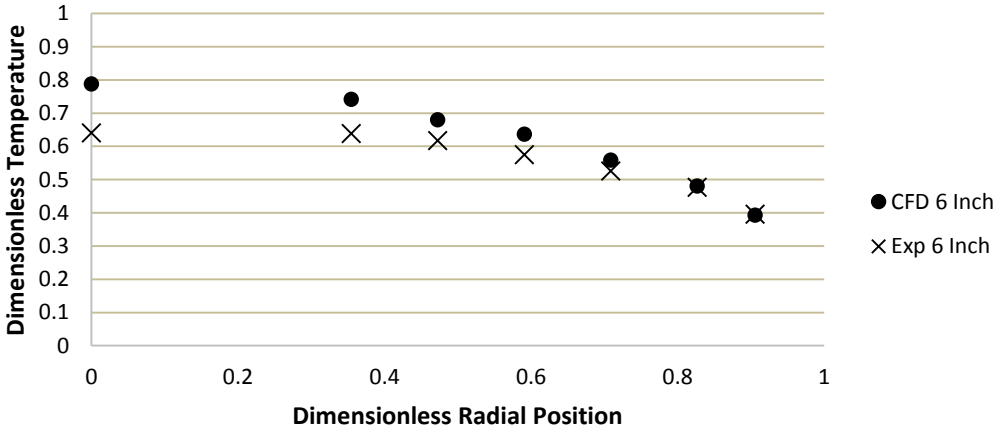

Air Flow 45% (Re=876) Bed Height 8 Inches

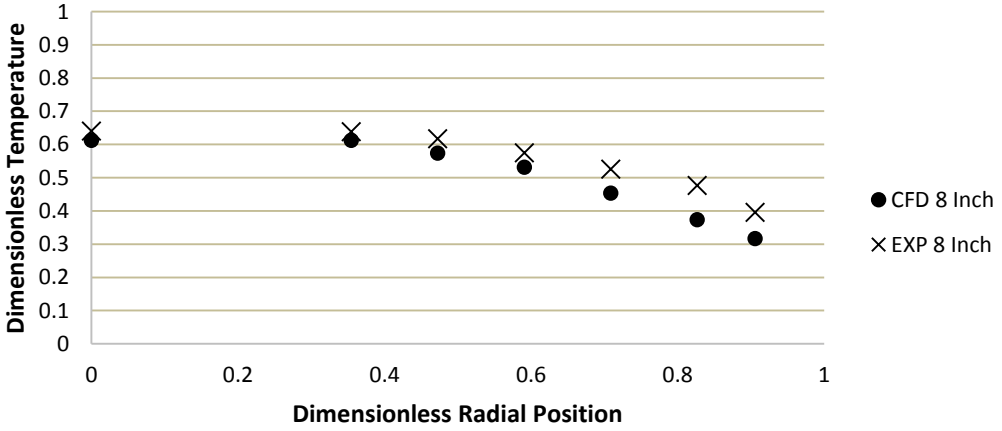

Air Flow 45% (Re=876) Bed Height 10 Inches

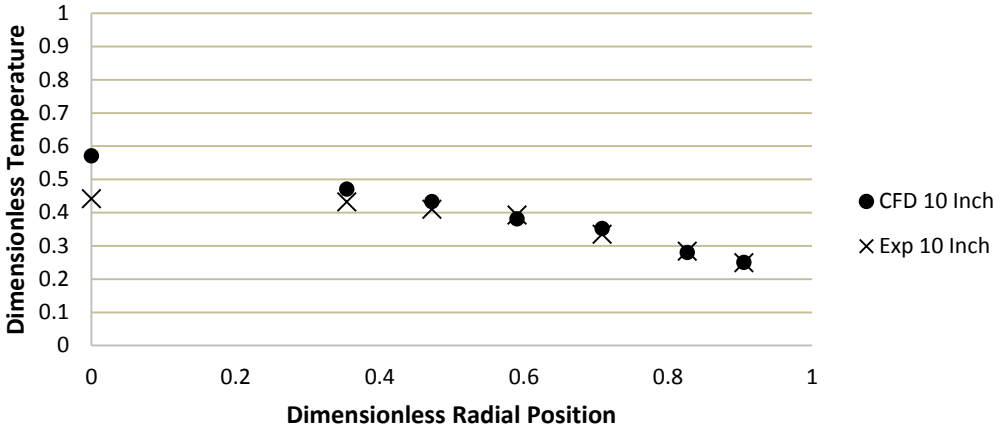

Air Flow 50% (Re=982) Bed Height 4 Inches

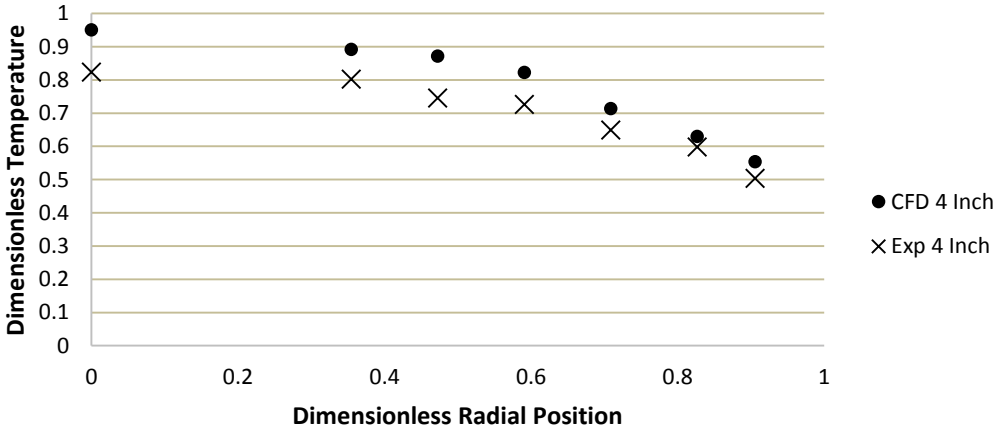

Air Flow 50% (Re=982) Bed Height 6 Inches

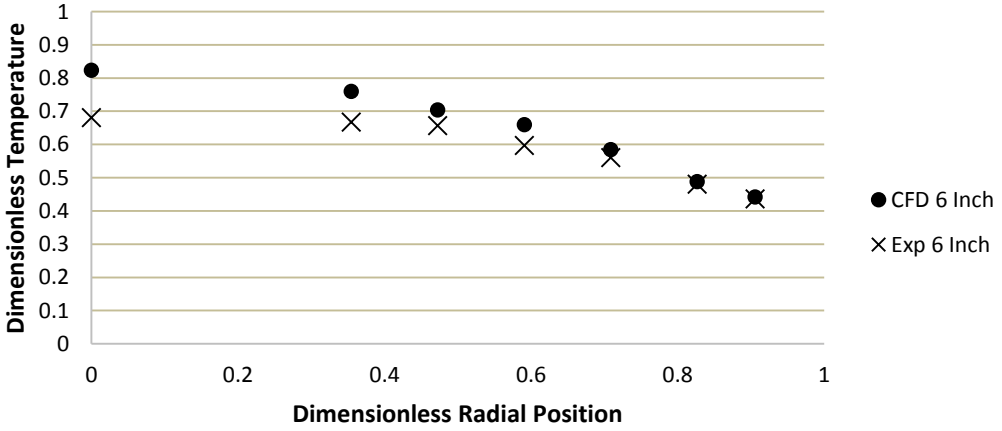

Air Flow 50% (Re=982) Bed Height 8 Inches

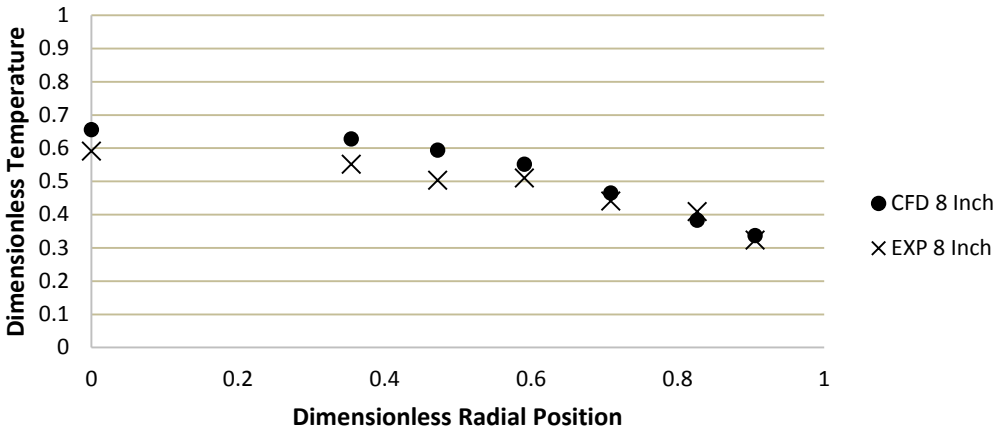

Air Flow 50% (Re=982) Bed Height 10 Inches

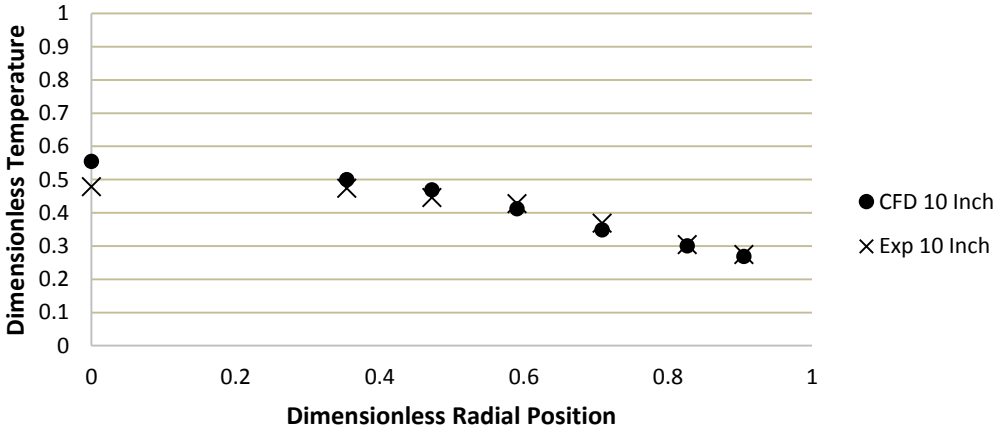

Simulation 1: Heating Experimental versus CFD (N=5.33)

Air Flow 28% Experimental Re= 630 and CFD Re= 689 Bed Height 4 Inches

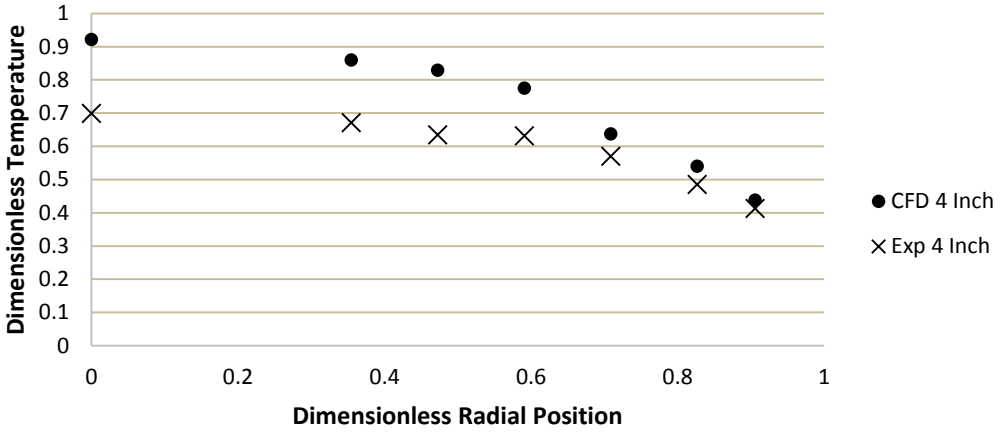

Air Flow 28% Experimental Re= 630 and CFD Re= 689 Bed Height 6 Inches

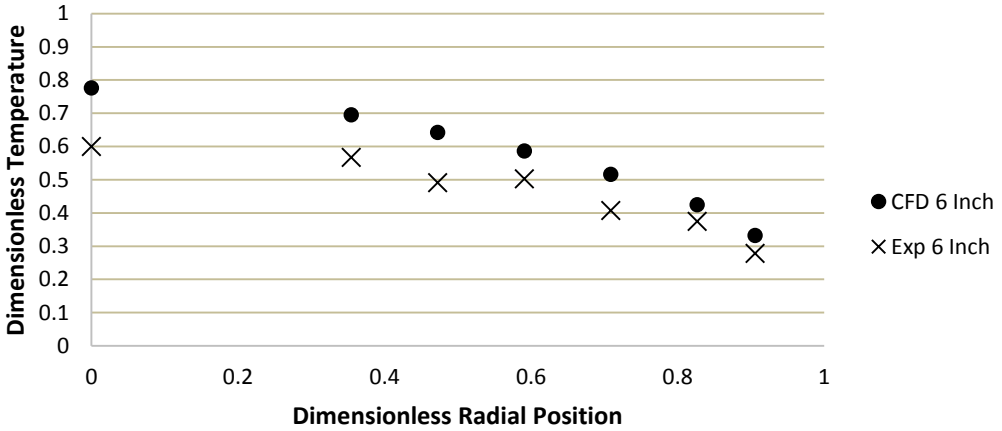

Air Flow 28% Experimental Re= 630 and CFD Re= 689 Bed Height 8 Inches

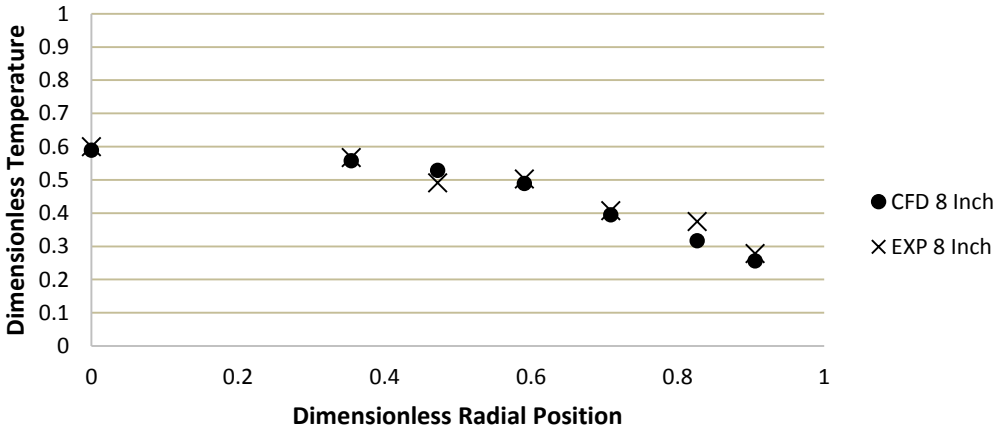

Air Flow 28% Experimental Re= 630 and CFD Re= 689 Bed Height 10 Inches

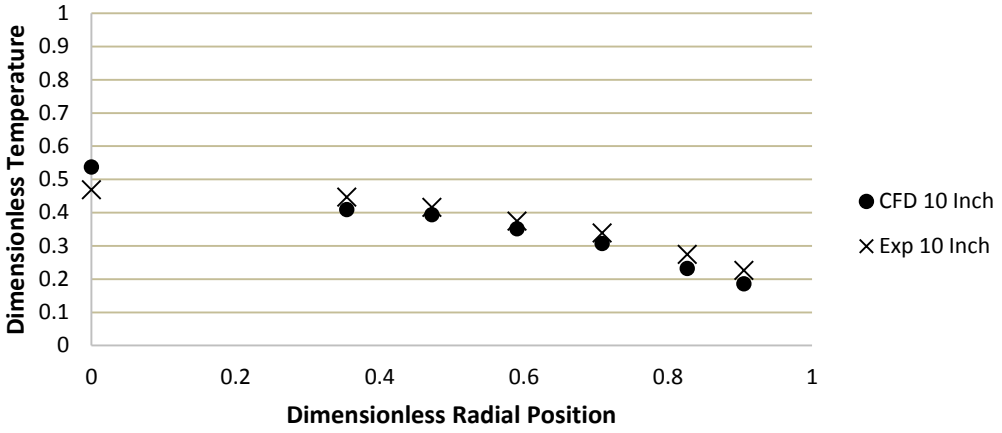

Air Flow 32% Experimental Re =702 and CFD Re=805 Bed Height 4 Inches

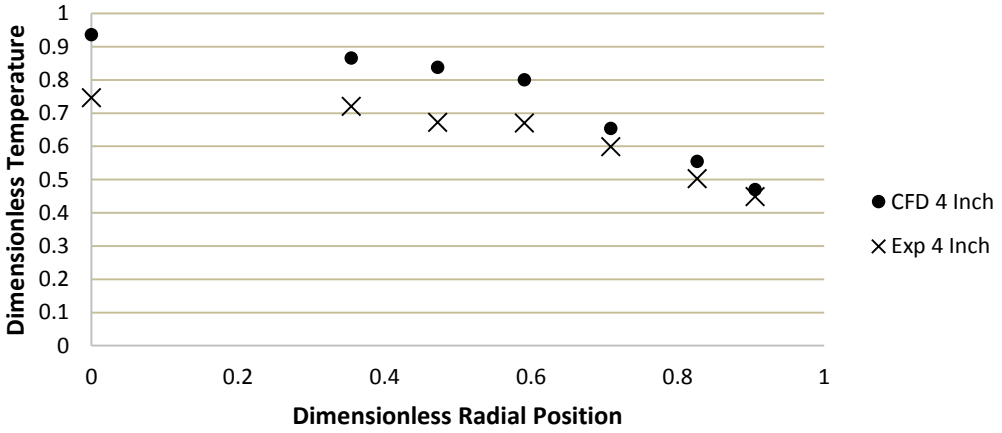

Air Flow 32% Experimental Re =702 and CFD Re=805 Bed Height 6 Inches

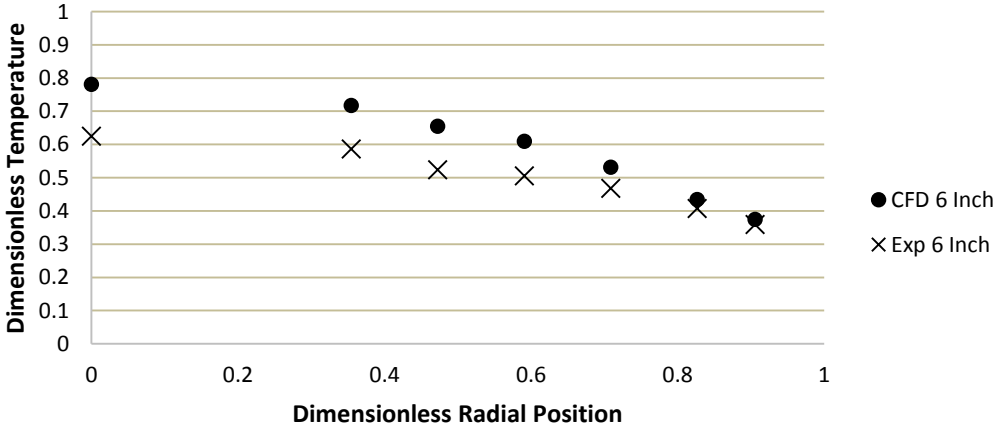

Air Flow 32% Experimental Re =702 and CFD Re=805 Bed Height 8 Inches

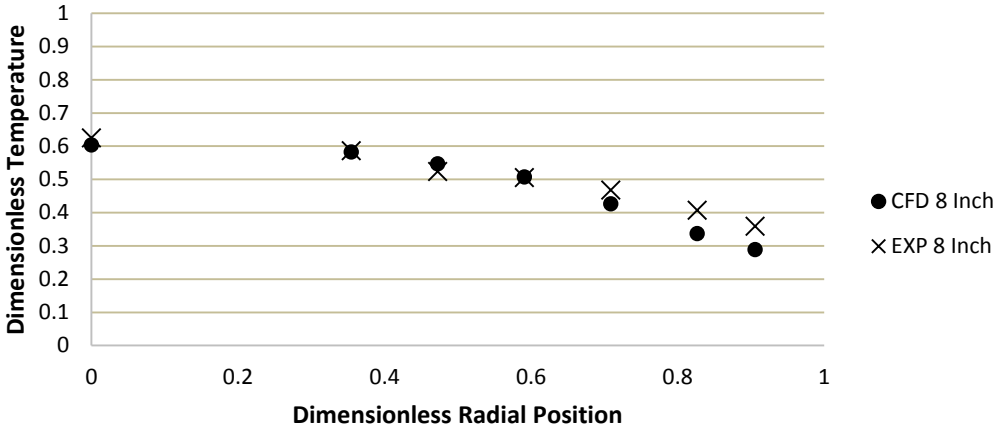

Air Flow 32% Experimental Re =702 and CFD Re=805 Bed Height 10 Inches

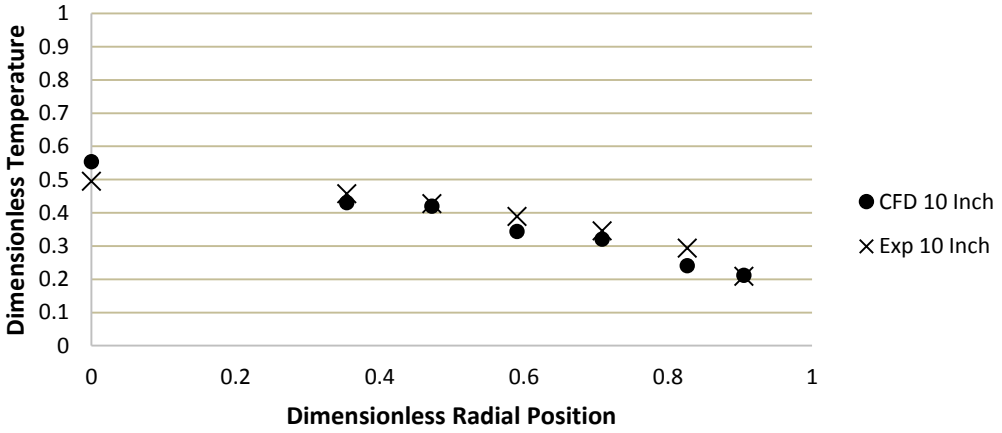

Air Flow 35% Experimental Re =789 and CFD Re=798 Bed Height 6 Inches

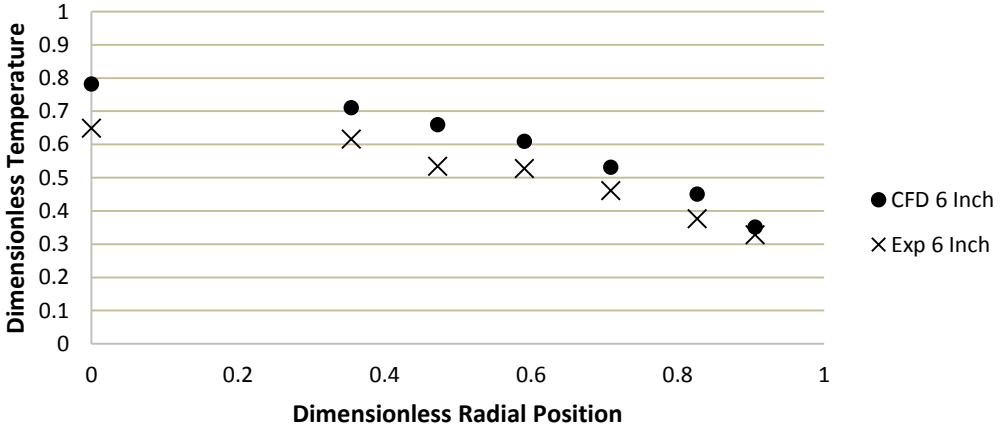

Air Flow 35% Experimental Re =789 and CFD Re=798 Bed Height 8 Inches

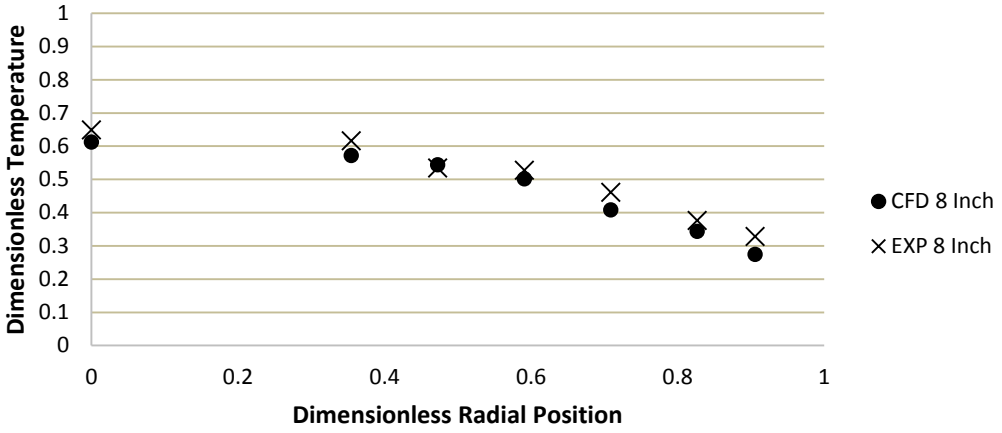

Air Flow 35% Experimental Re =789 and CFD Re=798 Bed Height 10 Inches

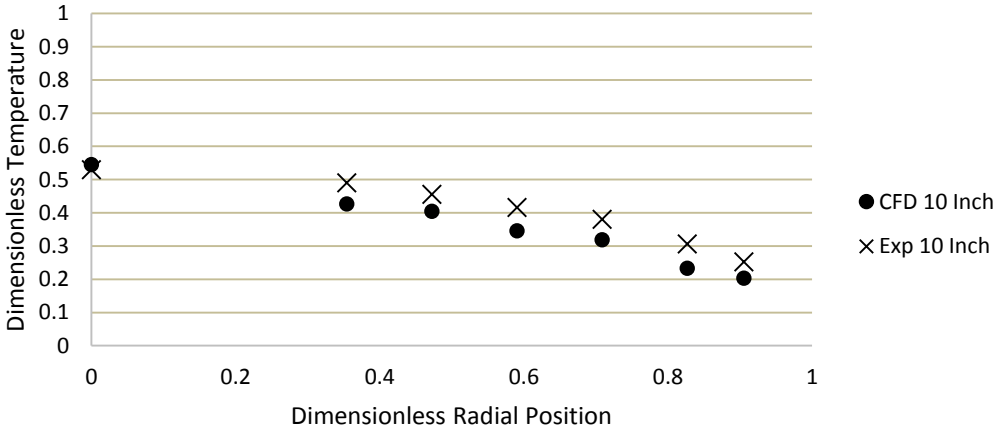

Air Flow 40% Experimental Re =901 and CFD Re=901 Bed Height 4 Inches

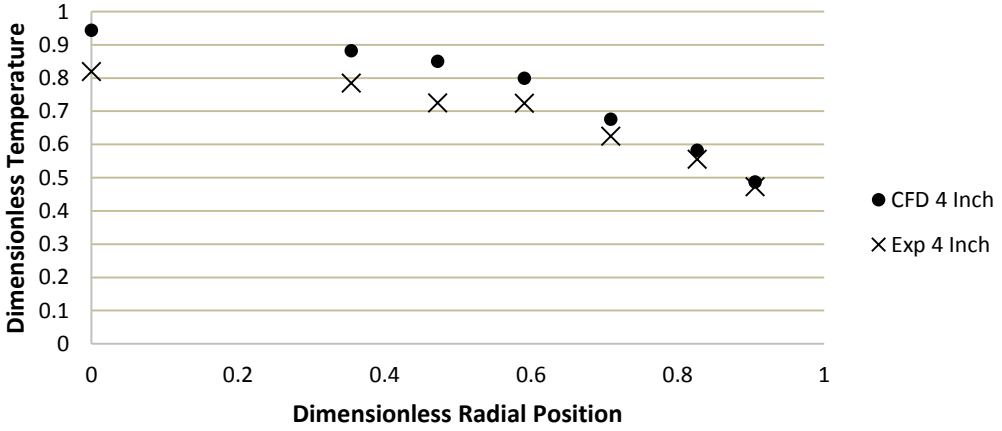

Air Flow 40% Experimental Re =901 and CFD Re=901 Bed Height 6 Inches

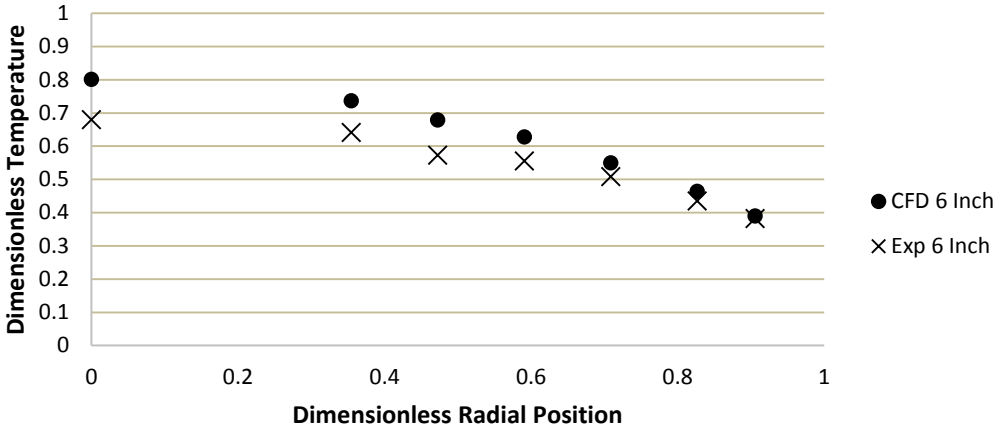

Air Flow 40% Experimental Re =901 and CFD Re=901 Bed Height 8 Inches

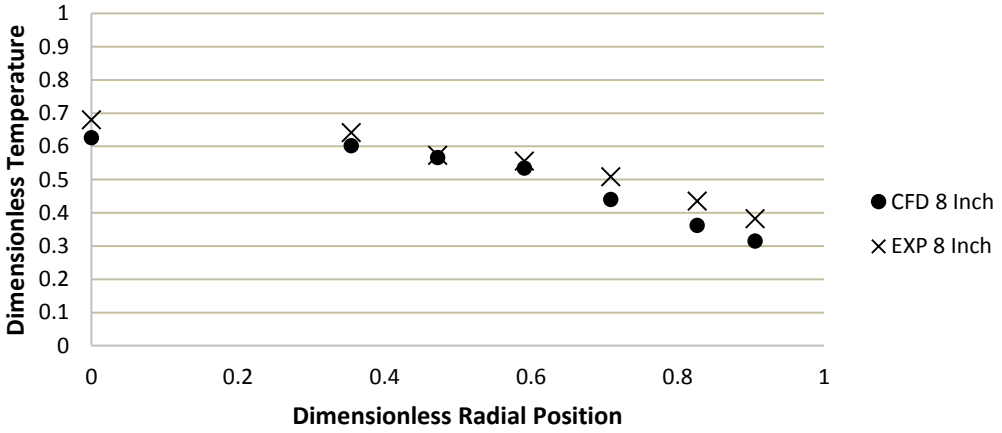

Air Flow 40% Experimental Re =901 and CFD Re=901 Bed Height 10 Inches

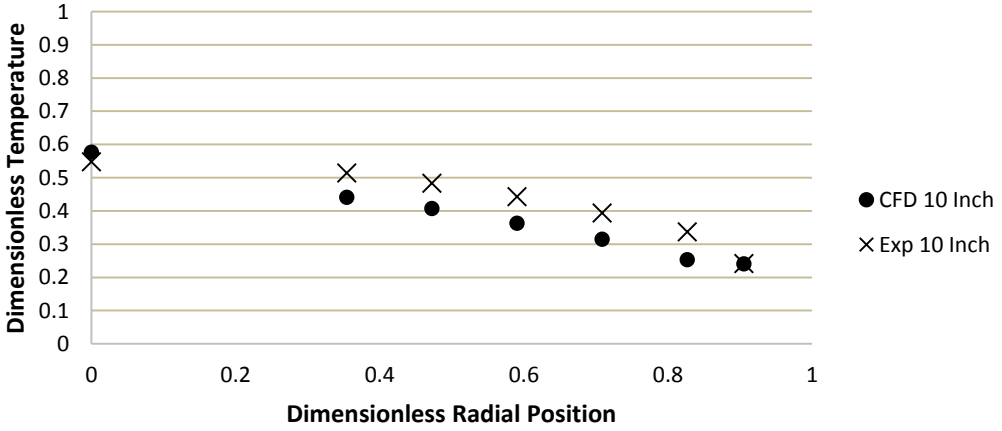

Air Flow 45% Experimental Re =1018 and CFD Re=1022 Bed Height 4 Inches

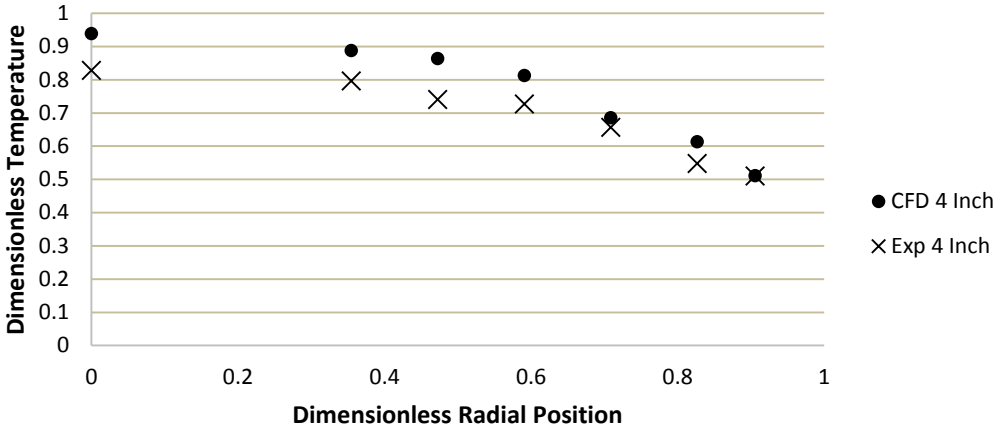

Air Flow 45% Experimental Re =1018 and CFD Re=1022 Bed Height 6 Inches

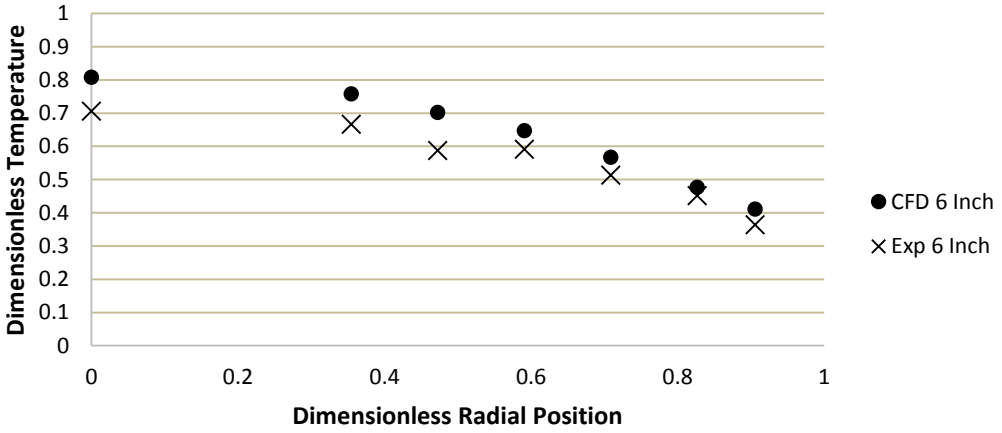

Air Flow 45% Experimental Re =1018 and CFD Re=1022 Bed Height 8 Inches

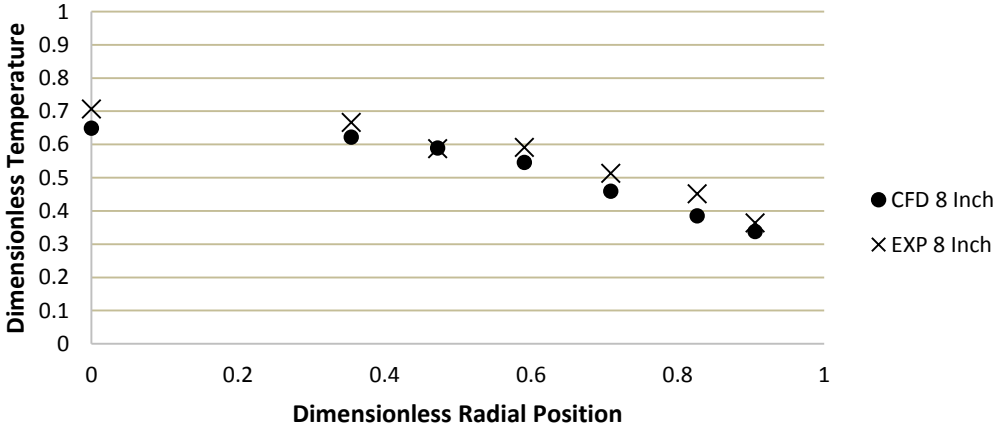

Air Flow 45% Experimental Re =1018 and CFD Re=1022 Bed Height 10 Inches

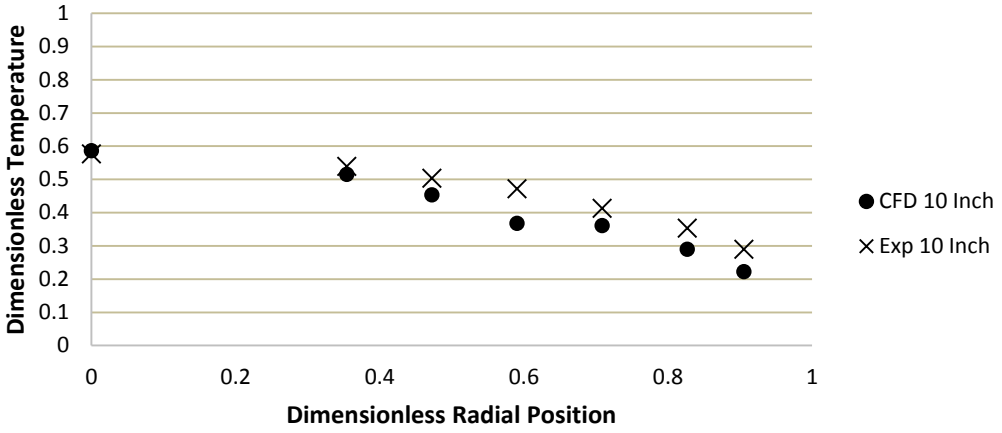

Air Flow 50% Experimental Re =1139 and CFD Re=1141 Bed Height 4 Inches

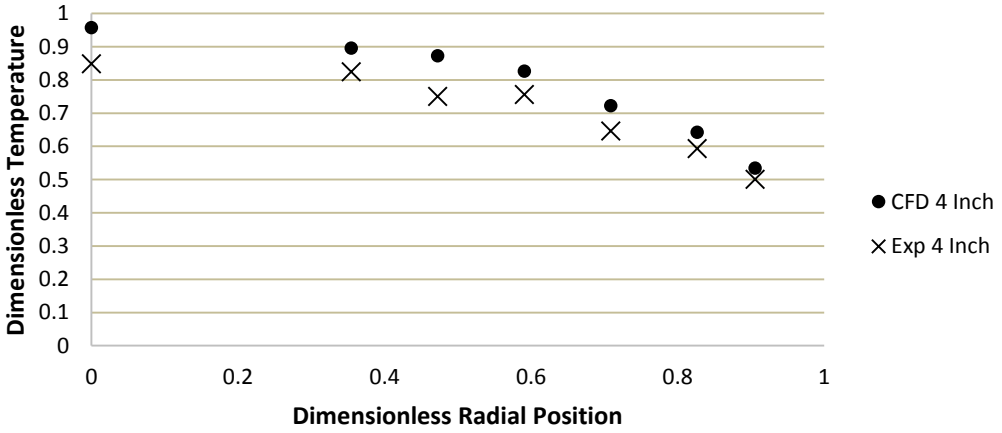

Air Flow 50% Experimental Re =1139 and CFD Re=1141 Bed Height 6 Inches

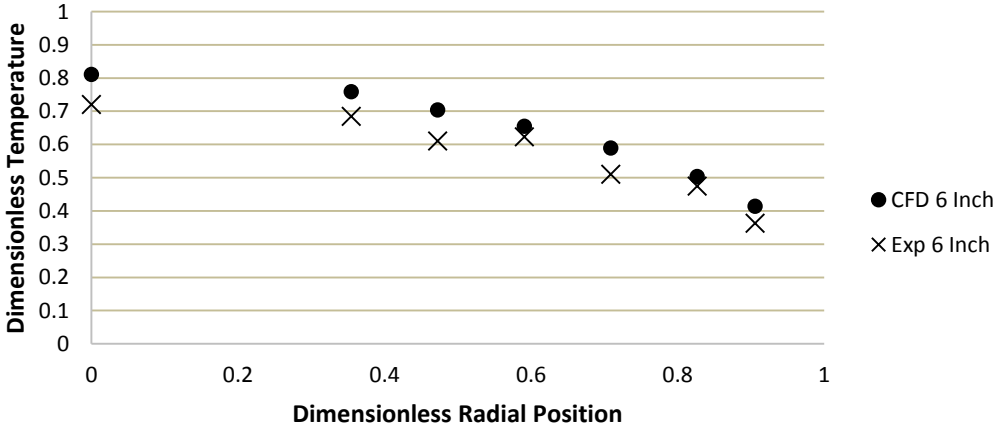

Air Flow 50% Experimental Re =1139 and CFD Re=1141 Bed Height 8 Inches

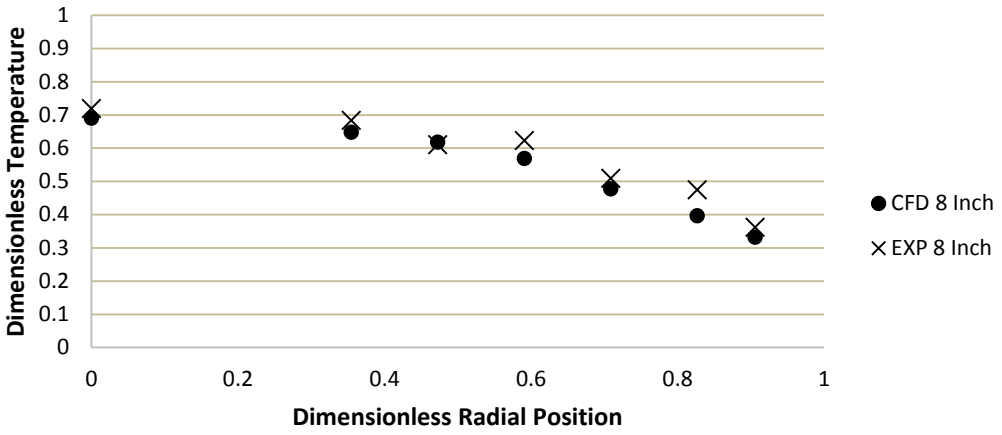

Air Flow 50% Experimental Re =1139 and CFD Re=1141 Bed Height 10 Inches

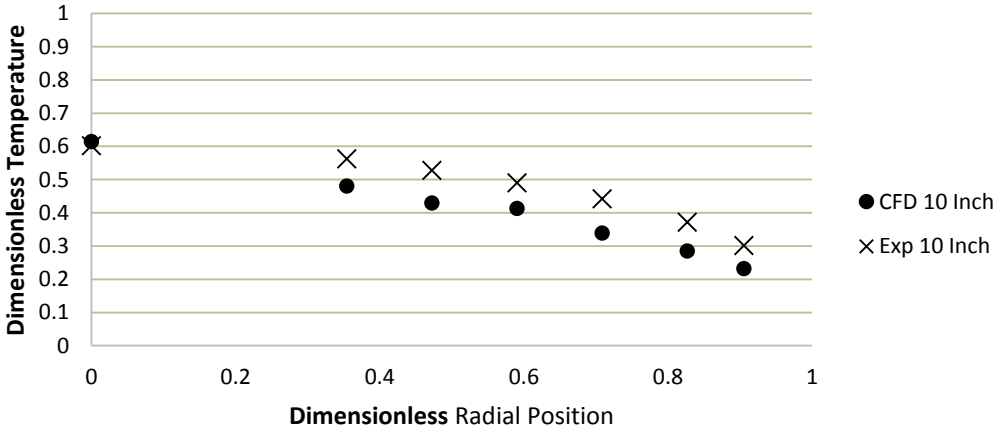

Simulation 1: CFD Heating versus Cooling

Air Flow 28% CFD Cooling Re=503 and Heating Re=689 Bed Height 4 Inches

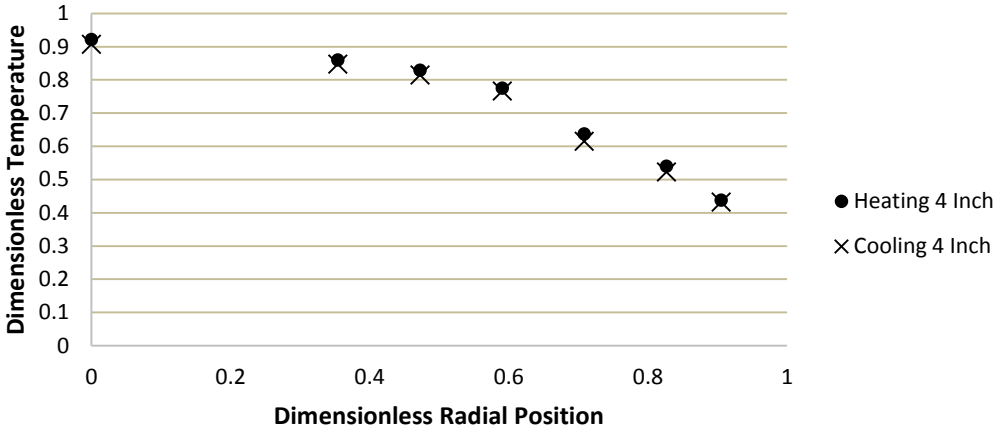

Air Flow 28% CFD Cooling Re=503 and Heating Re=689 Bed Height 6 Inches

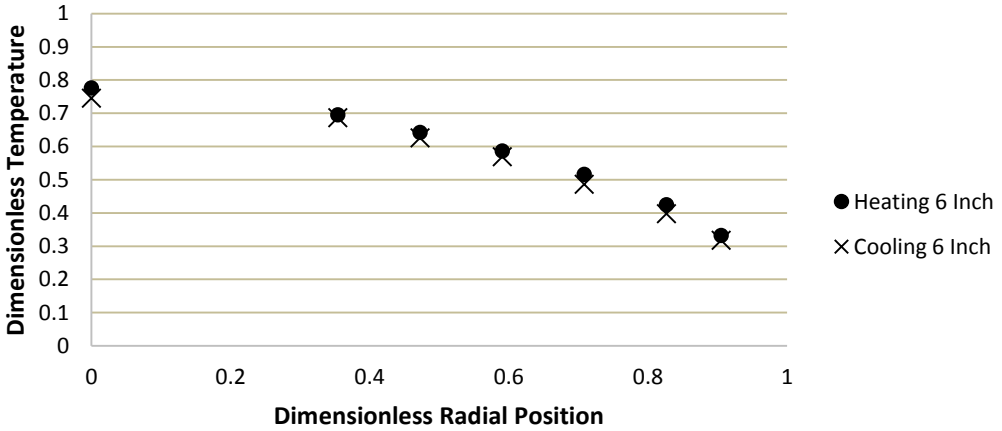

Air Flow 28% CFD Cooling Re=503 and Heating Re=689 Bed Height 8 Inches

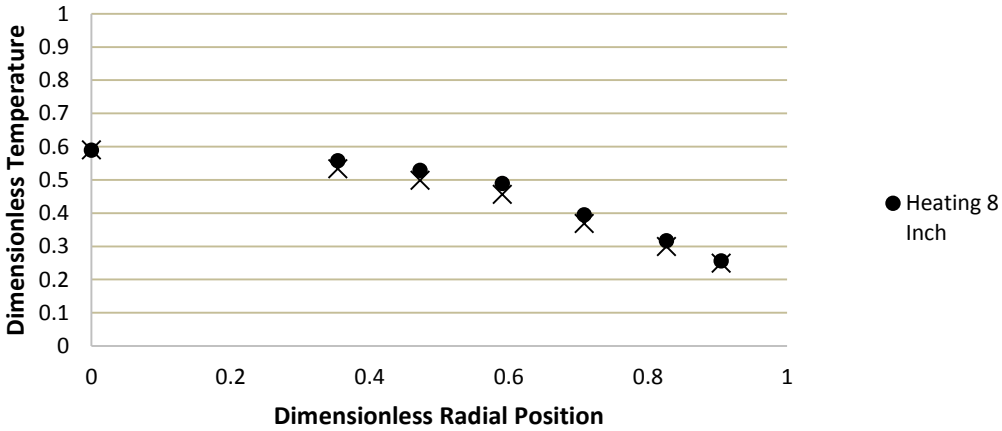

Air Flow 28% CFD Cooling Re=503 and Heating Re=689 Bed Height 10 Inches

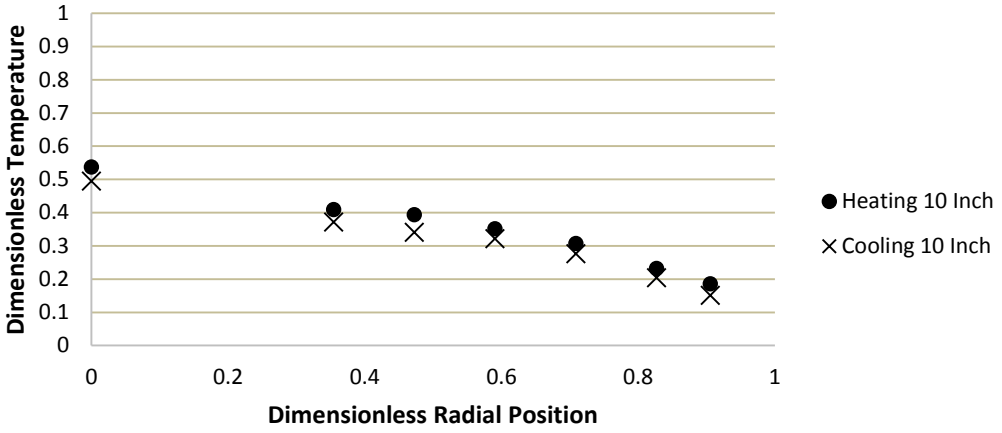

Air Flow 32% CFD Cooling Re=588 and Heating Re=805 Bed Height 4 Inches

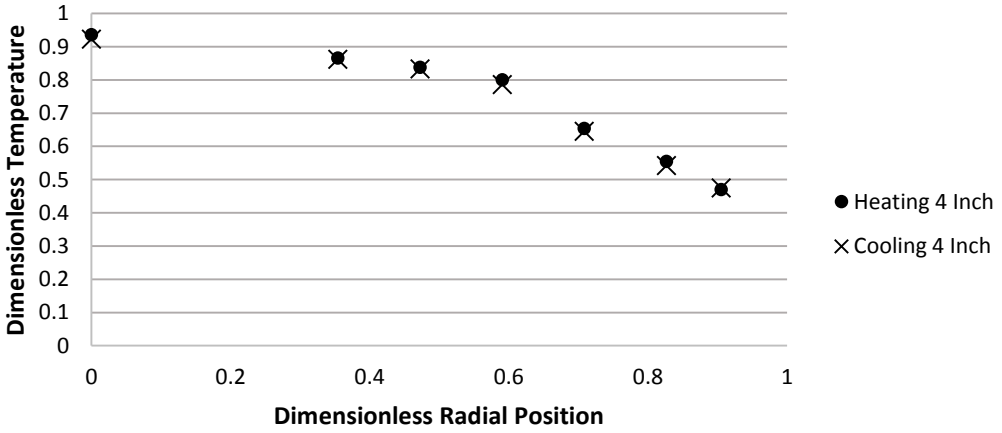

Air Flow 32% CFD Cooling Re=588 and Heating Re=805 Bed Height 6 Inches

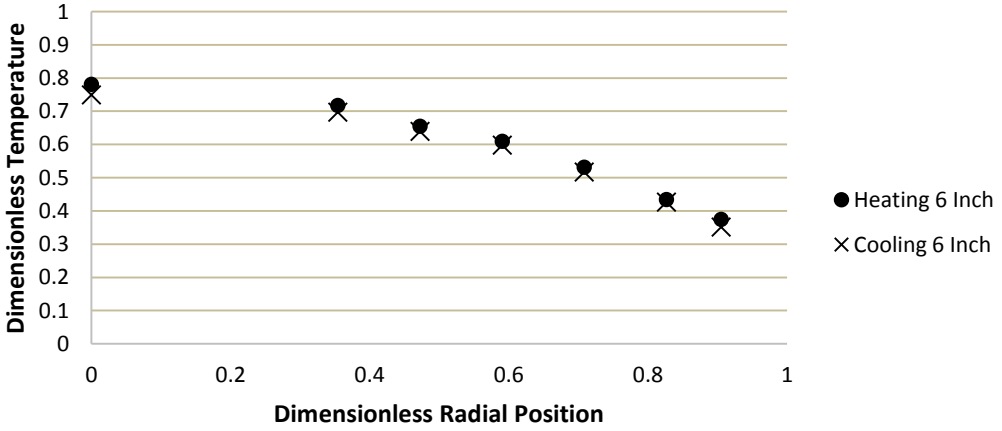

Air Flow 32% CFD Cooling Re=588 and Heating Re=805 Bed Height 8 Inches

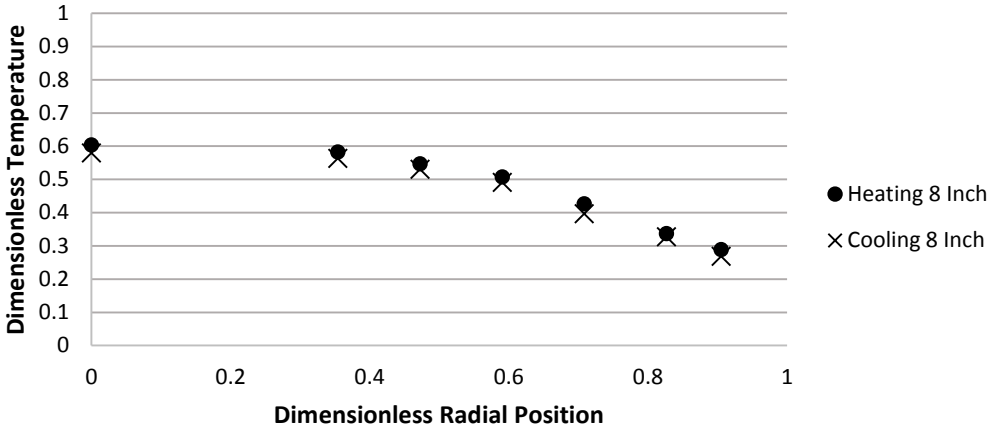

Air Flow 32% CFD Cooling Re=588 and Heating Re=805 Bed Height 10 Inches

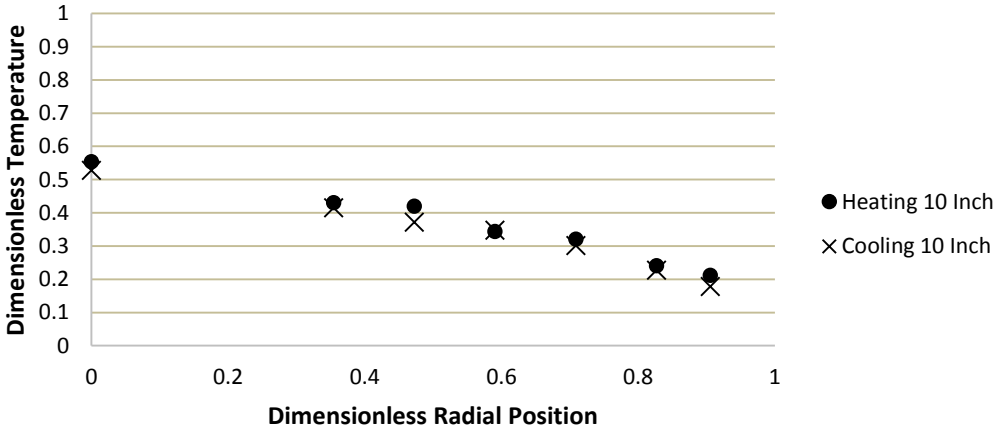

Air Flow 35% CFD Cooling Re=658 and Heating Re=798 Bed Height 6 Inches

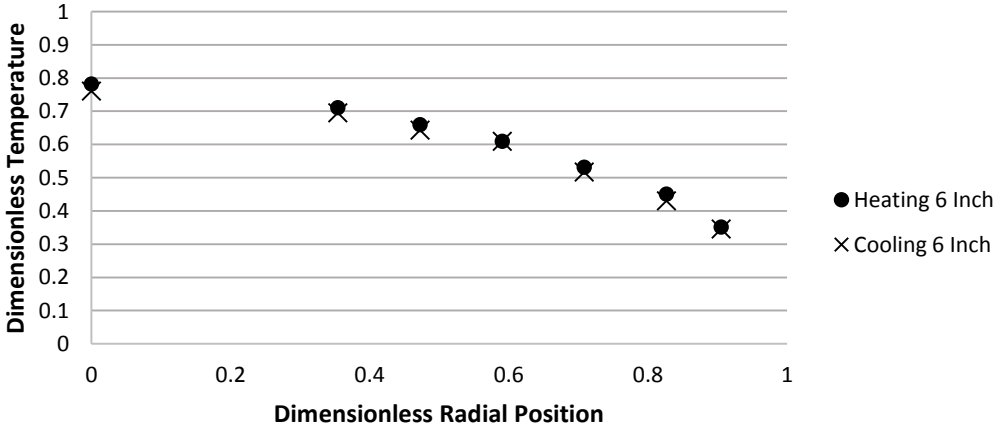

Air Flow 35% CFD Cooling Re=658 and Heating Re=798 Bed Height 8 Inches

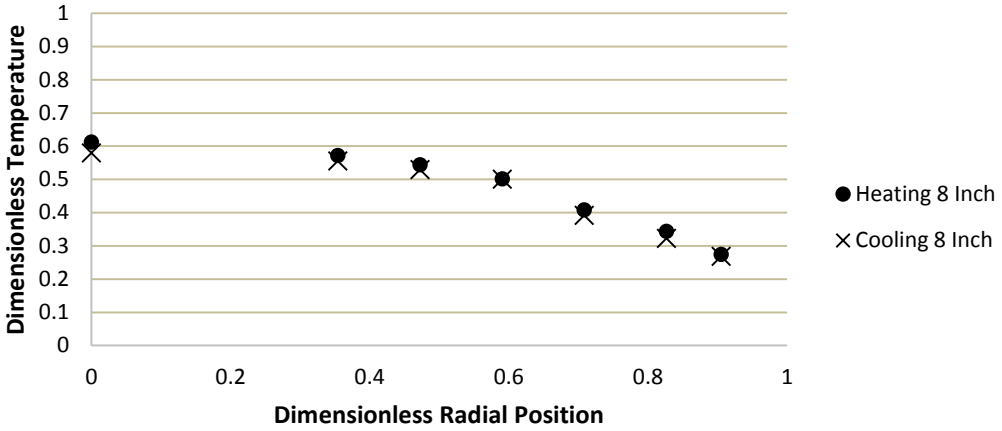

Air Flow 35% CFD Cooling Re=658 and Heating Re=798 Bed Height 10 Inches

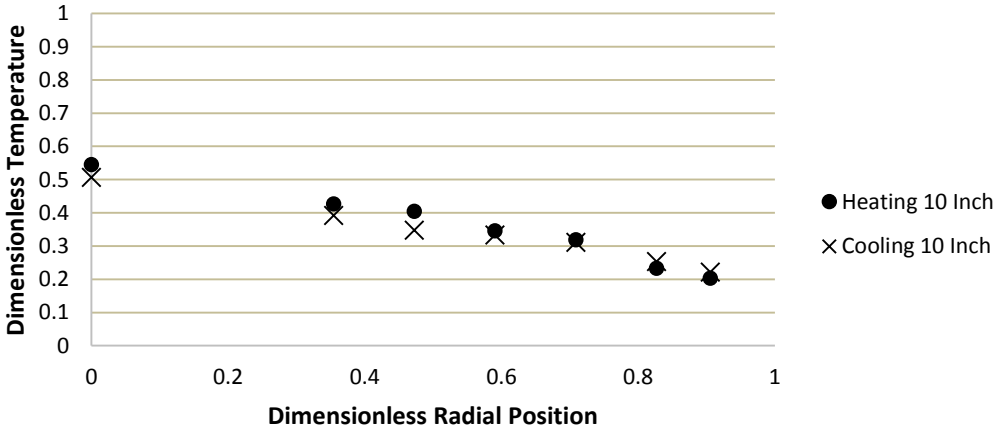

Air Flow 40% CFD Cooling Re=775 and Heating Re=901 Bed Height 4 Inches

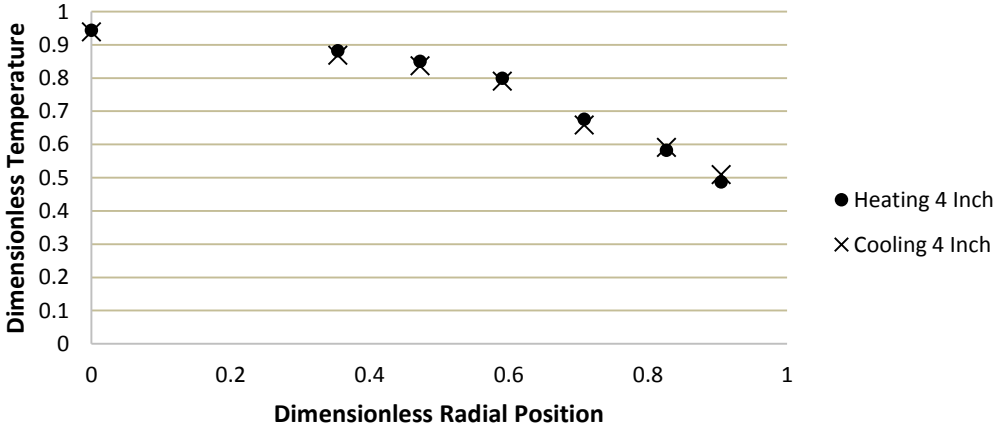

Air Flow 40% CFD Cooling Re=775 and Heating Re=901 Bed Height 6 Inches

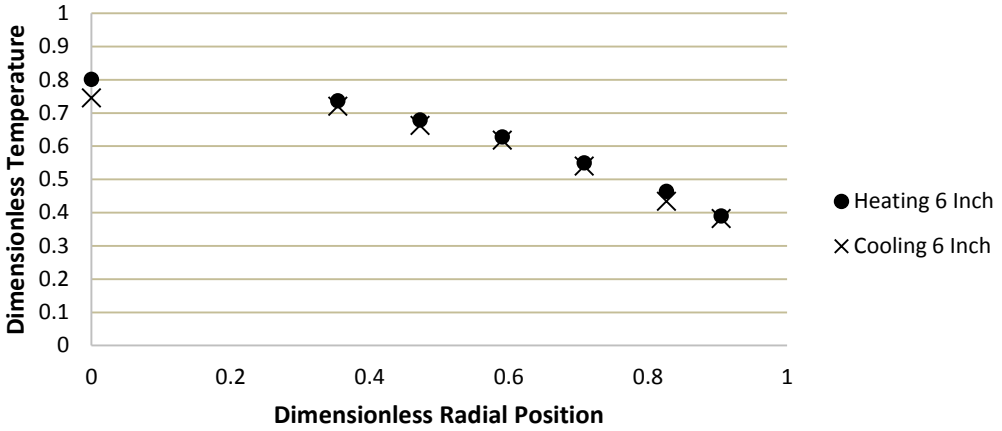

Air Flow 40% CFD Cooling Re=775 and Heating Re=901 Bed Height 8 Inches

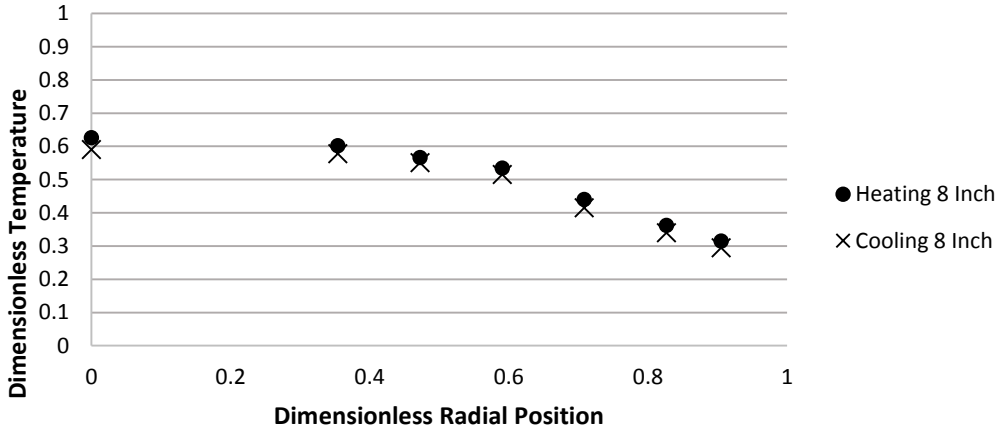

Air Flow 40% CFD Cooling Re=775 and Heating Re=901 Bed Height 10 Inches

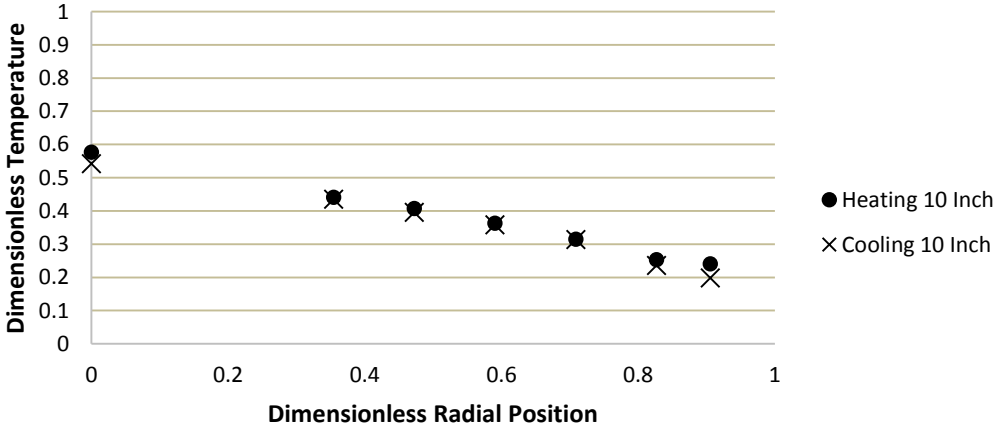

Air Flow 45% CFD Cooling Re=876 and Heating Re=1022 Bed Height 4 Inches

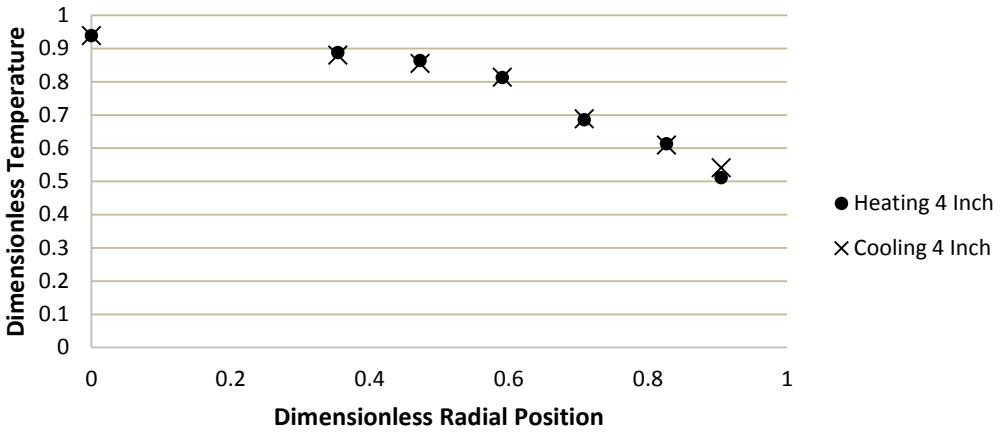

Air Flow 45% CFD Cooling Re=876 and Heating Re=1022 Bed Height 6 Inches

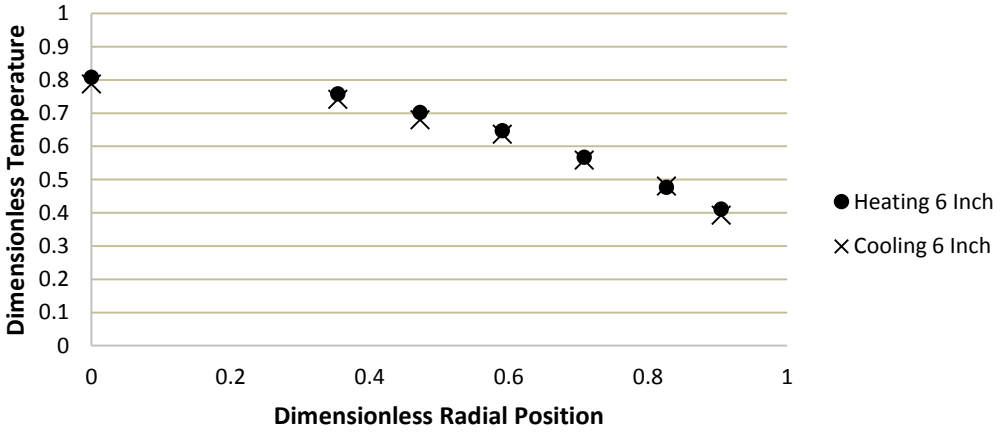

Air Flow 45% CFD Cooling Re=876 and Heating Re=1022 Bed Height 8 Inches

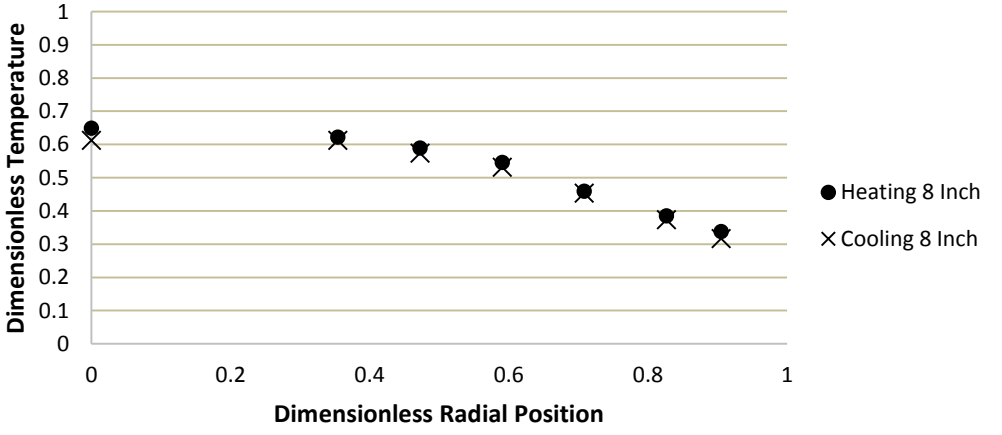

Air Flow 45% CFD Cooling Re=876 and Heating Re=1022 Bed Height 10 Inches

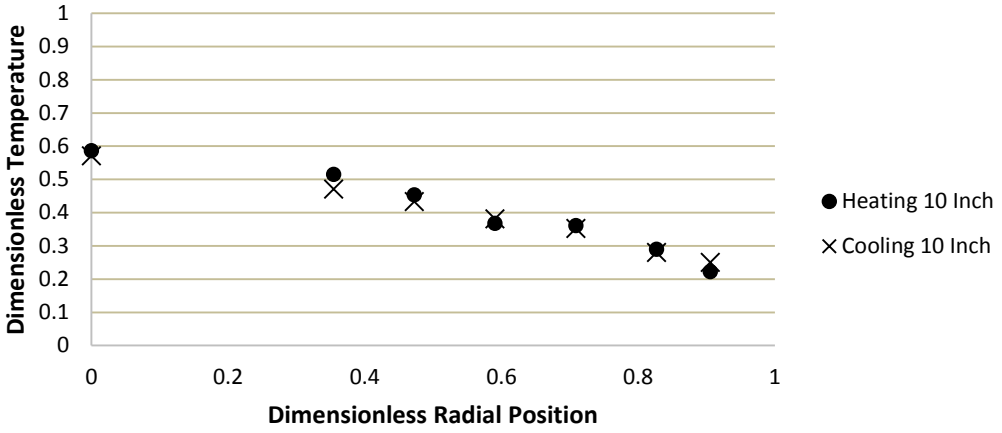

Air Flow 50% CFD Cooling Re=982 and Heating Re=1141 Bed Height 4 Inches

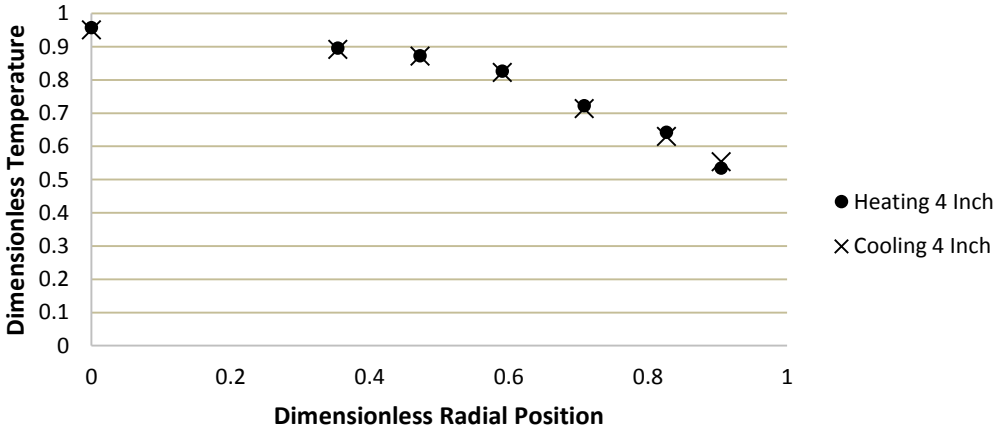

Air Flow 50% CFD Cooling Re=982 and Heating Re=1141 Bed Height 6 Inches

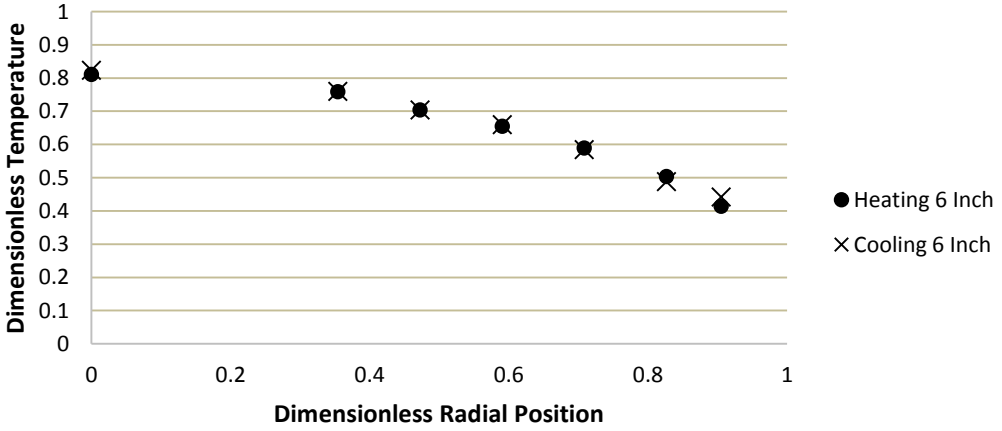

Air Flow 50% CFD Cooling Re=982 and Heating Re=1141 Bed Height 8 Inches

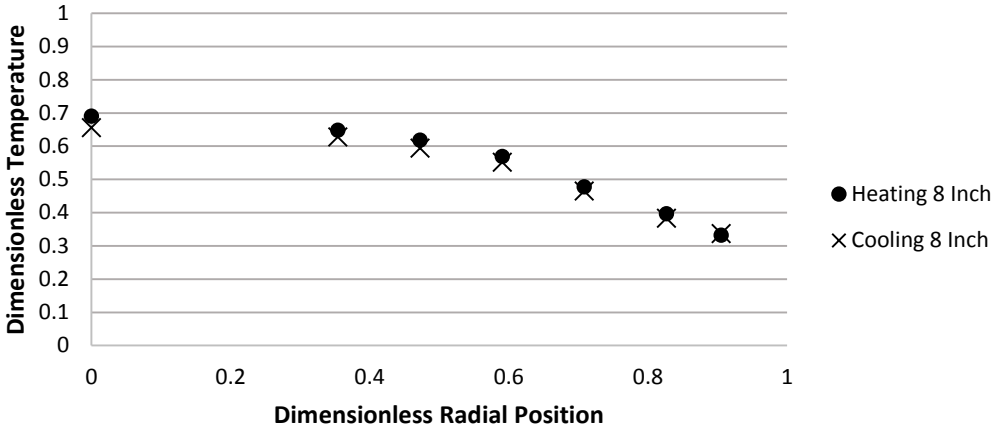

Air Flow 50% CFD Cooling Re=982 and Heating Re=1141 Bed Height 10 Inches

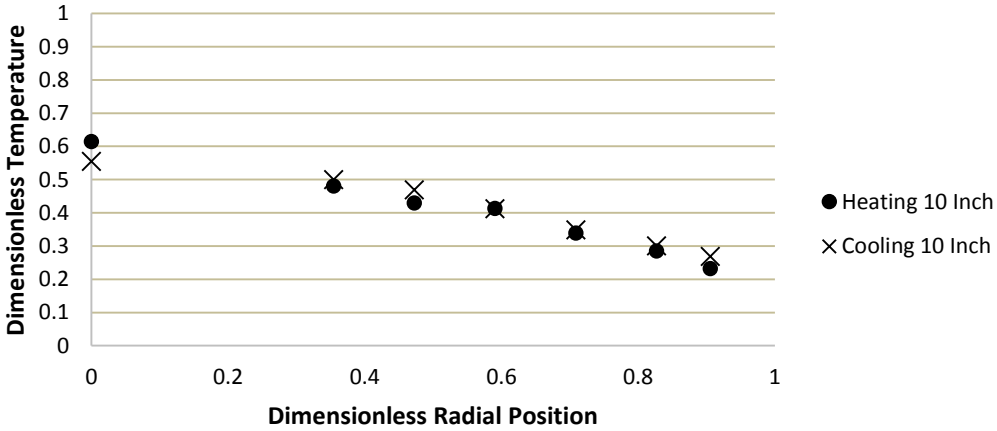

Simulation 2 Constant Viscosity: Cooling Experimental versus CFD (N=5.33)

Air Flow 28% (Re=503) Bed Height 6 Inches with Lower Particle Conductivity

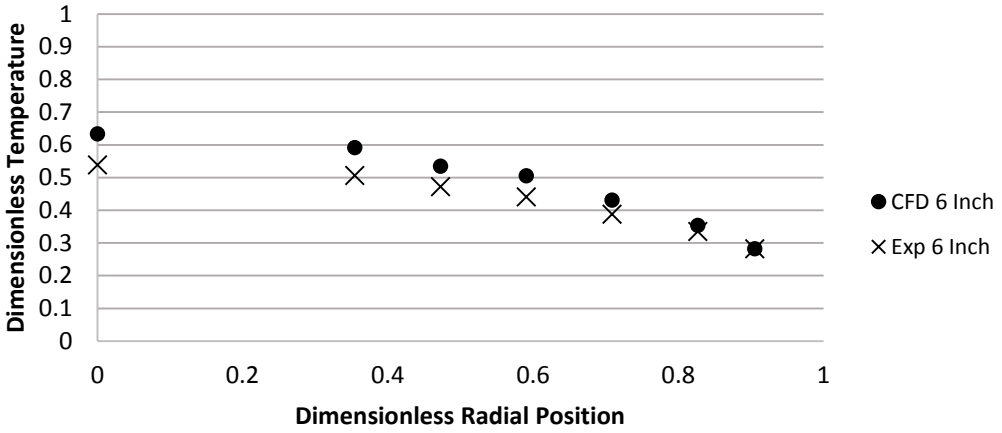

Air Flow 28% (Re=503) Bed Height 8 Inches with Lower Particle Conductivity

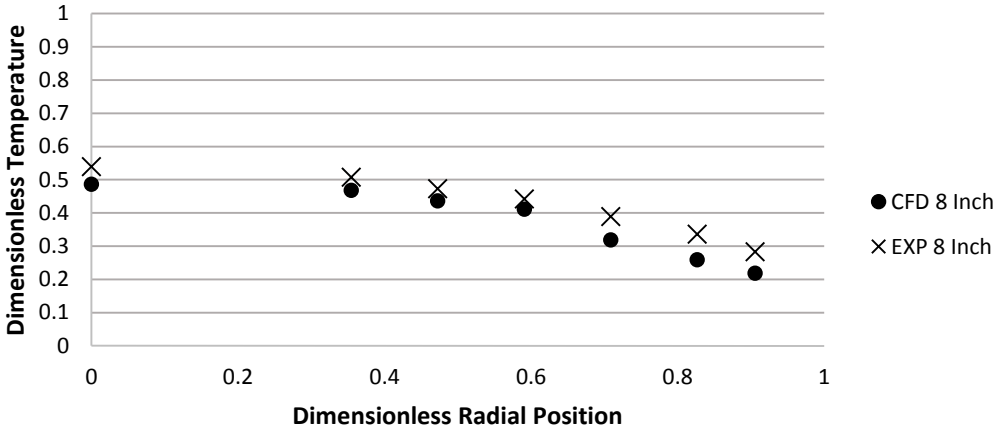

Air Flow 28% (Re=503) Bed Height 10 Inches with Lower Particle Conductivity

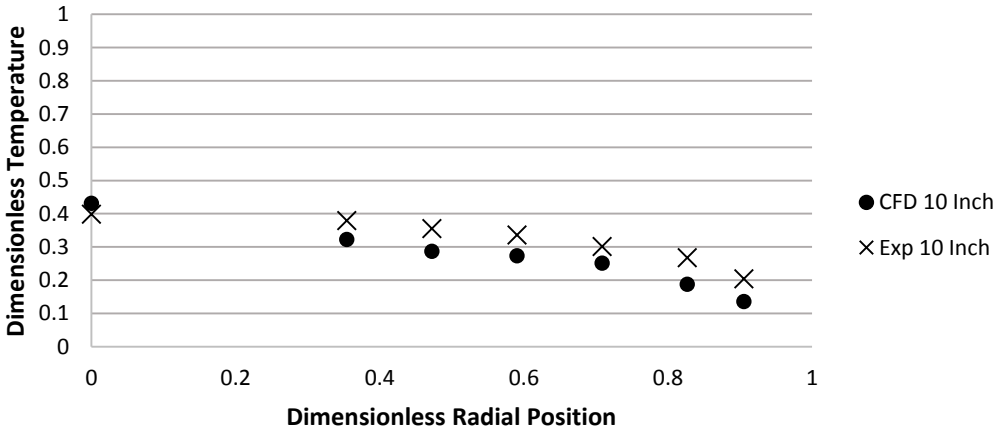

Air Flow 28% (Re=503) Bed Height 6 Inches with Higher Particle Conductivity

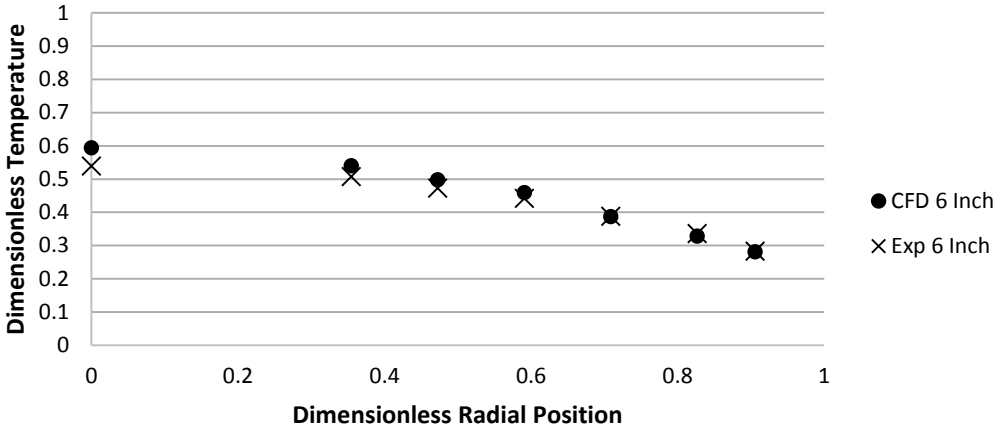

Air Flow 28% (Re=503) Bed Height 8 Inches with Correct Particle Conductivity

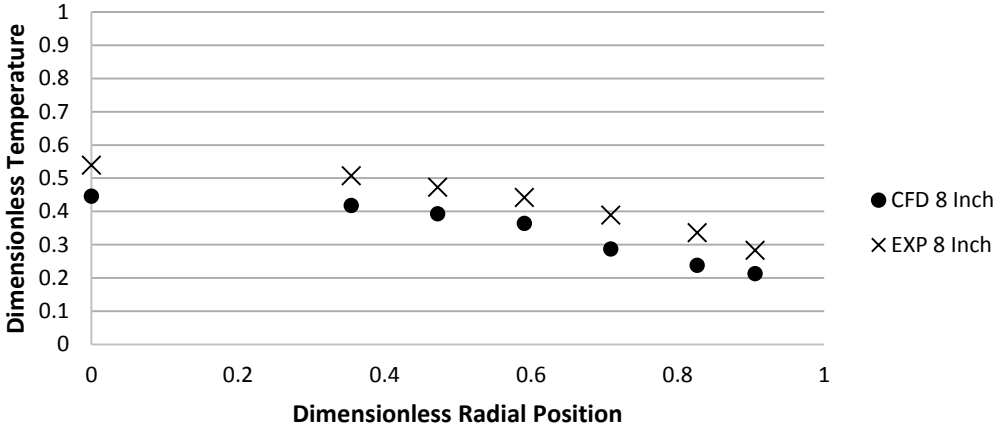

Air Flow 28% (Re=503) Bed Height 10 Inches with Correct Particle Conductivity

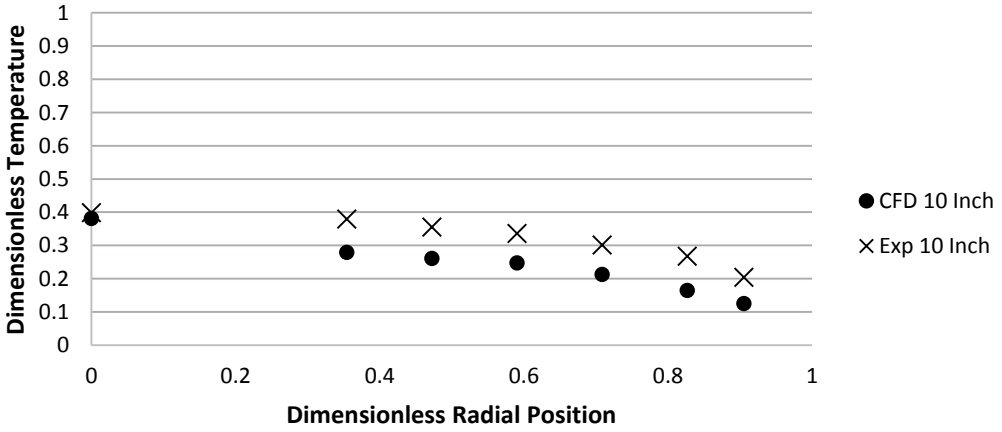

Air Flow 32% (Re=588) Bed Height 4 Inches

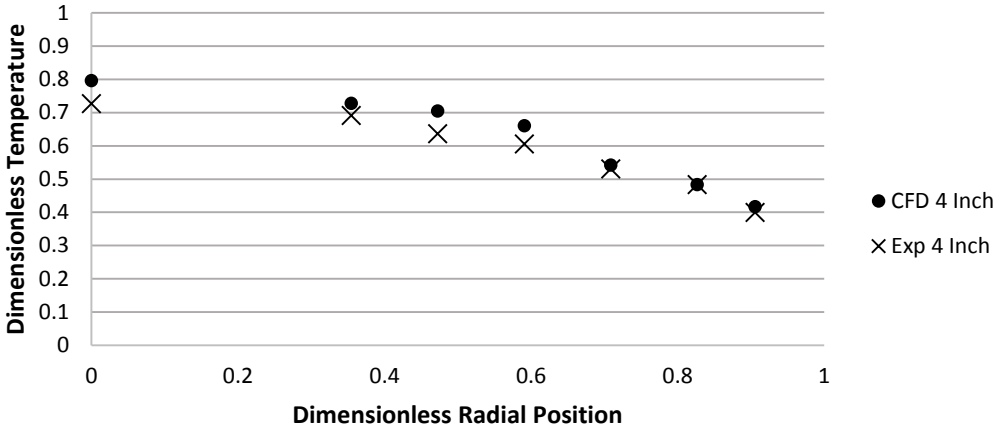

Air Flow 32% (Re=588) Bed Height 6 Inches

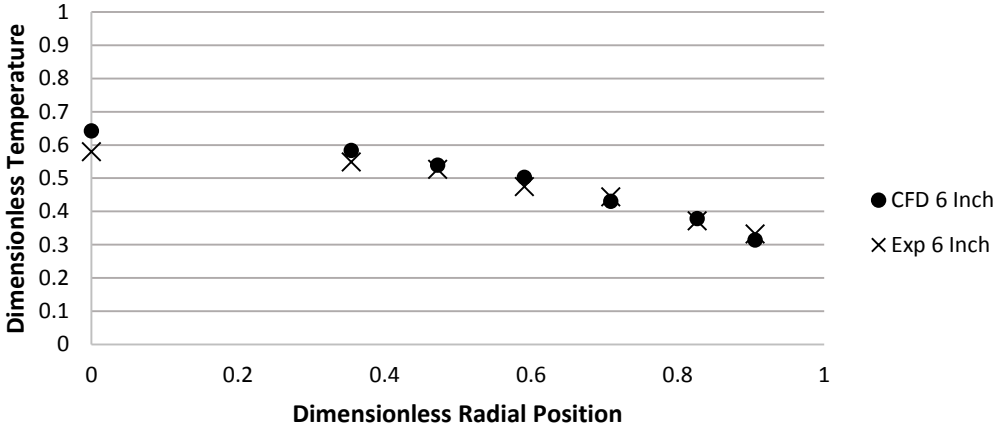

Air Flow 32% (Re=588) Bed Height 8 Inches

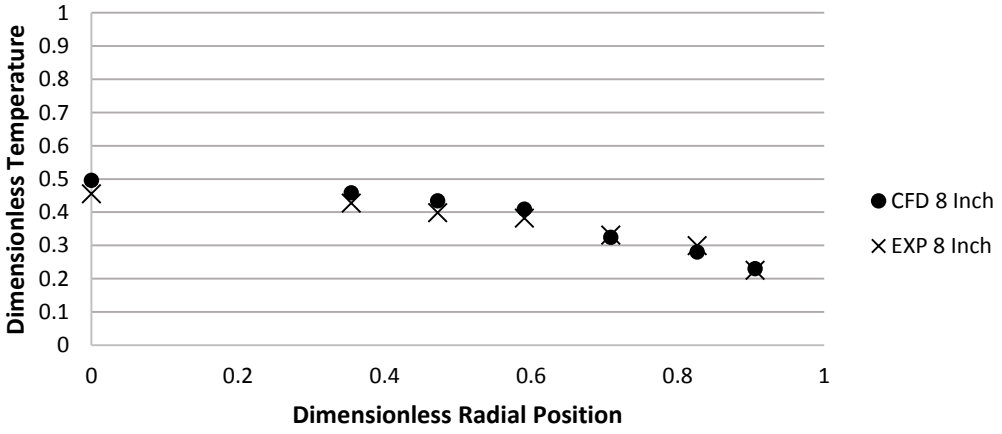

Air Flow 32% (Re=588) Bed Height 10 Inches

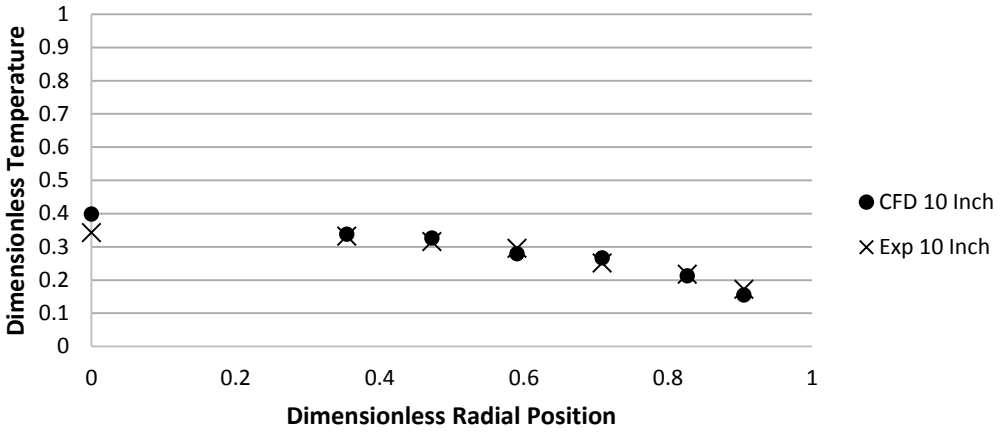

Air Flow 35% (Re=658) Bed Height 4 Inches

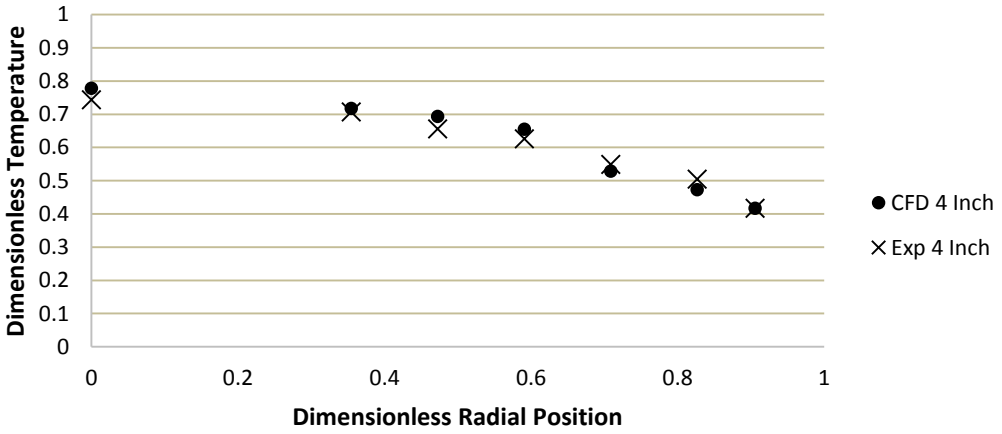

Air Flow 35% (Re=658) Bed Height 6 Inches

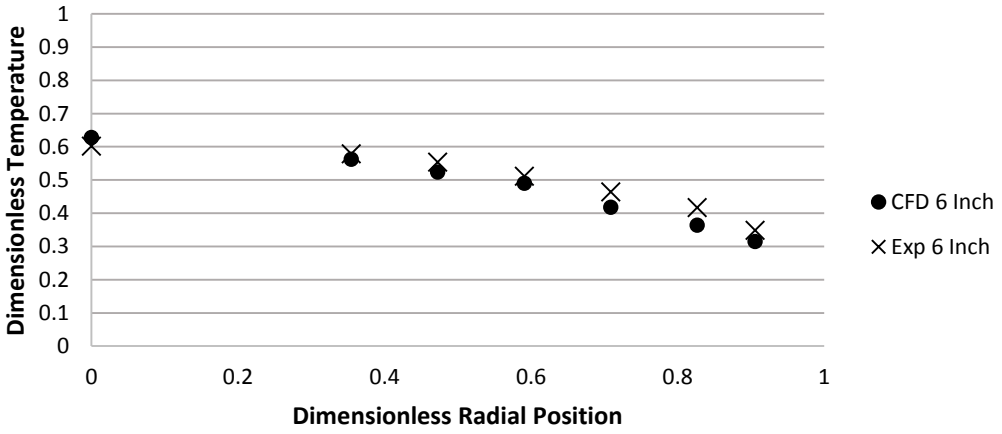

Air Flow 35% (Re=658) Bed Height 8 Inches

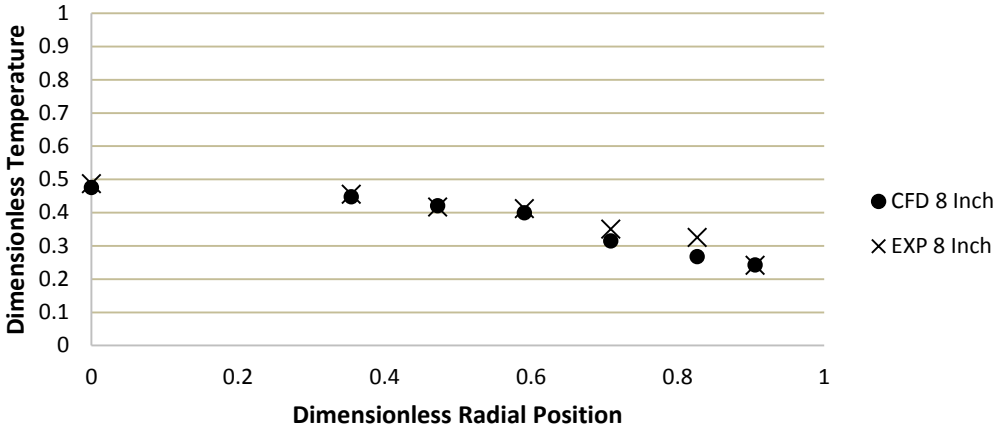

Air Flow 35% (Re=658) Bed Height 10 Inches

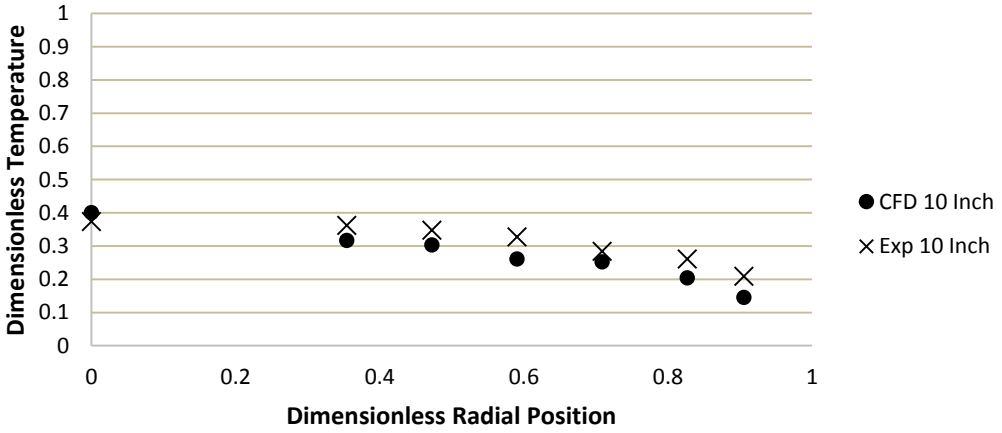

Air Flow 40% (Re=775) Bed Height 4 Inches

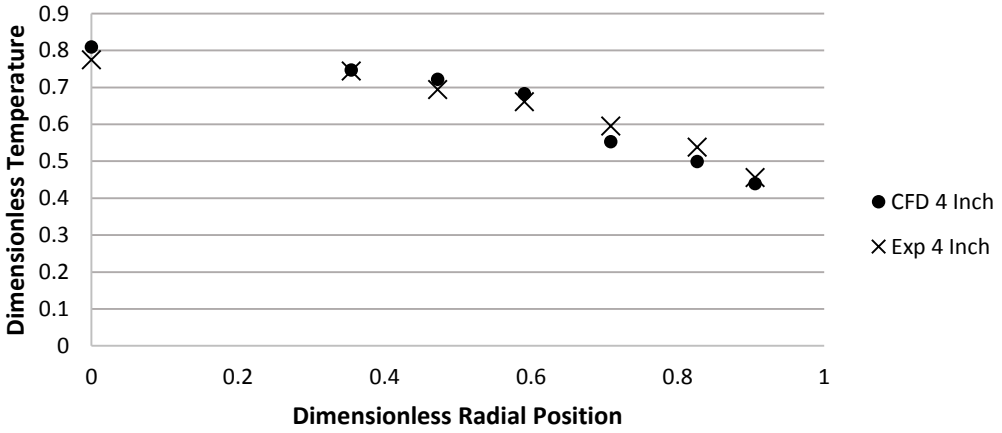

Air Flow 40% (Re=775) Bed Height 6 Inches

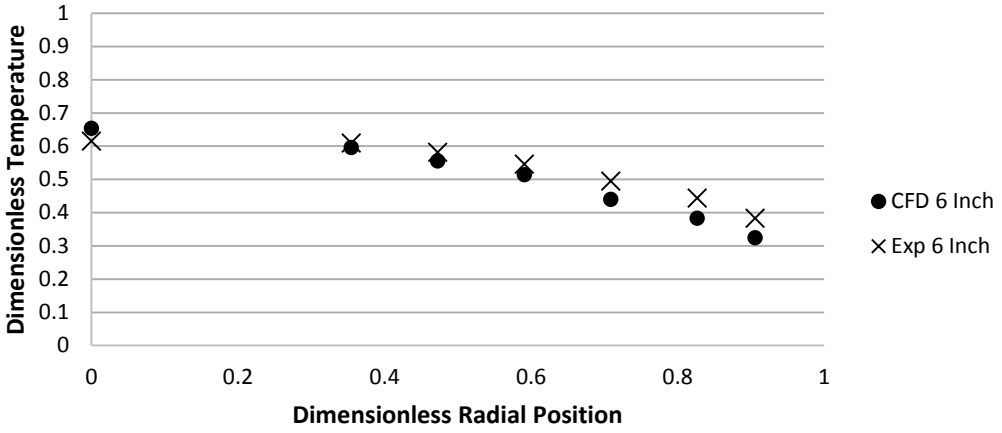

Air Flow 40% (Re=775) Bed Height 8 Inches

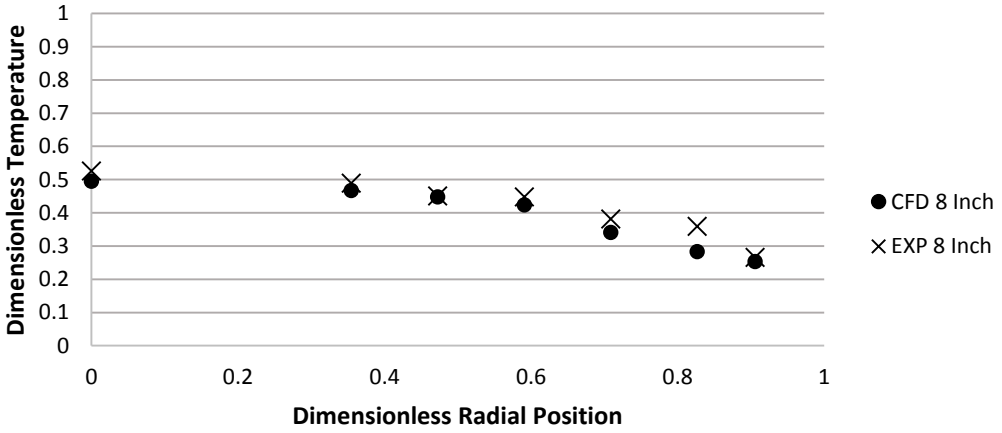

Air Flow 40% (Re=775) Bed Height 10 Inches

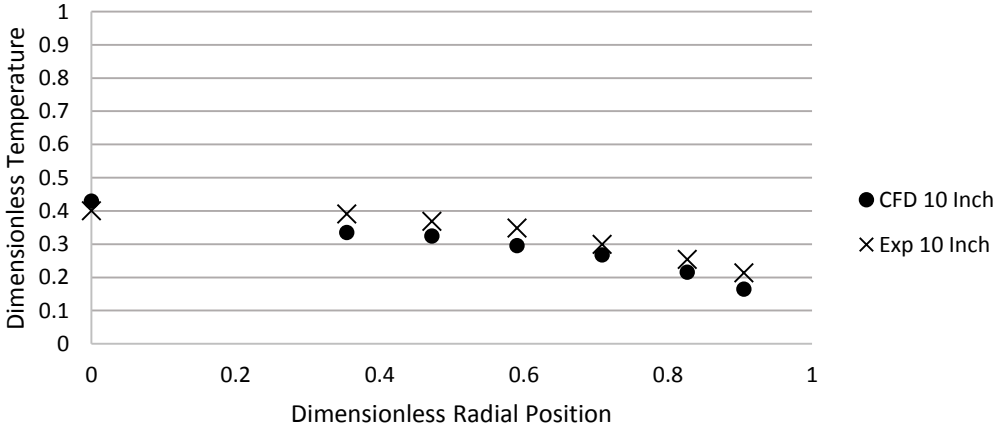

Air Flow 45% (Re=876) Bed Height 4 Inches

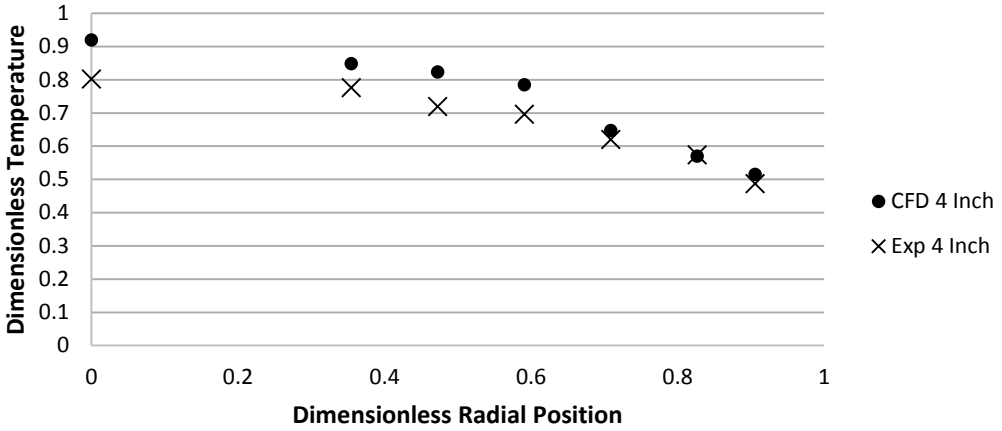

Air Flow 45% (Re=876) Bed Height 6 Inches

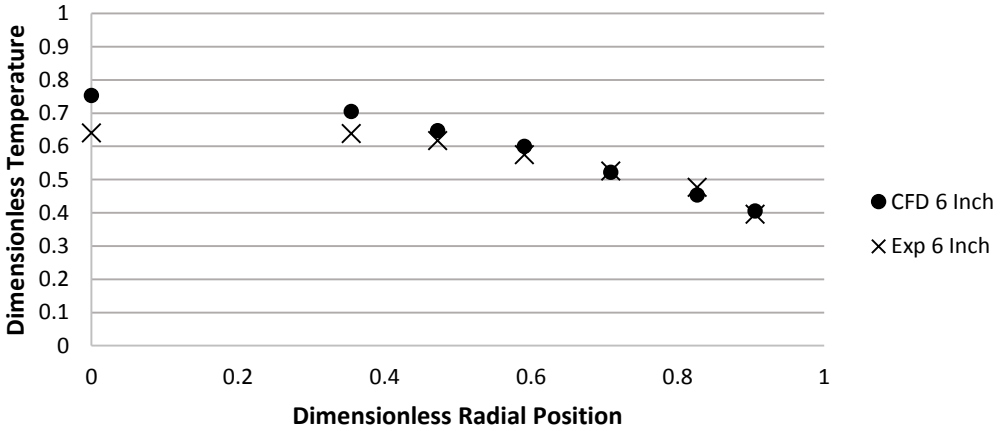

Air Flow 45% (Re=876) Bed Height 8 Inches

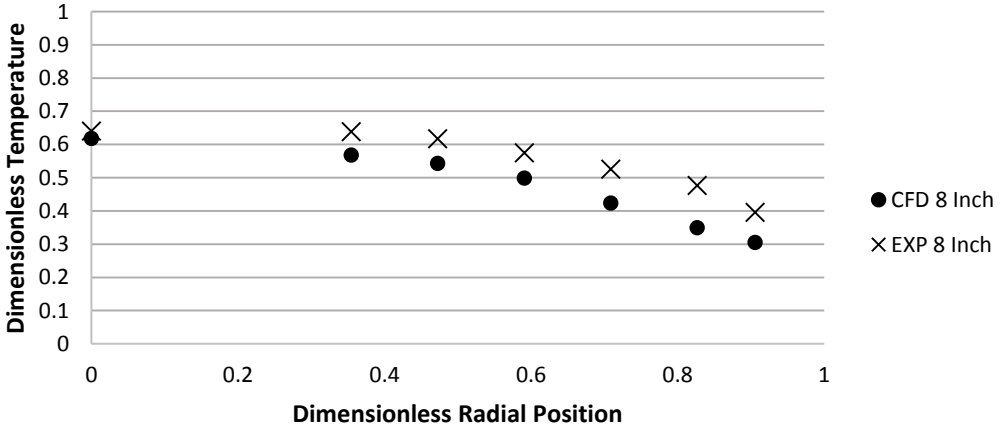

Air Flow 45% (Re=876) Bed Height 10 Inches

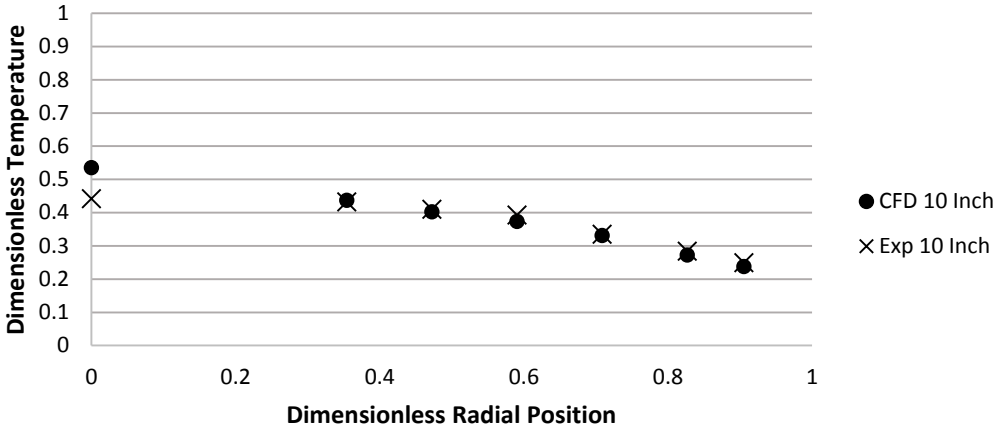

Air Flow 50% (Re=982) Bed Height 4 Inches

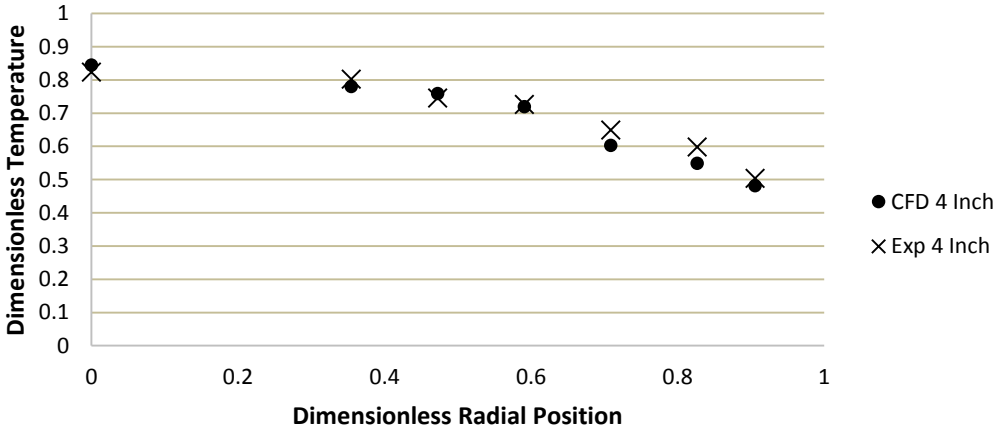

Air Flow 50% (Re=982) Bed Height 6 Inches

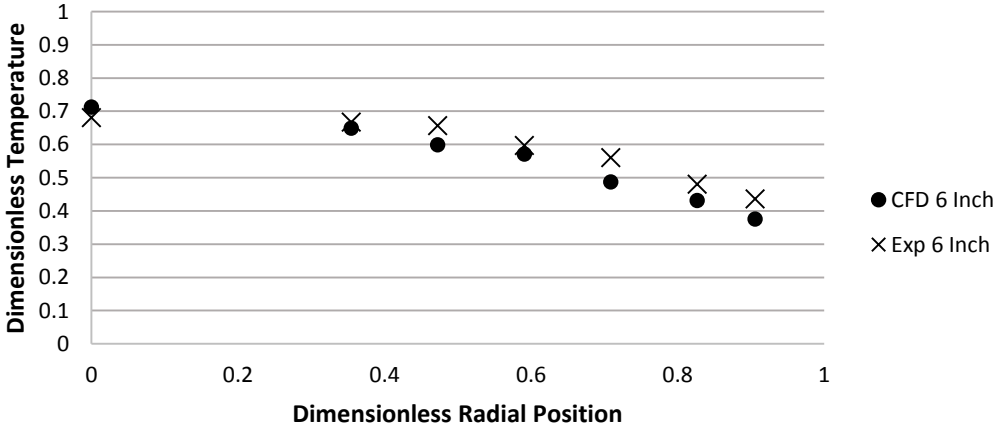

Air Flow 50% (Re=982) Bed Height 8 Inches

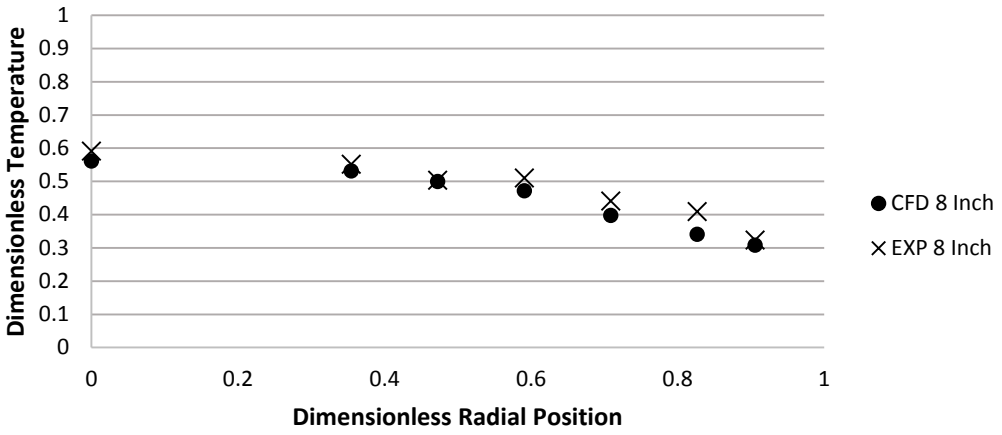

Air Flow 50% (Re=982) Bed Height 10 Inches

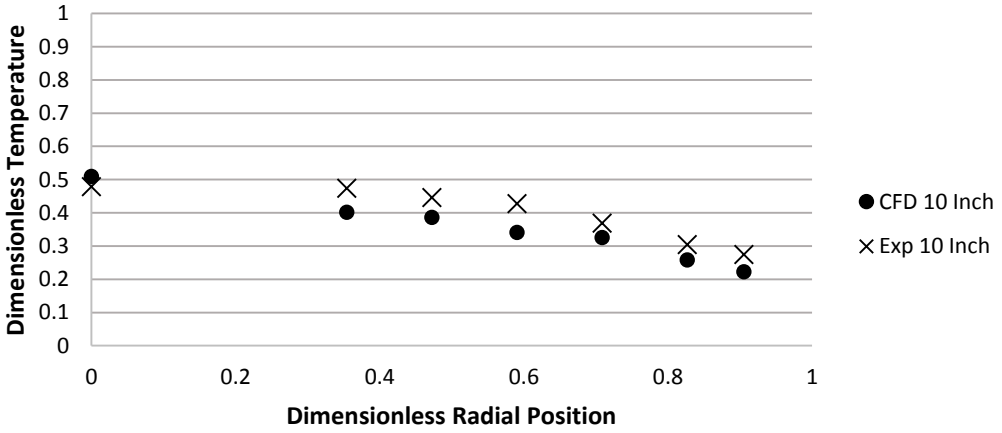

Simulation 2 Varying Viscosity: Cooling Experimental versus CFD (N=5.33)

Air Flow 28% (Re=503) Bed Height 4 Inches

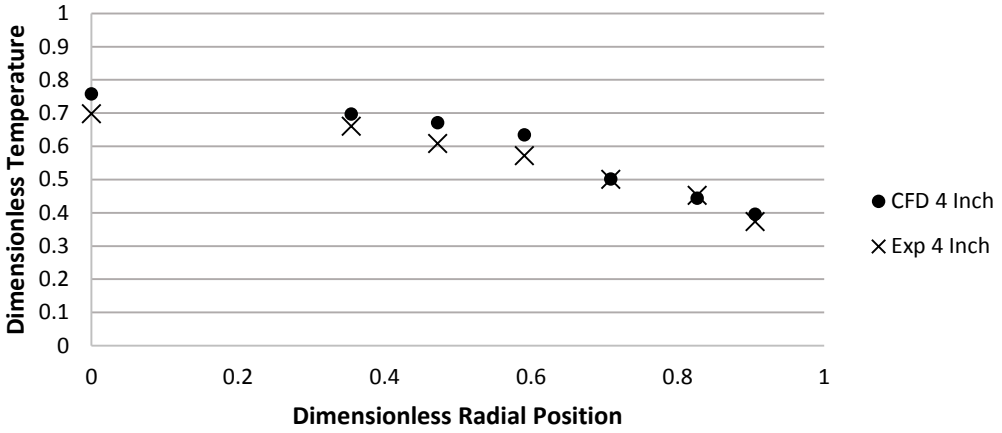

Air Flow 28% (Re=503) Bed Height 6 Inches

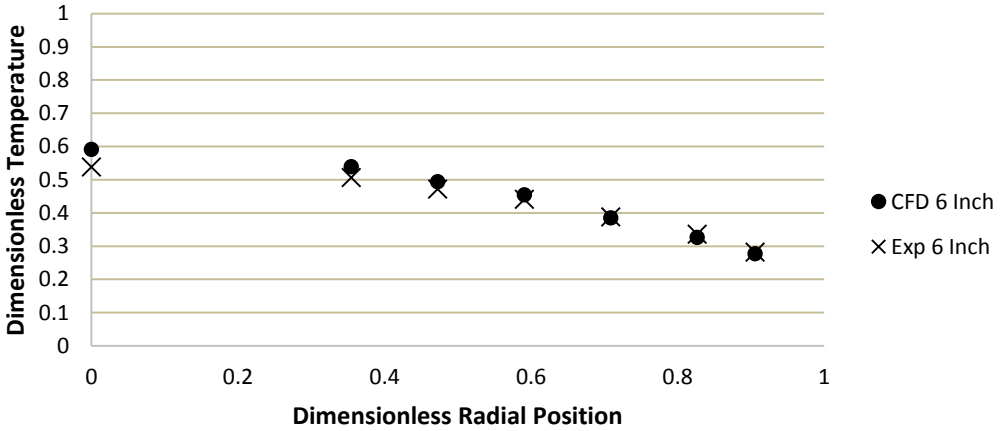

Air Flow 28% (Re=503) Bed Height 8 Inches

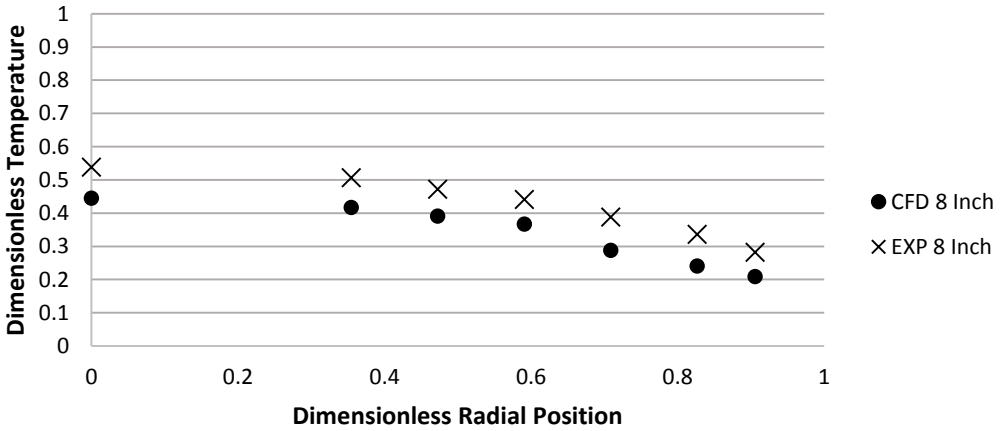

Air Flow 28% (Re=503) Bed Height 10 Inches

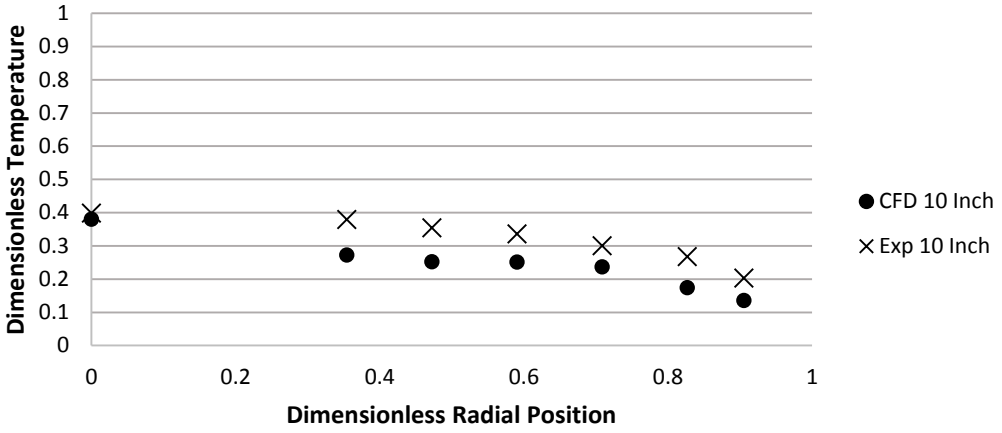

Air Flow 32% (Re=588) Bed Height 4 Inches

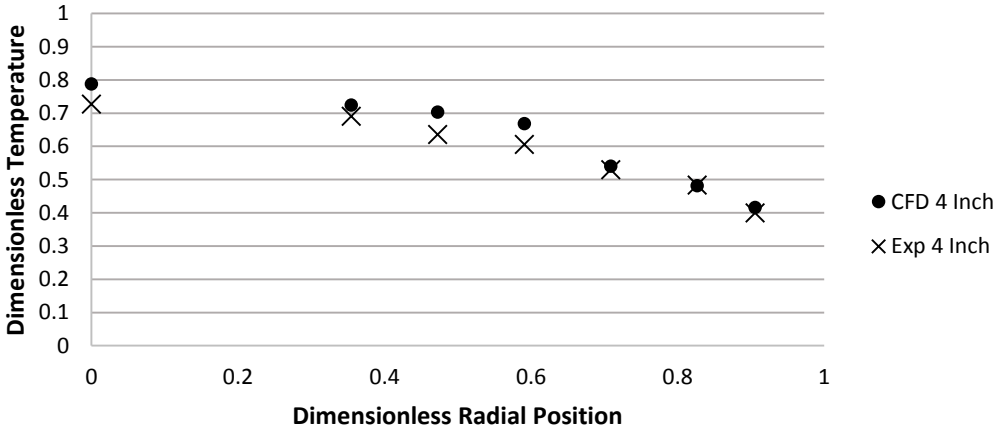

Air Flow 32% (Re=588) Bed Height 6 Inches

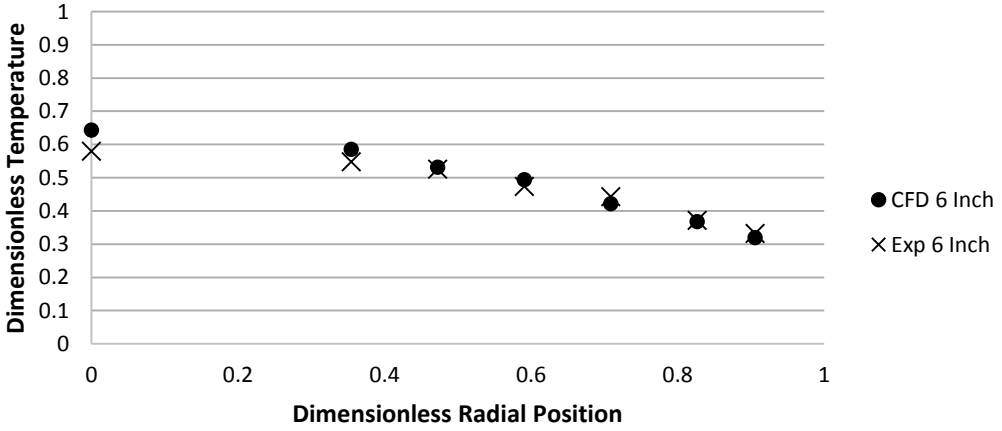

Air Flow 32% (Re=588) Bed Height 8 Inches

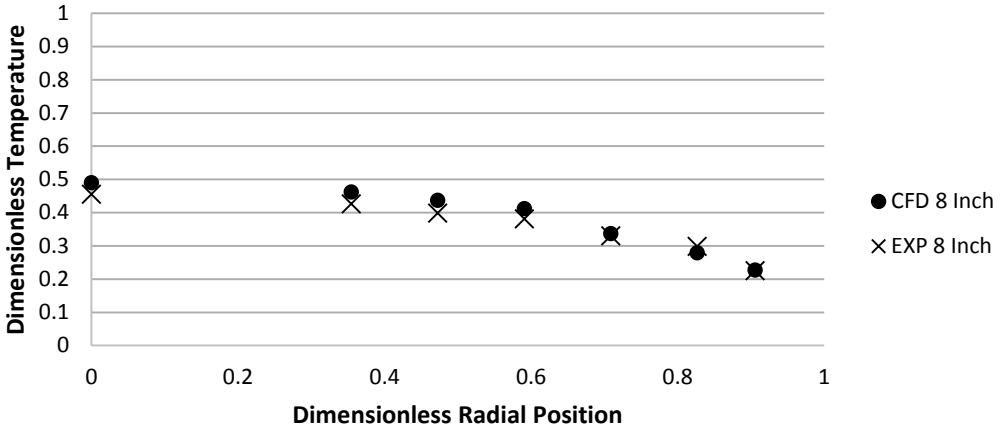

Air Flow 32% (Re=588) Bed Height 10 Inches

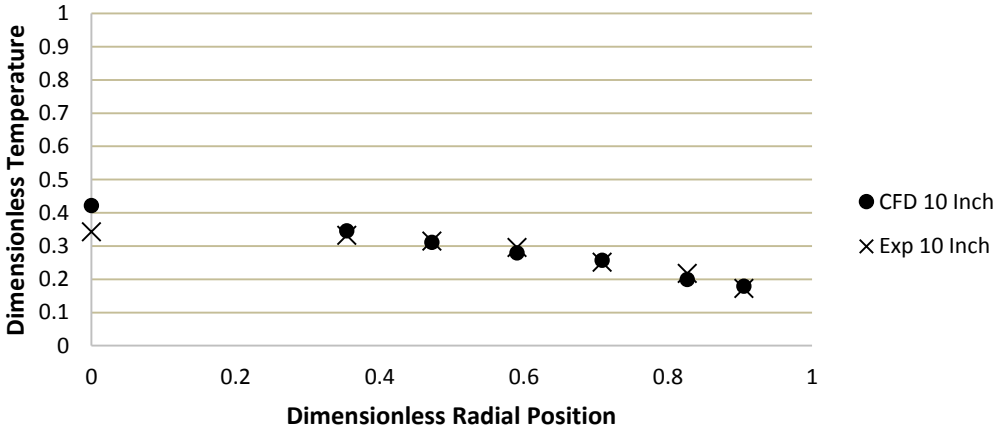

Air Flow 35% (Re=658) Bed Height 4 Inches

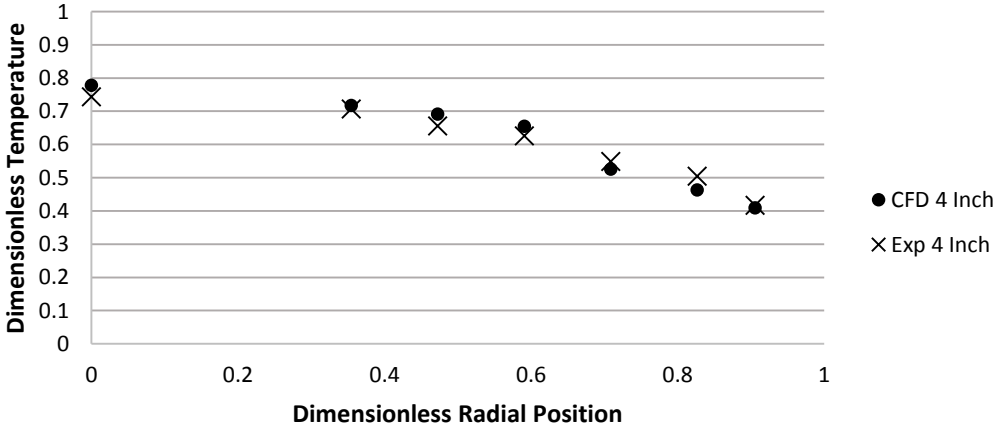

Air Flow 35% (Re=658) Bed Height 6 Inches

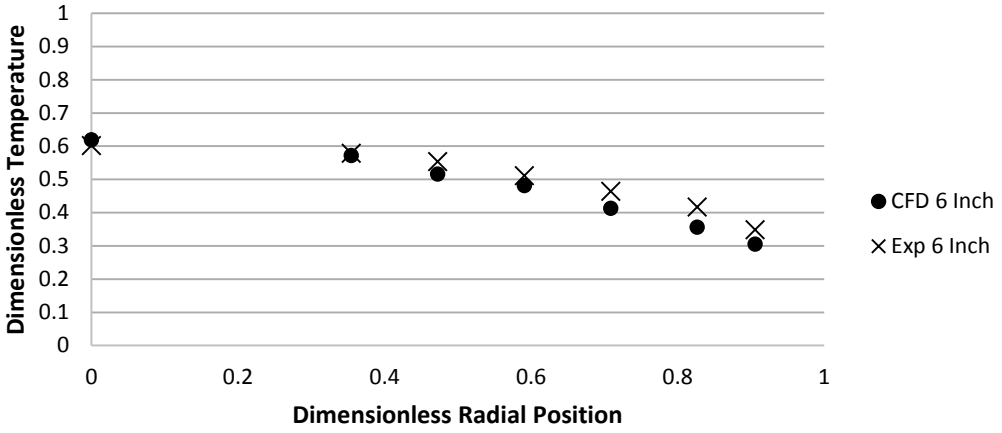

Air Flow 35% (Re=658) Bed Height 8 Inches

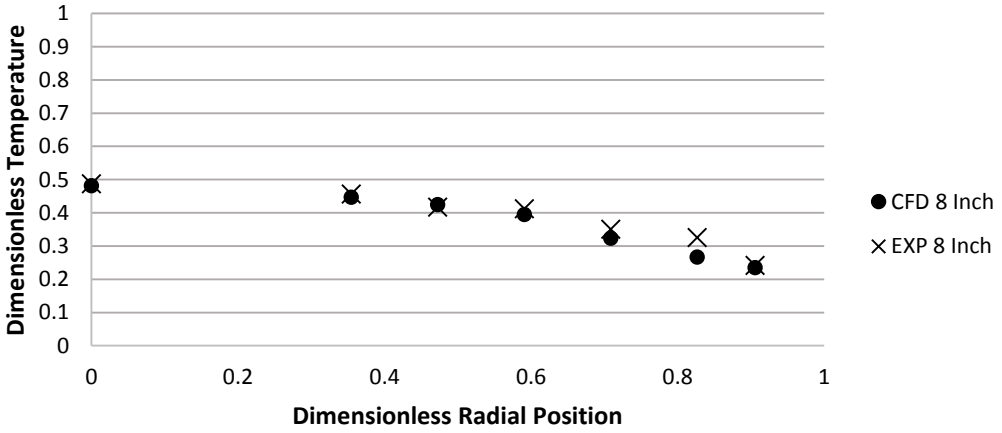

Air Flow 35% (Re=658) Bed Height 10 Inches

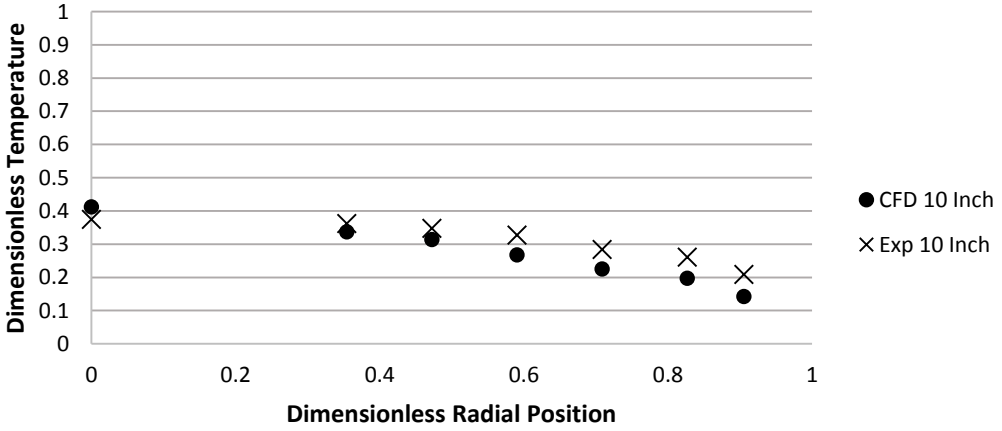

Air Flow 40% (Re=775) Bed Height 4 Inches

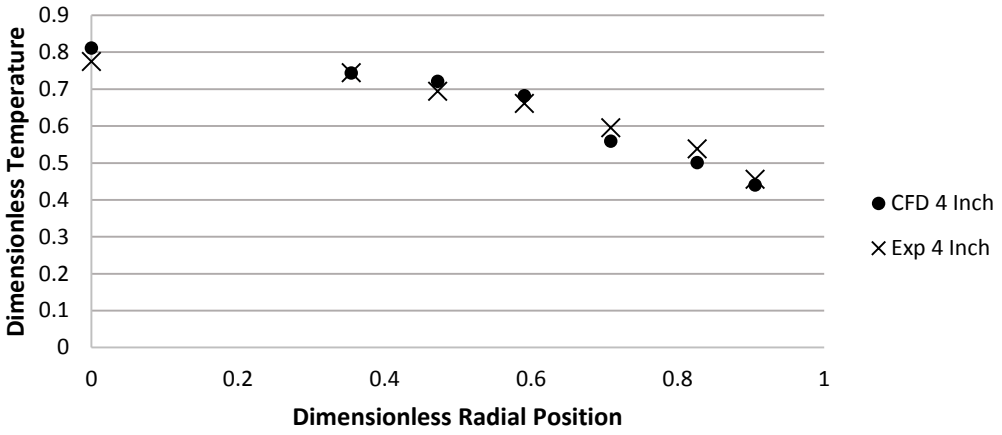

Air Flow 40% (Re=775) Bed Height 6 Inches

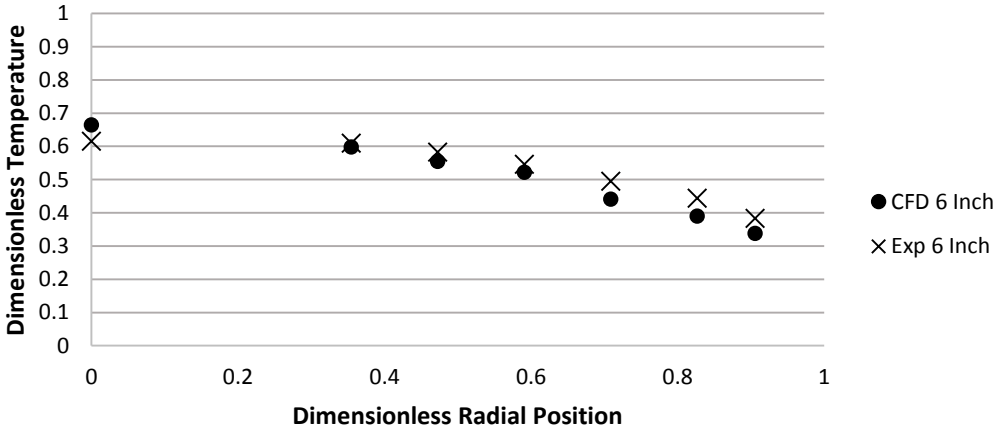

Air Flow 40% (Re=775) Bed Height 8 Inches

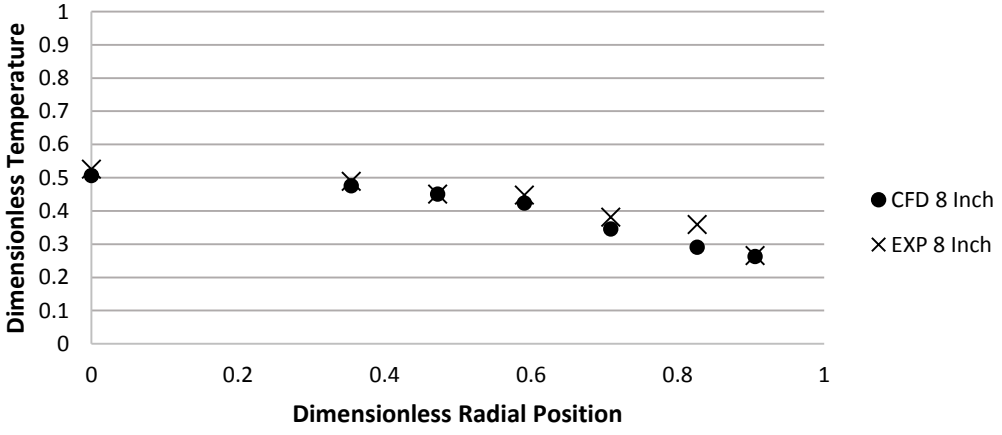

Air Flow 40% (Re=775) Bed Height 10 Inches

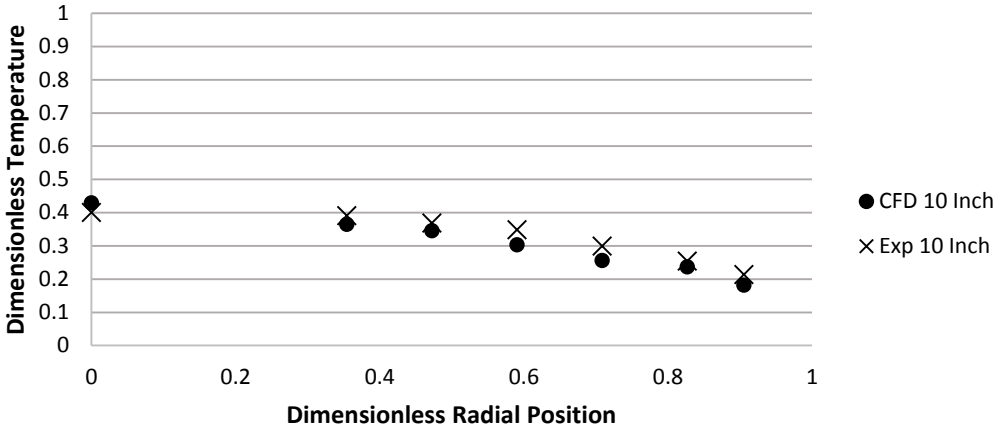

Air Flow 45% (Re=876) Bed Height 4 Inches

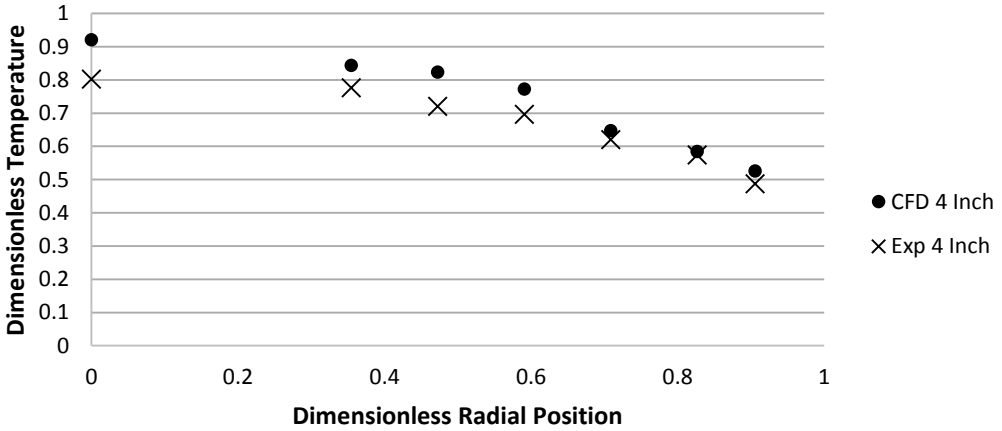

Air Flow 45% (Re=876) Bed Height 6 Inches

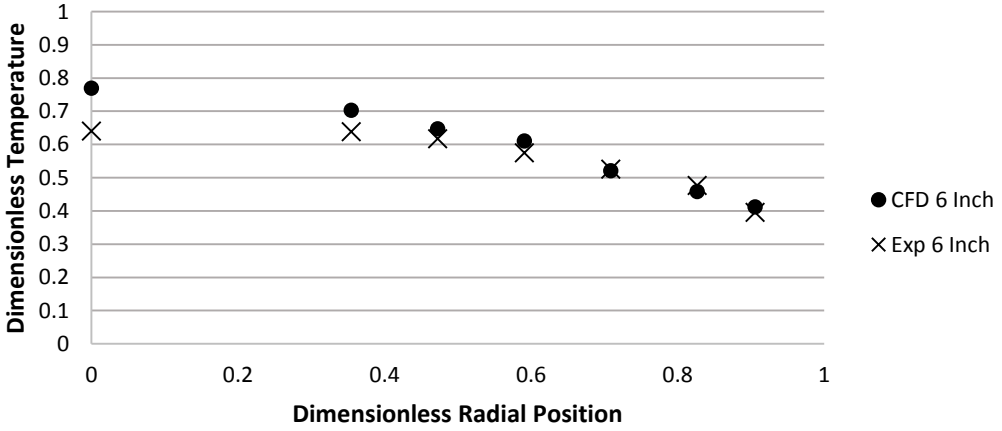

Air Flow 45% (Re=876) Bed Height 8 Inches

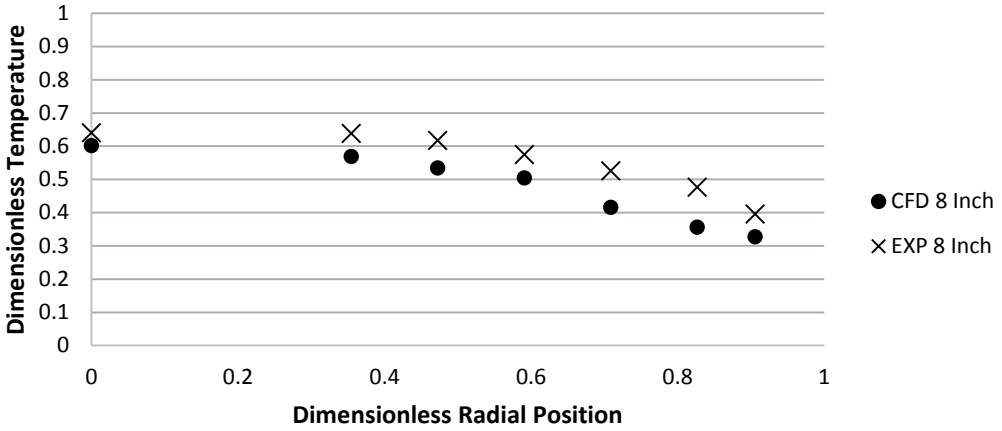

Air Flow 45% (Re=876) Bed Height 10 Inches

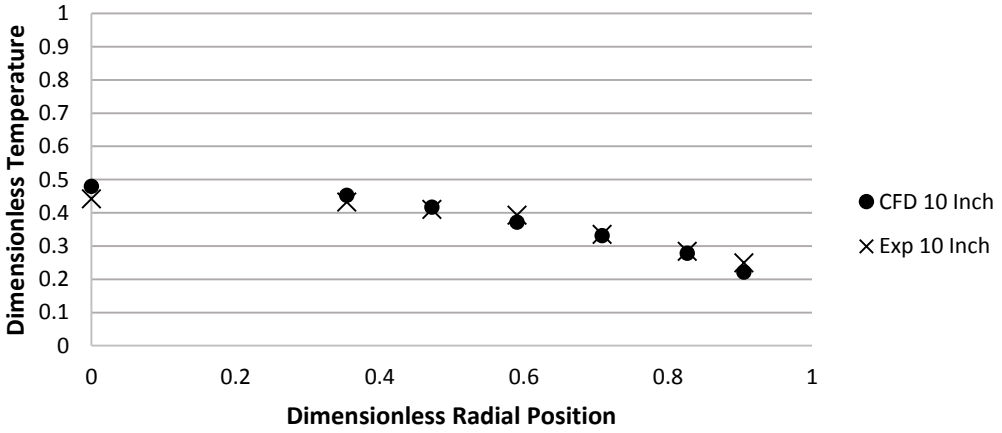

Air Flow 50% (Re=982) Bed Height 4 Inches

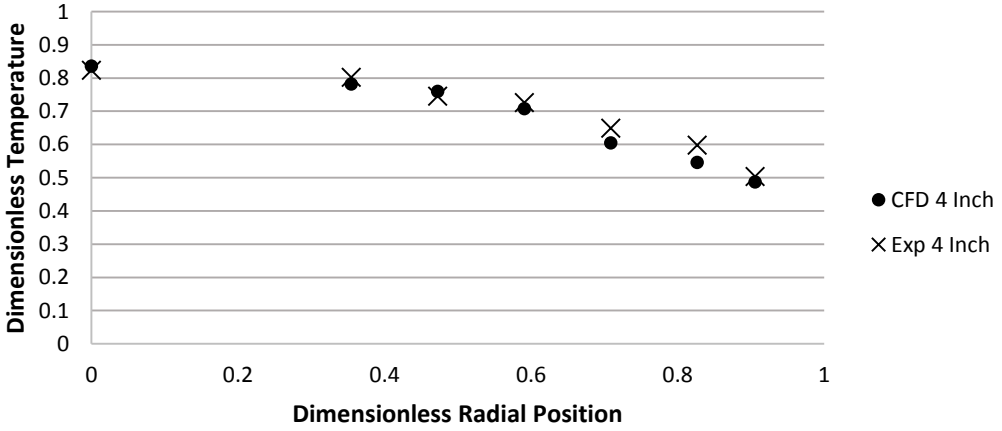

Air Flow 50% (Re=982) Bed Height 6 Inches

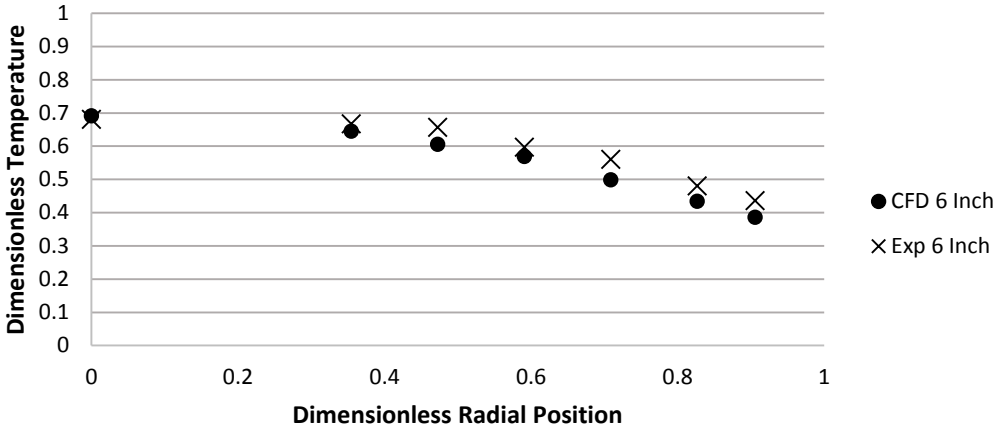

Air Flow 50% (Re=982) Bed Height 8 Inches

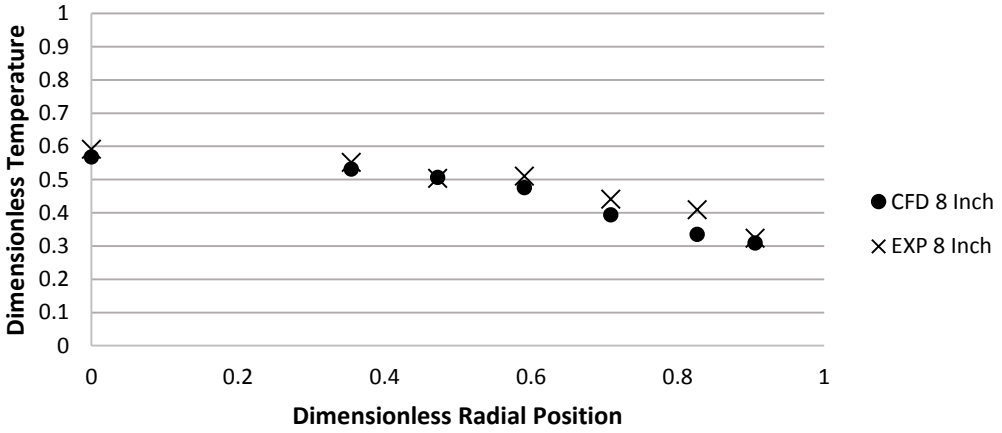

Air Flow 50% (Re=982) Bed Height 10 Inches

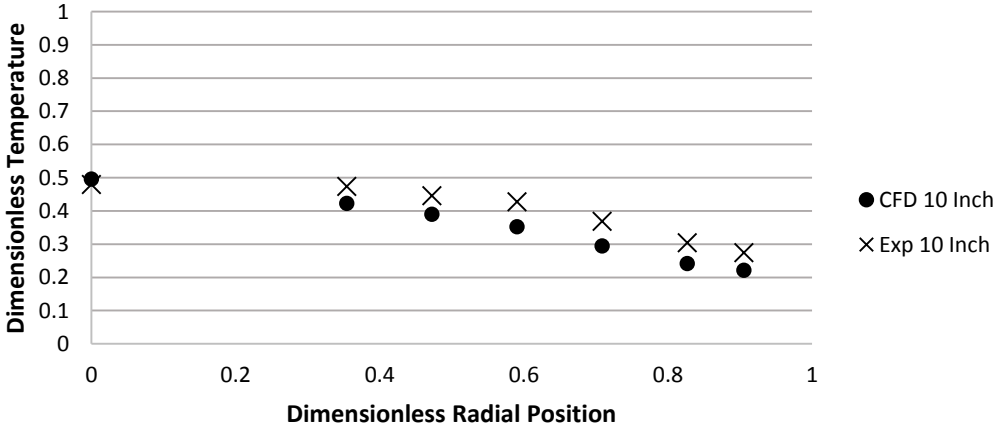

Simulation 2 Constant Viscosity: Heating Experimental versus CFD (N=5.33)

Air Flow 28% Experimental Re= 630 and CFD Re= 689 Bed Height 4 Inches

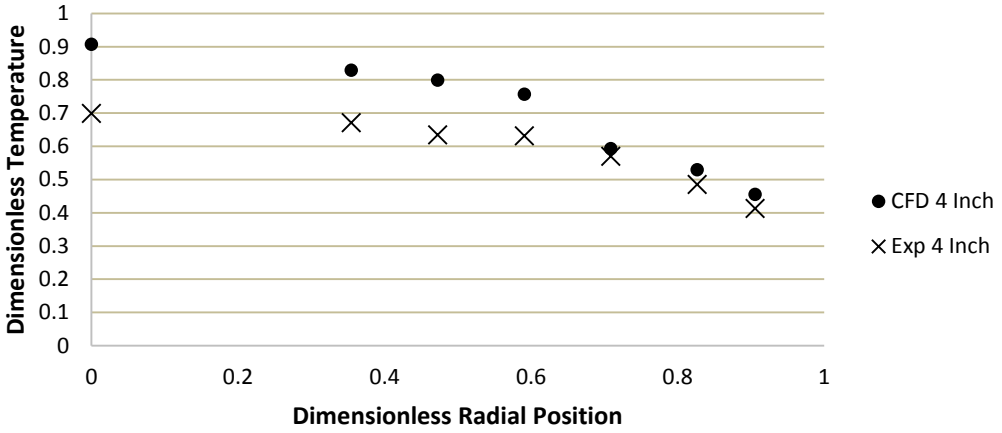

Air Flow 28% Experimental Re= 630 and CFD Re= 689 Bed Height 6 Inches

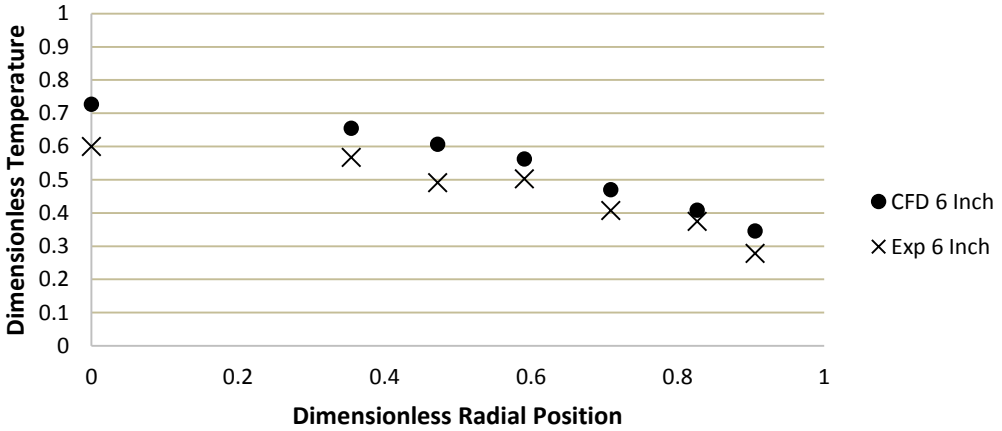

Air Flow 28% Experimental Re= 630 and CFD Re= 689 Bed Height 8 Inches

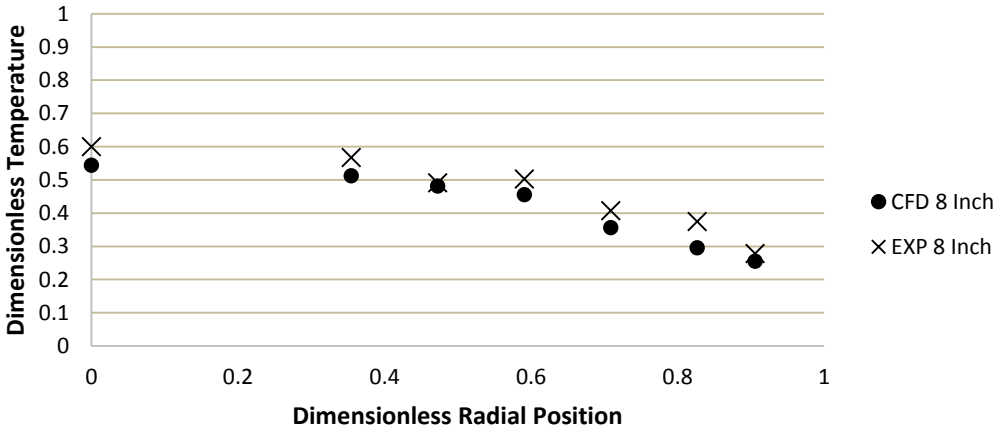

Air Flow 28% Experimental Re= 630 and CFD Re= 689 Bed Height 10 Inches

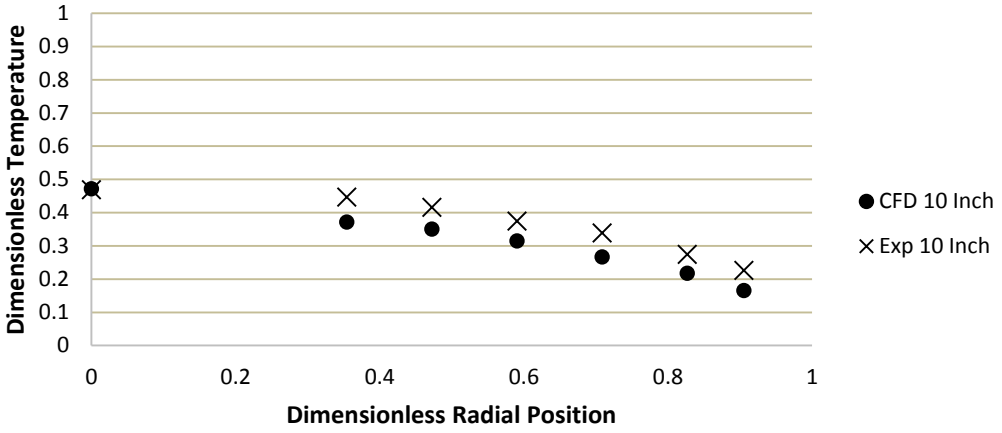

Air Flow 32% Experimental Re= 702 and CFD Re= 805 Bed Height 4 Inches

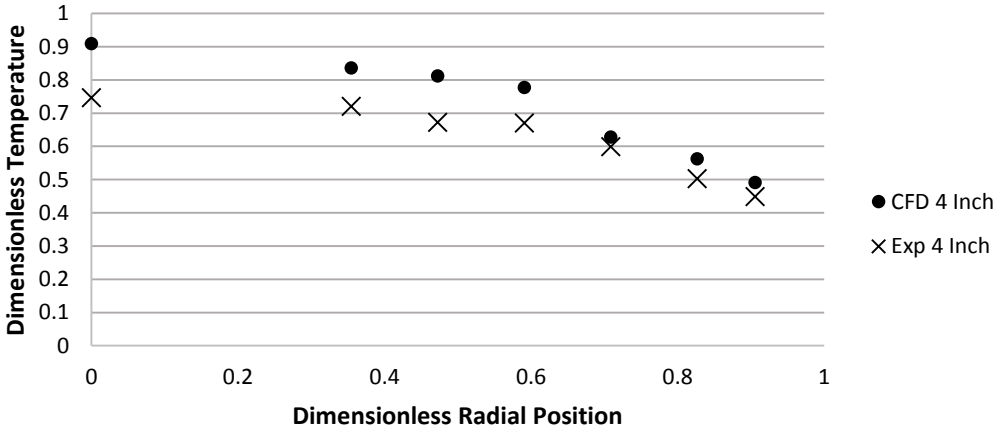

Air Flow 32% Experimental Re= 702 and CFD Re= 805 Bed Height 6 Inches

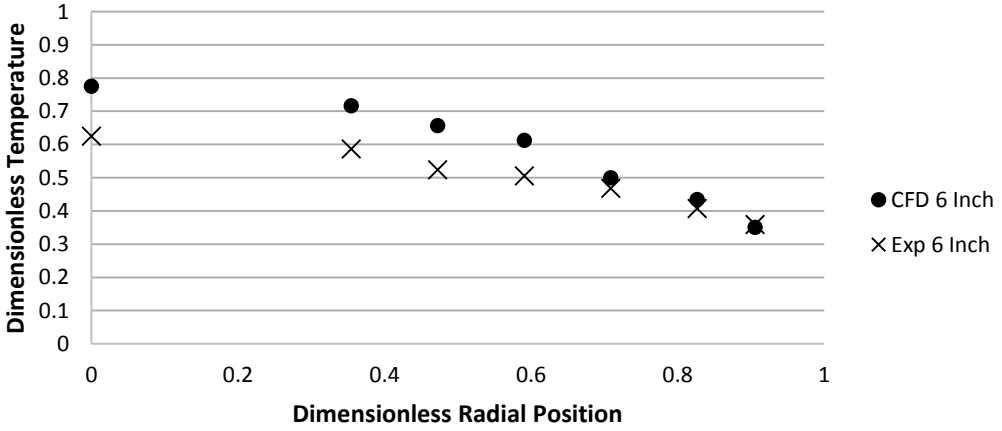

Air Flow 32% Experimental Re= 702 and CFD Re= 805 Bed Height 8 Inches

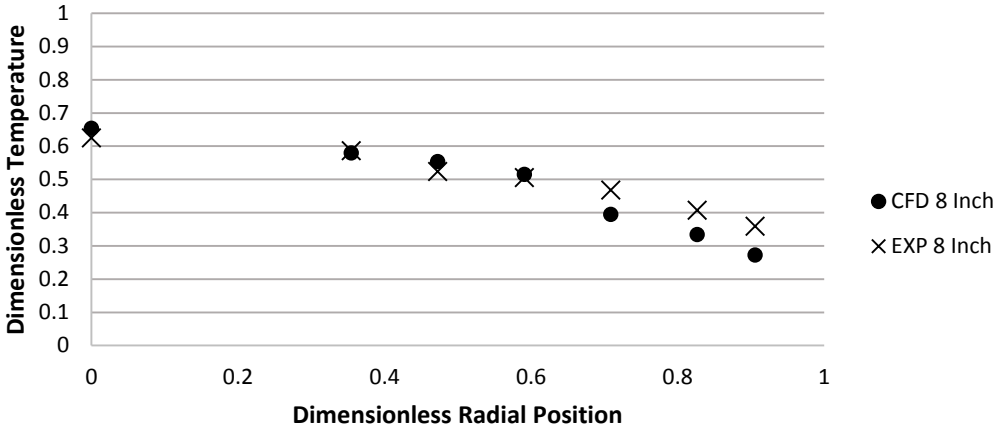

Air Flow 32% Experimental Re= 702 and CFD Re= 805 Bed Height 10 Inches

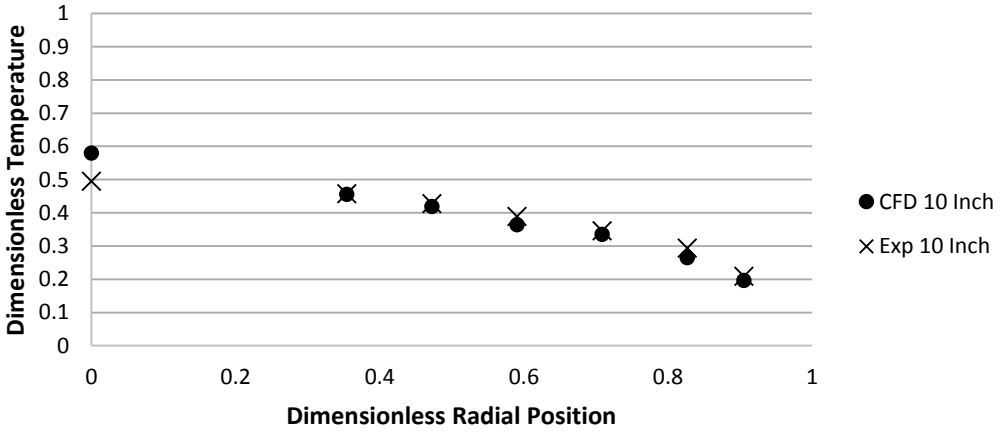

Air Flow 40% Experimental Re= 901 and CFD Re= 901 Bed Height 6 Inches

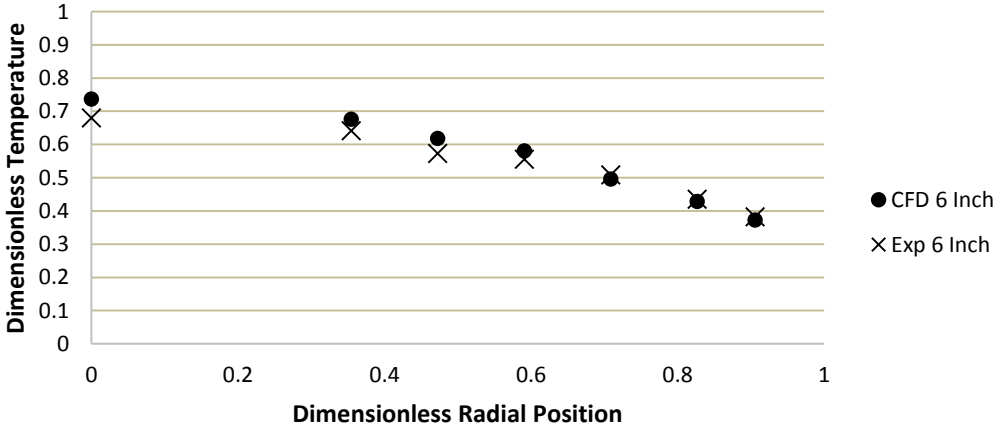

Air Flow 40% Experimental Re= 901 and CFD Re= 901 Bed Height 8 Inches

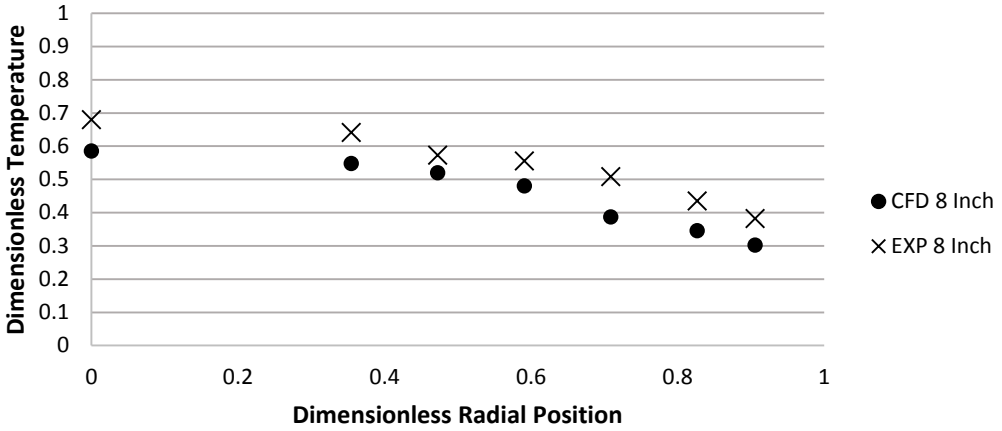

Air Flow 40% Experimental Re= 901 and CFD Re= 901 Bed Height 10 Inches

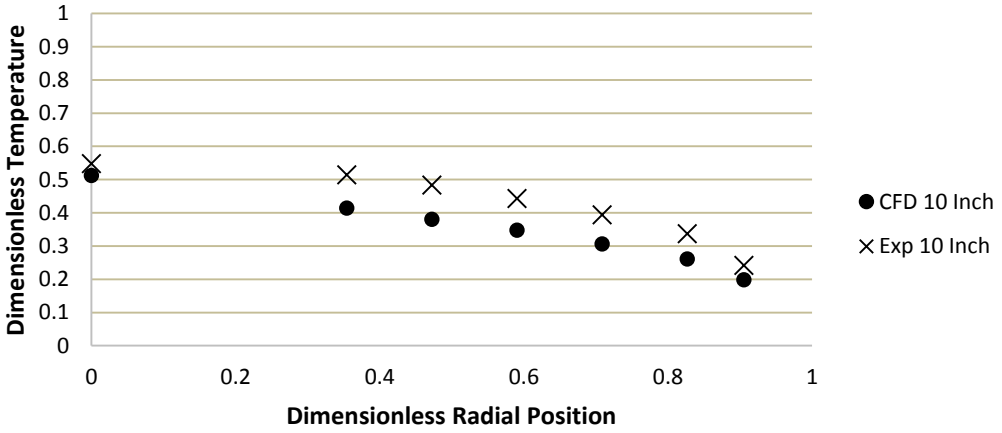

Air Flow 45% Experimental Re= 1018 and CFD Re= 1022 Bed Height 4 Inches

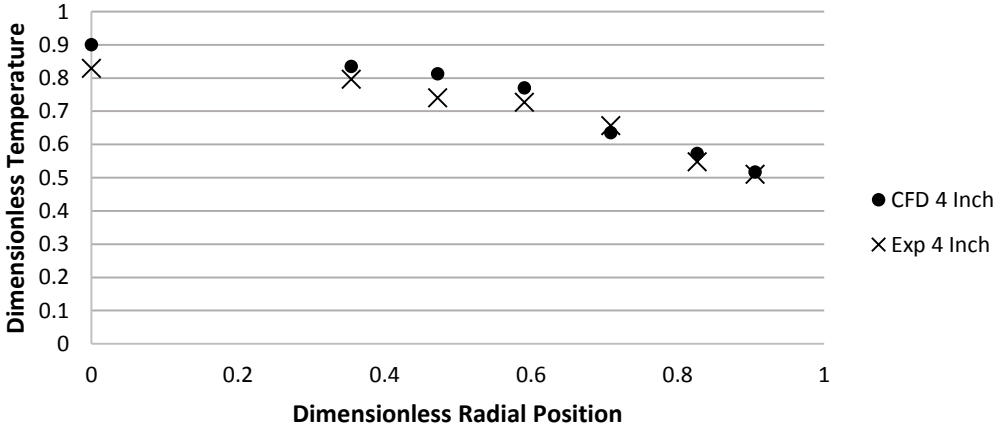

Air Flow 45% Experimental Re= 1018 and CFD Re= 1022 Bed Height 6 Inches

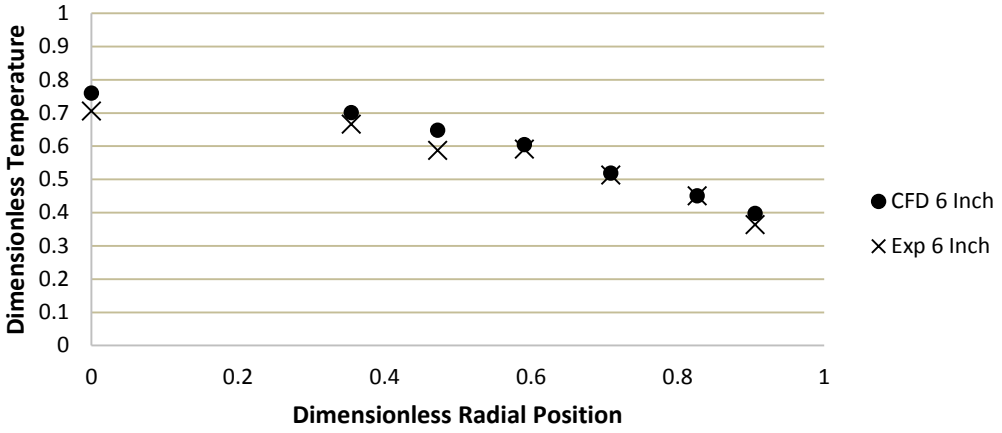

Air Flow 45% Experimental Re= 1018 and CFD Re= 1022 Bed Height 8 Inches

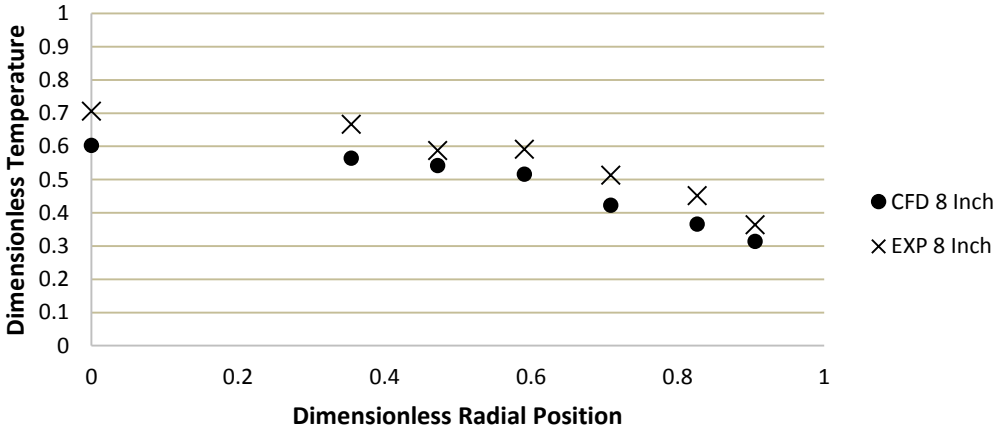

Air Flow 45% Experimental Re= 1018 and CFD Re= 1022 Bed Height 10 Inches

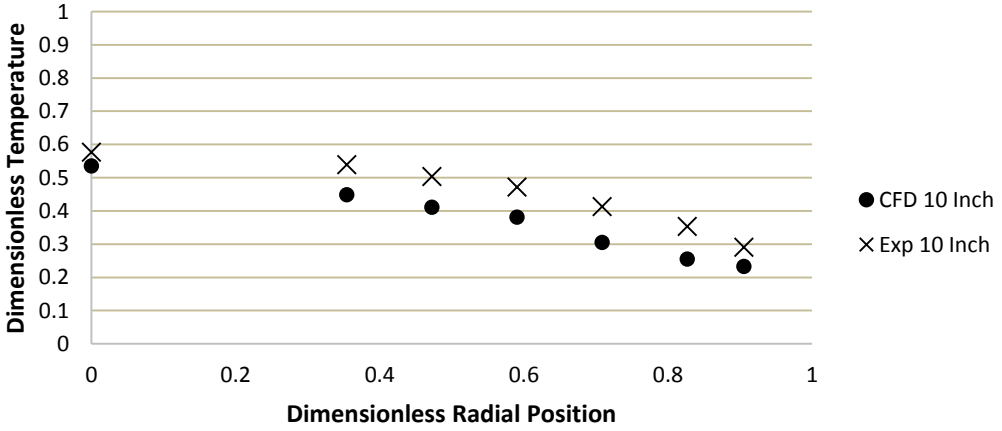

Air Flow 50% Experimental Re= 1139 and CFD Re= 1141 Bed Height 4 Inches

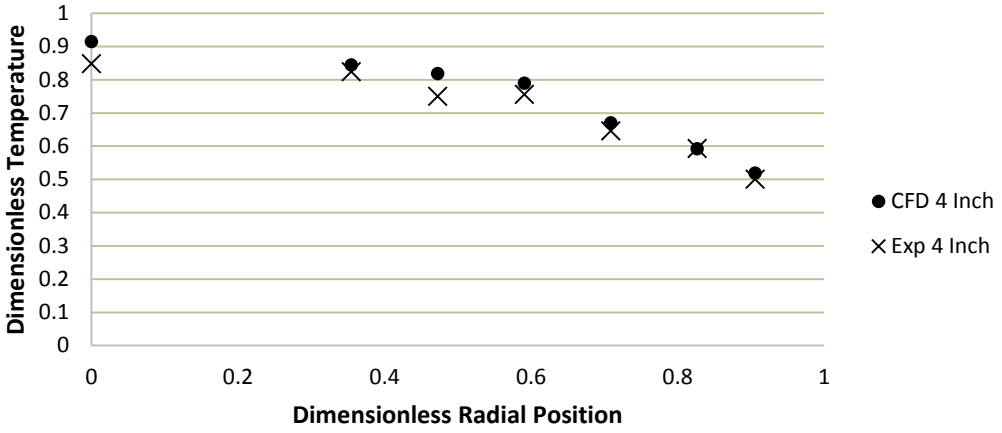

Air Flow 50% Experimental Re= 1139 and CFD Re= 1141 Bed Height 6 Inches

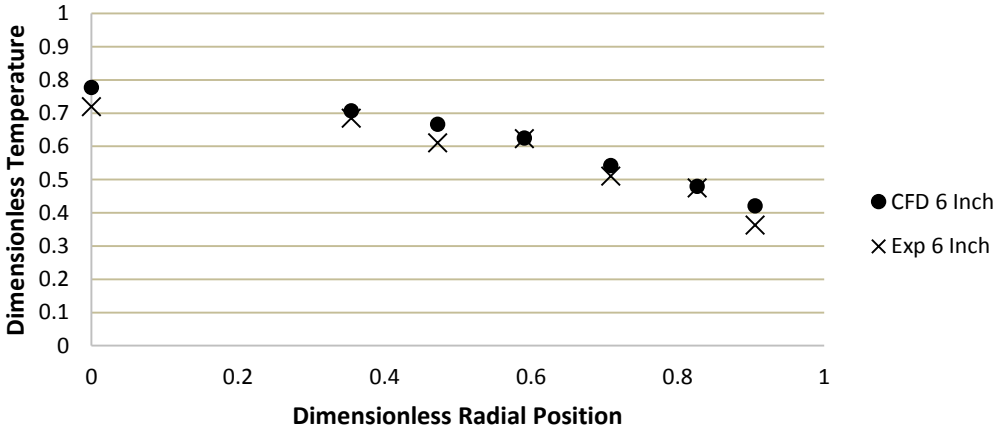

Air Flow 50% Experimental Re= 1139 and CFD Re= 1141 Bed Height 8 Inches

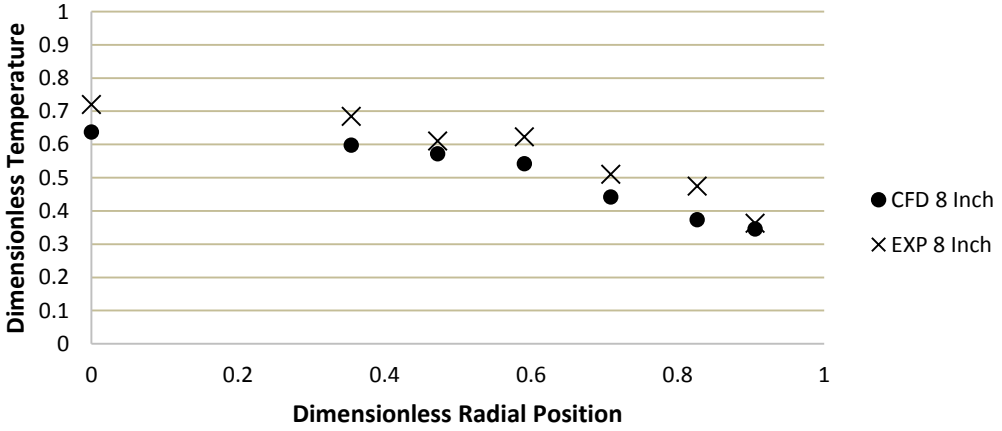

Air Flow 50% Experimental Re= 1139 and CFD Re= 1141 Bed Height 10 Inches

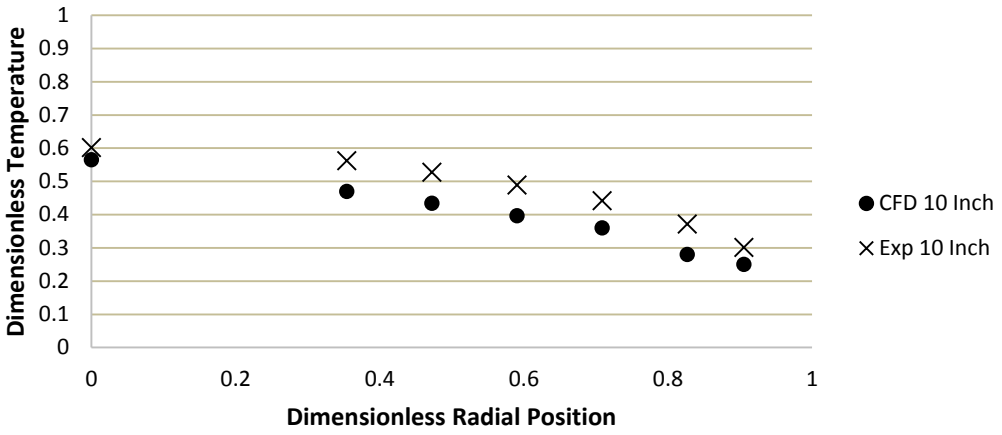

Simulation 2 Varying Viscosity: Heating Experimental versus CFD (N=5.33)

Air Flow 28% Experimental Re= 630 and CFD Re= 689 Bed Height 4 Inches

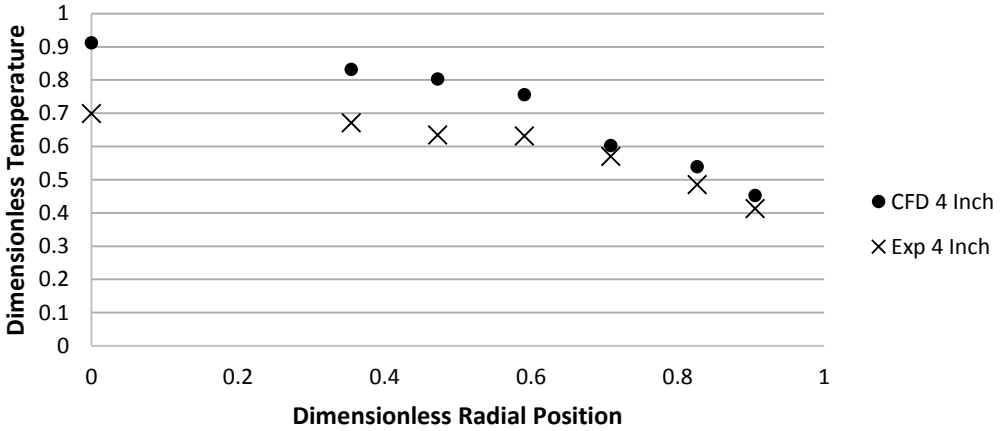

Air Flow 28% Experimental Re= 630 and CFD Re= 689 Bed Height 6 Inches

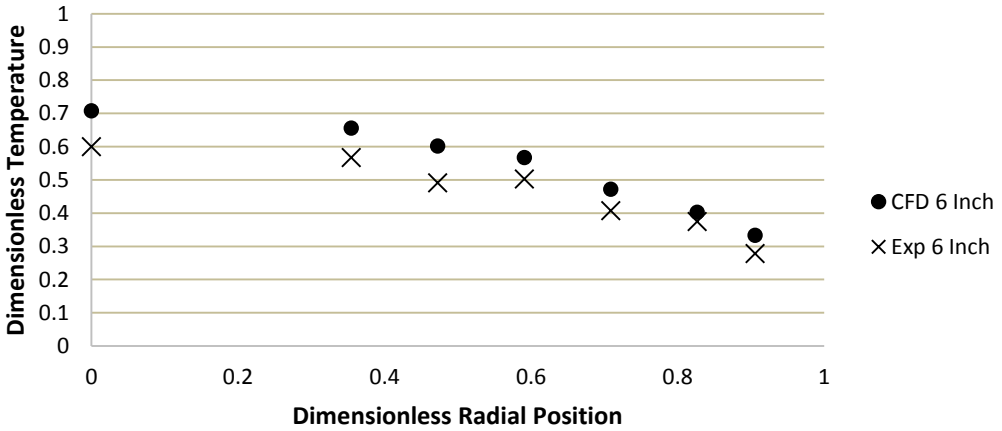

Air Flow 28% Experimental Re= 630 and CFD Re= 689 Bed Height 8 Inches

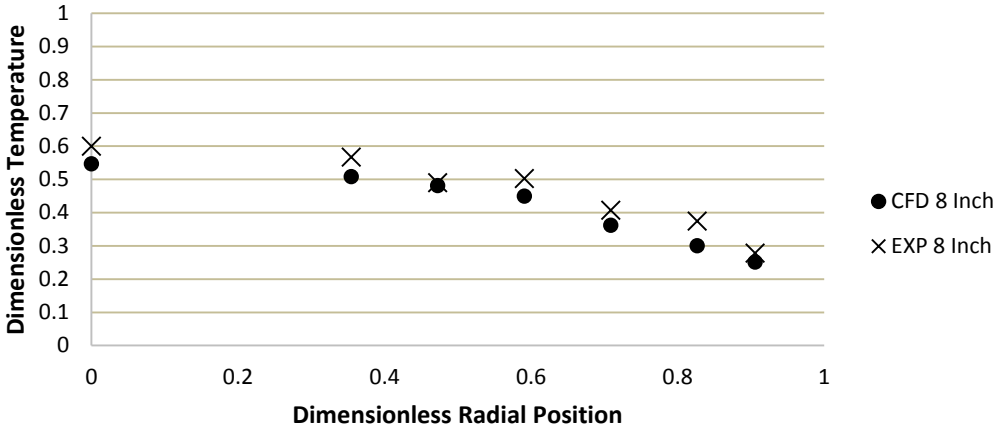

Air Flow 28% Experimental Re= 630 and CFD Re= 689 Bed Height 10 Inches

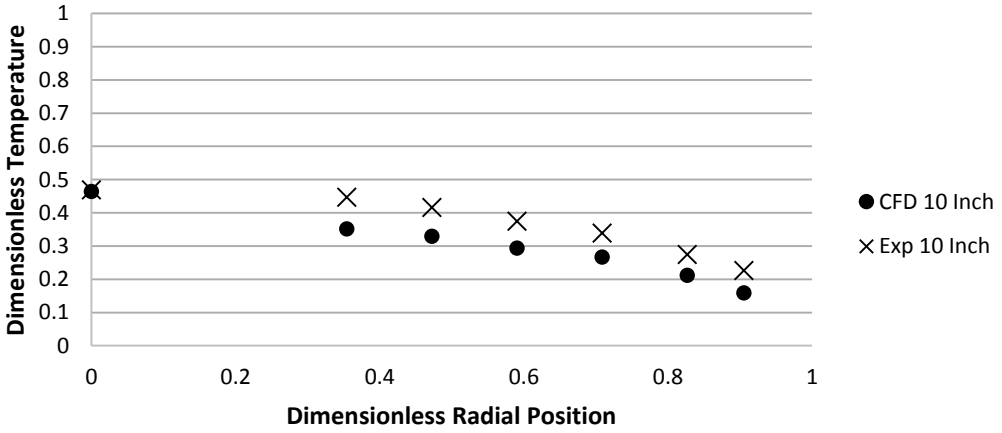

Air Flow 32% Experimental Re= 702 and CFD Re= 805 Bed Height 4 Inches

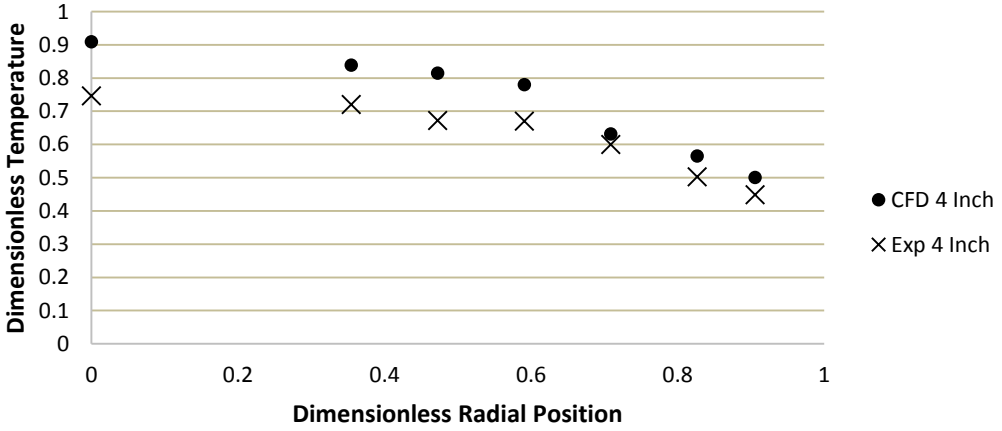

Air Flow 32% Experimental Re= 702 and CFD Re= 805 Bed Height 6 Inches

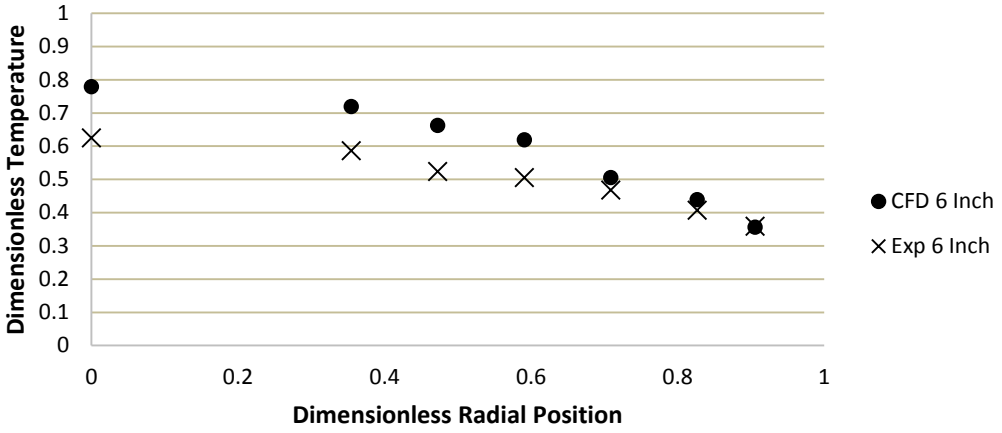

Air Flow 32% Experimental Re= 702 and CFD Re= 805 Bed Height 8 Inches

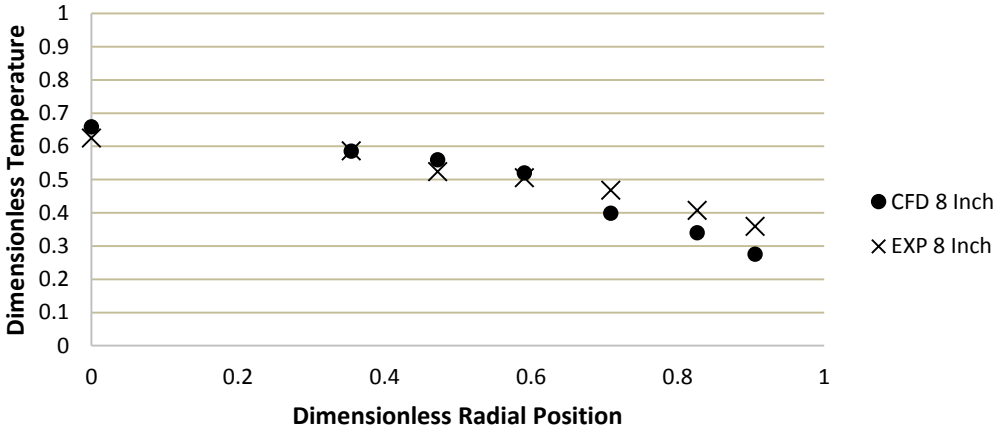

Air Flow 32% Experimental Re= 702 and CFD Re= 805 Bed Height 10 Inches

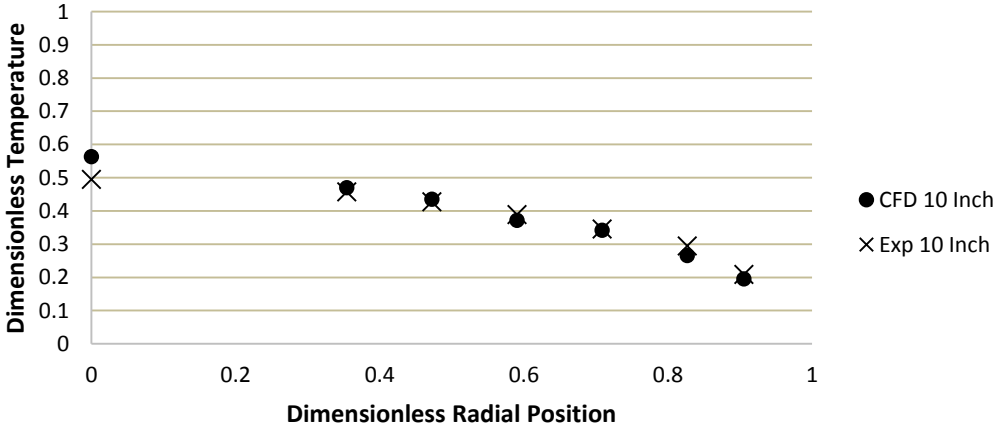

Air Flow 40% Experimental Re= 901 and CFD Re= 901 Bed Height 4 Inches

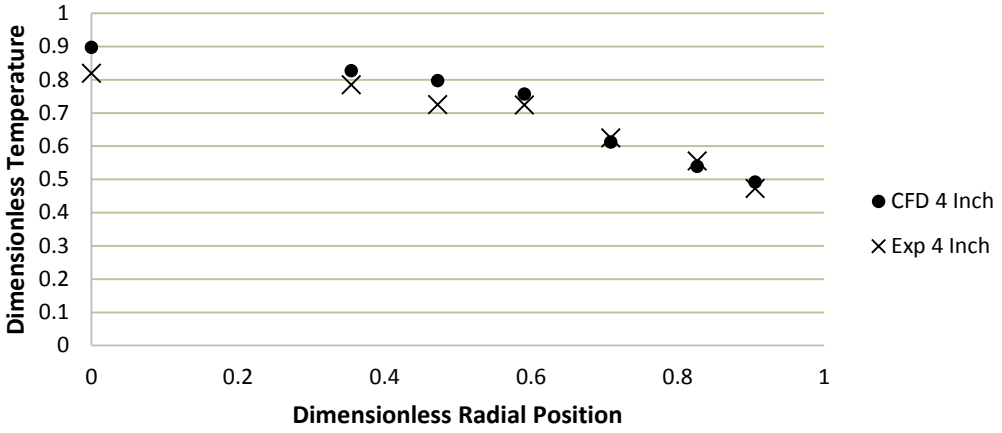

Air Flow 40% Experimental Re= 901 and CFD Re= 901 Bed Height 6 Inches

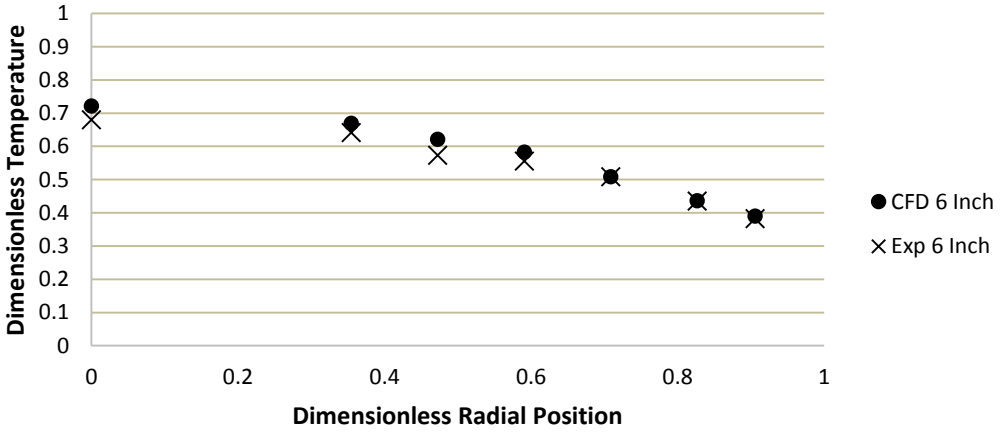

Air Flow 40% Experimental Re= 901 and CFD Re= 901 Bed Height 8 Inches

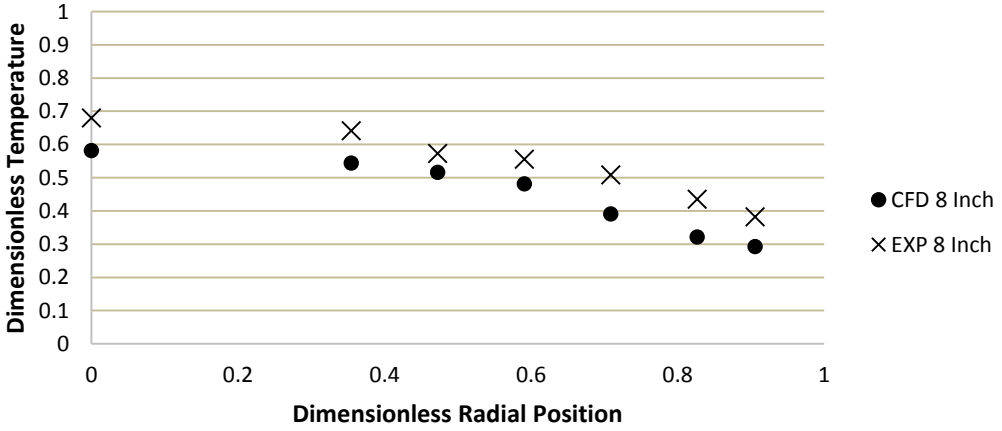

Air Flow 40% Experimental Re= 901 and CFD Re= 901 Bed Height 10 Inches

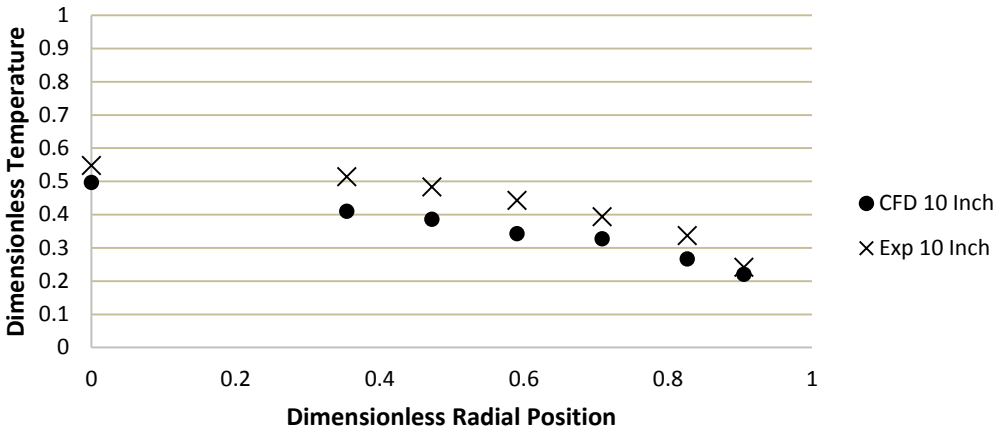

Air Flow 45% Experimental Re=1018 and CFD Re= 1022 Bed Height 4 Inches

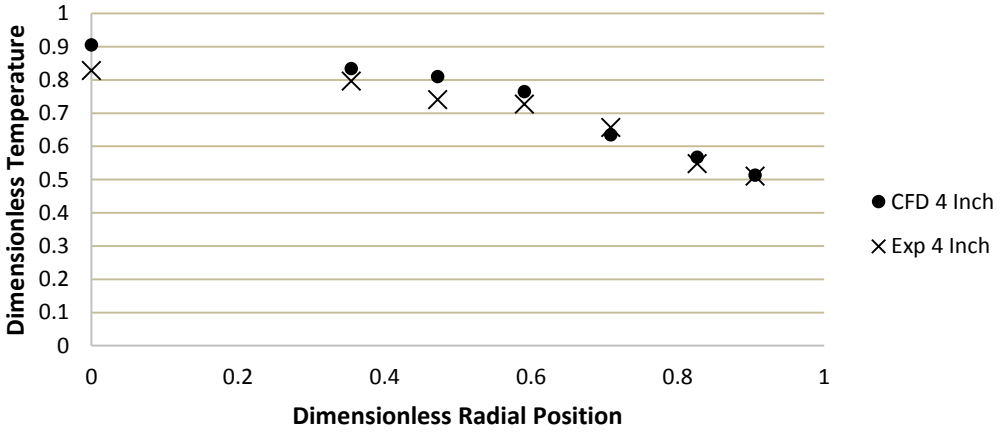

Air Flow 45% Experimental Re=1018 and CFD Re= 1022 Bed Height 6 Inches

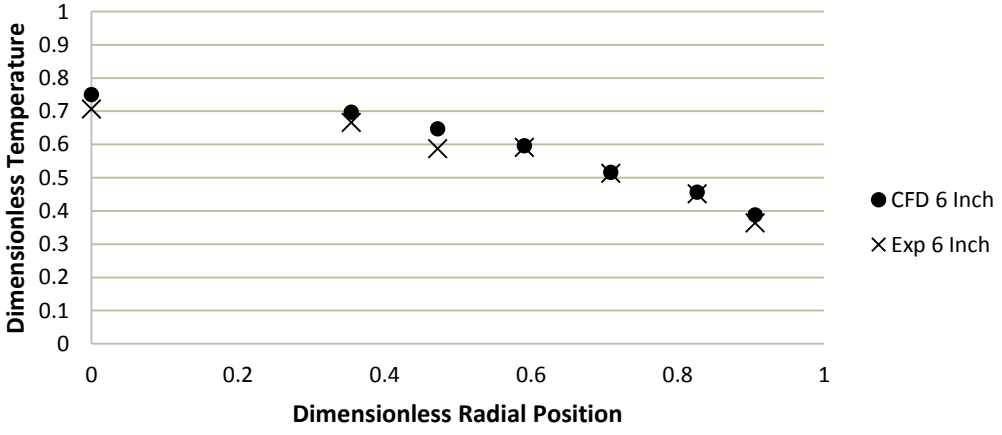

Air Flow 45% Experimental Re=1018 and CFD Re= 1022 Bed Height 8 Inches

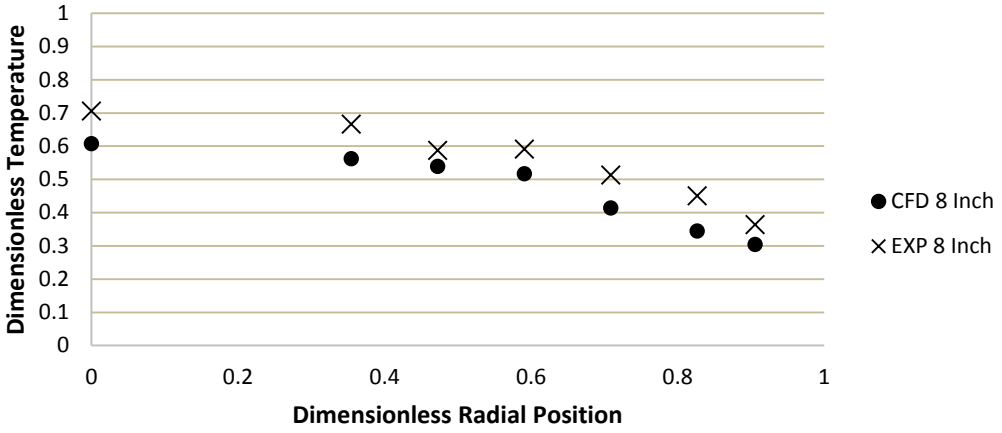

Air Flow 45% Experimental Re=1018 and CFD Re= 1022 Bed Height 10 Inches

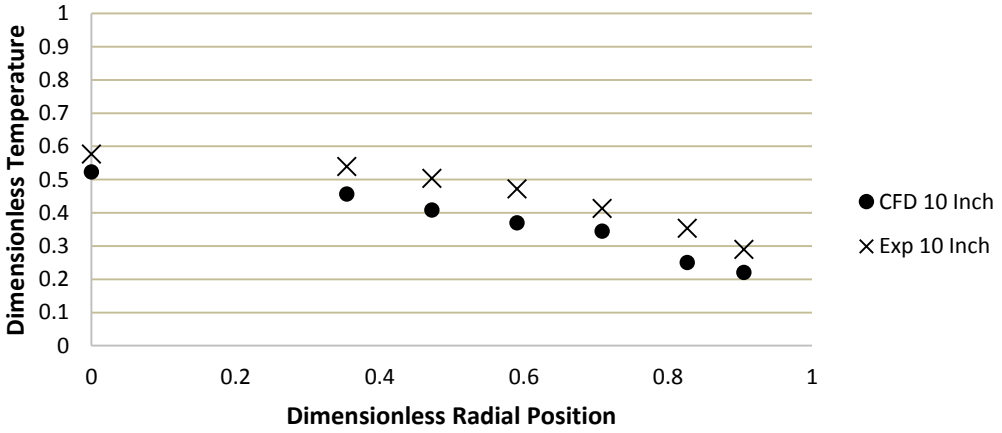

Air Flow 50% Experimental Re=1139 and CFD Re= 1141 Bed Height 4 Inches

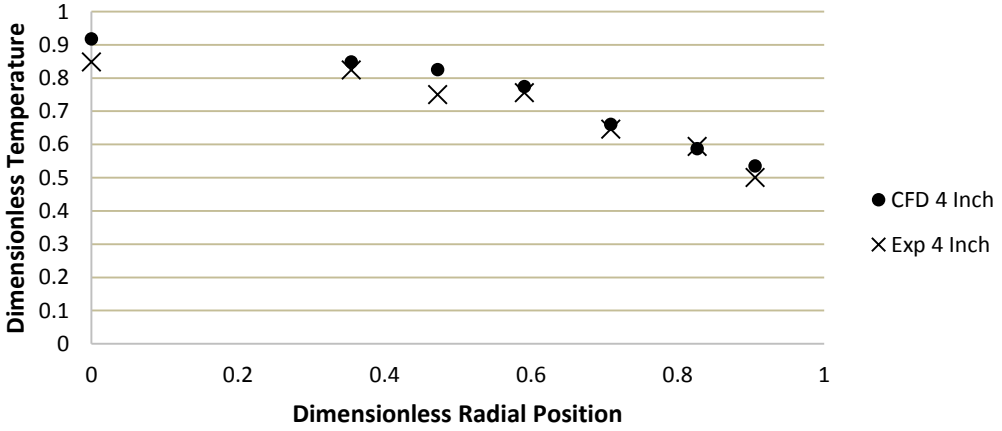

Air Flow 50% Experimental Re=1139 and CFD Re= 1141 Bed Height 6 Inches

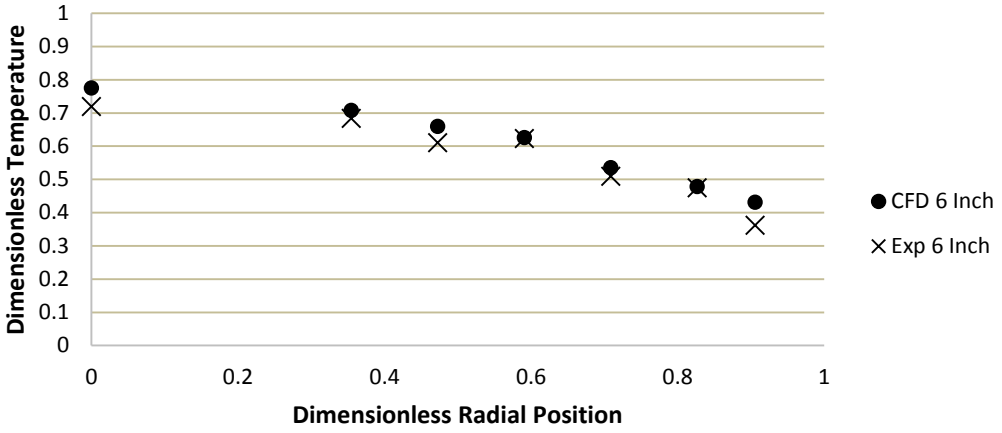

Air Flow 50% Experimental Re=1139 and CFD Re= 1141 Bed Height 8 Inches

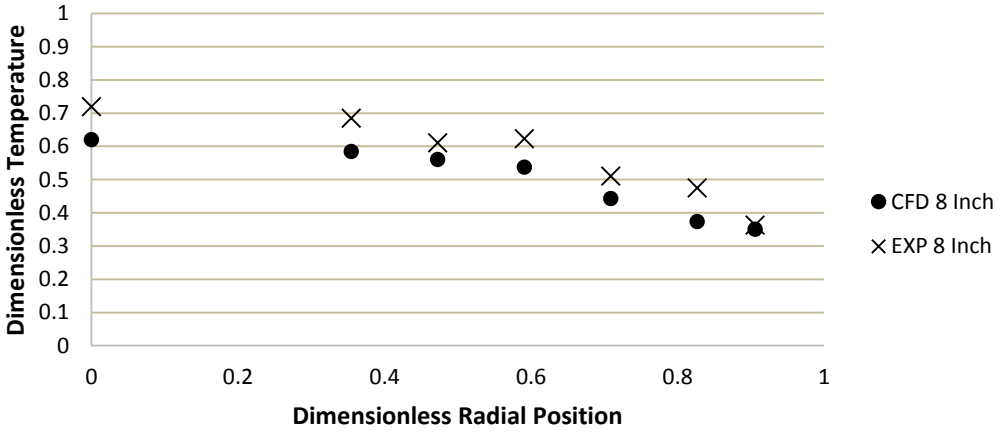

Air Flow 50% Experimental Re=1139 and CFD Re= 1141 Bed Height 10 Inches

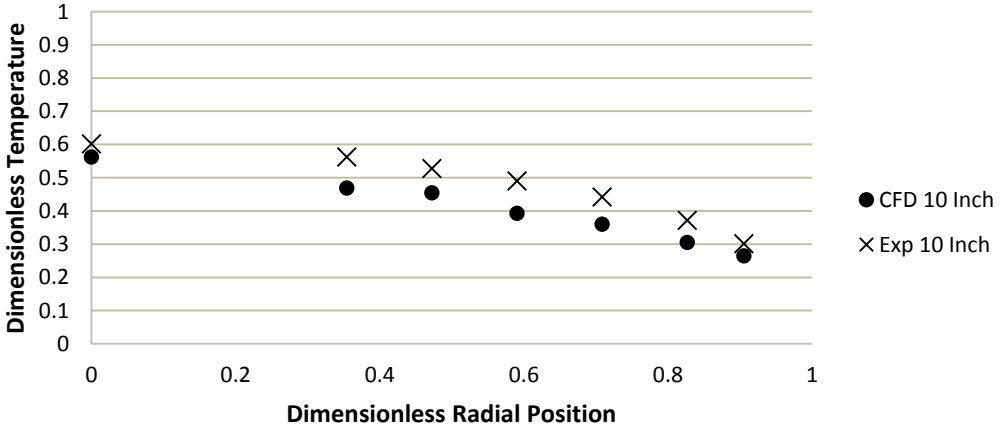

Simulation 2 Constant Viscosity: CFD Heating versus Cooling

Air Flow 28% CFD Cooling Re=503 and Heating Re=689 Bed Height 4 Inches

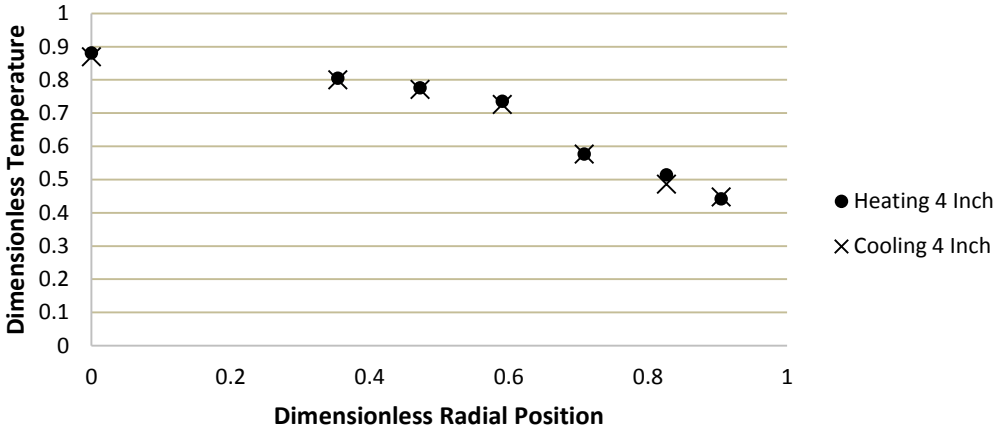

Air Flow 28% CFD Cooling Re=503 and Heating Re=689 Bed Height 6 Inches

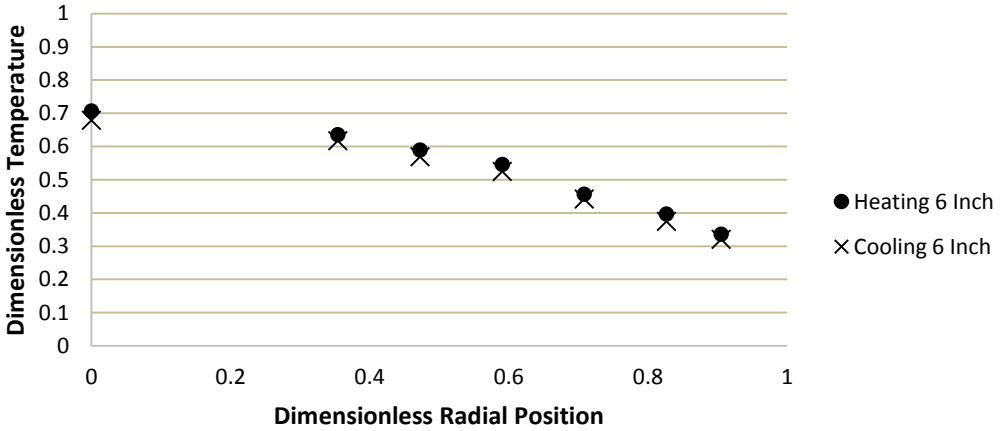

Air Flow 28% CFD Cooling Re=503 and Heating Re=689 Bed Height 8 Inches

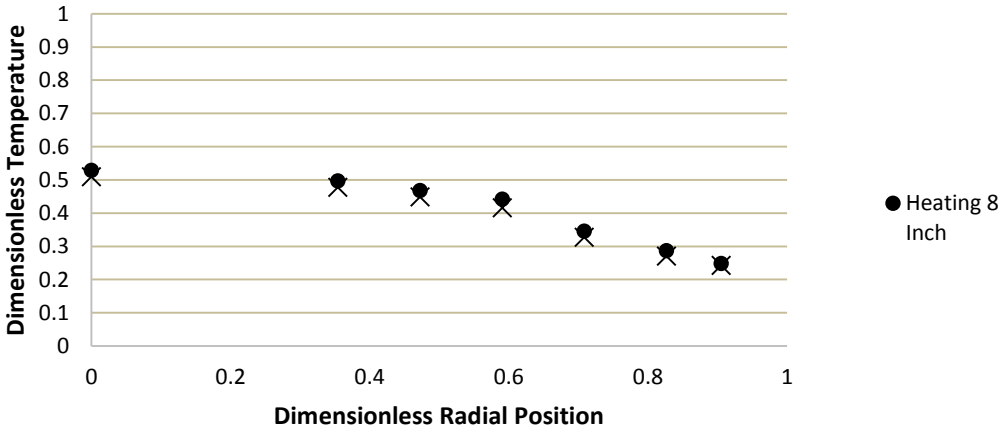

Air Flow 28% CFD Cooling Re=503 and Heating Re=689 Bed Height 10 Inches

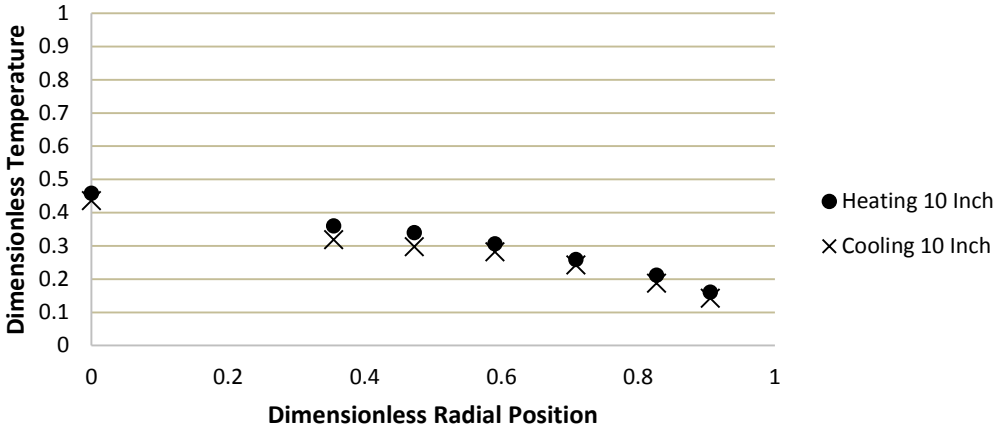

Air Flow 32% CFD Cooling Re=588 and Heating Re=805 Bed Height 4 Inches

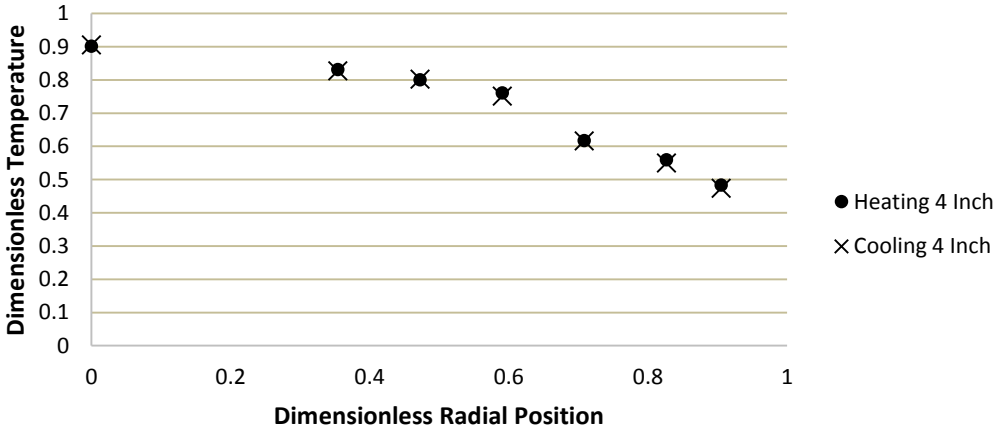

Air Flow 32% CFD Cooling Re=588 and Heating Re=805 Bed Height 6 Inches

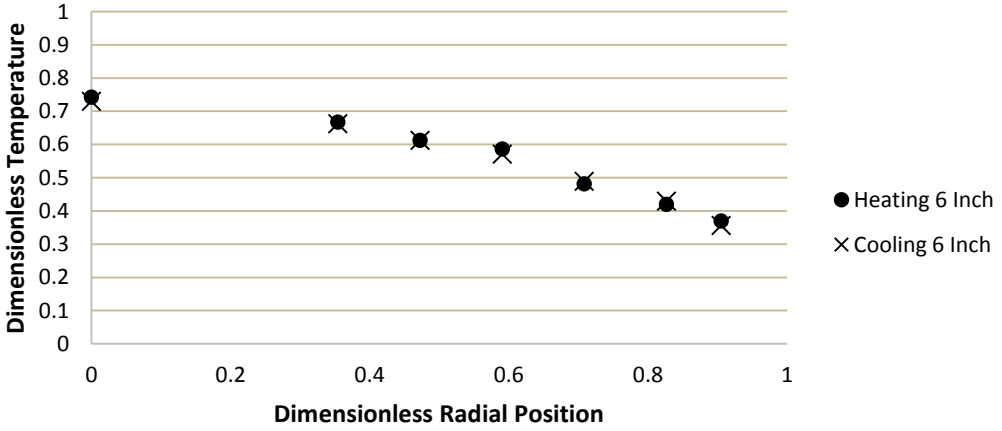

Air Flow 32% CFD Cooling Re=588 and Heating Re=805 Bed Height 8 Inches

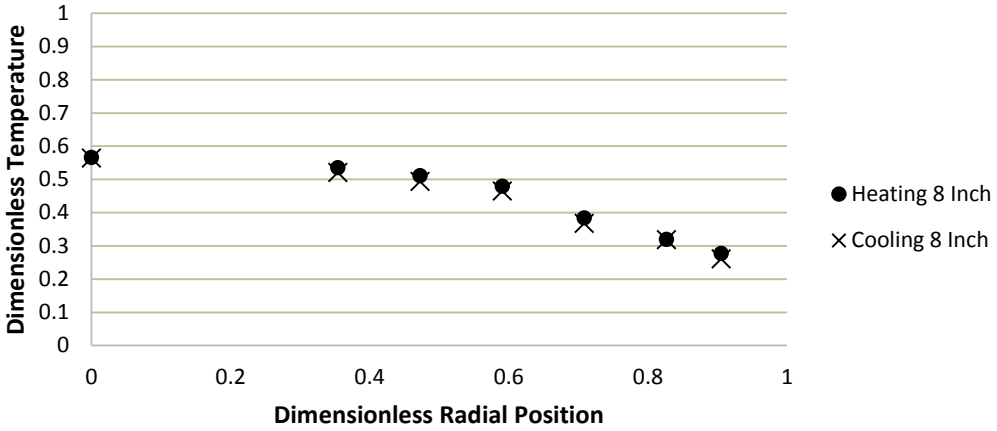

Air Flow 32% CFD Cooling Re=588 and Heating Re=805 Bed Height 10 Inches

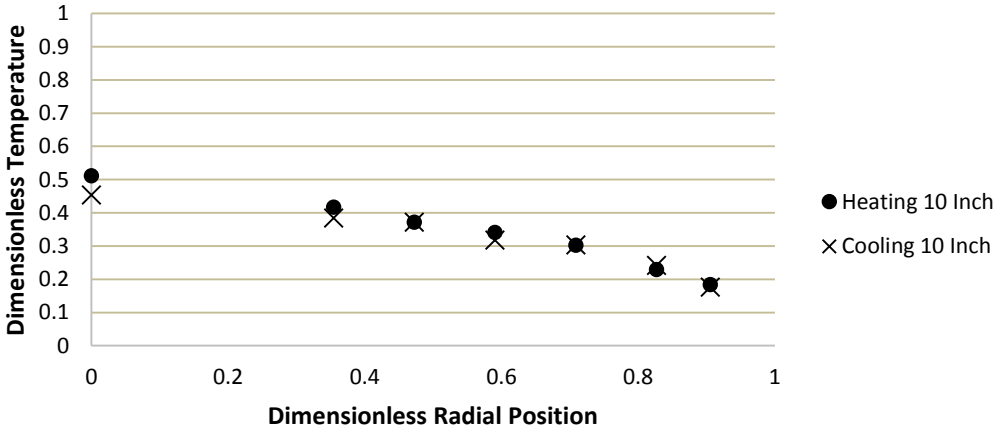

Air Flow 40% CFD Cooling Re=775 and Heating Re=901 Bed Height 6 Inches

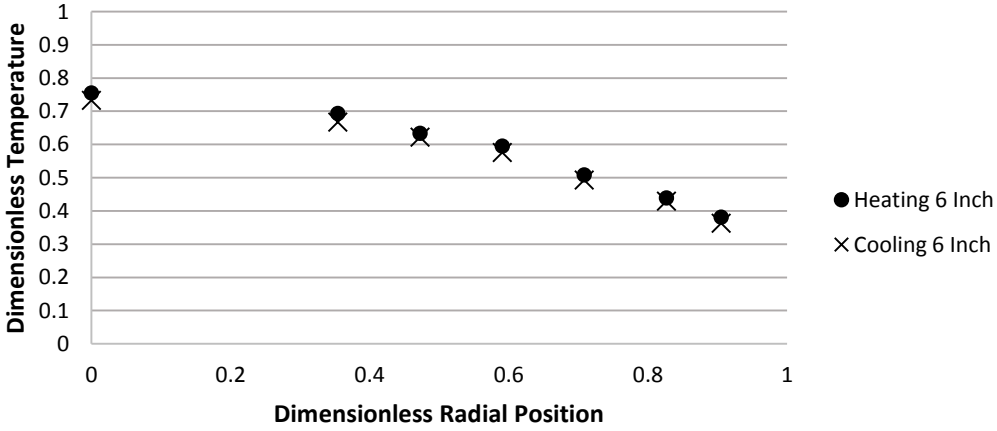

Air Flow 40% CFD Cooling Re=775 and Heating Re=901 Bed Height 8 Inches

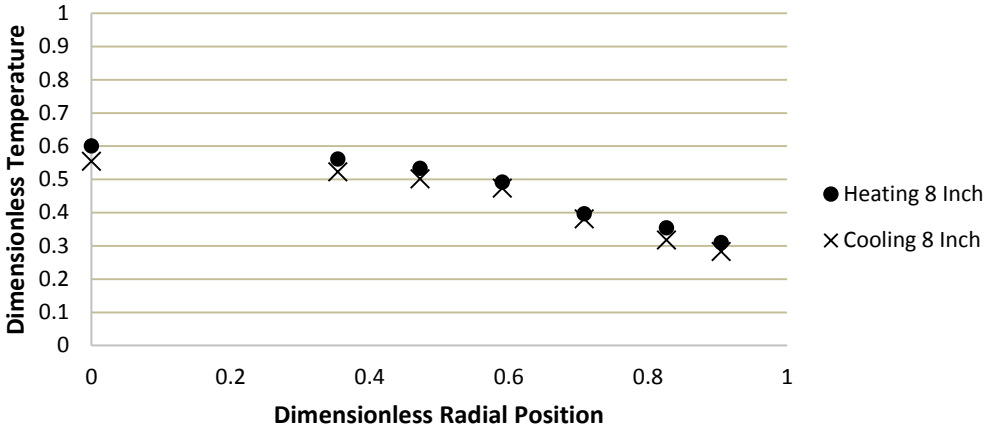

Air Flow 40% CFD Cooling Re=775 and Heating Re=901 Bed Height 10 Inches

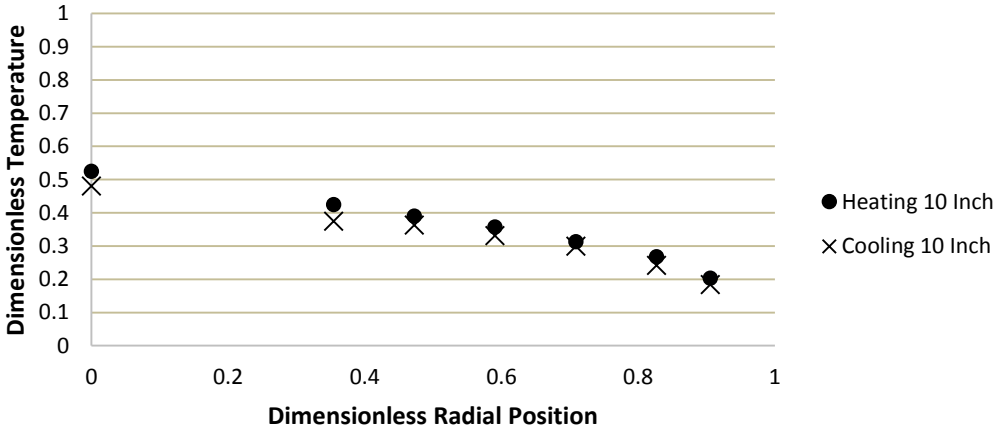

Air Flow 45% CFD Cooling Re=876 and Heating Re=1022 Bed Height 4 Inches

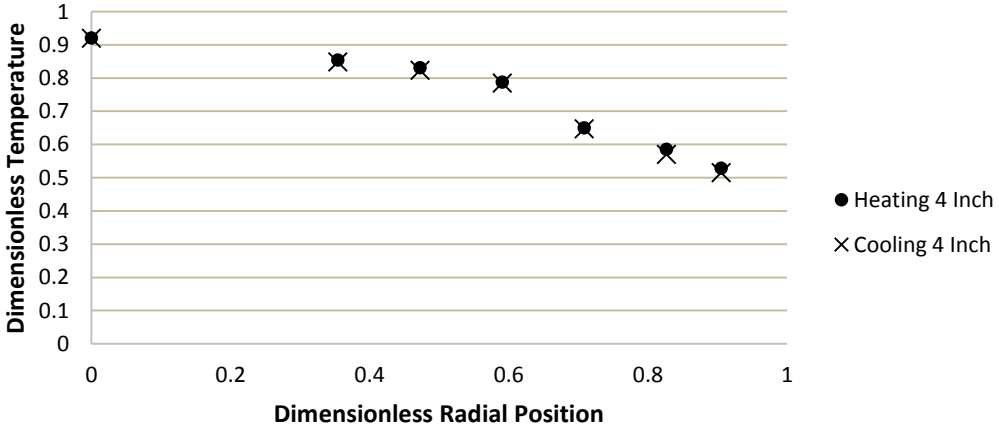

Air Flow 45% CFD Cooling Re=876 and Heating Re=1022 Bed Height 6 Inches

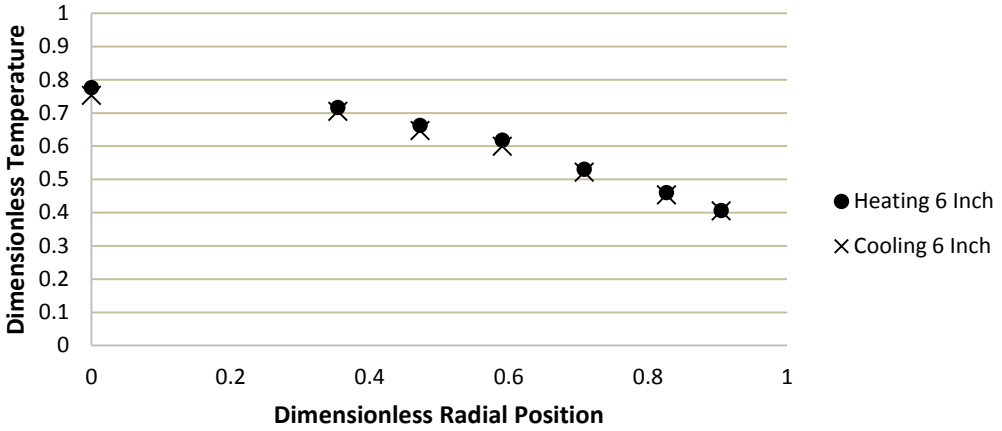

Air Flow 45% CFD Cooling Re=876 and Heating Re=1022 Bed Height 8 Inches

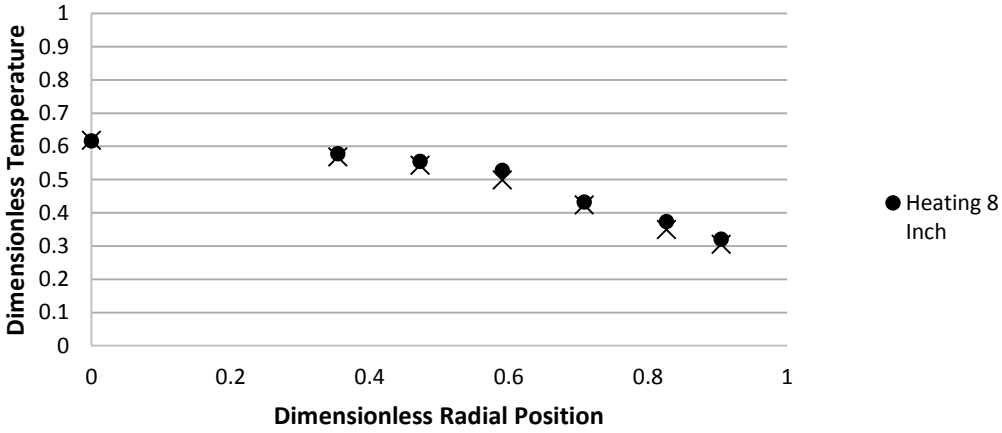

Air Flow 45% CFD Cooling Re=876 and Heating Re=1022 Bed Height 10 Inches

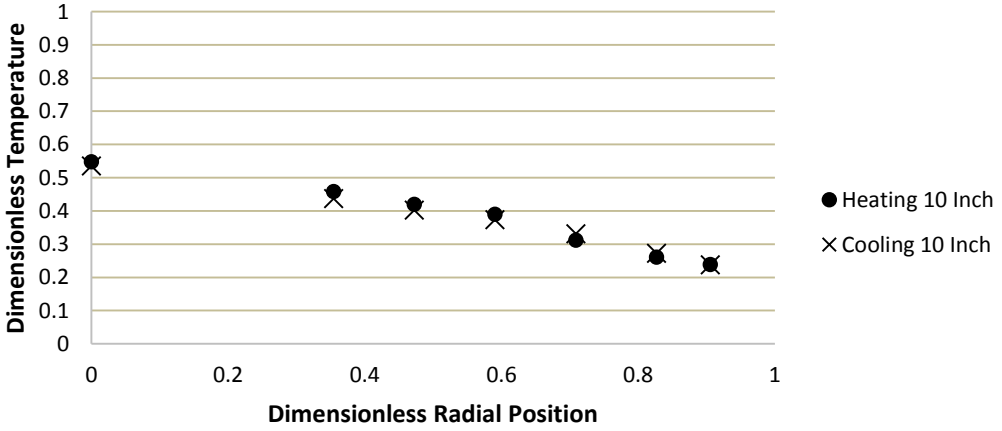

Air Flow 50% CFD Cooling Re=982 and Heating Re=1141 Bed Height 4 Inches

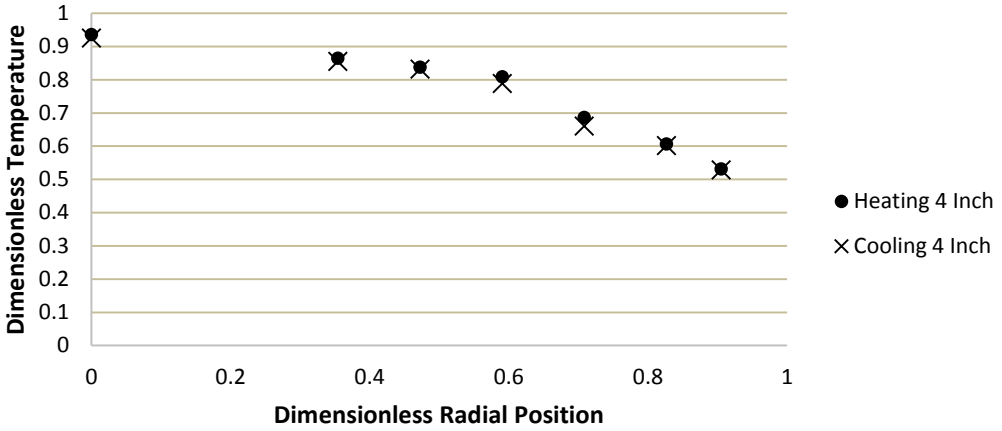

Air Flow 50% CFD Cooling Re=982 and Heating Re=1141 Bed Height 6 Inches

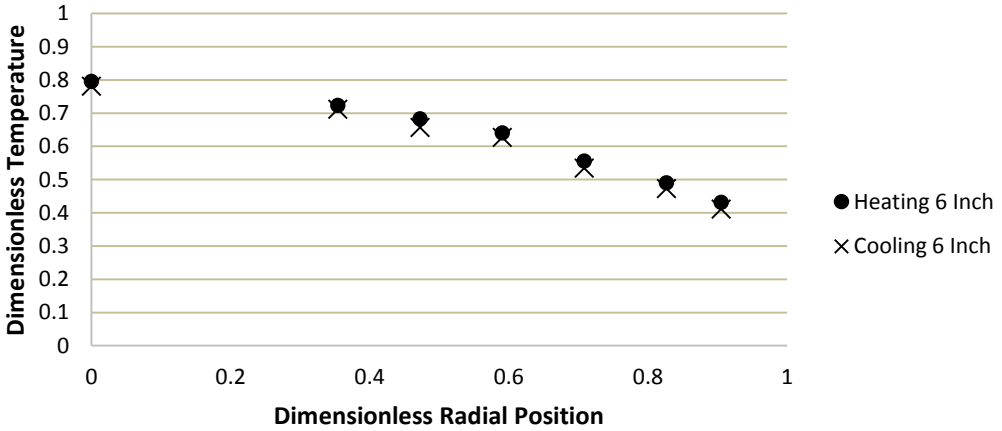

Air Flow 50% CFD Cooling Re=982 and Heating Re=1141 Bed Height 8 Inches

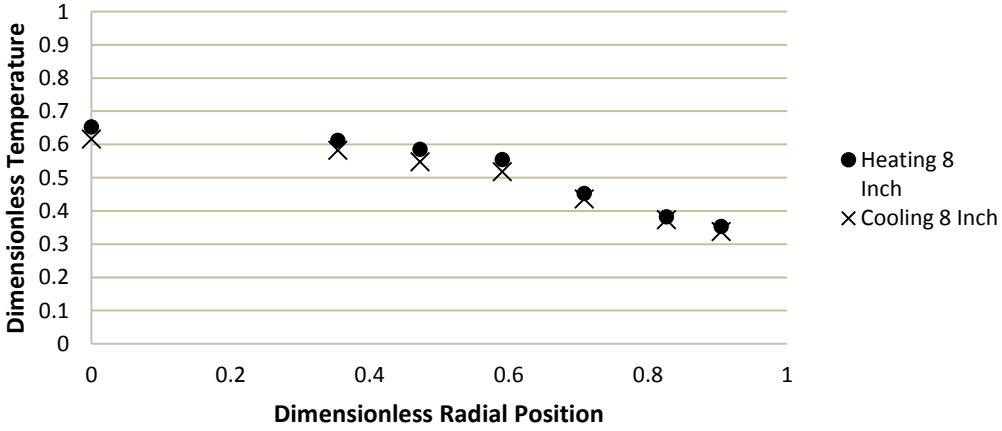

Air Flow 50% CFD Cooling Re=982 and Heating Re=1141 Bed Height 10 Inches

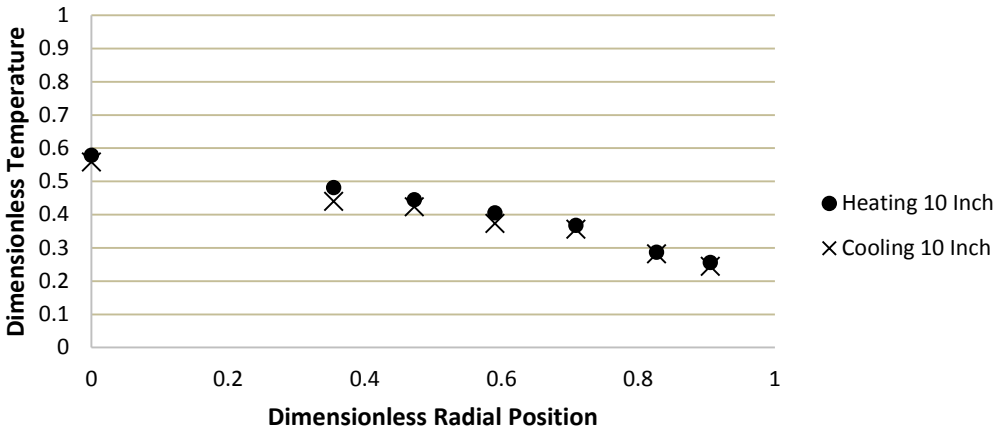

Simulation 2 Varying Viscosity: CFD Heating versus Cooling

Air Flow 28% CFD Cooling Re=503 and Heating Re=689 Bed Height 4 Inches

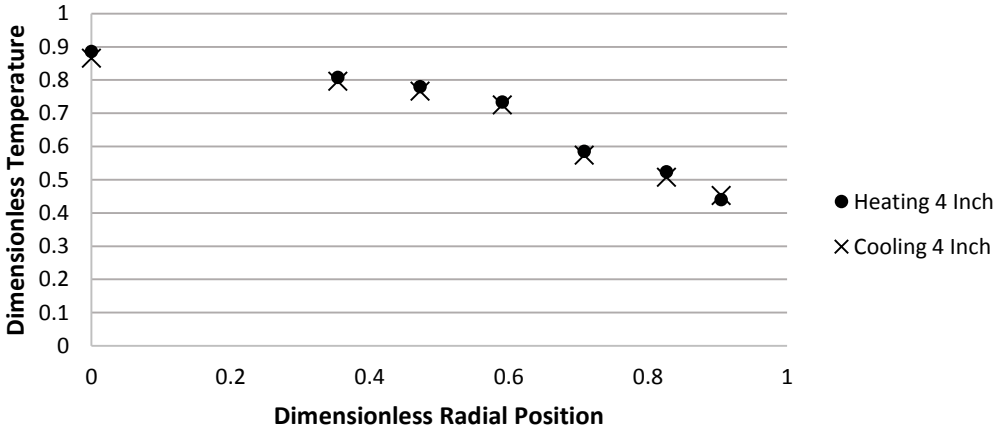

Air Flow 28% CFD Cooling Re=503 and Heating Re=689 Bed Height 6 Inches

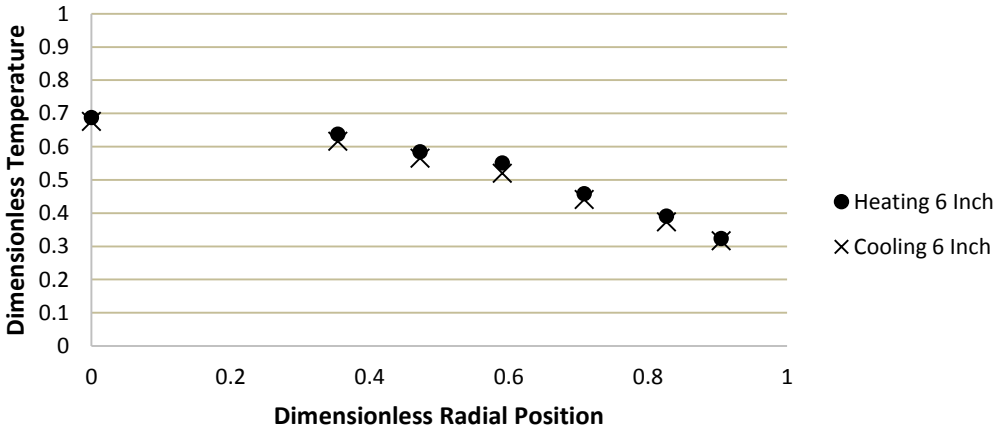

Air Flow 28% CFD Cooling Re=503 and Heating Re=689 Bed Height 8 Inches

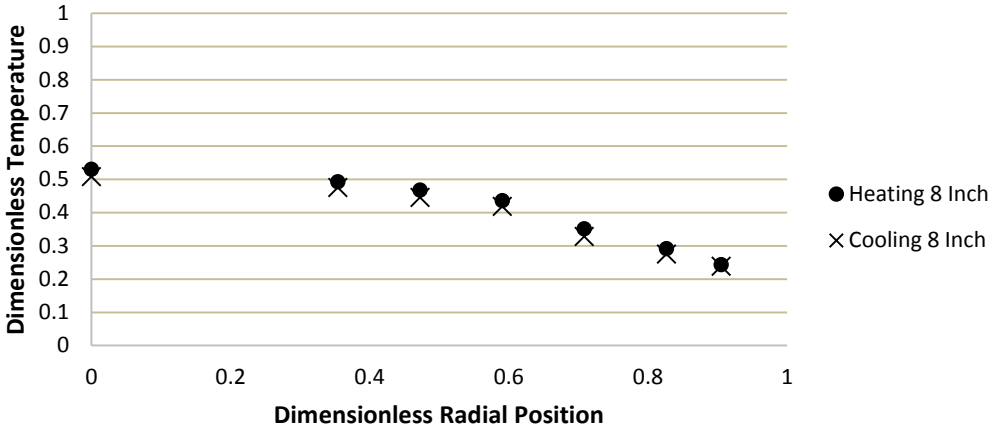

Air Flow 28% CFD Cooling Re=503 and Heating Re=689 Bed Height 10 Inches

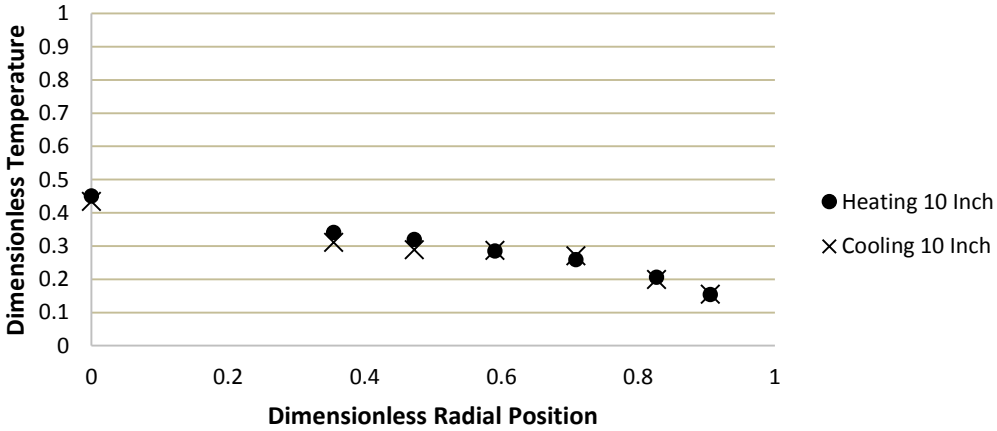

Air Flow 32% CFD Cooling Re=588 and Heating Re=805 Bed Height 4 Inches

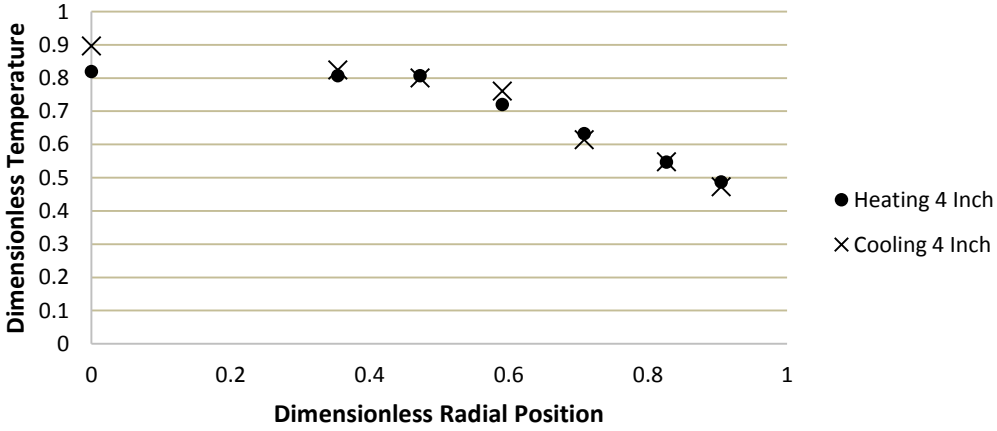

Air Flow 32% CFD Cooling Re=588 and Heating Re=805 Bed Height 6 Inches

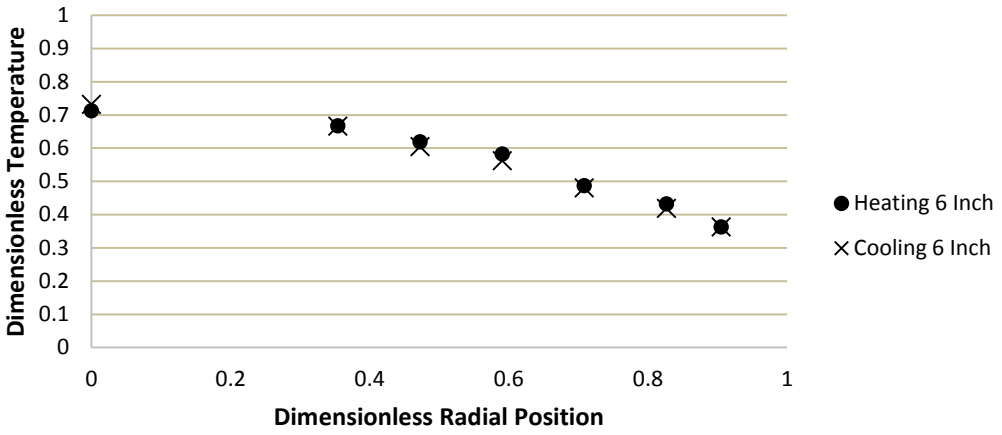

Air Flow 32% CFD Cooling Re=588 and Heating Re=805 Bed Height 8 Inches

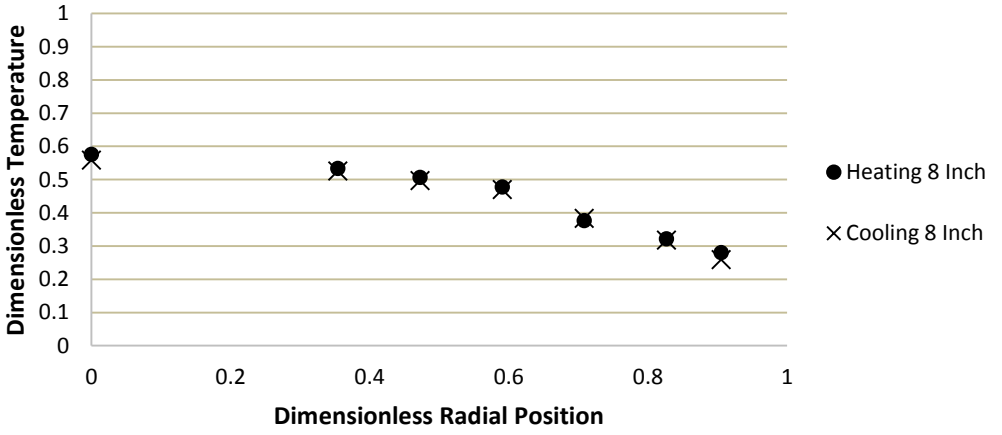

Air Flow 32% CFD Cooling Re=588 and Heating Re=805 Bed Height 10 Inches

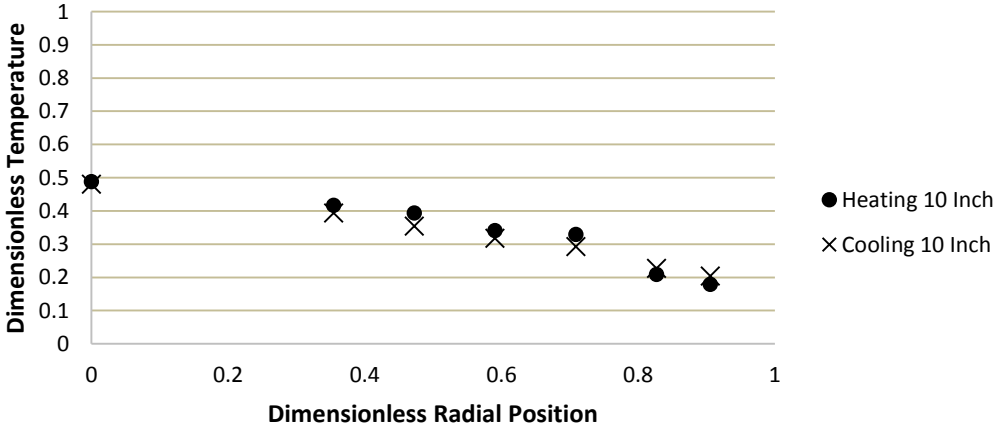

Air Flow 40% CFD Cooling Re=775 and Heating Re=901 Bed Height 4 Inches

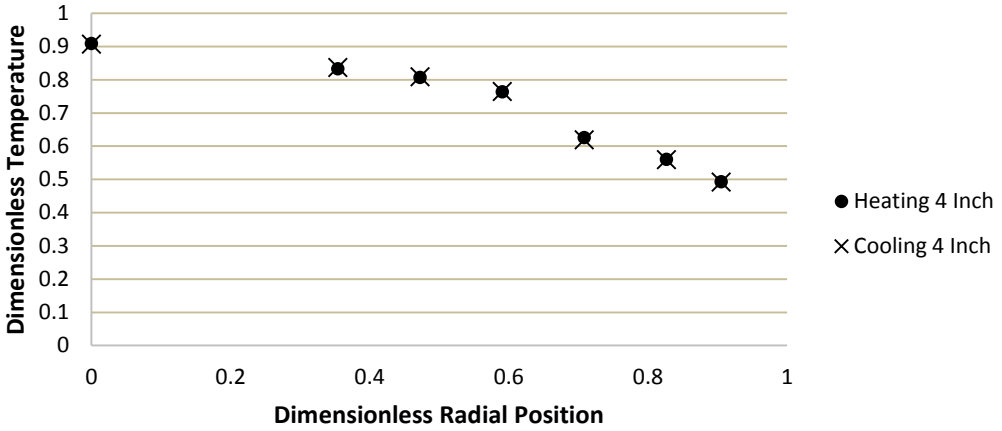

Air Flow 40% CFD Cooling Re=775 and Heating Re=901 Bed Height 6 Inches

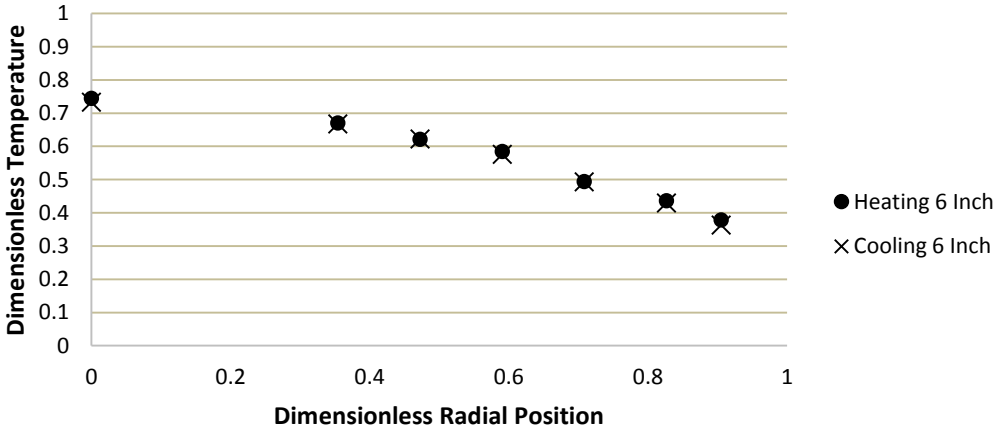

Air Flow 40% CFD Cooling Re=775 and Heating Re=901 Bed Height 8 Inches

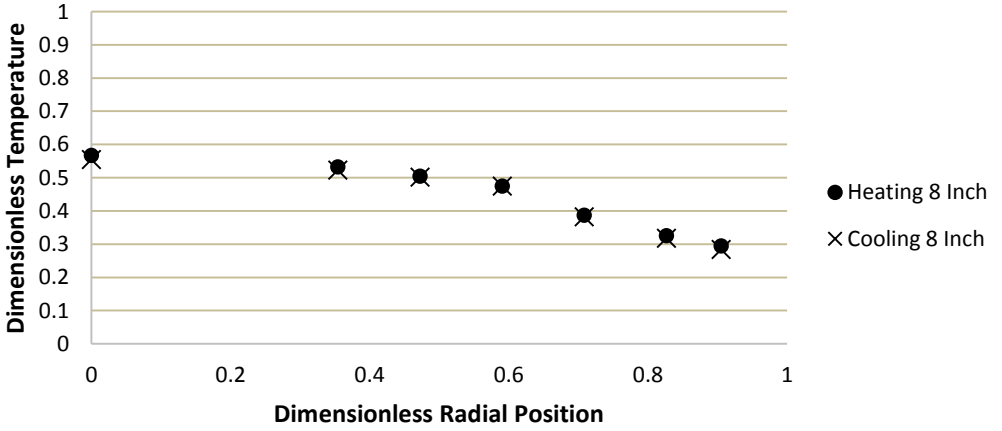

Air Flow 40% CFD Cooling Re=775 and Heating Re=901 Bed Height 10 Inches

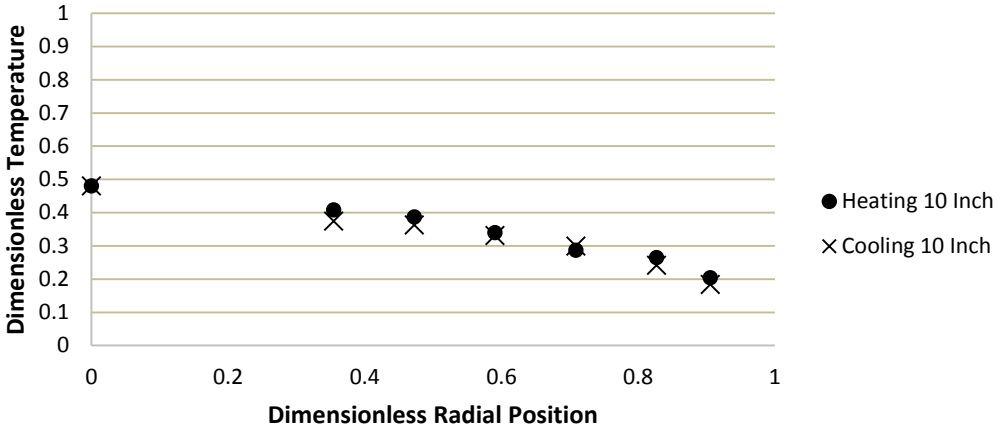

Air Flow 45% CFD Cooling Re=876 and Heating Re=1022 Bed Height 4 Inches

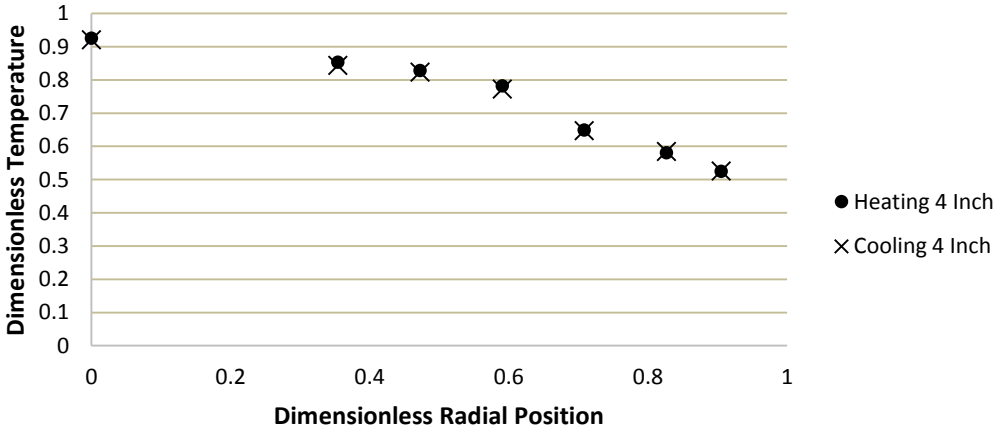

Air Flow 45% CFD Cooling Re=876 and Heating Re=1022 Bed Height 6 Inches

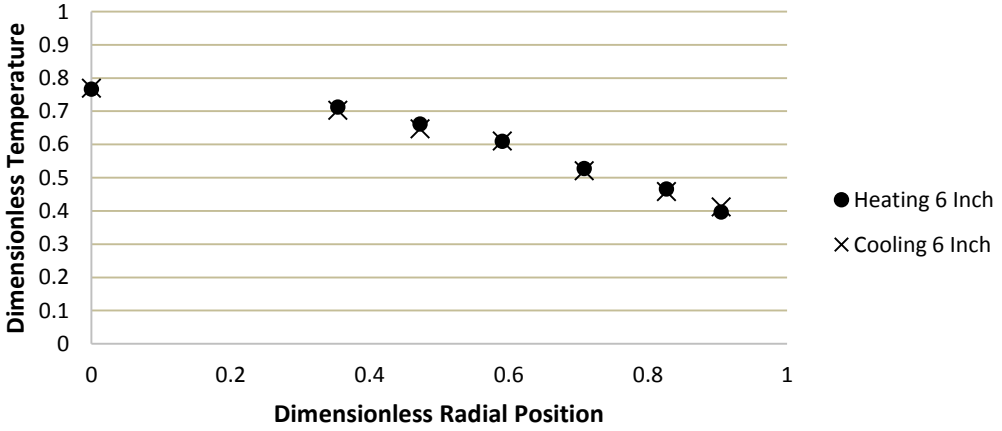

Air Flow 45% CFD Cooling Re=876 and Heating Re=1022 Bed Height 8 Inches

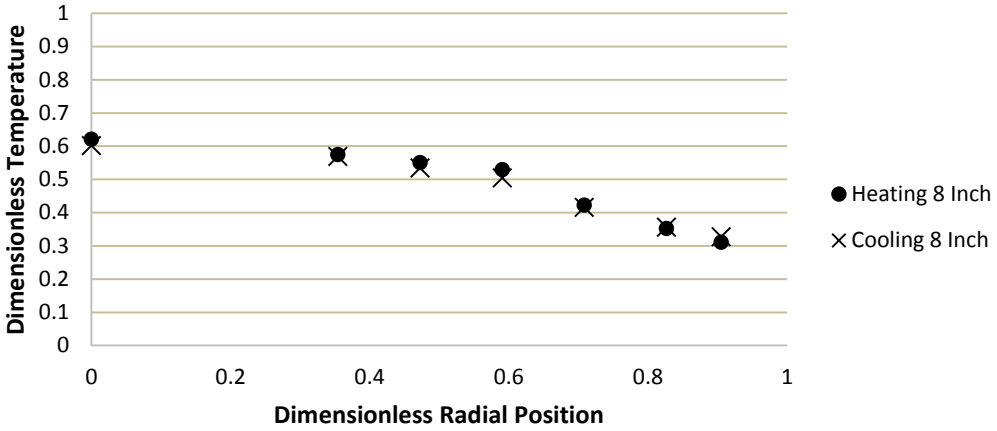

Air Flow 45% CFD Cooling Re=876 and Heating Re=1022 Bed Height 10 Inches

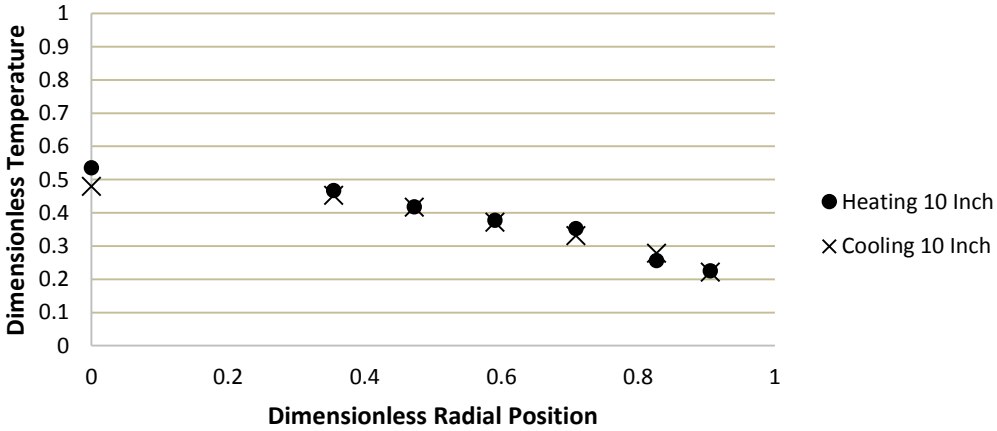

Air Flow 50% CFD Cooling Re=982 and Heating Re=1141 Bed Height 4 Inches

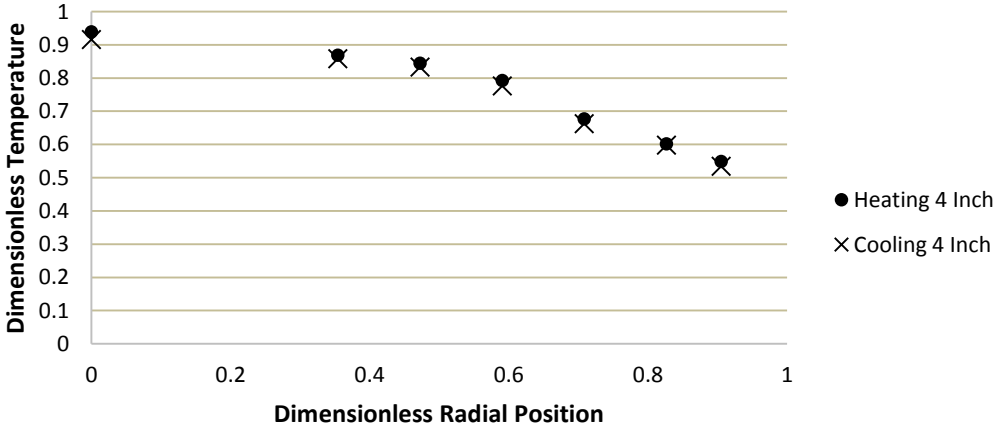

Air Flow 50% CFD Cooling Re=982 and Heating Re=1141 Bed Height 6 Inches

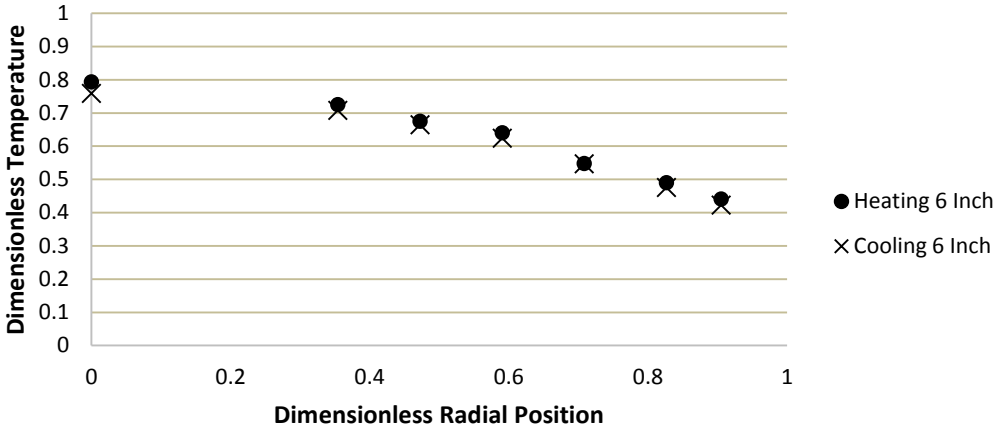

Air Flow 50% CFD Cooling Re=982 and Heating Re=1141 Bed Height 8 Inches

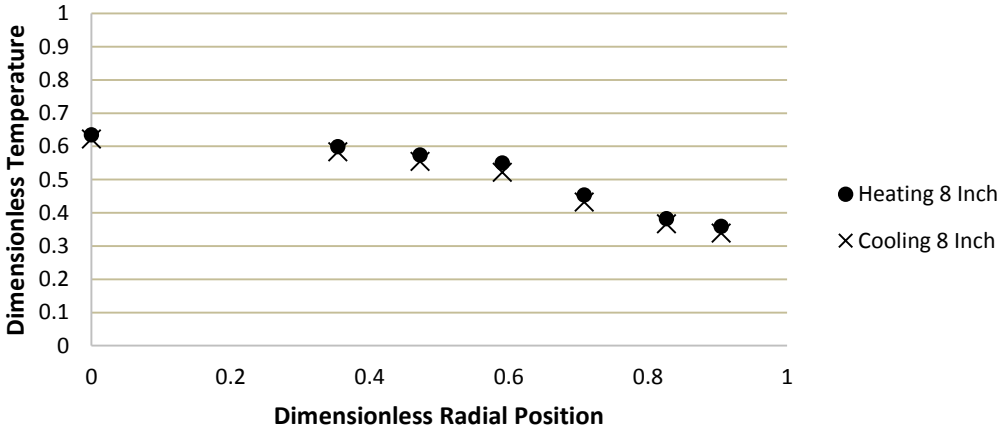

Air Flow 50% CFD Cooling Re=982 and Heating Re=1141 Bed Height 10 Inches